

GEOLOGICA ULTRAIECTINA

Mededelingen van de
Faculteit Aardwetenschappen
Universiteit Utrecht

No. 130

DYNAMICS OF ACTIVE CONTINENTAL MARGINS:
THE ANDES AND THE AEGEAN REGION

PAUL MEIJER

GEOLOGICA ULTRAIECTINA

Mededelingen van de
Faculteit Aardwetenschappen
Universiteit Utrecht

No. 130

DYNAMICS OF ACTIVE CONTINENTAL MARGINS:
THE ANDES AND THE AEGEAN REGION

PAUL MEIJER

27 - 014

CIP-GEGEVENS KONINKLIJKE BIBLIOTHEEK, DEN HAAG

Meijer, Paul Theodoor

Dynamics of active continental margins : the Andes and the
Aegean region / Paul Theodoor Meijer. - Utrecht :
Faculteit Aardwetenschappen, Universiteit Utrecht. -
(Geologica Ultraiectina, ISSN 0072-1026 ; no. 130)
Proefschrift Universiteit Utrecht. - Met lit. opg. - Met
samenvatting in het Nederlands.

ISBN 90-71577-84-8

Trefw.: aardbevingen ; Andes / aardbevingen ; Griekenland /
aardverschuivingen.

DYNAMICS OF ACTIVE CONTINENTAL MARGINS:
THE ANDES AND THE AEGEAN REGION

Dynamica van actieve continentale marges:
de Andes en het Egeïsche gebied

(met een samenvatting in het Nederlands)

PROEFSCHRIFT

TER VERKRIJGING VAN DE GRAAD VAN DOCTOR
AAN DE UNIVERSITEIT UTRECHT
OP GEZAG VAN DE RECTOR MAGNIFICUS, PROF. DR. J.A. VAN GINKEL
INGEVOLGE HET BESLUIT VAN HET COLLEGE VAN DEKANEN
IN HET OPENBAAR TE VERDEDIGEN
OP MAANDAG 23 OKTOBER 1995 DES OCHTENDS TE 10.30 UUR

DOOR

PAUL THEODOOR MEIJER

GEBOREN OP 25 JUNI 1965, TE AMERSFOORT

PROMOTOR: PROF. DR. M.J.R. WORTEL

The research reported in this thesis has been carried out at the Department of Geophysics, Institute of Earth Sciences, Utrecht University, Budapestlaan 4, 3584 CD Utrecht, The Netherlands. This is Geodynamics Research Institute (Utrecht University) contribution 95.043.

Voor Dolors

Contents

Chapter 1. Introduction

<i>Objective</i>	12
<i>Areas of Study</i>	12
<i>Western margin of South America</i>	12
<i>The Aegean region</i>	13
<i>The Use of a Numerical Model</i>	14
<i>Outline of the Analysis</i>	15
<i>Organisation of Thesis</i>	16

Chapter 2. The Dynamics of Motion of the South American Plate

Introduction	17
Model Description	18
<i>Plate boundaries: Geometry and Nature</i>	18
<i>Divergent boundaries</i>	18
<i>Scotia Sea region</i>	19
<i>Western boundary</i>	21
<i>Northern boundary</i>	21
<i>Force Modelling</i>	23
Analysis and Results	25
<i>First-Order Model</i>	26
<i>Distribution of Basal Shear Stress</i>	35
<i>Additional Plate Boundary Forces</i>	37
<i>Alternative Plate Geometry</i>	38
Discussion	41
<i>Model Limitations</i>	41
<i>Western Plate Margin</i>	41
<i>Northwestern South America</i>	43
<i>Basal Drag</i>	44
<i>Importance of Slab Pull on the South American Plate</i>	44
<i>General</i>	45
Conclusions	46
Appendix	46

Chapter 3. The Stress Field of the South American Plate

Introduction	49
Observed Present-Day Stress Field	51
<i>The Andes South of 5°N</i>	54
<i>Northwestern South America</i>	58
<i>Craton and Paleozoic Basins</i>	58

Methods	59
<i>Intra-Plate Stress Calculations</i>	59
<i>Effect of Topography</i>	60
<i>First approach</i>	61
<i>Second approach</i>	66
<i>Comparison of Model and Observations</i>	69
Analysis I. The First-Order Model	71
<i>Defining a Reference Model</i>	72
<i>Variation of Basal Shear</i>	74
<i>Variation of the Azimuth of F_{Car}</i>	78
<i>Reference Model vs. Observations in the Andes</i>	78
<i>Evaluation of Results Part I</i>	81
<i>Basal shear stress</i>	81
<i>Northwestern South America</i>	81
<i>Amazon basin</i>	84
<i>Western margin</i>	85
<i>General</i>	85
Analysis II. Additional Plate Boundary Forces	86
<i>Evaluation of Results Part II</i>	90
Analysis III. Lateral Variation of Plate Contact Resistance	91
<i>F_{pcr} Dependent on Slab Dip or Slab Age</i>	91
<i>Dependence on slab dip</i>	92
<i>Dependence on slab age</i>	96
<i>F_{pcr} Affected by Trench-Parallel Mantle Flow</i>	100
<i>Evaluation of Results Part III</i>	103
Analysis IV. Effects of Continent-Ocean Transition	103
<i>The Passive Margin</i>	103
<i>The Active Margin</i>	104
<i>Evaluation of Results Part IV</i>	108
Analysis V. The Effect of Topography: the Andes	111
<i>Reference Model as Background</i>	111
<i>Background Model With Driving Basal Shear</i>	115
<i>Evaluation of Results Part V</i>	122
<i>Dependence on density</i>	122
<i>Comparing the two approaches</i>	123
<i>Implications of strike-slip at low elevations</i>	123
General Discussion	124
<i>Combination of Model Results</i>	124
<i>The Forces of First-Order Importance</i>	125
<i>Does Ridge Push Constitute the Only Driving Force?</i>	126
<i>Stress Field in the Andes</i>	128
Conclusions	129

Chapter 4. Late Cenozoic Dynamics of the Aegean Region

Introduction	131
Outline of Geological History and Current Setting	134
Observations	137
<i>Stress Inferred From Field Observed Faulting</i>	137
<i>Western Peloponnese</i>	137
<i>Kythira</i>	140
<i>Regional compilation</i>	142
<i>Seismic Strain: Earthquake Focal Mechanisms</i>	145
<i>Horizontal Motions</i>	147
Suggested Mechanisms and Present Approach	151
<i>Westward Motion of Anatolia</i>	151
<i>The Hellenic Subduction Zone</i>	151
<i>Slab detachment</i>	152
<i>Present Approach</i>	153
Model Description	154
Model Analysis, Present-Day Situation	155
<i>Consequences of Westward Anatolian Push</i>	156
<i>Forces Associated With the Subduction Zone</i>	159
<i>Pull parallel to relative motion</i>	160
<i>Uniform arc-normal pull</i>	162
<i>Arc-normal pull, varying magnitude</i>	164
<i>Arc-normal pull and subduction zone resistance</i>	166
<i>Subduction Forces and Westward Push Combined</i>	168
<i>Results Analysis of Present Situation</i>	173
Model Analysis, Late Pliocene Situation	174
<i>Arc-Normal Pull as in Present-Day Model</i>	175
<i>Alternative Model</i>	176
Discussion of Model Results	178
<i>Role of Anatolian Push</i>	178
<i>Distribution of Forces Related to Subduction, Present-day</i>	179
<i>Distribution of Forces Related to Subduction, Pliocene</i>	181
Nature of the Subduction Related Forces	182
<i>Hinge-retreat and Roll-Back</i>	182
<i>Mechanism I: Secondary Convection</i>	184
<i>Mechanism II: Spreading That Forces Hinge Retreat</i>	184
<i>Distribution of associated pull</i>	185
<i>Forced hinge retreat</i>	187
<i>Mechanism III: Spreading Allowed by Roll-Back</i>	187
<i>Additional resistance</i>	189
<i>Geometry of roll-back</i>	190
<i>Mechanism IV: Spreading Caused by Roll-Back</i>	190

Role of Slab Detachment	191
Conclusions	193
Chapter 5. Conclusions	195
<i>The Two Overriding Margins Compared</i>	195
<i>Future Research</i>	196
<i>Concluding Remarks</i>	197
References	199
Samenvatting (summary in dutch)	217
Dankwoord (acknowledgements)	219
Curriculum Vitae	220

Introduction

Chapter 1

The large plates and numerous smaller units which make up the Earth's outer shell, or lithosphere, are in continuous motion. Together with flow at greater depth in the Earth's mantle, movement of the plates at the surface constitutes a complex pattern of convection that originates from, and is an expression of, the on-going cooling of the planet. As perhaps the most obvious manifestation of this cooling, oceanic lithosphere is continuously being created at zones of upwelling hot mantle material, the oceanic spreading ridges. Along boundaries where two adjacent plates converge, lithosphere (predominantly of the oceanic type) is returned into the mantle by the process of subduction. Although intra-oceanic subduction zones also exist, the upper or "overriding" plate often consists of continental lithosphere.

Subduction strongly affects the leading edge of the overriding plate, hence the term active continental margins. Reheating of the descending - initially cool - oceanic lithosphere leads to partial melting which is expressed at the surface of the overriding plate in the form of a volcanic arc. Moreover, subduction is commonly associated with deformation of the overriding plate. Active continental margins display a wide range of deformational styles. Whereas shortening occurs at the site of the trench, the overriding plate may be subject to either shortening or extension. Present-day active continental margins are characterised by conspicuous tectonic structures ranging from mountain belts to back-arc basins and island arcs. Many older orogenic belts mark the site of

closure of an oceanic basin and a large part of the rock sequences these mountain belts encompass will previously have occupied a position in an overriding margin.

Objective

The research presented in this thesis is aimed at contributing to our understanding of the forces that control the state of stress and associated deformation of overriding continental margins. For reasons outlined below, the study concentrates on two areas where deformation is currently active: the western margin of the South American plate, comprising the Andean Cordillera, and, secondly, the Aegean region, comprising the Aegean Sea, the Greek mainland, and western Turkey. The main objective of this thesis is not to provide additional observations regarding the tectonics of the regions under scrutiny, but rather, to investigate the causes of deformation by using the available data in a quantitative analysis based on a numerical modelling.

Areas of Study

Western margin of South America. The trench system off the west coast of South America extends along the entire western margin of the lithospheric plate, spanning a latitude range of about 60°. Apart from the southernmost Chile segment, where the descending lithosphere pertains to the Antarctic plate, the trench system marks the subduction of the Nazca plate. Viewed in an absolute frame of reference (such as formed by hotspots) the Nazca plate and the South American plate both advance towards the trench system (e.g. Chase, 1978a, b; Minster and Jordan, 1978; Gripp and Gordon, 1990). As is implied by the westward absolute motion of the South American plate, the trench system itself retreats oceanward.

Magmatic processes and compressional deformation have created the Andean Cordillera. This orogen consists of several parallel mountain belts and comprises, in its central part, the world's second largest highland plateau, the Altiplano-Puna, sitting at an average elevation of about 4 km. The tectonic evolution of the Andes has been long and complex. Whereas the current high topography was probably reached as recently as the Pliocene, the "Andean Orogeny" started in Triassic-Jurassic time. An outline of the geology of the Andes and an overview of recent developments in the study of the region are provided by e.g. Bell (1984), Şengör (1990), and Oliver *et al.* (1992).

The well-defined, relatively simple, plate tectonic setting of the Andean margin forms a suitable subject for our investigations. Since the overriding margin constitutes a large fraction of the total boundary of the South American plate, the forces associated with the active margin can be investigated by studying the dynamics of the plate as a whole, which - as explained below - offers additional constraints. In this respect a favourable condition is also formed by the fact that subduction of the South American plate itself is restricted to a small

portion of its circumference. Consequently, the large forces associated with subducted slabs do not dominate the plate dynamics. Of essential importance, finally, is the availability of a recent compilation of stress indicators, providing the observational basis for the model analysis. This data base has been compiled by *Assumpção* (1992) in the context of the World Stress Map Project (*Zoback*, 1992).

The investigation of the South American plate may be regarded as the continuation of previous work on plates made up mostly of oceanic lithosphere: the Farallon/Nazca plate (*Wortel and Cloetingh*, 1981; 1983), the Indo-Australian plate (*Cloetingh and Wortel*, 1985; 1986), and the Pacific plate (*Wortel et al.*, 1991). Questions other than that regarding the forces on the overriding margin will be addressed. Of specific interest, for this plate where ridge push constitutes the only evident driving force, is also the question whether shear stress at the contact between lithosphere and underlying mantle is resistive or acts as an additional driving force.

The Aegean region. The Aegean region forms a segment of the southern margin of the Eurasian plate where the latter overrides the lithosphere of the eastern Mediterranean Sea, pertaining to the African plate. The Hellenic subduction zone, bounding the Aegean region towards the south, extends from the island of Levkas to the southwestern part of Anatolia over a mere 1500 km. Apart from this difference in scale, the Andean margin and the Aegean region differ in terms of tectonic regime: whereas compressional deformation prevails in the Andes, the Aegean region has since Miocene time been subject to extension. This extension has left a pronounced expression in the present-day topography: much of the Aegean region is presently lying below sea-level and strong topographic gradients, typical of normal fault deformation, are characteristic. The Aegean region differs from the Andean margin significantly in terms of plate tectonic setting. As indicated by its name, the Mediterranean Sea forms a land-locked basin (*Le Pichon*, 1982). This is due to the fact that the continental masses carried by the approaching African and Eurasian plate are in contact in the region of northwestern Africa - southern Spain and in the Middle East. Consequently, active convergence between the plates bounding the Aegean region has all but halted completely. An introduction to various aspects of the geological/geodynamical evolution of the Aegean region is offered by e.g. *Robertson and Dixon* (1984), *Stanley and Wezel* (1985) and *Jacobshagen* (1986). A recent review by *Jackson* (1994) deals with the active deformation of the region. *Şengör* (1993) discusses problems concerning the evolution of the Aegean area in the context of the whole Mediterranean region.

The study of the Aegean region presented in this thesis was prompted by the wealth of available observations and the large number of proposed - but mainly qualitative - explanations. Recent developments such as tomographic studies of the structure of the upper mantle below the Mediterranean region (*Spakman*, 1991; *Spakman et al.*, 1988; 1993) and geodetical monitoring of horizontal motions (e.g. *Kahle et al.*, 1993; *Noomen et al.*, 1993), provide important additional

observational constraints and have raised new hypotheses regarding the acting tectonic forces. One of the objectives is to examine whether the tectonic evolution of the overriding Aegean lithosphere contains an expression of detachment of the plate subducted beneath the region, inferred to have taken place on the basis of tomography (Wortel and Spakman, 1992).

The fact that the Andes and the Aegean region represent two contrasting classes of upper plate deformation makes it interesting to consider them together in one study, which adds to the reasons for choosing these specific areas. Having first studied the large-scale setting of the western margin of the South American plate, the Aegean region serves to exemplify the complex smaller scale situation encountered in the irregular plate boundary zone of the Mediterranean. The two areas of study may be taken to represent subsequent stages in the process of oceanic basin closure and have their "fossil" counterparts in other areas. For example, the orogenic belt of western North America has, prior to initiation of the present transform boundary, been similar in setting to the present-day Andes. Likewise, the Aegean region may be considered an active example of a situation that existed in the past in the western Mediterranean region and in the Carpathians (e.g. Wortel and Spakman, 1992).

The Use of a Numerical Model

Both on a global scale (lithospheric plates) and - for many parts of the world - on a more local scale (orogenic belts, sedimentary basins, etc.) we have a considerable amount of information at our disposal regarding the active and past behaviour of the lithosphere. Still, knowledge of how the plates move at present and have moved in the past and the ability to reconstruct the evolution of the intensely deformed regions situated near the plate boundaries constitutes merely a first (albeit crucial) step in answering the question as to what causes the deformation. Careful analysis of the available observations and comparison of different manifestations of the same process may already provide much insight. An example is the elegant analysis of Forsyth and Uyeda (1975) dealing with the scale of plate tectonics. By examining the correlation between geometrical aspects of the lithospheric plates and their inferred absolute velocities these authors were able to draw some first-order conclusions regarding the controlling forces. For example, the lack of correlation between the fraction of the circumference of a plate occupied by transform faults on the one hand, and absolute velocity of the plates on the other, suggests that the resistive force associated with transforms is of minor importance.

In order to step beyond the qualitative conclusions obtained by straightforward interpretation of observations and arrive at more precise quantitative knowledge about the forces controlling deformation we can make use of numerical models. Generally speaking, numerical modelling allows us to quantitatively assess the role of the various factors and parameters that affect - or are considered to affect - a given process. Moreover, numerical modelling

provides a means of testing a hypothesis: a proposed mechanism is simulated and the model results are critically compared with the available data in order to assess if the assumed mechanism is realistic. The use of a numerical model allows us to assess the relevance of the available observations and to point out aspects (or regions) concerning which additional information is required.

Outline of the Analysis

The problem of the dynamics of the two regions under scrutiny is addressed adopting a plate-centered approach: the study is based on a model representation of the lithosphere and aims at finding the forces acting on the lithosphere, including those associated with the interaction with the underlying mantle. This approach was introduced by *Forsyth and Uyeda* (1975) and *Chapple and Tullis* (1977) and is the same as that used in the before-mentioned studies of individual oceanic plates. An alternative approach would be to concentrate on the process of mantle convection and incorporate the motion and internal deformation of the plates as the surface expression of mantle flow. At present, however, such an approach does not provide the spatial resolution required to analyse the densely-spaced geological observations.

In principle, both information regarding the motion of a plate as a whole and observations concerning its internal deformation offer constraints on the controlling forces. In the study of the South American plate observed plate motion is used in the sense that it demonstrates that the plate is not accelerating. This implies that the plate must be in equilibrium and, therefore, the sum of torques it experiences should be zero. Using the criterium of vanishing net torque it is possible to propose a series of feasible force models and assess the first-order characteristics of the plate's driving and resistive forces. With respect to the dynamics of the Aegean region little will be learned from a consideration of the torque balance of the Eurasian plate since the Aegean constitutes only a very small portion of that plate. Therefore, in the case of the Aegean the analysis proceeds directly to the step of stress field modelling.

In particular the large scale features of the lithospheric stress pattern are controlled by the forces exerted at plate boundaries, the forces associated with subducted slabs, shear at the base of the lithosphere, and ridge push, i.e. the body force associated with the gradual change in density in oceanic lithosphere. Smaller scale lateral variation in lithospheric structure, such as associated with a mountain range, may locally constitute an important additional source of stress. While the stress field thus offers the clue to the tectonic forces, our observations concern the result of these stresses: deformation. On the basis of several assumptions - which depend on the type of observation - it is possible to reconstruct the state of stress associated with the observed deformation. Whereas earthquake focal mechanisms clearly provide us with a view of the present-day intra-plate stress field, careful geological analysis ("neotectonic analysis") is required in order to reconstruct subsequent stress fields that existed in the past.

In this thesis the observed, or rather, inferred, stress fields will be compared with stress fields calculated with a forward numerical model in which the lithosphere is represented as a thin elastic shell.

Forming a second step in the analysis of the South American plate, intra-plate stress fields are calculated in order to further discriminate between the force sets that were found to satisfy the criterium of zero net torque. The observations used comprise mainly earthquake focal mechanisms and the results of field studies of recent faulting. In addition there is information from borehole break-outs. Both model and observations pertain to a momentary view of the present-day stress field. In order to achieve a complete representation of the state of stress in the Andes, the effect of topography and its compensating crustal root, is integrated in the plate-scale model.

A thin elastic shell model has also been applied to the study of the Aegean region. The various hypotheses that have been advanced for the region are translated into appropriate sets of forces and the model is used to assess the associated intra-plate stress field. Since recently the active deformation of the Aegean region is being examined also by means of geodetical monitoring. Space geodetic techniques such as Satellite Laser Ranging and the Global Positioning System provide information regarding the region as a whole and in more detail for several parts of great complexity. In order to use this source of information, also the model-derived instantaneous displacement fields are evaluated. Since the model experiments involve force (or stress) boundary conditions, examination of the corresponding displacement field has the additional advantage that it allows us to visualize the relation between forces and kinematics.

Having established the nature and relative importance of the forces controlling present-day deformation we are faced with the question: how did these forces evolve through time? In the case of the South American plate this question is as yet difficult to address in view of the restricted distribution of observations of the paleo-stress field. For the Aegean region, however, neotectonic studies have provided a relatively detailed documentation of temporal variations in the stress field. The elastic rheology applied in modelling does not allow us to simulate finite deformation. Therefore, the question of evolution is addressed using a model of instantaneous deformation for a specific point in time in the past. In this, a paleogeographical reconstruction of the region is used.

Organisation of Thesis

This thesis has been divided in three main chapters. Chapter 2 and 3 deal with the dynamics of the South American plate. In Chapter 2 the concept of torque balance is explored. Subsequently, Chapter 3 is devoted to the examination of the intra-plate stress field. The dynamics of the late Cenozoic evolution of the Aegean region are addressed in Chapter 4. A final chapter briefly summarizes the main results regarding the theme in common by two regions: the tectonics of overriding continental margins.

The Dynamics of Motion of the South American Plate¹

Chapter 2

Introduction

The principal aim of compiling and studying in situ stress data on a global scale, such as is done in the context of the World Stress Map Project, is to increase our understanding of the dynamics of the lithosphere, in particular, of the forces driving and resisting plate motion.

Stress data enter the study of the dynamics of the lithosphere through a comparison of theoretical stress modelling results with stress observations. The two main contributions to the lithospheric stress field to be considered in this context are the stress fields associated with (1) the plate tectonic forces acting on the lithosphere, and (2) the lateral heterogeneities in structure of the crust and the mantle part of the lithosphere, and the associated topography.

The theoretical stress modelling of the first contribution is based on models for the dynamics of the lithosphere. Examples of such studies are the work by *Richardson et al.* (1979) and, more recently, that by *Wortel and Cloetingh* (1981, 1983, 1985), and *Cloetingh and Wortel* (1985, 1986). In the study by *Richardson et al.* (1979) the emphasis was on a first-order global analysis, without much detail on individual plates and forces involved. Studying individual (largely) oceanic plates, *Wortel and Cloetingh* (1981, 1983, 1985) (see also *Cloetingh and Wortel*, 1985; 1986) included more physical aspects of the forces. The ridge push force was

¹Chapter published as: Meijer, P.Th., and M.J.R. Wortel, The dynamics of motion of the South American plate, *J. Geophys. Res.*, 97, 11,915-11,931, 1992.

incorporated not as a boundary force but as the integrated pressure gradient in the oceanic lithosphere resulting from the cooling of the lithosphere (*Lister, 1975*). The slab pull force was incorporated as a force dependent on the age of the downgoing lithosphere (*Vlaar and Wortel, 1976*).

The second contribution can be modelled on the basis of information concerning the structure of the crust and upper mantle (*Artyushkov, 1973; Fleitout and Froidevaux, 1982; Froidevaux and Isacks, 1984*).

In this chapter we address the dynamics of the South American plate, and we do so for two reasons:

1. We want to establish a basis for a detailed analysis of the stress field in this plate. Both stress contributions mentioned above are envisaged to be relevant in the South American plate (Andes!). New data have become available for the South American plate *Assumpção and Suárez, 1988* (see also *Zoback et al., 1989*). To fully exploit the information contained in these data, a thorough investigation of the underlying dynamical aspects is required.

2. From a dynamical point of view the South American plate is expected to be quite interesting. For the South American plate the slab pull force, which is the dominating driving force in the dynamics of oceanic plates, is likely to play a very modest role. A priori we therefore expect forces of smaller magnitude to play a (relatively) more important role in the dynamics of the South American plate. Thus, the South American plate may provide a good opportunity to investigate these minor forces.

Our dynamical analysis focuses on the plate tectonic forces acting on the South American plate. We consider a first-order model for these forces and deal with a series of pertinent second-order features of the force distribution in terms of superpositions onto the first-order model.

Model Description

Plate Boundaries: Geometry and Nature

The boundaries adopted for the models of the South American plate and the mesh used in the calculations, are shown in Figures 2.1 and 2.2, respectively. Also shown in Figure 2.1, are the relevant tectonic structures of the surrounding regions. The recently derived global plate motion model NUVEL-1 (*DeMets et al., 1990*) is followed in describing the present-day relative motion between the major plates. Although the geometry of the eastern and western margin of the South American plate is well defined, the geometry and tectonic nature of the southern and, in particular, the northern plate margin are complex.

Divergent boundaries. The geometry of the Mid-Atlantic Ridge was adopted after *Larson et al. (1985)*. The geometry of the American-Antarctic ridge is based on a map presented by *Lawver and Dick (1983)*. Parts of the divergent plate boundaries consisting of alternations of relatively short transform fault and spreading ridge segments are represented by a boundary following the general trend.

Scotia Sea region. Between the western termination of the American-Antarctic ridge and the southernmost Chile trench, slow relative motion between the South American plate and the Antarctic plate is accommodated by displacement along both the North and South Scotia ridge (Forsyth, 1975).

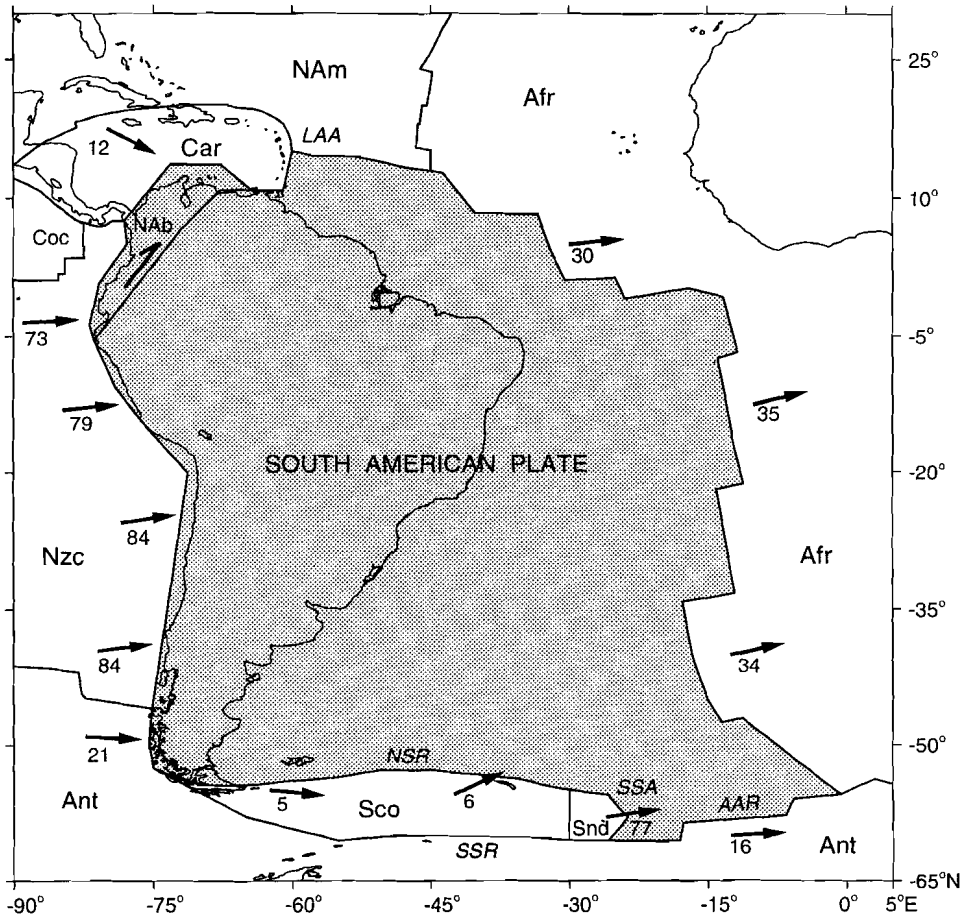


Fig. 2.1. Boundaries of the model for the South American plate and surrounding tectonic structures. Arrows denote current relative motion with respect to South America (DeMets *et al.*, 1990 and Pelayo and Wiens, 1989 for Sco-SAM and Snd-SAM); rates in millimeters per year; length of arrows not to scale. NAm-SAM motion is not indicated. Cartesian projection. Key: AAR, American-Antarctic Ridge; Afr, African plate; Ant, Antarctic plate; Car, Caribbean plate; CR, Carnegie Ridge; ChR, Chile Ridge; Coc, Cocos plate; JFR, Juan Fernandez Ridge; LAA, Lesser Antilles Arc; NAb, North Andes block; NAm, North American plate; NSR, North Scotia Ridge; NR, Nazca Ridge; Nzc, Nazca plate; Sco, Scotia plate; Snd, South Sandwich plate; SSA, South Sandwich Arc; SSR, South Sandwich Ridge.

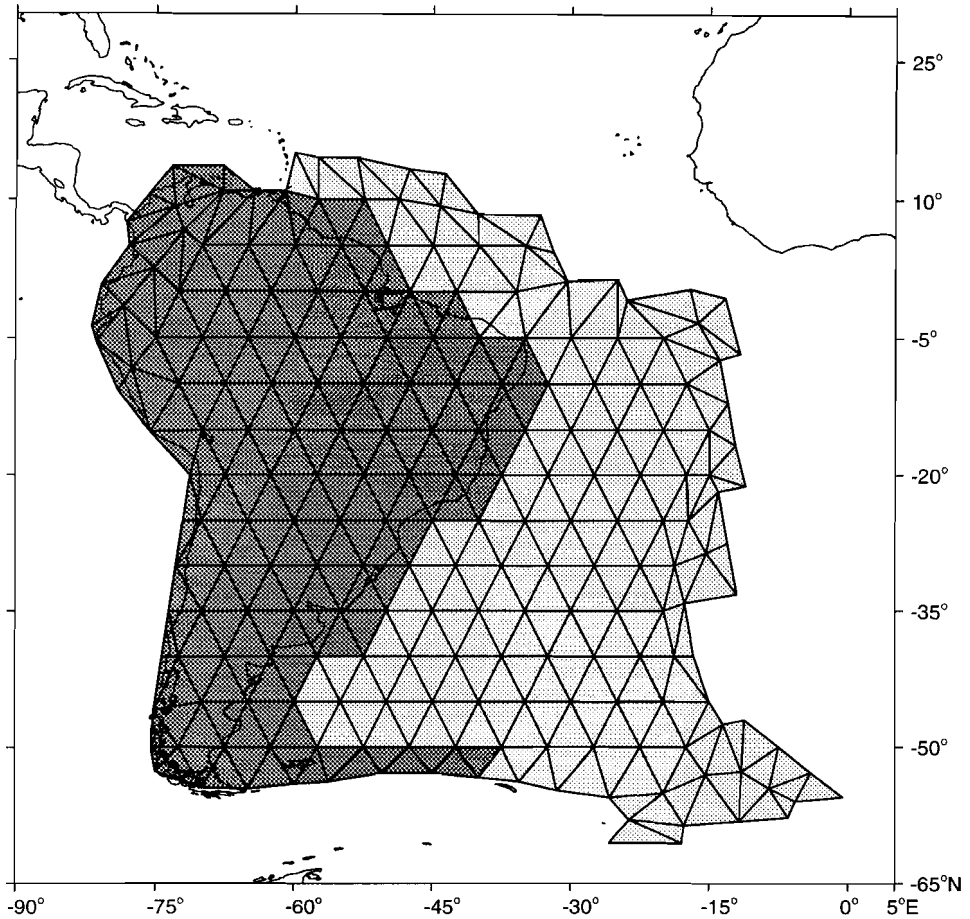


Fig. 2.2. Mesh of the South American plate. To enable incorporation of nonuniform basal shear stress the network of triangles is divided in a continental part (dark shading) and an oceanic part (light shading).

Along the South Sandwich arc, the South American plate subducts in westerly direction beneath the small South Sandwich plate (e.g., Forsyth, 1975). The South Sandwich plate advances eastward, separating from the Scotia plate by fast back arc spreading (Barker, 1970, 1972; Barker and Hill, 1980).

Although relative motion along the North and South Scotia ridges predominantly consists of left-lateral displacement, focal mechanisms of earthquakes along the North Scotia ridge additionally display a component of convergence, indicating the boundary is of transpressive nature (Pelayo and Wiens, 1989). Convergence along the North Scotia ridge is also evidenced by the presence

of a southward thickening wedge of deformed sediments on the northern side of the ridge, which has been interpreted as an accretionary prism created by active subduction of the South American plate beneath the Scotia plate (Ludwig *et al.*, 1978; Ludwig and Rabinowitz, 1982). The level of current activity is questioned, however, by Pelayo and Wiens (1989).

The strongly arched South Sandwich subduction zone is simply modelled as a two segment boundary centred at approximately 24°, 58°. Farther west, the adopted boundary runs just north of the North Scotia ridge, following its slight curvature (*International Hydrographic Organization/Intergovernmental Oceanographic Commission/Canadian Hydrographic Service (IHO/IOC/CHS)*, 1984, chart 5.16) and extending into Tierra del Fuego. Here, a system of left-lateral strike-slip faults may be interpreted as the on-land extension of the Scotia-South America boundary (Winslow, 1982).

Western boundary. Along the entire length of the western boundary of the South American plate subduction of oceanic lithosphere occurs. The adopted boundary approximately follows the axis of the trenches bordering the continent (*IHO/IOC/CHS*, 1981, charts 5.08, 5.11 and 5.16). Of possible relevance with respect to the forces exerted on the overriding South American plate are along-strike variations in the subduction process. Subduction of the Antarctic plate beneath the South American plate, south of the intersection between the Chile ridge and the Chile trench at latitude 496°, occurs at lower rate than subduction of the Nazca plate (Figure 2.1). In contrast with the major part of the western plate boundary, the southernmost Chile segment is characterized by a low level of seismic activity (Forsyth, 1975).

The subduction of the Nazca plate beneath South America occurs in several segments with varying angle of dip of the descending slab, as is evidenced by the spatial distribution of hypocenters (e.g., Barazangi and Isacks, 1976). The lateral variation in dip of the subducted slab can be correlated with variations in trench morphology (Kulm *et al.*, 1977), Quaternary volcanic activity (Sacks, 1977; Isacks, 1988), heat flow (Henry and Pollack, 1988), and age of the descending lithosphere (Wortel and Vlaar, 1978; Wortel, 1984). Localized anomalies in the process of convergence along the western plate margin are caused by aseismic ridges and seamount chains carried by the descending Nazca plate (Pennington, 1981; Pilger, 1981).

Northern boundary. The geometry and nature of the northern boundary of the South American plate are complicated. On the basis of a recent analysis D.F. Argus and R.G. Gordon (unpublished manuscript, 1989) propose that the boundary between the North American and South American plates is diffuse rather than discrete. The plate boundary zone may intersect the Lesser Antilles arc along its northern part (D.F. Argus and R.G. Gordon, unpublished manuscript, 1989). In modelling, however, a sharp boundary must be adopted, and in the present study only the Atlantic seafloor subducting along the southern half of the Lesser Antilles arc (south of latitude ≈15°N) is considered part of the

South American plate (Minster *et al.*, 1974). West of the Lesser Antilles arc, the Caribbean-South America plate boundary consists of a zone of complex deformation. In northeastern Venezuela, deformation is dominated by right-lateral strike-slip along approximately east-west striking faults, reflecting east-west relative motion of the Caribbean and South American plates (e.g., Molnar and Sykes, 1969). Additional deformation is indicative of a component of north-south compression (Jordan, 1975). Off northeastern Venezuela, obduction of the Caribbean plate onto the South American plate occurs in southeasterly direction (Speed, 1985).

West of about longitude 70°W, beneath northern Colombia and northwestern Venezuela, the spatial distribution of earthquake hypocentres points to the presence of an approximately east-southeast dipping lithospheric slab, continuous with the Caribbean plate (Isacks and Molnar, 1971; Dewey, 1972; Pennington, 1981). Present-day subduction of the Caribbean plate beneath northwestern South America is evidenced by deformation of the most recent sediments in the South Caribbean deformed belt (Lu and McMillen, 1982; Lehner *et al.*, 1983; Ladd *et al.*, 1984). In the plate model, the northern boundary parallels the El Pilar fault zone of northeastern Venezuela (e.g., Pérez and Aggarwal, 1981) and approximately follows the South Caribbean marginal fault westward (Kellogg and Bonini, 1982). The Panama-Colombia border region constitutes a zone of diffuse deformation (Pennington, 1981; Adamek *et al.*, 1988).

While subduction of the Caribbean plate beneath northwestern South America is not outlined by shallow focus earthquakes, an active zone of shallow seismicity follows the eastern front of the northern Andes, including the Boconó fault zone of western Venezuela (e.g., Molnar and Sykes, 1969; Dewey, 1972). The approximately NE-SW striking fault zone is interpreted as constituting the eastern boundary of a separate microplate, the Andean block (Pennington, 1981) or North Andes block (Kellogg and Bonini, 1985). The North Andes block is moving to the northeast with respect to the South American plate along right-lateral strike-slip faults forming the eastern boundary (Pennington, 1981; Kellogg and Bonini, 1985).

An Euler vector unambiguously describing Caribbean-South America relative motion proves difficult to assess (e.g., Stein *et al.*, 1988). Assuming that the direction of maximum compressive stress in the South American plate is parallel to the direction of convergence, seismological and geological data from northeastern Venezuela are interpreted as indicating WNW-ESE relative motion (Pérez and Aggarwal, 1981). In the northern Andes, Late Cenozoic deformation as well as earthquake focal mechanisms are indicative of NW-SE convergence (Kellogg and Bonini, 1982, 1985). Since the North Andes block moves to the northeast with respect to the South American plate, motion of the Caribbean plate with respect to South America will probably be directed easterly from SE (Kellogg and Bonini, 1985).

Force Modelling

In studying the dynamics of plate motion, the South American plate is modelled as part of a spherical shell of unit thickness. For the numerical integration of the forces acting on the plate we divide the South American plate into an assembly of 362 triangular elements (349, when excluding the North Andes block). Except near the margins, the network of triangles is regular with a 5° spacing between east-west grid lines, as well as between subsequent grid points along individual lines (Figure 2.2). In the Chapter 3 the mesh will be used in finite element calculations of the regional intraplate stress field, analogous to the studies of *Wortel and Cloetingh* (1981, 1983, 1985), *Cloetingh and Wortel* (1985, 1986), and *Wortel et al.* (1991).

Plate tectonic forces incorporated in all models considered in the present study are ridge push F_{rp} (driving force), transform fault force F_{tf} (resistive force), basal drag force F_{dr} (of which we consider the sense to be unknown, hence driving or resistive), plate contact resistance F_{pcr} (resistive force), and F_{Car} (or an alternative force, see below) representing the resistive force exerted along the northwestern plate margin. The basal drag force is a surface force. Although the nature of the ridge push force is that of an integrated pressure gradient, it enters the analysis as a surface force (see below). All other types of force are boundary forces. Suffixes used to identify forces are listed in Table 2.1.

The ridge push (F_{rp}) is calculated according to *Richter and McKenzie* (1978) and *England and Wortel* (1980). The ridge push force should be considered a horizontal pressure gradient, resulting from the cooling and contraction of oceanic lithosphere with age, integrated over the area of the oceanic part of the plate (*Lister*, 1975). Since lithosphere older than approximately 90 Ma is no longer subject to any significant continued cooling, contributions to the ridge push come from parts of the lithosphere younger than this age. The total driving force produced by a section, normal to the ridge axis, of oceanic lithosphere ranging in age from 0 Ma to 90 Ma, amounts to 2.0×10^{12} N per metre ridge length. The inverse dependence of ridge push per unit area on the rate of spreading with which a specific part of lithosphere was formed, is incorporated in the calculations via the magnitude of the local age gradient. The orientation of the ridge push force per unit area is assumed to be parallel to the local age gradient. Age gradients are determined using magnetic isochrons digitized from the map of *Larson et al.* (1985) and reconstruction poles describing Africa-South America and Antarctica-South America relative motion through time (*C.R. Scotese*, personal communication, 1986).

The transform fault force (F_{tf}) is everywhere taken parallel to the plate boundary. It is expressed in Newton per metre transform fault and must be considered the integral of the transform shear stress exerted on a vertical section of lithosphere of unit width.

The drag force (F_{dr}) is dealt with in terms of a constant shear stress σ_{dr} at the base of the plate, integrated over the area of the plate. This implies that any

Table 2.1 Force Types

Explanation	
<i>First-Order Model</i>	
rp	ridge push force
tf	transform fault force
dr	basal drag force
pcr	plate contact resistance
Car	resistance along the contact with the Caribbean plate
<i>Basal Drag</i>	
dro	drag force at base of oceanic lithosphere
drc	drag force at base of continental lithosphere
<i>Additional Forces</i>	
LA	force exerted in Lesser Antilles subduction zone
SS	force exerted in South Sandwich subduction zone
suc	trench suction force
Chi	plate contact resistance along South Chile overriding margin
Sco	resistance normal to eastern Scotia-South America boundary
NAM	force parallel to North America-South America boundary
<i>North Andes Block Excluded</i>	
dr-ex	basal drag force
pcr-ex	plate contact resistance
NW-tf	force parallel to northwestern margin
NW	force at angle to northwestern margin

variations of the shear stress along the base of the plate due to variations in the magnitude of absolute plate velocity are not taken into account. The orientation of the basal shear stress is assumed to be parallel to the direction of absolute plate motion. In order to allow for differentiation between the drag on the base of continental lithosphere and drag beneath oceanic lithosphere, the network of triangles is divided as indicated in Figure 2.2. Since the drag force is a surface integrated shear stress, the obviously rough approximation of the actual continent-ocean boundary (Figure 2.2) will only result in a small error.

The plate contact resistance, F_{pcr} , is the resistive force exerted on the overriding plate in a subduction zone, at the contact with the descending slab. This force is equal in magnitude, but opposite in sense, to the force exerted on the subducting plate. The plate contact resistance is assumed to be parallel to the direction of convergence of the two plates. In the models the plate contact resistance is incorporated as a horizontal boundary force, in reality, however, F_{pcr} is the result of a shear stress distributed over the subduction thrust interface, dipping toward the plate interior.

Additional forces incorporated in the various models will be introduced below. In the present study, no attempt is made to analyze in detail the forces acting on the South American plate in the Lesser Antilles and South Sandwich subduction zones.

For each type of force included in a given model, the resultant torque about the center of the Earth is computed. The magnitude of the resultant ridge push torque is 11.1×10^{25} N m. For all other types of force, only the orientation of the corresponding vectors can be determined. With the assumption that the present-day South American plate is in mechanical equilibrium, the sum of the torques on the plate is required to be zero. The assumption of mechanical equilibrium implies that the rate and direction of absolute motion of the South American plate are considered constant in time. The constancy of the rate and direction of spreading, since 20 Ma, between the South American plate and the African plate (*Cande et al.*, 1988) and between the South American plate and the Antarctic plate (*Barker and Lawver*, 1988), may indicate that the absolute motion of the South American plate is not subject to significant change and therefore validate the assumption of mechanical equilibrium.

The constraint of zero net torque enables us to solve for the magnitudes of three forces, under the premises that the magnitudes of the other forces are known. In the present study, the linear relation between each of three unknown forces and the basal shear stress is derived. In order for the analysis to be relevant, the torque vectors of the forces the magnitude of which is solved for, should constitute an independent system. The principle of the calculations is further explained in the first part of the appendix.

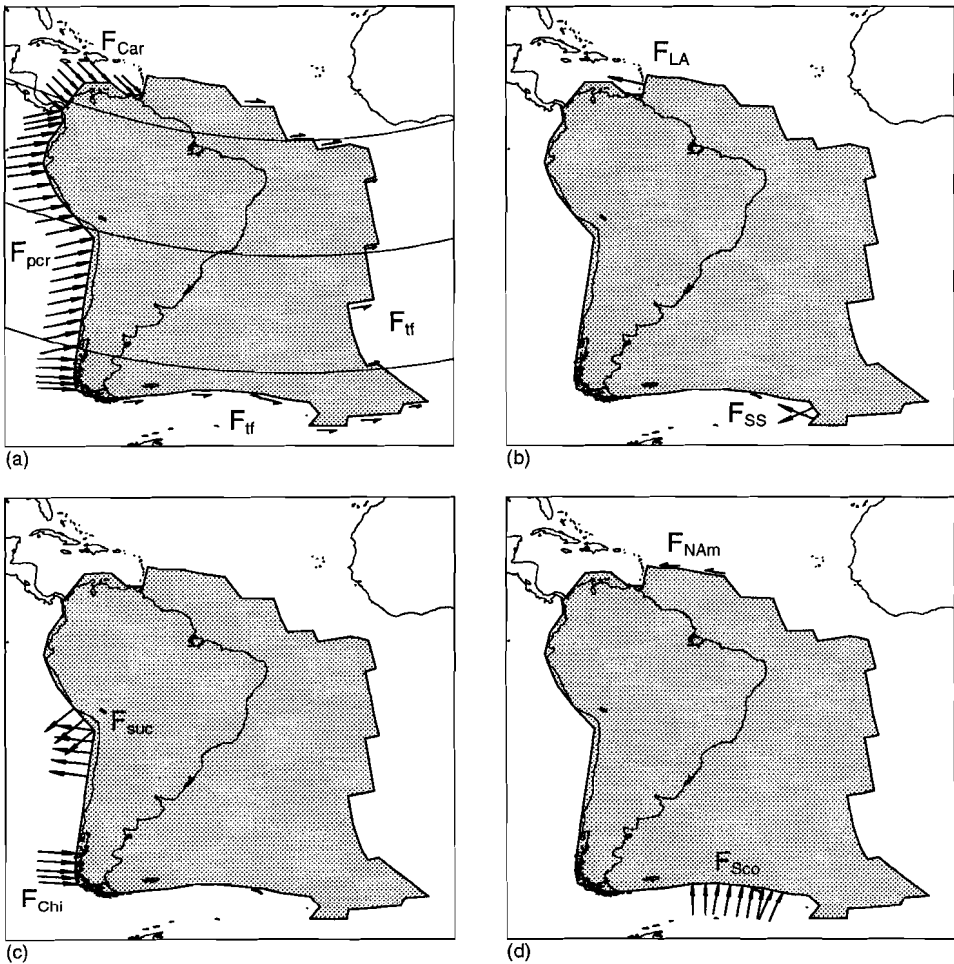
Analysis and Results

In analyzing the dynamics of motion of the South American plate a step-wise approach is adopted. A starting model is defined on the basis of a first-order approximation of plate boundary nature. This first-order model incorporates the forces which are expected to be of major importance: ridge push (F_{rp}), transform fault force (F_{tf}), basal drag force (F_{dr}), plate contact resistance (F_{pcr}), and the resistive force exerted along the contact with the Caribbean plate (F_{Car}). Subsequently, the effect of the various simplifications adopted in the first-order model on the obtained results is examined. We investigate the role of nonuniform basal shear stress, and we consider the effect of additional plate boundary forces by superpositions onto the first-order model. Finally, an alternative plate geometry is analyzed in order to examine the forces exerted on the northwestern plate margin.

In the following analysis and discussion we adopt the convention that positive values for the forces indicate forces driving plate motion. Negative values indicate resistance to plate motion. In discussing the results, to avoid confusion, we refer strictly to the numerical values of the various forces. This implies for instance, that an increase in value of a resistive force means that this force becomes less resistive.

First-Order Model

The distribution of boundary forces incorporated in the first-order model is illustrated in Figure 2.3a. The North Andes block is considered an integral part of the South American plate. Along the overriding western margin, a plate contact resistance of uniform magnitude is assumed to act. The orientation of this force is defined by Nazca-South America relative motion, north of the intersection between the Chile ridge and the Chile trench, and by Antarctica-South America relative motion, south of the intersection. The southern plate boundary, west of the South Sandwich trench, is modelled as a transform fault. No discrimination is made between the transform fault force acting along the southern plate boundary and the force exerted on the transform segments which off-set the Mid-Atlantic Ridge and the American-Antarctic ridge. A uniform shear stress is



assumed to act on the base of the plate. Ridge push is included in the equations as the single known torque. To first approximation, any forces exerted on the South American plate in the Lesser Antilles and South Sandwich subduction zones are neglected, as are forces at the contact with the North American plate.

The complex Caribbean-South America boundary is modelled by assigning a force of uniform magnitude and constant azimuth (F_{Car}) to the entire boundary segment between the southern terminus of the Lesser Antilles arc and the Panama isthmus. Calculations are performed for a range of azimuths of F_{Car} , increasing from 90° to 180° (clockwise from north).

In order to investigate the role of the orientation of the basal drag force, we consider four different Euler vectors describing the present-day absolute motion of the South American plate. Adopted are (1) model AM1-2, derived by *Minster and Jordan* (1978) by combination of global relative plate motion model RM2 with a hotspot reference frame; (2) the Euler vector used by *Gordon and Jurdy* (1986) to describe the absolute motion of the South American plate during the last 10 Ma; (3) the absolute motion model determined by *Chase* (1978a); (4) an Euler vector obtained by relating the relative plate motion model NUVEL-1 (*DeMets et al.*, 1990) to the hotspot reference frame of *Minster and Jordan* (1978) ("HS2-NUVEL1", *Gripp and Gordon*, 1990). Small-circle trajectories indicating the plate motion defined by each Euler vector are depicted in Figure 2.4. The rate of absolute motion does not enter the model calculations.

Numerical data concerning the orientation and magnitude of all torque vectors incorporated in the present study are listed in Table 2.2. Furthermore, torque magnitudes are graphically displayed in a histogram (Figure 2.5) and torque orientations are illustrated by means of equal-area projection (Figure 2.6). In Table 2.2 and Figure 2.5 the magnitudes of the drag torques are scaled by adopting a basal shear stress of 1 bar. The magnitudes of the boundary forces correspond to a scaling force of 1×10^{12} N m⁻¹ plate boundary. These scaling values correspond with the order of magnitude of the forces.

Fig. 2.3. (previous page) Forces of models including the North Andes block. Length of vectors not to scale. (a) Force distribution of first-order model. Small circles are with respect to the ridge push torque, driving the plate towards the west. Incorporated boundary forces are F_{tr} , transform fault force; F_{pcr} , plate contact resistance, and F_{Car} , resistance due to Caribbean-South America convergence, shown here with azimuth 135° (clockwise from north). No (net) forces are assumed to act on the plate in the Lesser Antilles and South Sandwich subduction zones or on the contact with the North American plate. Basal drag force not shown. (b)-(d) Additional boundary forces superimposed onto first-order model. Key: F_{LA} , net force exerted in Lesser Antilles trench; F_{SS} , net force exerted in South Sandwich trench; F_{suc} , suction force, exerted along the central part of the Peru-Chile trench; F_{Chiv} , plate contact resistance along southernmost Chile trench; F_{NAMv} , boundary-parallel force along NAM-SAM boundary; F_{Scov} , normal force acting on eastern Sco-SAM boundary.

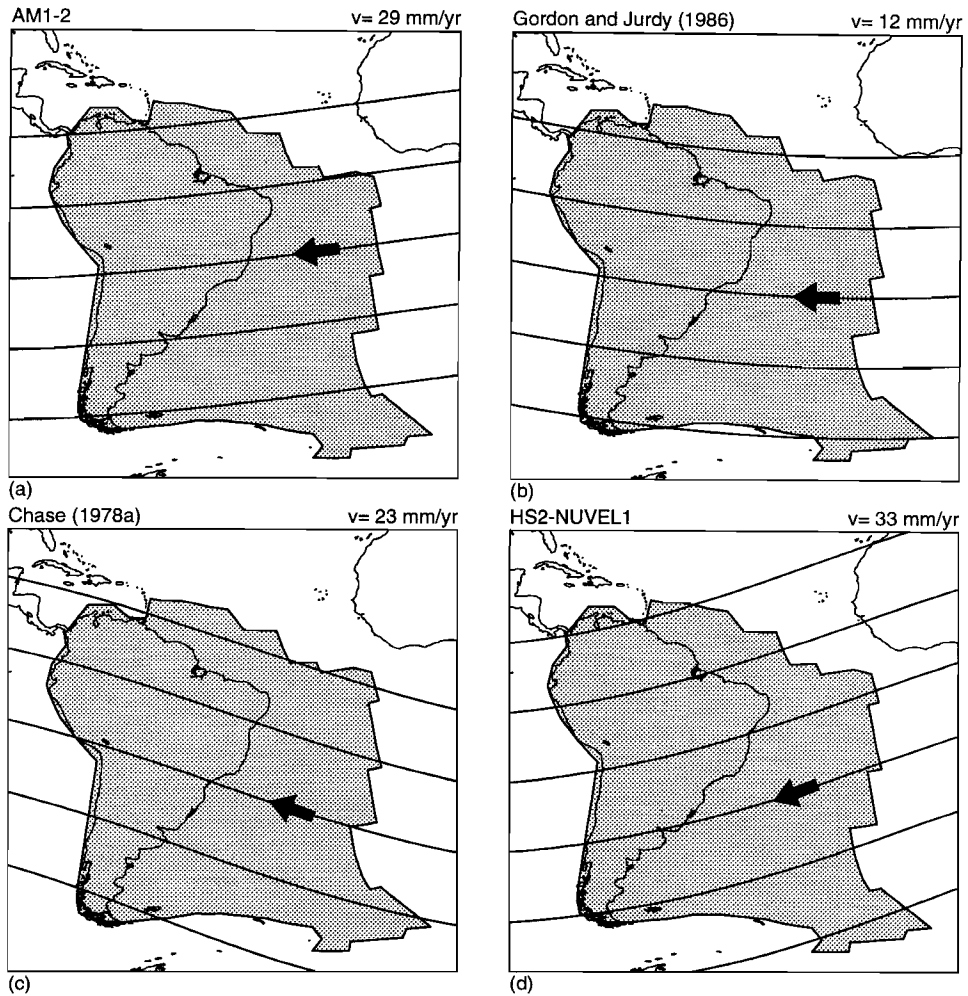


Fig. 2.4. Small circle trajectories indicating present-day absolute motion of the South American plate according to various studies. Absolute motion is assumed to define the orientation of basal shear stress. Average velocity of absolute motion is indicated at top right. (a) Model AM1-2, *Minster and Jordan* (1978). (b) *Gordon and Jurdy* (1986). (c) Model PO73, *Chase* (1978a). (d) Model HS2-NUVEL1, *Gripp and Gordon* (1990).

Table 2.2 (next page) T_1 , T_2 , and T_3 are torque components in a frame with x_1 : 0°E , 0°N ; x_2 : 90°E , 0°N ; x_3 : 90°N . Ridge push quantified as described in text. Drag torques correspond to a basal shear of 1 bar; other torques to a force of 1×10^{12} N m^{-1} . Abbreviations as in Table 2.1. Numbers of Car and NW give azimuth. Absolute motion used for drag torques indicated. Key: AM1-2, *Minster and Jordan* (1978); GJ, *Gordon and Jurdy* (1986); Chase, *Chase* (1978a); HS2, *Gripp and Gordon* (1990). “-ex” indicates North Andes block is excluded.

Table 2.2. Torque Data

Force	T_1 10^{25} Nm	T_2 10^{25} Nm	T_3 10^{25} Nm	Magnitude 10^{25} Nm	Longitude °E	Latitude °N
rp	-3.799	2.068	-10.214	11.092	151.4	-67.0
tf	-2.101	1.676	-3.716	4.586	141.4	-54.1
pcr	0.273	1.717	-4.002	4.363	81.0	-66.5
Car, 90	0.086	-0.288	-1.433	1.464	-73.4	-78.2
Car, 105	-0.271	-0.404	-1.380	1.463	-123.9	-70.6
Car, 120	-0.611	-0.493	-1.233	1.462	-141.1	-57.5
Car, 135	-0.909	-0.548	-1.003	1.461	-148.9	-43.4
Car, 150	-1.145	-0.567	-0.705	1.459	-153.7	-28.9
Car, 165	-1.304	-0.547	-0.357	1.459	-157.2	-14.2
Car, 180	-1.374	-0.489	0.016	1.459	-160.4	0.6
dr, AM1-2	-0.414	0.802	-2.444	2.606	117.3	-69.7
dr, GJ	-0.848	0.415	-2.448	2.624	153.9	-68.9
dr, Chase	-1.252	-0.138	-2.305	2.627	-173.7	-61.3
dr, HS2	-0.064	1.129	-2.346	2.604	93.3	-64.3
dro, AM1-2	-0.344	0.415	-1.144	1.265	129.7	-64.8
drc, AM1-2	-0.070	0.387	-1.300	1.358	100.3	-73.2
dro, GJ	-0.492	0.194	-1.154	1.270	158.5	-65.4
drc, GJ	-0.356	0.221	-1.294	1.360	148.1	-72.1
dro, Chase	-0.660	-0.177	-1.080	1.278	-165.0	-57.7
drc, Chase	-0.592	0.039	-1.225	1.361	176.2	-64.2
dro, HS2	-0.174	0.641	-1.081	1.269	105.2	-58.4
drc, HS2	0.110	0.488	-1.265	1.360	77.3	-68.4
LA	-0.028	-0.091	-0.287	0.302	-106.9	-71.6
SS	-0.274	0.132	-0.189	0.358	154.2	-31.9
suc	0.064	0.437	-0.970	1.066	81.7	-65.5
Chi	0.114	-0.339	0.307	0.471	-71.4	40.6
Sco	-0.440	-0.673	0.082	0.808	-123.2	5.8
NAm	0.042	-0.313	-1.089	1.133	-82.3	-73.8
pcr-ex	0.106	1.706	-3.020	3.470	86.4	-60.5
NW-tf	1.168	0.171	-1.419	1.845	8.3	-50.2
NW, 90	0.069	-0.152	-1.957	1.964	-65.5	-85.1
NW, 105	-0.420	-0.301	-1.890	1.959	-144.4	-74.7
NW, 120	-0.881	-0.430	-1.692	1.956	-154.0	-59.9
NW, 135	-1.281	-0.530	-1.378	1.954	-157.5	-44.8
NW, 150	-1.592	-0.593	-0.968	1.955	-159.6	-29.7
NW, 165	-1.794	-0.615	-0.491	1.959	-161.1	-14.5
NW, 180	-1.871	-0.595	0.017	1.963	-162.4	0.5
dr-ex, AM1-2	-0.421	0.808	-2.371	2.540	117.5	-69.0
dr-ex, GJ	-0.838	0.426	-2.375	2.555	153.0	-68.4
dr-ex, Chase	-1.235	-0.125	-2.234	2.556	-174.2	-61.0
dr-ex, HS2	-0.080	1.133	-2.273	2.541	94.1	-63.5

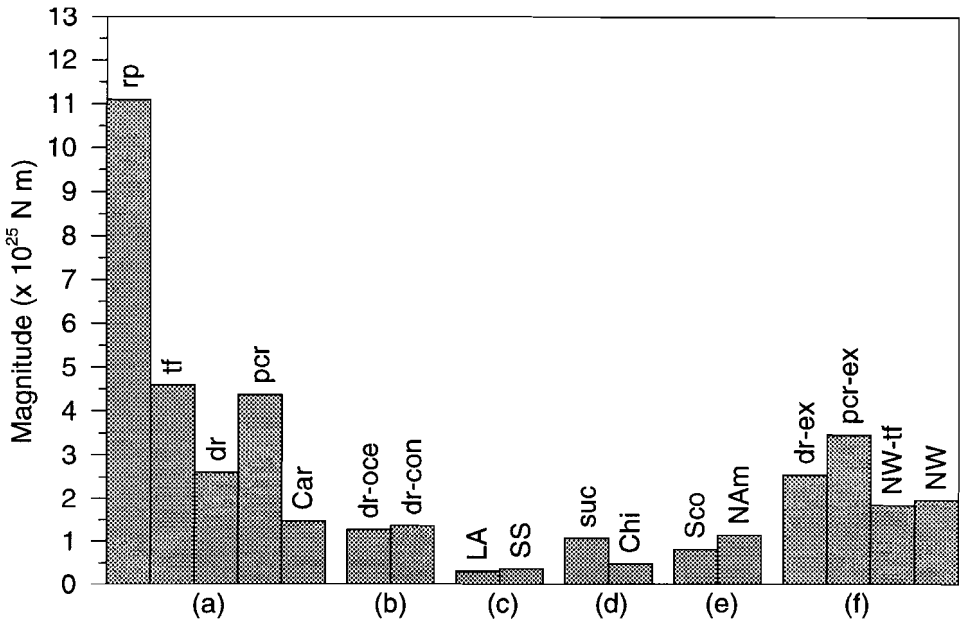


Fig. 2.5. Histogram of torque magnitudes. Six sets are given corresponding to (a) forces incorporated in the first-order model, (b) separated oceanic and continental drag, (c)-(e) three sets of additional forces, (f) newly defined or modified forces incorporated in the model excluding the North Andes block. The ridge push torque has been quantified as a basal shear stress of 1 bar. The displayed magnitudes of the basal drag torques correspond to a force of $1 \times 10^{12} \text{ N m}^{-1}$ plate boundary. The basal drag torques are approximately of equal magnitude for each of the adopted models of absolute motion; the magnitude of F_{Car} and F_{NW} is approximately independent of the chosen azimuth (Table 2.2). Forces are identified by abbreviations explained in Table 2.1.

The magnitude of transform fault force, plate contact resistance and F_{Car} as a function of basal shear stress, computed for each of the absolute motion models and varying azimuth of F_{Car} , are shown in Figure 2.7. The derived values are of course equal for all adopted models of absolute motion, when basal shear stress is zero. Assuming the force exerted on the South American plate by the convergence with the Caribbean plate is parallel to the direction of relative motion, the azimuth of F_{Car} will be in the range 90° - 135° . The corresponding range of solutions is shaded in Figure 2.7.

With absolute motion models AM1-2 and HS2-NUVEL1, the values derived for transform fault force magnitude and F_{Car} display the correct sign; that is, the forces are indeed resistive, over the entire range of basal shear stress studied for azimuths of F_{Car} between 90° and 135° . The range of basal shear stress for which realistic solutions are obtained is constrained, however, by the

corresponding plate contact resistance. For each azimuth of F_{Car} , a minimum value of basal drag exists (i.e., maximum amount of resistive drag), below which the derived plate contact resistance is implied to be driving plate motion. This minimum value of basal shear stress decreases with increasing azimuth of F_{Car} to about -2.5 bars when the azimuth of F_{Car} is 135° .

If absolute motion is defined according to *Gordon and Jurdy (1986)* or *Chase (1978a)*, the derived F_{Car} constrains the range of basal shear stress yielding realistic solutions. The minimum value of basal shear stress for which F_{Car} is indeed a

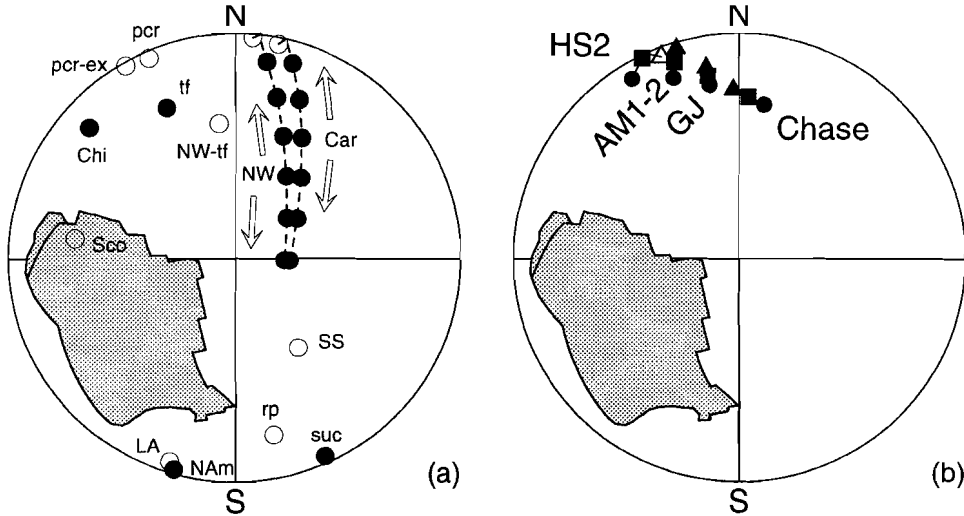
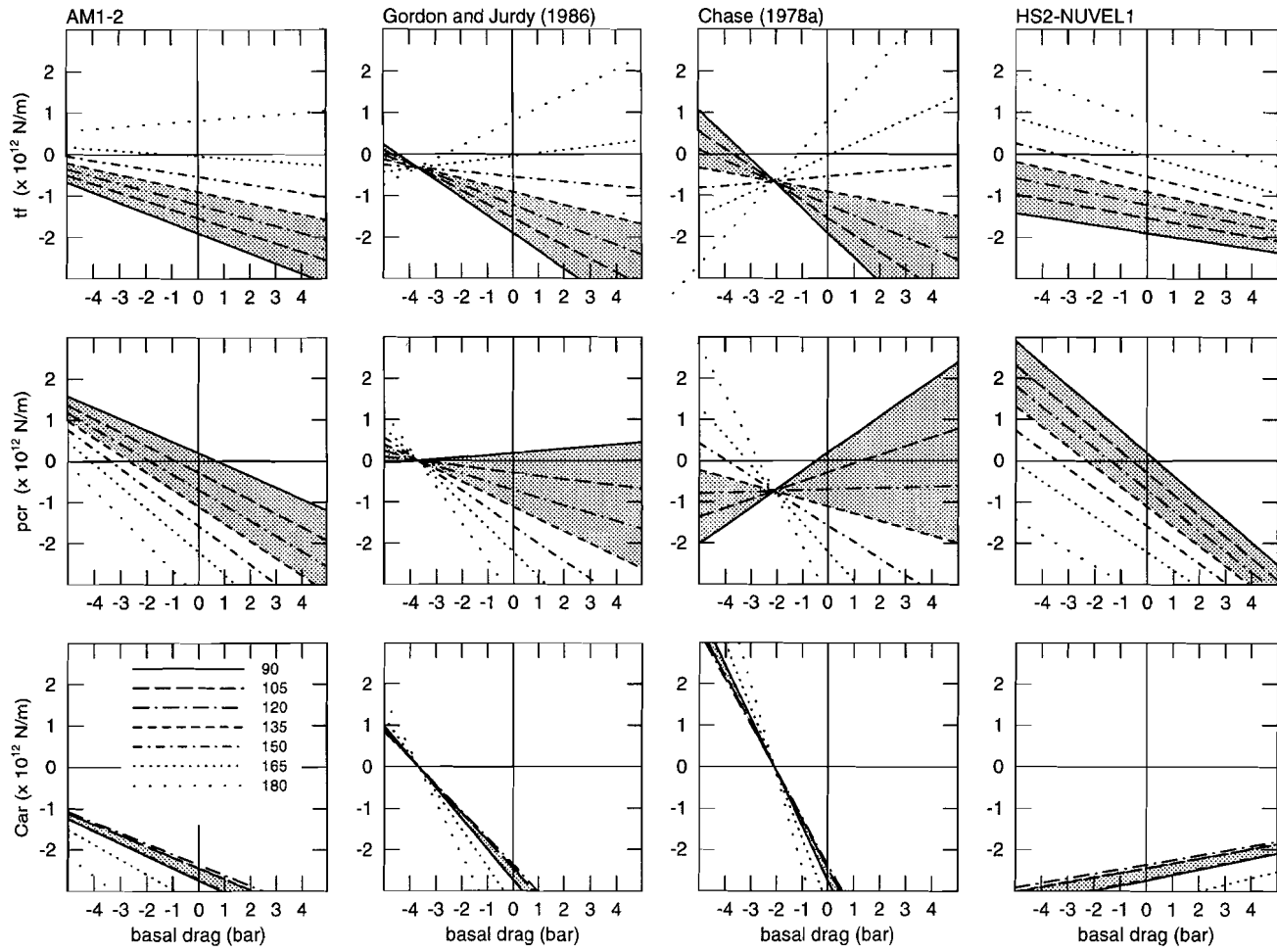


Fig. 2.6. Equal-area projection of the Earth illustrating the orientation of the torques of the various plate tectonic forces. Symbols indicate points of emergence of the positive end of torque vectors as listed in Table 2.2, with exception of the torques of F_{dr} , F_{tr} , F_{pcr} , F_{Car} , and F_{NW} which are assumed to be resistive forces and for which negative ends are plotted. Solid symbols are located on upper hemisphere of projection, open symbols on lower hemisphere. Poles of torques corresponding to driving forces plot in southern hemisphere of the Earth, poles of torques of resistive forces in northern hemisphere. (a) All torques except basal drag. Poles of the torques of F_{Car} and F_{NW} approximately describe great circles as a function of the azimuth of the force. Poles are shown with a 15° spacing of the azimuth; minimum and maximum azimuth are indicated. Abbreviations are listed in Table 2.1. (b) Basal drag torques. For each of the four absolute motion models used, three poles are given, corresponding to the total drag force (circle), drag below the oceanic part of the lithosphere (square), and drag below the continental part (triangle). Poles corresponding to a specific absolute motion model are located along a great circle segment. Labels give corresponding absolute motion model. Key: AM1-2, model AM1-2 of *Minster and Jordan (1978)*; GJ, *Gordon and Jurdy (1986)*; Chase, *Chase (1978a)*; HS2, model HS2-NUVEL1 of *DeMets et al. (1990)*. The orientation of the basal drag torques is only slightly affected when the North Andes block is excluded (Table 2.2).



resistive force, is approximately -3.5 bars in case of the *Gordon and Jurdy* (1986) Euler vector and approximately -2 bars in case of the *Chase* (1978a) model. Especially in case of the *Chase* (1978a), absolute motion model low azimuths of F_{Car} are found to imply positive values of F_{pcr} .

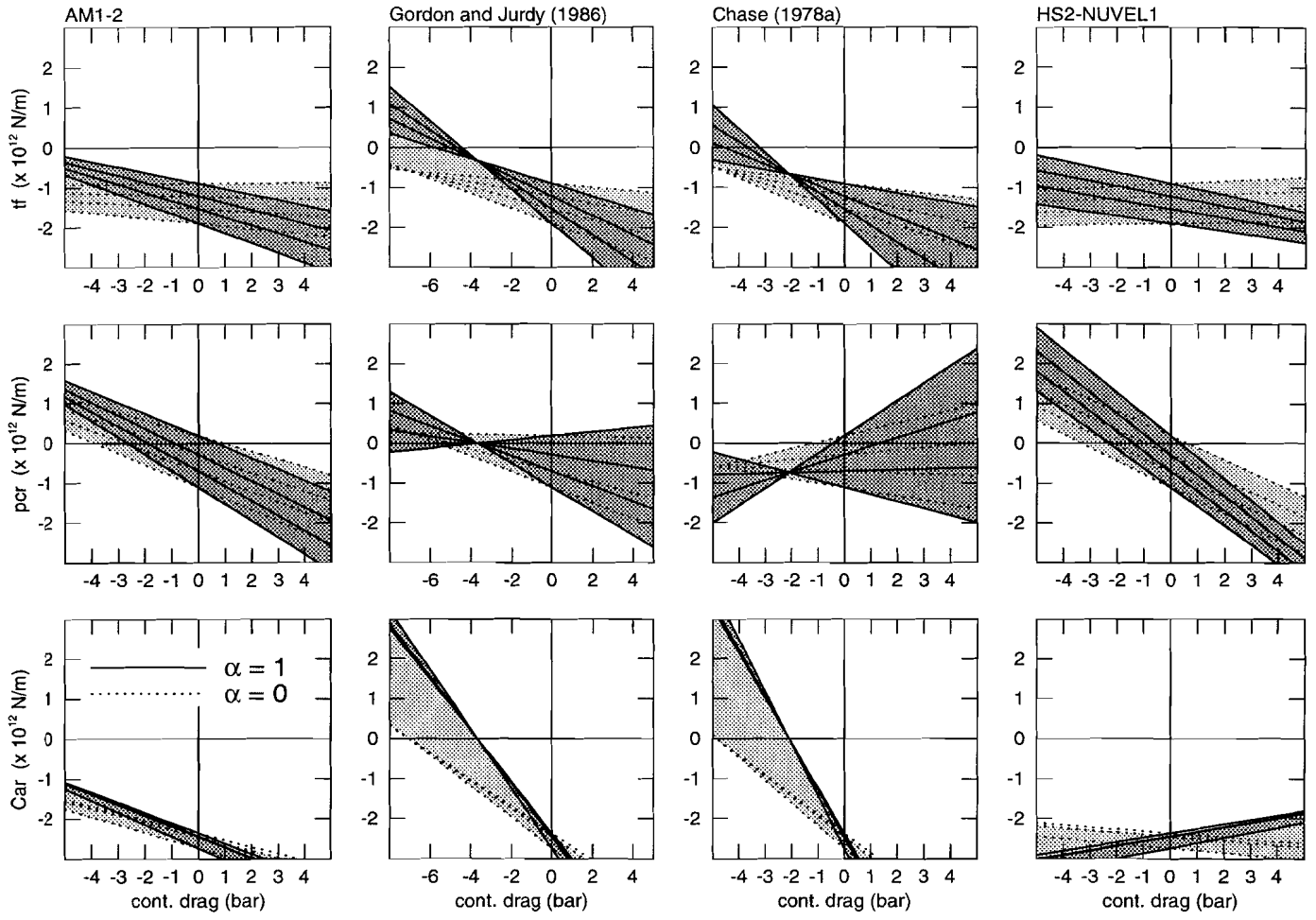
The effect on the derived solutions of the adopted absolute motion model is demonstrated in particular by the results obtained with the *Gordon and Jurdy* (1986) Euler vector. In this case, regardless of the azimuth of F_{Car} , a basal shear stress of approximately -3.5 bars corresponds to zero F_{pcr} and F_{Car} and a small negative F_{tf} ; that is, basal drag almost entirely balances the ridge push.

In case of absolute motion models AM1-2 and HS2-NUVEL1, a resistive force exerted on the northwestern plate margin (F_{Car}) is found to be required in order to balance the torques realistically. When absolute motion is defined according to *Chase* (1978a), realistic solutions are also obtained if F_{Car} is equal to zero. The magnitudes derived for F_{tf} and F_{pcr} are clearly dependent on the azimuth of F_{Car} for all absolute motion models.

When it is assumed that basal shear stress acts to resist plate motion, it can be derived from Figure 2.7 that F_{tf} and F_{pcr} are greater than approximately $-1.8 \times 10^{12} \text{ N m}^{-1}$ and $-1 \times 10^{12} \text{ N m}^{-1}$ respectively, regardless of the adopted absolute motion model, for F_{Car} in the range 90° - 135° . The lowest values of F_{tf} correspond to an azimuth of F_{Car} of 90° , the minimum values of F_{pcr} are obtained at azimuth 135° . For the range of basal shear stress yielding realistic solutions, F_{Car} is greater than about $-2.5 \times 10^{12} \text{ N m}^{-1}$.

Errors in the derived magnitudes of F_{tf} , F_{pcr} , and F_{Car} due to errors in the orientation of the incorporated torques are difficult to assess because they stem from assumptions concerning plate boundary geometry and the orientation and distribution of the various forces. However, the dependence of the results on the magnitude of the ridge push torque can be determined. A 10% increase in the magnitude of the ridge push torque results in a shift of F_{tf} by $-0.19 \times 10^{12} \text{ N m}^{-1}$ if the azimuth of F_{Car} is 90° and by $-0.09 \times 10^{12} \text{ N m}^{-1}$ if the azimuth of F_{Car} is 135° . Similarly, the corresponding shift of F_{pcr} ranges from $0.02 \times 10^{12} \text{ N m}^{-1}$ to $-0.11 \times 10^{12} \text{ N m}^{-1}$ and the shift of F_{Car} from $-0.27 \times 10^{12} \text{ N m}^{-1}$ to $-0.24 \times 10^{12} \text{ N m}^{-1}$. These shifts are independent of the magnitude of basal shear stress and the adopted absolute motion model and are linearly proportional to shift in the magnitude of the ridge push torque.

Fig. 2.7. (previous page) Magnitude of transform fault force (tf), plate contact resistance (pcr), and resistance due to Caribbean-South America convergence (Car), as a function of uniform basal shear stress, determined with the first-order model. Forces are identified by suffixes only; Table 2.1 gives key. Basal shear is expressed in bar (1 bar = 10^5 Pa). Panels in the same column correspond to a specific absolute motion model indicated near the top. Panels in one row correspond to a specific type of force (top, F_{tf} ; middle, F_{pcr} ; bottom, F_{Car}). Solutions are obtained for a range of azimuths of F_{Car} ; legend is shown in panel at lower left. Shaded area in each panel corresponds to an azimuth of F_{Car} in the range 90° - 135° .



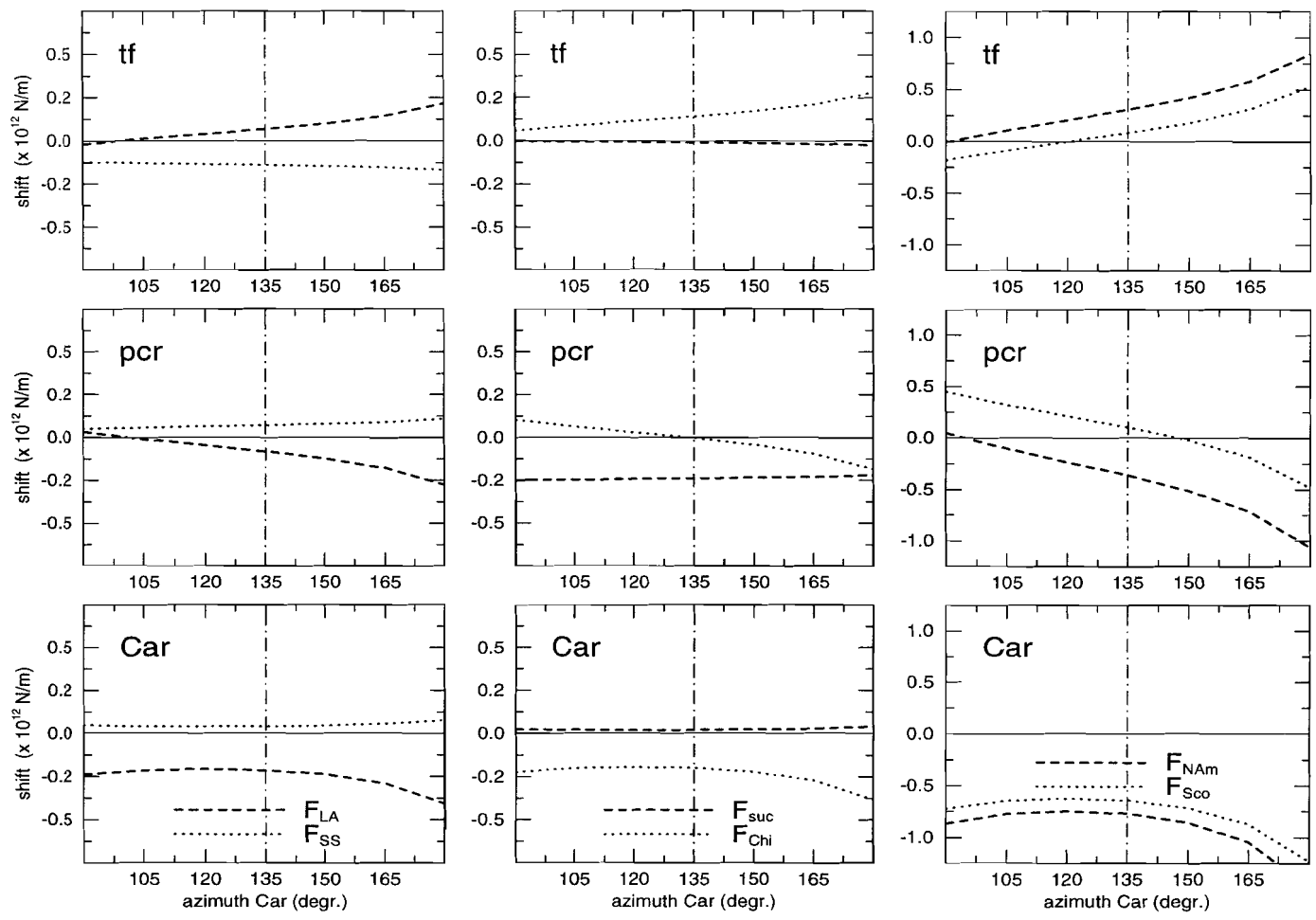
Distribution of Basal Shear Stress

In several previous studies of the dynamics of plate motion, it was concluded that resistive drag at the base of continental lithosphere is stronger than drag beneath oceanic lithosphere (Forsyth and Uyeda, 1975; Chapple and Tullis, 1977). Here, it is assumed that the shear stress at the base of oceanic lithosphere can be written as $\alpha\sigma_{dr}$, where α is a factor between 0 and 1, and σ_{dr} is the shear stress beneath continental lithosphere. In Figure 2.8, the line depicting the relation between a computed force and σ_{dr} , rotates about the intersection with the ordinate from the line corresponding to zero oceanic drag ($\alpha = 0$) to the line representing equal shear stress below the entire lithosphere ($\alpha = 1$).

In general, a decrease in the value of α at a fixed value of continental drag, results in a shift of the solutions towards magnitudes corresponding to lower absolute values of continental drag. Although the areas of the continental part and the oceanic part of the plate (Figure 2.2) are almost equal, the slope of the lines for $\alpha = 0$, is not simply equal to half the slope of the corresponding lines for $\alpha = 1$, because the torques of continental drag and oceanic drag are not parallel (Figure 2.6b).

An estimate of the minimum value of continental drag can be made by assuming that drag is entirely concentrated below the continent ($\alpha = 0$). The azimuth of F_{Car} is considered to fall in the range 90° - 135° . With absolute motion models AM1-2 and HS2-NUVEL1 the derived plate contact resistance is negative for continental drag greater than about -4 and -3.5 bars, respectively. When defining absolute motion according to Chase (1978a), the basal drag is constrained by the corresponding magnitude of F_{Car} and the minimum amounts to about -5 bars. The lowest basal shear stress is obtained in case of the Gordon and Jurdy (1986) absolute motion pole, a minimum value of continental drag of -5.5 bars is constrained by the corresponding F_{per} .

Fig. 2.8. (previous page) Results derived with the first-order model taking into account a different magnitude of basal shear stress between the continental part and the oceanic part of the plate. Arrangement of results as in Figure 2.7. Derived magnitudes are shown as a function of continental basal drag. Oceanic basal drag is taken as a factor α times continental drag, with $0 < \alpha < 1$. The lines depicting the relation between a computed force and continental drag rotate about the intersection with the ordinate as a function of α . If $\alpha = 1$ (drawn lines), the solution is equal to the solution for uniform basal drag (Figure 2.7), $\alpha = 0$ (dotted lines) implies zero oceanic drag. Solutions are displayed for azimuths of F_{Car} in the range 90° - 135° . Azimuths corresponding to the drawn lines can be found by reference to Figure 2.7; azimuths of dotted lines can be found by finding intersection with drawn lines along the ordinate. Dark shaded areas correspond to shaded areas in Figure 2.7; light shading indicates the extension of the range of solutions due to nonuniform basal shear stress.



Additional Plate Boundary Forces

Along certain segments of the plate circumference, the first-order model is not an adequate description of the actual situation. Although the actual processes are probably complicated, their precise nature is not known, and we attempt to determine their role in the dynamics of plate motion using simple representations. By modelling each deviation from the first-order model as an additional force, use can be made of the linearity of the torque balance equations. The effect of a superposition of an additional force on the solutions, is a shift of the lines presented in Figures 2.7 and 2.8, parallel to the ordinate. The slope of the lines is not affected. The magnitude of the shift is linearly proportional to the magnitude of the added force. The effects of individual deviations from the starting model are mutually independent. Moreover, the effect of an additional force is independent of the drag torque and hence is not sensitive to uncertainties concerning the orientation and distribution of basal shear stress. The calculations are further explained in the appendix, part 2. Three sets of additional forces, schematically depicted in Figures 2.3b-d, are studied. The associated shifts are displayed in Figure 2.9.

The driving and resistive forces exerted on the South American plate in the Lesser Antilles and South Sandwich subduction zones are in each zone represented by a net force acting perpendicular to the trench segments (F_{LA} and F_{SS} , Figure 2.3b).

An additional force possibly exerted on the western margin of the South American plate is the trench suction force (*Elsasser, 1971; Chase, 1978b*). Since a trenchward pull on the overriding plate is unlikely to exist along boundary segments with strong coupling between the converging plates, we assume trench suction acts only along the South Peru-North Chile segment, where the subducting slab dips relatively steeply (*Barazangi and Isacks, 1976*). The trench suction is assumed to act perpendicular to the margin and is superimposed onto the plate contact resistance (F_{suc} , Figure 2.3c). The probably anomalous nature of the southernmost Chile segment of the overriding margin (south of latitude $46^\circ S$)

Fig. 2.9. (previous page) Effect on the magnitude of transform fault force (tf), plate contact resistance (pcr) and resistance due to Caribbean-South America convergence (Car) of additional forces, superimposed onto the first-order model. A positive shift implies an increase in the value of the corresponding force. Shifts are shown as a function of the azimuth of F_{Car} . Panels in the same row give shifts of a specific force (top, F_{tf} ; middle, F_{pcr} ; bottom, F_{Car}). Panels in one column each show the shifts resulting from two additional forces. Added are a net driving force in the Lesser Antilles trench (F_{LA}) and in the South Sandwich trench (F_{SS}), a driving suction force along the central part of the Peru-Chile trench (F_{suc}), an additional plate contact resistance along the southernmost Chile segment (F_{Chi}), a boundary-parallel driving force along the contact with the North American plate (F_{NAm}) and a boundary-normal resistive force acting along the eastern Sco-SAM boundary (F_{Sco}). Absolute magnitude of added forces is $1 \times 10^{12} \text{ N m}^{-1}$. Shifts are linearly proportional to the magnitude of the added forces.

is accounted for, by calculation of an additional torque for the plate contact resistance acting along this stretch (F_{Chir} , Figure 2.3c).

The Euler vector for Scotia-South America relative motion derived by *Pelayo and Wiens (1989)* shows a component of convergence to exist along the eastern half of the Scotia-South America boundary. This transpressive nature is accounted for by adding a boundary-normal force of uniform magnitude to the boundary-parallel transform fault force (F_{Sco} , Figure 2.3d). The possible relevance of normal forces across transform boundaries in general, was recently emphasized by *Barker and Lawver (1988)*. A boundary-parallel shear force, either driving or resisting plate motion, is assumed to act at the North America-South America boundary (F_{NAm} , Figure 2.3d).

The shifts of the lines giving the relation with basal shear stress of transform fault force, plate contact resistance, and F_{Car} are computed for the following magnitudes of the additional forces, $+1 \times 10^{12} \text{ N m}^{-1}$ (outward directed, driving plate motion): F_{LA} , F_{SS} , F_{suc} , F_{NAm} , and $-1 \times 10^{12} \text{ N m}^{-1}$ (inward directed, resisting plate motion): F_{Chir} , F_{Sco} (Figure 2.9). In particular for the additional forces F_{LA} , F_{SS} , and F_{NAm} , the actual character (driving or resistive) is uncertain. The effects of a resistive F_{LA} , F_{SS} , and F_{NAm} can be derived from Figure 2.9 by reversing the sign of the indicated shifts.

The effect on each of the computed forces of a driving force exerted in the Lesser Antilles trench is opposite to that of a driving force exerted in the South Sandwich trench, over almost the entire range of azimuth of F_{Car} .

Adding a trench suction force to the first-order model results in a decrease in the value of F_{pcr} regardless of the azimuth of F_{Car} . The transform fault force and F_{Car} are hardly affected. Increasing the plate contact resistance along the southernmost Chile segment of the western margin renders the overall F_{pcr} less resistive, only if the azimuth of F_{Car} is between 90° and approximately 135° .

The shifts of F_{tfr} , F_{pcr} , and F_{Car} due to the superposition of F_{NAm} and F_{Sco} are greater than the shifts due to the other additional forces. This can only partially be explained by the greater length of plate boundary along which F_{NAm} and F_{Sco} act. In general, Figure 2.9 illustrates that the addition of a driving force to the first-order model does not simply result in more resistive F_{tfr} , F_{pcr} , and F_{Car} or vice versa.

Alternative Plate Geometry

To investigate further the relevance of forces exerted along the northwestern margin of the South American plate, an alternative plate geometry, excluding the North Andes block, is examined with two associated distributions of boundary forces. In a first model (Figure 2.10a) the forces acting at the contact with the North Andes block and the east-west striking boundary segment, west of the Lesser Antilles trench, are assumed to be parallel to the plate margin. This would be appropriate if the segments are essentially transcurrent boundaries. The forces exerted along the two segments are included in a single torque. The remainder

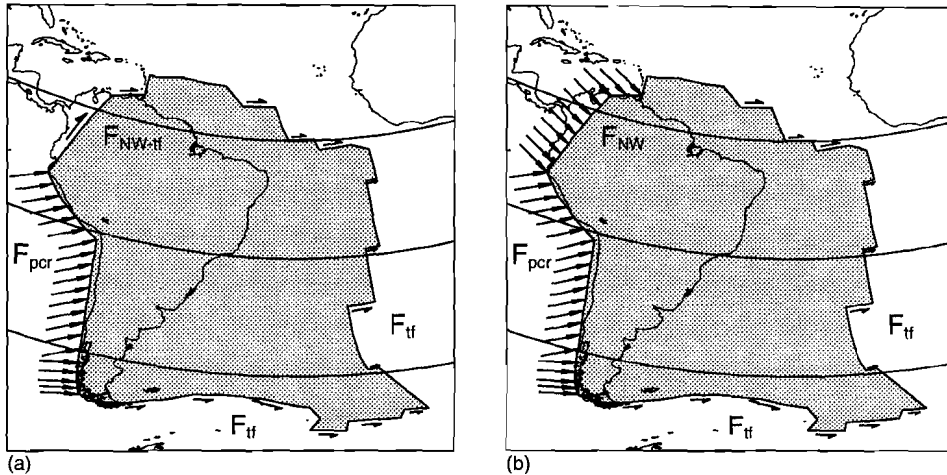


Fig. 2.10. Forces adopted in models excluding the North Andes block. Two models are defined, differing in the force exerted along the northwestern margin. Apart from the northwestern margin, incorporated forces are equivalent to first-order model illustrated in Figure 2.3a. Length of vectors is not to scale. Small circles are drawn with respect to the ridge push torque, driving the plate in westerly direction. (a) Forces exerted along contact with North Andes block and east-west striking segment just west of the Lesser Antilles arc are orientated parallel to the boundary (F_{NW-tf}). (b) Northwestern margin is assigned a force of uniform magnitude and constant azimuth (F_{NW}). The azimuth is varied between 90° and 135° (clockwise from north).

of the plate is modelled equivalent to the first-order model defined previously. The computed magnitude of the plate contact resistance is of the wrong sign, for almost the entire range of continental basal shear stress studied, when absolute motion models AM1-2 and HS2-NUVEL1 are adopted (Figure 2.11). When the *Gordon and Jurdy* (1986) or *Chase* (1978a) Euler vectors are incorporated, the plate contact resistance is negative for the lowest values of basal shear stress studied, but the corresponding force acting at the northwestern margin is implied to be driving plate motion (Figure 2.11).

In the second model, the northwestern boundary is assigned a force of uniform magnitude and constant azimuth (Figure 2.10b), analogous to the Caribbean-South America boundary in the model including the North Andes block. The obtained solutions (Figure 2.12) are essentially equivalent to the results obtained with the starting model defined above (cf. Figure 2.7).

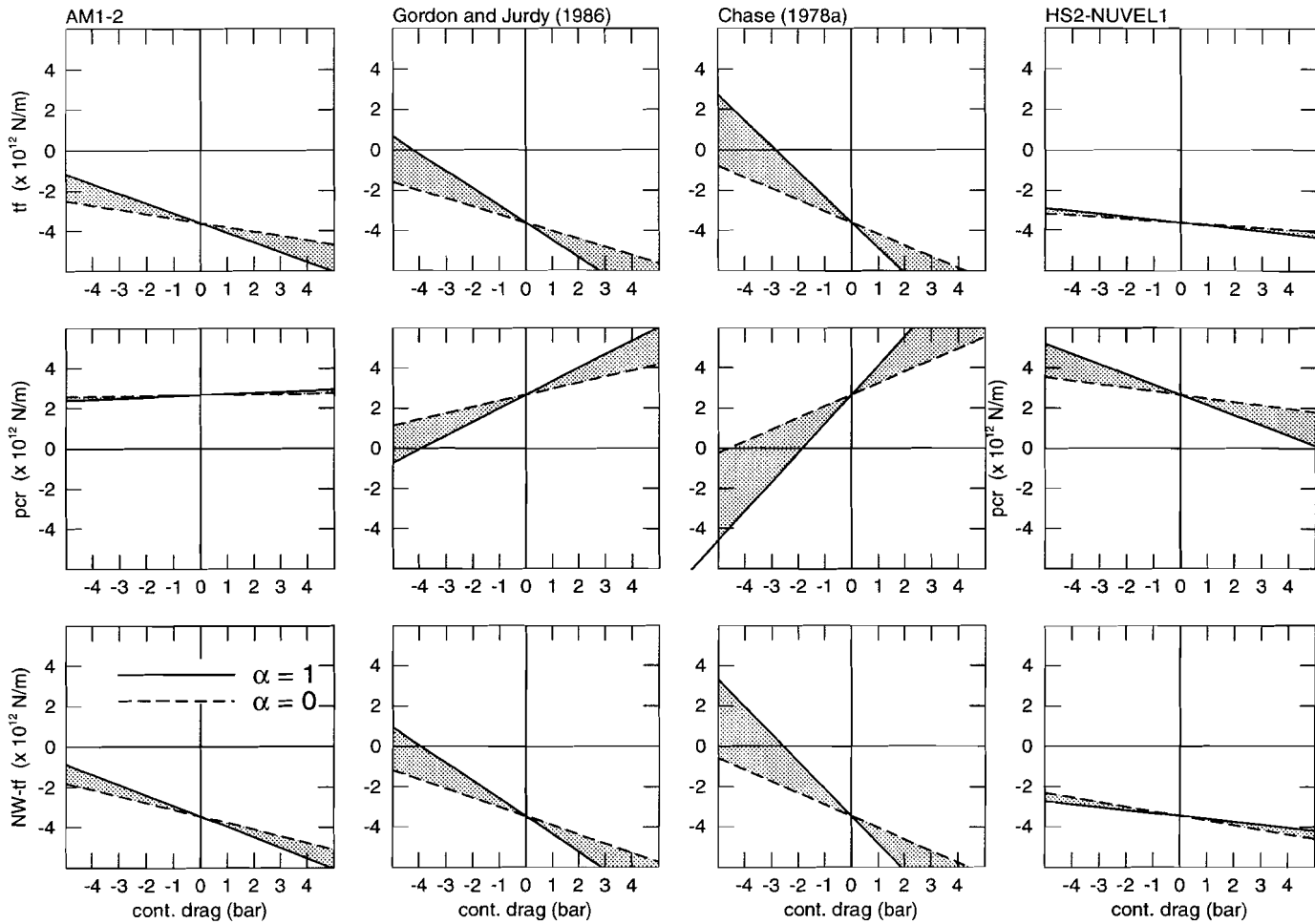


Fig. 2.11. (previous page) Results derived with the plate model excluding the North Andes block incorporating a boundary parallel force acting along the northwestern margin. Arrangement of results as in Figure 2.7. Derived magnitudes of transform fault force (tf), plate contact resistance (pcr), and transform force exerted along northwestern margin (NW-tf) are shown as a function of continental basal shear stress. Note that the range along the ordinate is twice that in Figures 2.7, 2.8, and 2.12. Drawn lines correspond to uniform basal shear stress ($\alpha = 0$); dotted lines give solution for zero oceanic drag ($\alpha = 1$). Shading indicates range of solutions as a function α .

Discussion

Model Limitations

Plate tectonic forces not incorporated in the present study include the resistive forces presumably exerted on the western margin of the South American plate by collision with the continent of the Chile ridge and aseismic ridges and seamount chains carried by the descending Nazca plate. Ridge-trench collision of the Chile ridge has a pronounced expression in the regional geology (e.g., *Cande et al.*, 1987). Subduction of the Juan Fernandez ridge and the Nazca ridge is thought to affect the dip of the descending slab, thereby possibly increasing the coupling between the overriding and the subducting plate (*Pilger*, 1981). Ridge-trench collision of the Chile ridge is further considered to be the cause of northward displacement of the Chiloe block (*Forsythe and Nelson*, 1985) and northeastward motion of the North Andes block may be partially driven by collision of the Nazca ridge (*Pennington*, 1981). Although neglect of the effects of ridge-trench collision may result in local errors in any intraplate stress fields calculated on the basis of the present study, the accompanying forces are considered to be of minor importance in the dynamics of plate motion. The latter also holds for an additional push perhaps exerted at the trailing edge of the South American plate by hotspots localized below the Mid-Atlantic Ridge (*Harper*, 1990).

Western Plate Margin

A question of debate with respect to the dynamics of plate motion in general is the importance and nature of the so-called trench suction force possibly acting on the overriding plate in a subduction zone. In their global study, *Chapple and Tullis* (1977) consistently found a net trenchward pull to be exerted on the upper plate in a subduction zone. The different expression of the various forces in the *Chapple and Tullis* (1977) study and the present analysis inhibits straightforward comparison of results. However, it should be noted that the ridge push torque incorporated in the present study is about 10 times larger than the ridge push on the South American plate found by *Chapple and Tullis* (1977). This difference is expected to alleviate some of the necessity of an extra driving trench suction force. Furthermore, in general, the resistive force exerted on the overriding plate in a subduction zone may have been overestimated by *Chapple and Tullis* (1977)

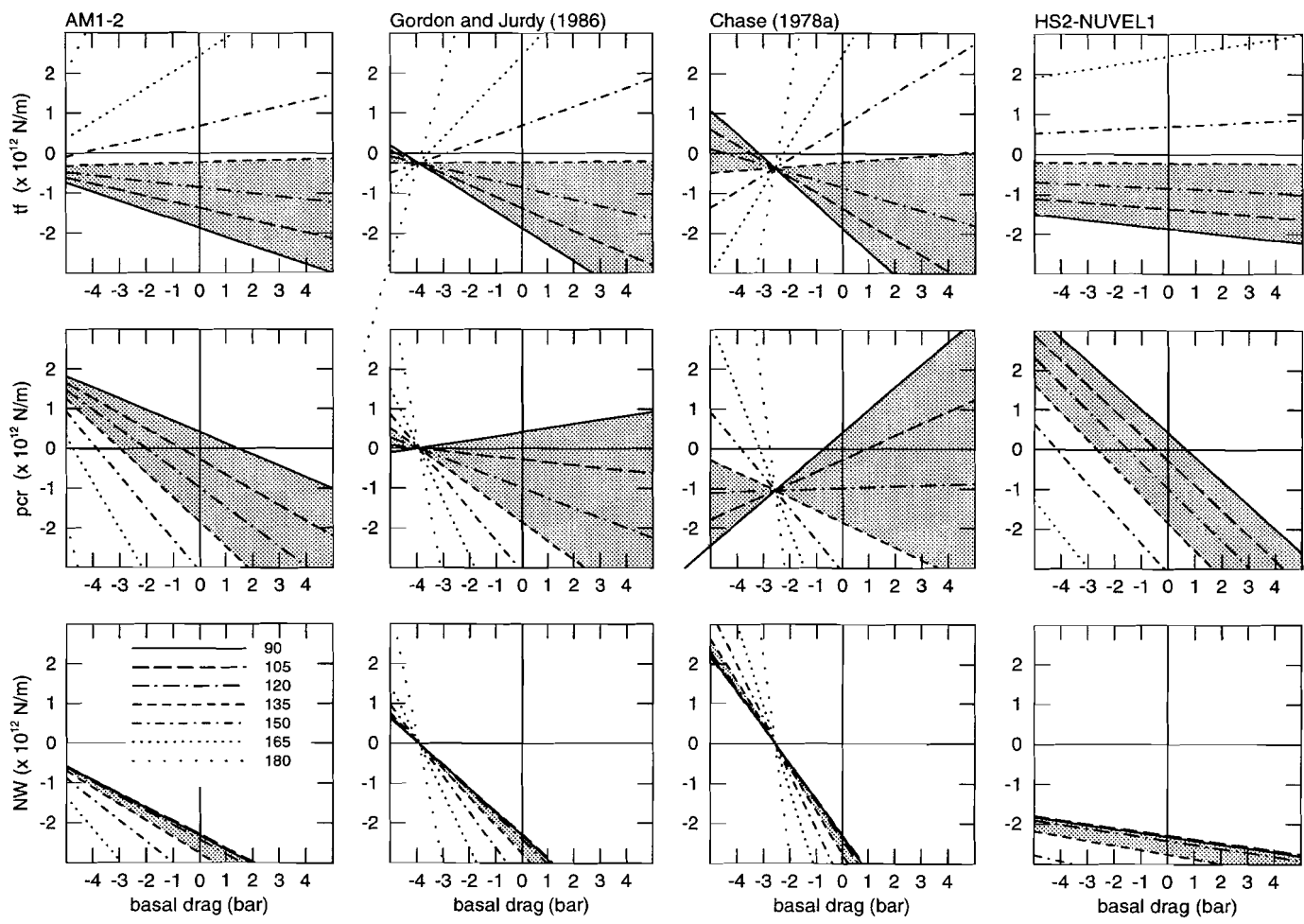


Fig. 2.12. (previous page) Solutions obtained with model excluding the North Andes block and a force of uniform magnitude and constant azimuth on the northwestern margin. Arrangement of results as in Figure 2.7. Magnitudes of transform fault force (t_f), plate contact resistance (p_{cr}), and force on northwestern margin (NW) are shown as a function of uniform basal shear stress. Solutions are obtained for a range of azimuths of F_{NW} ; legend in panel at lower left. Shading corresponds to an azimuth of F_{NW} in the range 90° - 135° .

because the trench-normal component of this force is assumed to be equal in magnitude to the trench-normal component of the resistance exerted on the subducting plate. The latter, however, results only partially from friction along the contact with the overriding plate, a second part results from shearing along the slab-mantle interface.

Assuming basal shear stress acts to resist plate motion and the azimuth of F_{Car} lies between 90° and 135° , we find a maximum resistive plate contact force of $-1 \times 10^{12} \text{ N m}^{-1}$. Only under the simplifying assumption that trench suction is of constant magnitude along the entire western plate margin and is everywhere orientated antiparallel to $F_{p_{cr}}$, the magnitudes derived for $F_{p_{cr}}$ may be considered the net force exerted on the overriding plate. In this case, Figure 2.7 can be used to infer the magnitude of basal shear stress (for a specific absolute motion model and azimuth of F_{Car}) corresponding to a transition from net pull to net resistance at the overriding margin. In case of the probably more realistic situation of a trench suction force acting perpendicularly to the overriding margin only above the steeply dipping slab of the central Peru-Chile trench, a more resistive $F_{p_{cr}}$ is obtained, while only locally a net pull is exerted.

A conclusion concerning the importance of trench suction, based solely on an analysis of the dynamics of motion, requires constraints on the magnitude of plate contact resistance and basal shear stress. Since the plate contact resistance is exerted on both the overriding South American plate and the subducting Nazca plate, modelling of the dynamics of motion of the Nazca plate may yield independent constraints on its magnitude.

Northwestern South America

From the first-order model, it can be concluded that the resistive force exerted on the South American plate constitutes a significant contribution to the dynamics of motion. Only when absolute motion is defined according to *Chase (1978a)*, a realistic solution is also obtained if F_{Car} equals zero. Magnitudes derived for transform fault force and plate contact resistance strongly depend on the azimuth of F_{Car} . These observations, together with the results obtained with the model excluding the North Andes block, strongly suggest that an important compressive force is transferred to the South American plate over the contact with the North Andes block. The fault system bounding the North Andes block to the east is unlikely to be a purely transcurrent boundary. These findings are consistent with analysis of the regional tectonics (e.g. *Kellogg and Bonini, 1982; Henneberg, 1983*).

Basal Drag

With respect to the drag force exerted on the base of the South American plate, several inferences can be made. A noteworthy conclusion is that the obtained results do not rule out the possibility of a basal shear stress acting to drive plate motion. This can be concluded from the fact that realistic solutions are also obtained for positive values of basal shear stress. The present analysis allows estimation of the minimum (i.e., maximum resistive) basal shear stress. The minimum values of basal shear stress yielding realistic solutions in case of the first-order model, -2 to -3.5 bars, may be less resistive than expected. This may be especially so in view of the suggestion that resistive drag beneath continental lithosphere is stronger than on the base of oceanic lithosphere (*Forsyth and Uyeda, 1975; Chapple and Tullis, 1977*). It should be noted, however, that basal shear stress is likely to be proportional to the velocity of absolute motion, which is low in case of the South American plate (Figure 2.4).

Assuming that basal drag is entirely concentrated below the continental lithosphere ($\alpha = 0$), minimum values of continental drag of -3.5 to -5.5 bars, depending on the incorporated absolute motion model, have been derived. These estimates are again strictly valid for the first-order model and will be affected when additional plate boundary forces are considered relevant. In particular, an active trench suction force will decrease the minimum value of continental drag resistance in case of absolute motion models AM1-2 and HS2-NUVEL1.

Finally, it must be noted that the present analysis does not account for any effects on the magnitude and orientation of the basal drag force which might be caused by the lithospheric root of the Andean cordillera.

Importance of Slab Pull on the South American Plate

With respect to the Lesser Antilles subduction zone, the assumption adopted in the first-order model, that no net force is exerted on the subducting South American plate, may be justified by the absence of indications for either compression or extension in the overriding Caribbean plate (*England and Wortel, 1980*). The situation in the South Sandwich subduction zone is more complex, inhibiting a qualitative statement concerning the exerted forces.

The importance of slab pull as a driving force of motion of the South American plate, compared with ridge push, cannot be assessed unambiguously by computation. Apart from uncertainties concerning the dip and length of the slab subducted beneath the southern South Sandwich trench, factors affecting the thermal state of the lithosphere exist in both subduction zones. These are the thick sediment cover present on the oceanic lithosphere subducting beneath the Lesser Antilles arc (*Wortel, 1980*) and the fracture zone offsetting the slab descending in the South Sandwich trench. Assuming a slab pull of $1 \times 10^{12} \text{ N m}^{-1}$ in both subduction zones, the magnitude of the resulting slab pull torque only amounts to approximately 3% of the magnitude of the ridge push torque (Figure 2.5). This relative magnitude is not expected to increase by more than a factor of 3 when

the resultant of the slab pull force, and the resistive forces due to plate-plate and plate-mantle interaction, and crustal buoyancy, is considered.

General

The South American plate constitutes an example of a plate for which the balance of forces is not dominated by slab pull. Consequently, forces which may be of minor importance in the case of purely oceanic plates attached to subducting slabs along much of their circumference, are relatively more important. Examples are the transform fault force and the resistive force exerted along the contact with the Caribbean plate. Further, it has been demonstrated that the choice of an absolute motion pole, taken to define the orientation of the basal drag force, strongly influences conclusions concerning the importance of forces other than basal drag and ridge push. It is expected that assumptions concerning the orientation and distribution of basal shear stress will be important for the other slowly moving plates.

The presented results strongly emphasize that an analysis based solely on the requirement of mechanical equilibrium does not suffice in determining the forces controlling motion of the South American plate. Additional constraints may come from two sources. First, if more insight is provided into the nature of forces the magnitude of which is solved for in the present analysis, they may perhaps be quantified in advance in subsequent work. Second, comparison of data from the World Stress Map Project with intraplate stress fields computed according to various force distributions found possible from the dynamical analysis, may lead to the choice of preferred models. Moreover, this will clarify the importance of those forces which are not resolvable from the torque balance but are expected to have a local expression in the intraplate stress field. In this way the nature of net forces exerted on the South American plate in the Lesser Antilles and South Sandwich subduction zones and the importance of trench suction can be examined.

The uneven distribution of the observations complicates the use of data from the World Stress Map Project. The major part of the observations concerns focal mechanism solutions of earthquakes which occurred within the Andes. Furthermore, the state of stress within the Andes is likely to result from a superposition of a regional intraplate stress field with a more local field representing the effect of lithospheric heterogeneity. The magnitude and orientation of this additional contribution must be quantified before observations of intraplate stress can be used to compare with theoretical results.

Instead of using data on the current state of intraplate stress, information pertaining to the distribution of strain may also be used to compare with model results. For example, the recently initiated CASA project (*Kellogg et al.*, 1989) may be used to analyze further the complex dynamics of northwestern South America.

Conclusions

An analysis of the dynamics of motion of the South American plate, adopting as sole constraint the assumption of mechanical equilibrium, does not yield a unique solution. Instead the relation between the values of the major resistive forces and basal shear stress are assessed.

Combination of a first-order model, incorporating the forces which are expected to be of major importance, with several determinations of the Euler vector of absolute motion of the South American plate, shows that the possibility of a basal drag force acting to drive plate motion, cannot be discarded. By assuming that basal drag is entirely concentrated below the continental part of the South American plate, estimates of the minimum continental basal shear stress (i.e., maximum resistive drag), can be obtained.

Comparison of the results obtained with models including and excluding the North Andes block, clearly demonstrates that the resistive force exerted on the South American plate due to convergence with the Caribbean plate constitutes a significant contribution to the dynamics of plate motion.

Information on the state of intraplate stress, such as compiled and studied by the World Stress Map Project, may be used to compare with stress modelling results based on the various derived dynamical models to further constrain the range of feasible force models. However, this requires a correct assessment of the contribution to the intraplate stress field of lithospheric heterogeneity associated with the Andean cordillera.

Appendix

1. The principle of the calculations is explained examining a model in which five different types of force are incorporated: ridge push force (\mathbf{F}_{rp}), basal drag force (\mathbf{F}_{dr}), transform fault force (\mathbf{F}_{tf}), plate contact resistance (\mathbf{F}_{pcr}), and the force due to convergence with the Caribbean plate (\mathbf{F}_{car}). For each type of force the resultant torque about the center of the Earth is computed. Taking into account the local age gradient, the contribution to the ridge push torque of each element in the oceanic part of the plate can be computed according to *Richter and McKenzie (1978)* and *England and Wortel (1980)*. Integration yields the orientation and magnitude of the ridge push torque T_{rp} . The magnitude of the other forces is not known in advance. Each force is factored into a product of a scalar parameter representing the magnitude per unit length (for \mathbf{F}_{tf} , \mathbf{F}_{pcr} , and \mathbf{F}_{car}) or area (\mathbf{F}_{dr}), and a unit vector \hat{e} giving the orientation of the force, e.g., $\mathbf{F}_{tf} = F_{tf} \hat{e}_{tf}$. The magnitude is considered to be characteristic for the type of force and is therefore independent of position. The torque of transform fault force, \mathbf{T}_{tf} , can be written

as follows:

$$\mathbf{T}'_{if} = \int_L \mathbf{r} \times F_{if} \hat{\mathbf{e}}_{if} dL = F_{if} \int_L \mathbf{r} \times \hat{\mathbf{e}}_{if} dL = F_{if} \mathbf{T}'_{if} \quad (1)$$

where dL is an increment of transform boundary L and \mathbf{r} indicates position. The dimension of F_{if} is Newton per metre and the dimension of \mathbf{T}'_{if} is square metres. The torques of the other boundary forces F_{pcr} and F_{Car} are computed equivalent to (1). The basal drag force is assumed to be orientated parallel to the direction of absolute plate motion which is expressed by unit vector $\hat{\mathbf{e}}_{dr}$. If $\boldsymbol{\Omega}$ is the Euler vector of absolute plate motion, then

$$\hat{\mathbf{e}}_{dr} = \frac{\boldsymbol{\Omega} \times \mathbf{r}}{\|\boldsymbol{\Omega} \times \mathbf{r}\|} \quad (2)$$

The drag torque is expressed as:

$$\mathbf{T}'_{dr} = \int_A \mathbf{r} \times \sigma_{dr} \hat{\mathbf{e}}_{dr} dA = \sigma_{dr} \int_A \mathbf{r} \times \hat{\mathbf{e}}_{dr} dA = \sigma_{dr} \mathbf{T}'_{dr} \quad (3)$$

where integration is over area A , the dimension of σ_{dr} is Newtons per square metre, and the dimension of \mathbf{T}'_{dr} is cubic metres.

The assumption of mechanical equilibrium yields the following equation

$$F_{if} \mathbf{T}'_{if} + F_{pcr} \mathbf{T}'_{pcr} + F_{Car} \mathbf{T}'_{Car} = -(\sigma_{dr} \mathbf{T}'_{dr} + \mathbf{T}'_{rp}) \quad (4)$$

From this, F_{if} , F_{pcr} , and F_{Car} are solved for a range of values of σ_{dr} . The calculation is performed for four different Euler vectors of absolute plate motion.

2. The effect of additional forces is studied by means of superpositions onto the first-order model. This implies that a torque vector of known magnitude is added to equation (4). The result is a shift of the values of the three forces obtained from equation (4), which is the same for each value of σ_{dr} . For example, the shifts, δ_{if}^{LA} , δ_{pcr}^{LA} , and δ_{Car}^{LA} , due to an additional driving force in the Lesser

Antilles zone (F_{LA}) follow from:

$$\delta_{if}^{LA} T'_{if} + \delta_{pcr}^{LA} T'_{pcr} + \delta_{Car}^{LA} T'_{Car} = -T_{LA} \quad (5)$$

where T_{LA} is the resultant torque of F_{LA} . At a given value of σ_{dr} , e.g., the magnitude of the transform fault force in a model incorporating F_{LA} is equal to F_{if} as obtained from equation (3) at this value of σ_{dr} plus the shift δ_{if}^{LA} . The magnitude of the shifts is linearly proportional to the magnitude of the added force. The effects of additional forces are mutually independent.

The Stress Field of the South American Plate

Chapter 3

Introduction

In the investigation of the driving and resistive forces that act on the South American plate we can make use of two principal constraints. Firstly, it can be assumed that the plate is in a state of dynamical equilibrium which implies that a proposed set of forces should yield a zero net torque. In the previous chapter we analysed the plate dynamics using solely this criterium. Secondly, the intra-plate stress field associated with a given force model should be in agreement with the observed pattern of stress. In this chapter we concentrate on the use of observations of the intra-plate stress field as a means of further discrimination between the force models that satisfy the criterium of no net torque.

Viewed upon from a different angle, our study may be considered to contribute to a general understanding of the factors controlling the state of stress in the lithosphere. Moreover, the use of a model will reveal the relevance and limitations of the available observations regarding the stress field. The present study may be considered the first detailed analysis of the South American stress field, based on numerical modelling, that uses the recent compilation of stress indicators obtained by the World Stress Map Project. The South American plate was previously included in the global study of *Richardson et al.* (1979). In this early study, however, the notion of torque balance was not considered and the authors had only few observations at their disposal. Recently, the World Stress

Map data for South America were analysed also by *Stefanick and Jurdy* (1992). The latter authors used a strongly simplified representation of the plate (e.g. a flat plate geometry), offering limited insight.

The plate tectonic forces considered in the previous chapter are not the only factor controlling the South American stress field. The Andean Cordillera and the (Atlantic) passive continental margin represent a second source of intra-plate stress: lateral heterogeneities in the structure of the lithosphere, including topography variations. Since a large part of the available stress observations is situated within the Andes, the South American plate offers a good opportunity to study the interaction between the two sources of lithospheric stress in the case of a mountain range. We will not consider the mountain range and the passive margin as isolated features, but study both as an integral part of the whole plate. As such, our approach forms an improvement over previous work regarding the Andes, in which the state of stress in the mountain range has been addressed only in terms of a vertical cross section (e.g. *Dalmayrac and Molnar*, 1981; *Froidevaux et al.*, 1988; *Richardson and Colblentz*, 1994). Our approach allows us to investigate geometrical aspects such as the role of the orientation of the range with respect to, for example, the direction of convergence along the west margin and the state of stress near changes in the strike of the mountain range. Moreover, orientation and magnitude of the "background" stresses are those constrained by a model of the plate tectonic forces.

The plate tectonic force to which the stress field in the Andes is expected to be particularly sensitive is the resistance associated with subduction below the western margin (plate contact resistance). Therefore, we will make use of the high density of observations along the western margin to learn more about the nature of this resistive force. We have extended the set of forces considered in the previous chapter by examining various possible types of lateral variation of the magnitude of plate contact resistance.

The model analysis has been structured in the following manner. At the onset we define a reference model by choosing a specific value for each of the variables involved in the first order model which was introduced in Chapter 2. Next, the characteristic effect on the intra-plate stress field of each of the factors of interest is assessed by incorporating these factors one by one into the reference model. The analysis has been divided into five parts. The first and second part treat, respectively, the first order model and the set of additional forces defined in the previous chapter. Next, part three addresses the possibility of lateral variation of the resistance associated with subduction. The final two parts deal with the effects of lateral variation in lithospheric structure: in part four we investigate the continent-ocean transition, in part five the Andean Cordillera is examined.

To some extent, the various parts of the analysis each have their own flavour and it proved best not to maintain a strictly uniform structure. In the first two parts we will first assess how the intra-plate stress field varies as a function

of the relevant variables and only then evaluate the results in the light of the observations. In contrast, in the other three parts evaluation of the correspondence between a calculated stress field and the observations is presented as an intrinsic part of the experiments. Furthermore, while in parts two through four a given aspect is examined against the background of the same reference model, examination of the effect of topography requires consideration of an alternative background model as well.

The probability that a given deviation from the reference model is realistic will be commented upon by evaluating whether this deviation provides a better fit to the observations than the reference model. Clearly, this practice implies the assumption that the given deviation is the only factor of relevance. When, for example, a certain additional force leads to a worse fit with part of the observations this may be taken to speak against the presence of that force but may also imply that other additional forces are present in reality mitigating the negative effects of the force under scrutiny. Thus, it is only after having established the effects of all possible factors that definitive conclusions can be reached. The model analysis is preceded by a presentation of the available stress observations and a discussion of the various methods that are used.

Observed Present-Day Stress field

As mentioned in the introduction, our main source of information regarding the current stress field has been the World Stress Map data base ("WSM", Zoback, 1992). The South American part of the WSM was compiled by Assumpção (1992) and includes various types of observations (Figure 3.1). Earthquake focal mechanisms and geological field observations of recent and active faulting constitute the majority of the data. In addition there is information from borehole breakouts and volcanic alignments. Except for two focal mechanisms near the South Sandwich arc all of the available observations pertain to the continent. Within the continent most of the observations are located near the western and northwestern plate margin, i.e. along the Andean Cordillera.

The WSM data have been supplemented with observations published in more recent years, listed in Table 3.1. Data quality was assigned according to WSM criteria which divide the significant observations in three groups. Observations of quality "A" are considered to give the azimuth of the horizontal direction of maximum compressive stress to within $\pm 10^\circ$ - 15° , that of quality "B" to within $\pm 15^\circ$ - 20° , and that of quality "C" to within $\pm 25^\circ$ (Zoback, 1992). Data of lesser quality are considered of questionable significance and have not been included in the present study. Most earthquake focal mechanisms recorded in the WSM have qualities B or C; inversion of fault slip observations may yield quality A data.

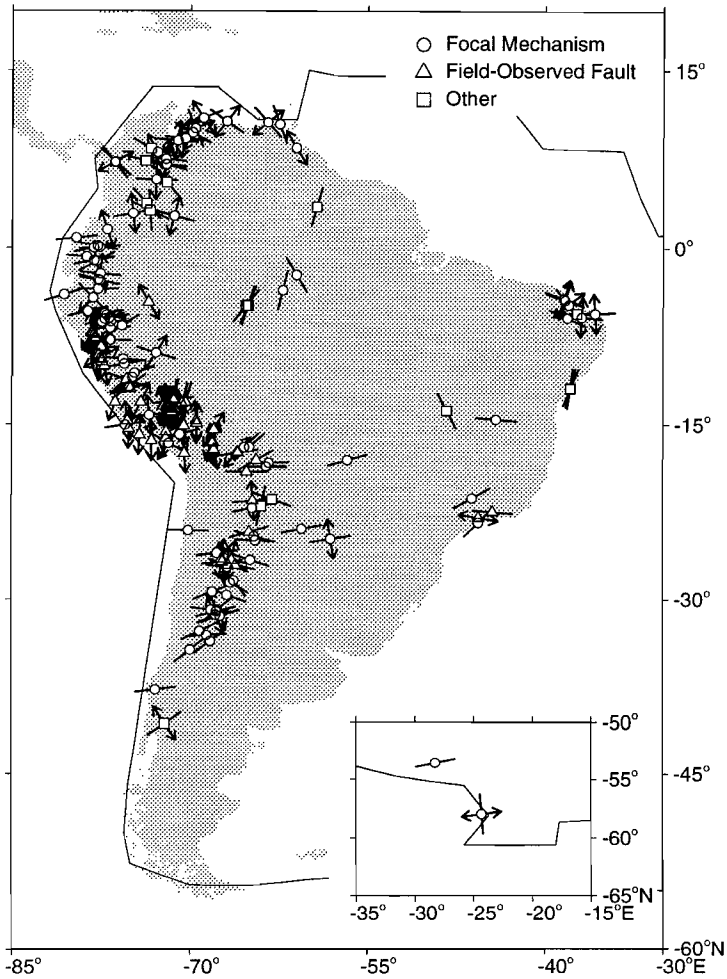


Fig. 3.1. Compilation of observations of the present-day stress field of the South American plate. Short line: principal axis of compression (σ_1) or P-axis. Double arrow: principal axis of tension (σ_3) or T-axis. Symbol denotes type of stress indicator as explained by legend. Data quality is not accounted for in this overview. Convention regarding tectonic regime as follows; σ_1 or P-axis plunges less than 45° while σ_3 /T-axis more than 45° : reverse faulting, only compressional axis is plotted; σ_1 /P-axis and σ_3 /T-axis both plunge less than 45° : strike-slip faulting, both axes are shown; σ_1 /P-axis plunges more than 45° while σ_3 /T-axis plunges less than 45° : normal faulting, only tensional axis is shown. In case the orientation of the axis of maximum horizontal compression is known but tectonic regime is not (borehole breakouts) only the compressional axis is plotted. Shown are horizontal projections of the various axes.

Table 3.1. Additional Stress Indicators

No	Date	Latitude °N	Longitude °E	Depth km	P-axis or σ_1 Azi. Plu.		T-axis or σ_3 Azi. Plu.		Type	Quality	Ref.
<i>Andes South of 5°N</i>											
1	660131	-24.93	-64.48	25	93	1	309	89	FMS	B	a
2	670425	-32.72	-69.17	27	64	4	194	84	FMS	B	a
3	770125	-33.59	-68.27	18	53	13	159	51	FMS	B	a
4	791224	-29.63	-66.87	27	290	7	28	46	FMS	B	a
5	860623	-27.17	-66.84	6	275	15	185	2	FMC	C	a
6	890624	-28.35	-66.30	22	324	3	156	87	FMS	B	a
7	900606	-6.29	-77.46	27	52	36	207	51	FMS	C	b
8	900609	-5.70	-77.07	31	79	46	282	42	FMS	C	b
9	900811	0.01	-78.15	15	258	6	156	64	FMS	C	b
10	901125	-2.70	-77.79	25	284	10	80	79	FMS	C	b
11	910404	-6.24	-76.72	27	91	25	282	64	FMS	C	b
12	910405	-5.93	-76.84	40	81	13	226	74	FMS	C	b
13	910723	-15.85	-70.88	24	74	9	342	9	FMS	C	b
14	920817	-4.25	-78.21	52	315	0	225	40	FMS	C	b
15	921226	-1.15	-77.92	15	62	22	170	38	FMS	C	b
16		-4.60	-73.50	0	0	90	150	0	GFI	A	c
17		-24.20	-65.00	0	74	0	0	90	FMA	C	d
<i>Northwestern South America</i>											
18	910625	5.76	-72.90	15	272	0	182	0	FMS	C	b
19	910817	9.74	-69.83	15	299	5	209	1	FMS	C	b
20	921017	7.22	-76.39	15	142	8	246	59	FMS	C	b
21	921018	7.27	-76.34	15	132	23	241	38	FMS	C	b
22	740612	10.61	-63.47	11	318	8	52	19	FMS	C	e
23	840820	10.45	-62.45	10	160	7	61	50	FMS	C	e
<i>Atlantic Coast, Brazil</i>											
24	-----	-21.33	-46.15	2	61	11	163	46	FMC	C	f
25	94----	-4.42	-38.29	-	109	16	199	2	FMS	C	g
26	90----	-5.86	-36.88	-	95	19	4	3	FMS	C	g
27	93----	-5.93	-38.10	-	114	15	1	5	FMS	C	g

Key to indicator type, FMA: average or inversion of focal mechanisms; FMC: composite focal mechanism; FMS: single focal mechanism; GFI: inversion of geological fault slip observations (names follow WSM convention, see *Zoback, 1992*). Key to references, a: *Assumpção and Araujo (1993)* and personal communication M. Assumpção, 1995; b: CMT Catalogue; c: *Dumont (1993)*; d: *Cahill et al. (1992)*; e: *Russo et al. (1993)*; f: *Bassay Blum (1993)*; g: *Ferreira et al. (1995)*.

Additional earthquake focal mechanisms were taken from *Assumpção and Araujo (1993)* for the Andes of Chile and northwest Argentina, from *Russo et al. (1993)* for Venezuela, and from *Bassay Blum (1993)* and *Ferreira et al. (1995)* regarding Brazil. The Harvard Centroid Moment Tensor (CMT) Catalogue (*Dziewonski and Woodhouse, 1983*; now published with the U.S. National Earthquake Information Center (NEIC) Preliminary Determination of Epicenters Catalog) was scanned for

the period June 1990 through December 1992, i.e. posterior to the period for which CMT data are included in the WSM. Also, we included the result of an inversion of earthquake data by Cahill *et al.* (1992) concerning northwest Argentina. Supplementary geological observations are reported by Dumont (1993) for the Andean foreland of eastern Peru.

The Andes South of 5°N

Focal mechanisms of earthquakes in the Andes south of 5°N mainly indicate reverse faulting consistent with WSW-ENE to E-W orientated compression (Figure 3.2). Seismic intra-plate faulting is concentrated east of the high ranges, in particular, it occurs in the Sub-Andean foreland fold-and-thrust belt of Peru, Bolivia, and Argentina. Whereas reverse faulting dominates, strike-slip faulting is also observed. The existence of horizontal compression is confirmed by geological observations. This type of observations also shows that normal faulting associated with roughly N-S orientated tensional stress characterises the high Andes at several places. Observations of the state of stress in the high Andes are not evenly distributed along the length of the orogen. Most notably, the widest segment of the Altiplano-Puna plateau - between 18°-26°S - remains as yet unexplored. The extensional regime of the higher regions of the cordillera would remain essentially unnoticed on the basis of earthquake data alone.

Thus, ascending the Andes from the east we find a change in tectonic regime from reverse faulting to normal faulting. As shown in Figure 3.3 most reverse faulting occurs there where the topography (averaged over an 1°x1° area centered on the epicentre or field site) is less than about 2 km. Normal faulting is observed at elevations exceeding 3 km. We may note that the two regimes are apparently not separated by an elevation interval where strike-slip faulting prevails. Indicated with deviating symbols in Figure 3.3 are data from the western flank. Close to the Pacific coast of south Peru normal faulting is observed to take place also at low elevations.

There exists only scant evidence on the behaviour of tectonic regime versus depth in a given vertical column through the mountain range. In the Cordillera Blanca of northern Peru normal faulting extending from the surface to a depth of about 20 km is suggested by three observations: the focal mechanism of the 1946 Ancash earthquake (Suarez *et al.*, 1987; Doser, 1987) and the composite solutions of two separate microearthquake surveys (Grange *et al.*, 1984; Deverchère *et al.*, 1989). Further south, normal faulting at a depth of presumably 51 km below the northern Altiplano is evidenced by a CMT solution reported by Assumpção (1992; event date 860405, misprinted as 850405). In contrast, at a depth of 11 km below the southern Puna plateau event #68 of Chinn and Isacks (1983) expresses reverse or strike-slip faulting. The latter observation led Allmendinger *et al.* (1989) to suggest that the normal faulting observed at the surface in the southern Puna is a shallow feature.

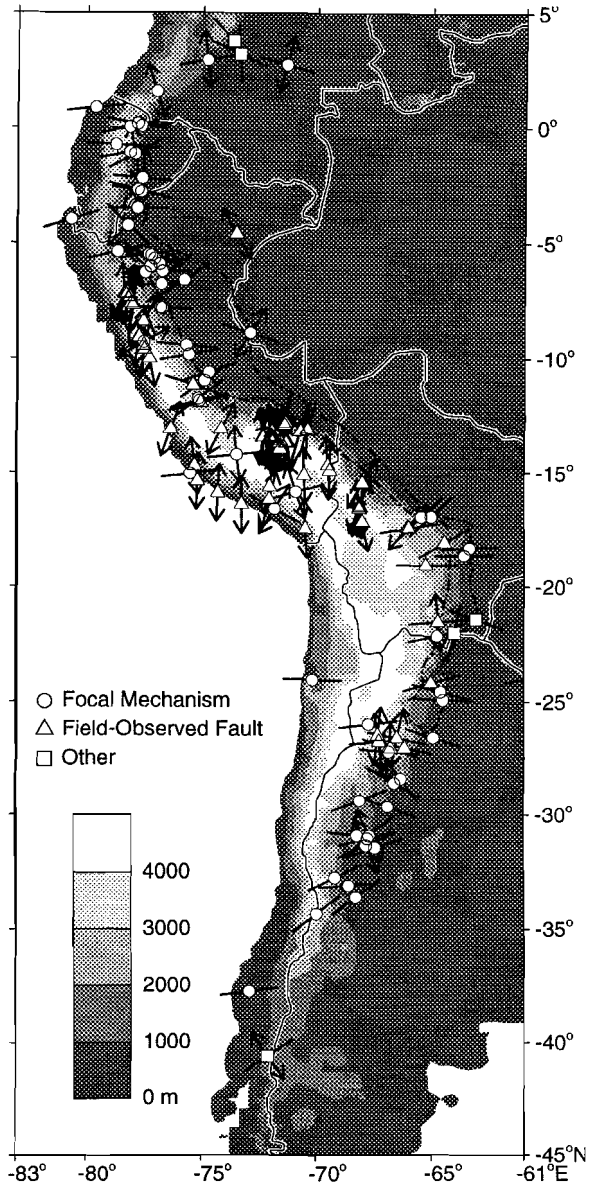


Fig. 3.2. Stress observations in the Andes shown against the background of a contour map of topography. Political borders are indicated for reference. Dash-dotted line delimits the Sub Andean foreland fold-and-thrust belt. Conventions adopted in plotting of observations are explained in caption of Figure 3.1.

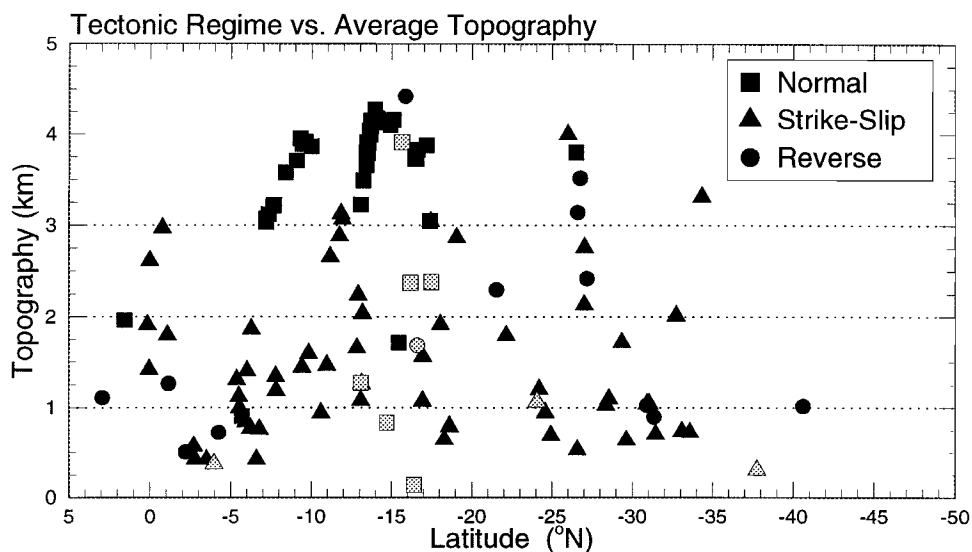
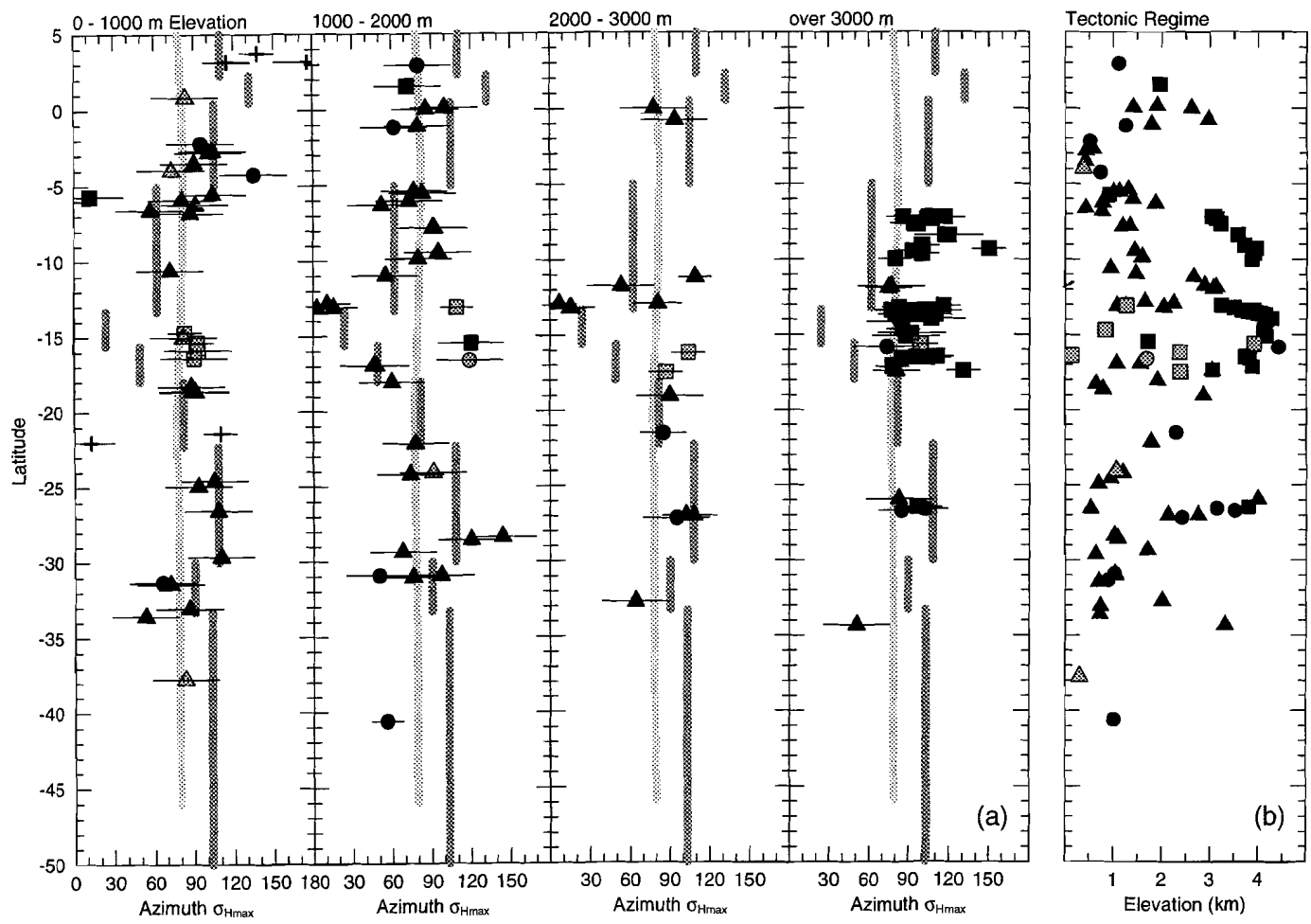


Fig. 3.3. Tectonic regime observed in the Andes as a function of latitude and topographic elevation. The latter corresponds to the average elevation of the Earth's surface within a $1^\circ \times 1^\circ$ area centered on the epicentre or field site. Symbol type now indicates tectonic regime; triangle: reverse faulting; circle: strike-slip faulting; square: normal faulting. Grey symbols pertain to the Andes west of the Altiplano-Puna plateau.

It has been noted previously that, on average, the direction of maximum horizontal compression ($\sigma_{H_{max}}$) expressed by observations from the Andes is close to both the direction of Nazca - South America convergence and the direction of absolute plate motion (e.g. *Assumpção*, 1992). When looked at in more detail subtle trends in the orientation of $\sigma_{H_{max}}$ are discernable. Figure 3.4 shows the available observations as a function of latitude and grouped according to average topographic elevation. For topography up to 1 km going south from

Fig. 3.4. (next page) (a) Observed azimuth of the axis of maximum horizontal compression ($\sigma_{H_{max}}$) in the Andes as a function of latitude for four intervals of average topographic elevation. For earthquake focal mechanisms and geological data $\sigma_{H_{max}}$ corresponds, respectively, to the horizontal projection of the P-axis and σ_1 -axis. Symbol type as in previous figure. Grey symbols refer to west flank of the Andes. Horizontal lines give uncertainty in azimuth of $\sigma_{H_{max}}$ as indicated by World Stress Map quality measure. Also shown as a function of latitude are the azimuth of Nazca-South America convergence according to NUVEL-1 (continuous light grey line; *DeMets et al.*, 1990) and the orientation of the vector approximately perpendicular to the strike of the Andean Cordillera (dark grey segmented line). Nazca-South America convergence has been evaluated at the trench. Both grey lines are the same for all elevation intervals. (b) Observed tectonic regime as a function of latitude and elevation; identical to Figure 3.3.



Stress Field of the South American Plate

5°N to 11°S an overall decrease in the azimuth of $\sigma_{H_{max}}$ can be observed. This trend is lost, however, in the data pertaining to the interval 1-2 km. Data for the latter interval do show a general increase in azimuth from 13°S to 28°S. This increase is only vaguely present in the data below 1 km but is confirmed by the observations between 2 and 3 km. All three groups below 3 km demonstrate a decrease in the azimuth of $\sigma_{H_{max}}$ from about 29°S southwards. Regarding the normal faults above 3 km we may infer that data from central Peru (including the Cordillera Blanca) show a $\sigma_{H_{max}}$ azimuth - taken as the direction perpendicular to the axes of tension - that is on average slightly larger than that for the observations to the south. The last panel shows the non-uniform distribution of observations in the high Andes.

Also shown in Figure 3.4 is the approximate azimuth of the direction perpendicular to the strike of the cordillera at each latitude. Although correlation is far from perfect we may note that both the decrease in azimuth of $\sigma_{H_{max}}$ from 5°N to 11°S, and the gradual increase from 13°S to 28°S are mirrored by similar trends in the normal-to-strike direction. The observations of roughly NE directed $\sigma_{H_{max}}$ between 30°S-34°S more or less coincide with a segment where the Andes deviates from its general trend. A correlation between $\sigma_{H_{max}}$ orientation and normal-to-strike direction for the focal mechanisms around 30°S was pointed out by *Assumpção and Araujo* (1993). The normal faults above 3 km are characterised by $\sigma_{H_{max}}$ that significantly deviates from the normal-to-strike direction. In other words: tension is not directed parallel to the mountain range (cf. *Assumpção*, 1992; *Mercier et al.*, 1992). A final inference from Figure 3.4 is that segments where normal faults have been observed in Peru and Bolivia appear to coincide with segments with relatively little reverse faulting. Since investigation of the high Andes has not been uniform along the cordillera this apparent correlation may well be coincidental.

Northwestern South America

In northwestern South America the available focal mechanisms display a considerable scatter (Figure 3.5). The orientation of horizontal compression is markedly different from that along the Andes south of 5°N and varies from WNW-ESE to NW-SE. A roughly NW-SE orientation of compression is also indicated by borehole breakouts in Colombia. Most of the focal mechanisms inferred for the region indicate strike-slip faulting, a characteristic which also sets northwestern South America apart from the main body of the Andes.

Craton and Paleozoic Basins

Between about latitudes 15°-25°S the reverse faulting regime with WSW-ENE orientated compression extends eastwards from the Andes to the Atlantic coast (Figure 3.1). To the north, compression deviates significantly from this trend.

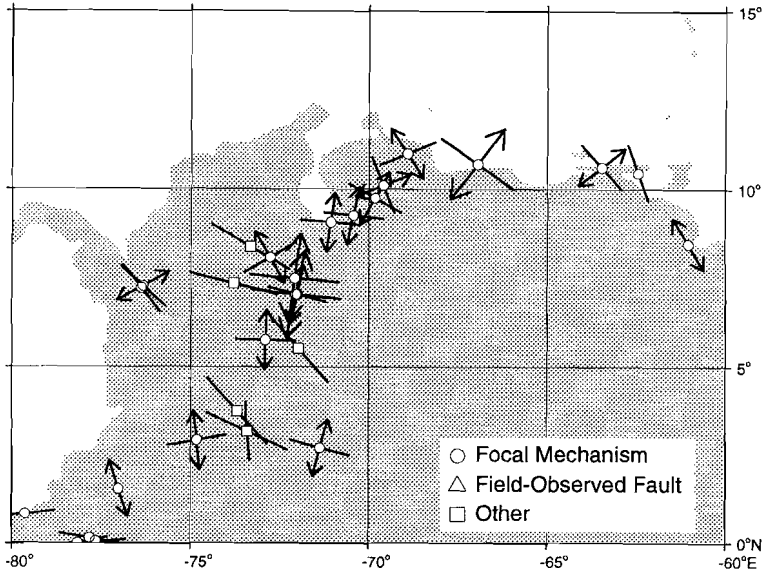


Fig. 3.5. Stress observations available for the northwestern part of South America. Size proportional to data quality, large symbol: quality A and B; small symbol: quality C. Conventions as in Figure 3.1.

In the Amazon basin roughly NNE-SSW compression is evidenced by both focal mechanisms and borehole breakouts. Near the Atlantic coast of Brazil strike-slip deformation takes place. The associated axis of compression is found to be orientated parallel to the coast line.

Methods

The manner in which all forces other than those associated with the Andes are calculated has been explained in detail in Chapter 2. In this section we will concentrate on the method of calculation of the intra-plate stress field and the manner in which the effect of topography is accounted for. Furthermore, we present a technique for the comparison of a computed stress field with earthquake focal mechanisms.

Intra-Plate Stress Calculations

The South American plate is modelled as a thin elastic shell using the finite element ("FE") method. This approach has previously been applied successfully to other plates (see Wortel *et al.*, 1991 and references therein). In the previous chapter two alternative geometries of the South American plate have been considered, either in- or excluding the North Andes block (see Figure 2.1). The results that were obtained indicate that the contact between the North Andes

block and South America transfers the forces exerted on the western and northern margin of the block and should not be considered a transform fault. Therefore, in our study of the intra-plate stress field we will consider the North Andes block to be an integral part of the plate.

The plate's curved surface is approximated by a total of 3848 flat triangular elements of the linear displacement type. The distance between two E-W rows of nodal points and between subsequent nodes of a given row amounts to 150 km. These dimensions were chosen in order to be able to examine the stress field in the Andes and constitute a considerable reduction in element size in comparison with the mesh adopted in the previous chapter. Torques for the various forces calculated using the new mesh differ only slightly from those found with the less detailed mesh. Stress fields are calculated assuming plane stress, Young's modulus is taken as 7×10^{10} N/m², Poisson's ratio as 0.25. A reference thickness of 100 km has been adopted for the plate. Stresses obtained with the FE model are horizontal non-lithostatic stresses integrated over the plate's thickness. In subsequent figures the stresses will be displayed as average values for a plate with the reference thickness of 100 km.

In the calculations of the stress field associated with a given set of forces, a minimum of three degrees of freedom needs to be constrained in order to prevent rigid body motion. This was done by taking one nodal point fixed in both the N-S and E-W direction, and a second only in the E-W direction. In general the fixed nodal points will introduce undesired "boundary effects" when the in-plane sum of the forces is not equal to zero. Whereas each of the force sets studied satisfies the requirement of zero net torque this does not guarantee the in-plane sum of forces to vanish. The problem is solved by distributing evenly over the area of the plate the force required to balance any existing net in-plane force. In all experiments discussed below the nodal point forces associated with balancing are small compared to the average nodal point force due to the plate tectonic forces. Expressed in terms of a basal shear stress the balancing force seldomly exceeds a magnitude of 1 bar (0.1 MPa). Throughout the analysis the fixed nodes were placed at the spreading ridge which already restricts undesired effects to the oceanic domain. Applying the balancing provides an undisturbed stress pattern in the oceanic part of the plate. It was found that balancing does not significantly affect the stress field in the continental domain where almost all of the available observations are located.

Effect of Topography

Surface elevation has been derived from the ETOPO5 data base (U.S. National Oceanic and Atmospheric Administration) which provides topography on a 5'x5' grid. In order to account for the effect of topography we require knowledge about the density structure. Specifically, we need to know how the topographic mass is compensated isostatically at depth. It has been suggested that the Altiplano-Puna plateau is compensated not only by a crustal root but also by a thermal root

due to a hot asthenosphere (Froidevaux and Isacks, 1984). The relative importance of the two contributions is not known, however. In view of this uncertainty we will, as a first approximation of the actual situation, assume surface elevation to be compensated by a crustal root only, and assume constant, i.e. temperature independent, densities for crust and lithospheric mantle. Although the model thus incorporates a simplified density structure it will allow us to gain important insight. The role of a possible thermal root will be discussed later. Calculations presented below are based on a crustal density of 2800 kg/m^3 and a mantle density of 3200 kg/m^3 . We adopt a reference thickness for the continental crust of 35 km. Stresses or forces caused by topography are averaged over the plate thickness of 100 km.

We will account for the effect of topography following two different approaches. Previously, the state of stress in mountain ranges has been examined mainly in terms of a vertical cross section perpendicular to the strike of the range (references given below). The first approach outlined below serves to illustrate the concepts based on these vertical sections in the context of our plate model. An alternative procedure, yielding a more complete description of the effect of topography and consistent with the manner in which, for example, ridge push is accounted for, is formed by the second approach.

First approach. The first approach follows the reasoning of *Dalmayrac and Molnar* (1981) and, in particular, *Froidevaux and Isacks* (1984) and *Froidevaux et al.* (1988). These authors built on earlier studies by *Frank* (1972), *Artyushkov* (1973), and *Fleitout and Froidevaux* (1982). We consider a schematic vertical cross section perpendicular to the strike of a mountain range (Figure 3.6a). A coordinate system is introduced with x giving horizontal position along profile and the z -axis pointing vertically downwards. For this two-dimensional situation the equations of equilibrium are written as:

$$\frac{\partial \sigma_{xx}}{\partial x} + \frac{\partial \sigma_{xz}}{\partial z} = 0 \quad (1)$$

and:

$$\frac{\partial \sigma_{xz}}{\partial x} + \frac{\partial \sigma_{zz}}{\partial z} = \rho g \quad (2)$$

where σ_{xx} and σ_{zz} are the normal stresses in the x and z direction respectively, σ_{xz} shear stress along the x or z direction, ρ density, and g gravitational acceleration. Assuming that shear stress at the base of the lithosphere is negligible and that

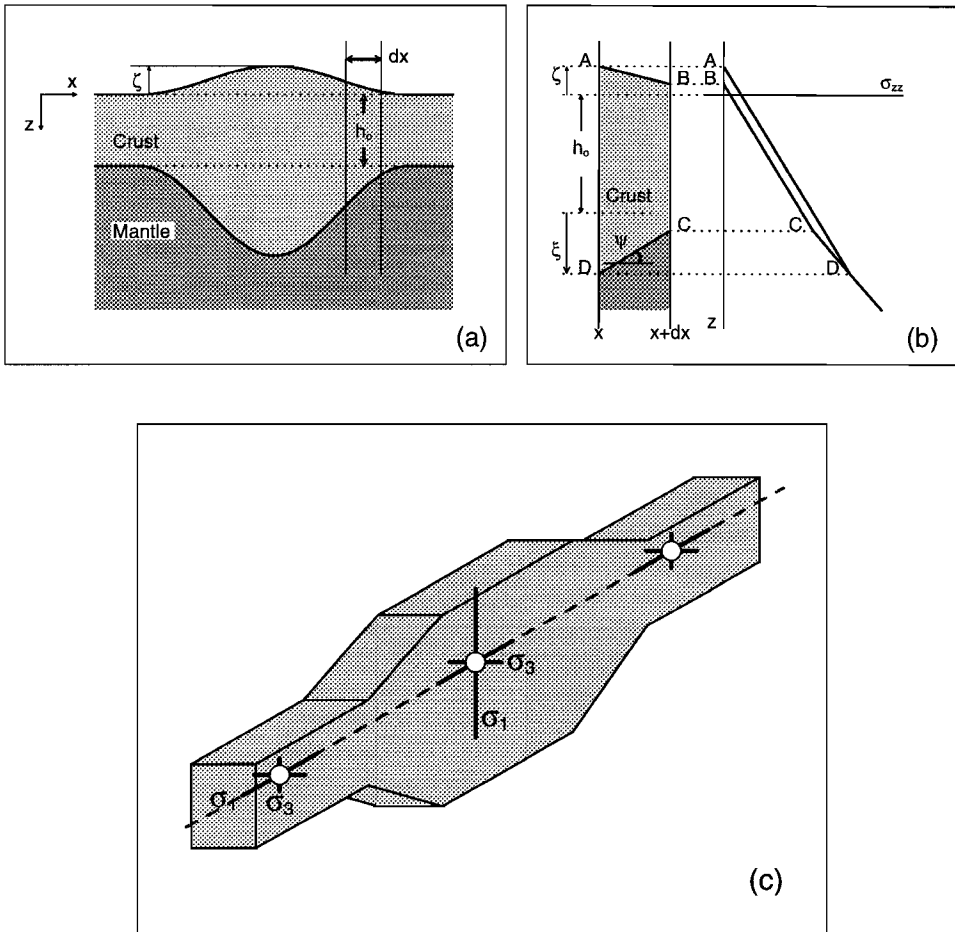


Fig. 3.6. (a) Schematised vertical cross section perpendicular to the strike of a mountain range. Topography ζ is compensated by a crustal root. The segment limited by two vertical lines is shown in detail in the next panel. (b) Segment of the cross section of the previous panel juxtaposed to a diagram showing schematically the variation of the vertical principal stress (= lithostatic pressure) with depth at both sides of the segment. Indicated are the positions in σ_{zz} - z space corresponding to points A through D. Figures not to scale. See text for explanation. (c) Schematic representation of a slice of crust comprising a mountain range, shown to illustrate the concept of average excess vertical stress as employed by *Mercier et al. (1992)*. Whereas the topography and crustal root do not affect the horizontal principal axes, they result in increased compression along the vertical axis. A permutation of the principal stresses takes place, such that normal faulting occurs in the mountain.

crustal thickness varies on a length scale large compared to the thickness of the lithosphere, shear stresses σ_{xz} may be neglected. This is equivalent to assuming that the crust is in a state of local isostatic equilibrium. Consequently, the equations of equilibrium reduce to

$$\frac{\partial \sigma_{xx}}{\partial x} = 0 \quad (3)$$

and

$$\frac{\partial \sigma_{zz}}{\partial z} = \rho g \quad (4)$$

It follows from (3) that topography does not affect the vertically averaged value of the horizontal stress $\bar{\sigma}_{xx}$. By expressing the density structure in the mountain as the difference with respect to a reference structure where topography is zero we may, using (4), introduce the excess vertical stress due to topography ζ , averaged over thickness L , as

$$\Delta \bar{\sigma}_{zz} = \frac{g}{L} \int_{-\zeta}^L \Delta \rho(z) z dz = \frac{gM}{L} \quad (5)$$

Where:

$$M = \int_{-\zeta}^L \Delta \rho(z) z dz \quad (6)$$

is the moment of the density anomalies with respect to the level $z=0$ (Fleitout and Froidevaux, 1982). The notion that $\bar{\sigma}_{xx}$ remains constant while $\bar{\sigma}_{zz}$ becomes increasingly compressive going from lowland to high mountain has been suggested (in the studies referred to in the above) to explain why high mountain regions exhibit normal faulting. The lowest elevation at which normal faulting is observed allows an estimate of the magnitude of $\bar{\sigma}_{xx}$ to be made: at this elevation the vertical stress - which can be calculated using (5) - is approximately equal to the horizontal stress. Our implementation of the above concept firstly involves an extension of the theory to three dimensions. Introducing the y -axis in the

direction parallel to the mountain range the equations of equilibrium now are:

$$\begin{aligned}
 \frac{\partial \sigma_{xx}}{\partial x} + \frac{\partial \sigma_{xy}}{\partial y} + \frac{\partial \sigma_{xz}}{\partial z} &= 0 \\
 \frac{\partial \sigma_{yx}}{\partial x} + \frac{\partial \sigma_{yy}}{\partial y} + \frac{\partial \sigma_{yz}}{\partial z} &= 0 \\
 \frac{\partial \sigma_{zx}}{\partial x} + \frac{\partial \sigma_{zy}}{\partial y} + \frac{\partial \sigma_{zz}}{\partial z} &= \rho g
 \end{aligned}
 \tag{7}$$

in which σ_{yy} is the normal stress in the y direction and σ_{xy} and σ_{yz} are shear stresses in that direction. Making the reasonable assumption that crustal thickness varies slowly also in the direction parallel to the mountain range, shear stress σ_{yz} is negligible, as was σ_{xz} . Consequently, we may write

$$\begin{aligned}
 \frac{\partial \sigma_{xx}}{\partial x} + \frac{\partial \sigma_{xy}}{\partial y} &= 0 \\
 \frac{\partial \sigma_{yx}}{\partial x} + \frac{\partial \sigma_{yy}}{\partial y} &= 0 \\
 \frac{\partial \sigma_{zz}}{\partial z} &= \rho g
 \end{aligned}
 \tag{8}$$

In other words, in the three dimensional situation we again find that the horizontal components of stress are not affected by topography and that expression (5) is retained. Implicitly the latter notion was already incorporated in the study of *Mercier et al.* (1992) who applied the reasoning of *Froidevaux et al.* (1988) in a qualitative manner to explain the behaviour of all *three* principal axes of stress in a cross section through the Andes. The concept is illustrated schematically in Figure 3.6c. In order to visualise the notion of excess vertical stress in the context of our numerical modelling we apply the concept on an element by element basis. Firstly, for each element situated in the Andes we calculate its average surface elevation. The result is compared to the actual topography in Figure 3.7. The major topographic characteristics of the Andes are represented well by the model. Secondly, using equation (5) we calculate for each element the corresponding average excess vertical stress. In contrast to the above-mentioned previous studies we now do not assume the horizontal principal stresses to be constant throughout the Andes (both in terms of orientation and magnitude), but use the intra-plate stresses calculated to result from a given set of plate tectonic forces. By subtracting - for each element - the excess vertical stress from the two horizontal stresses the latter again represent the difference

with respect to the vertical stress and their sign and magnitude is a direct indication of tectonic regime.

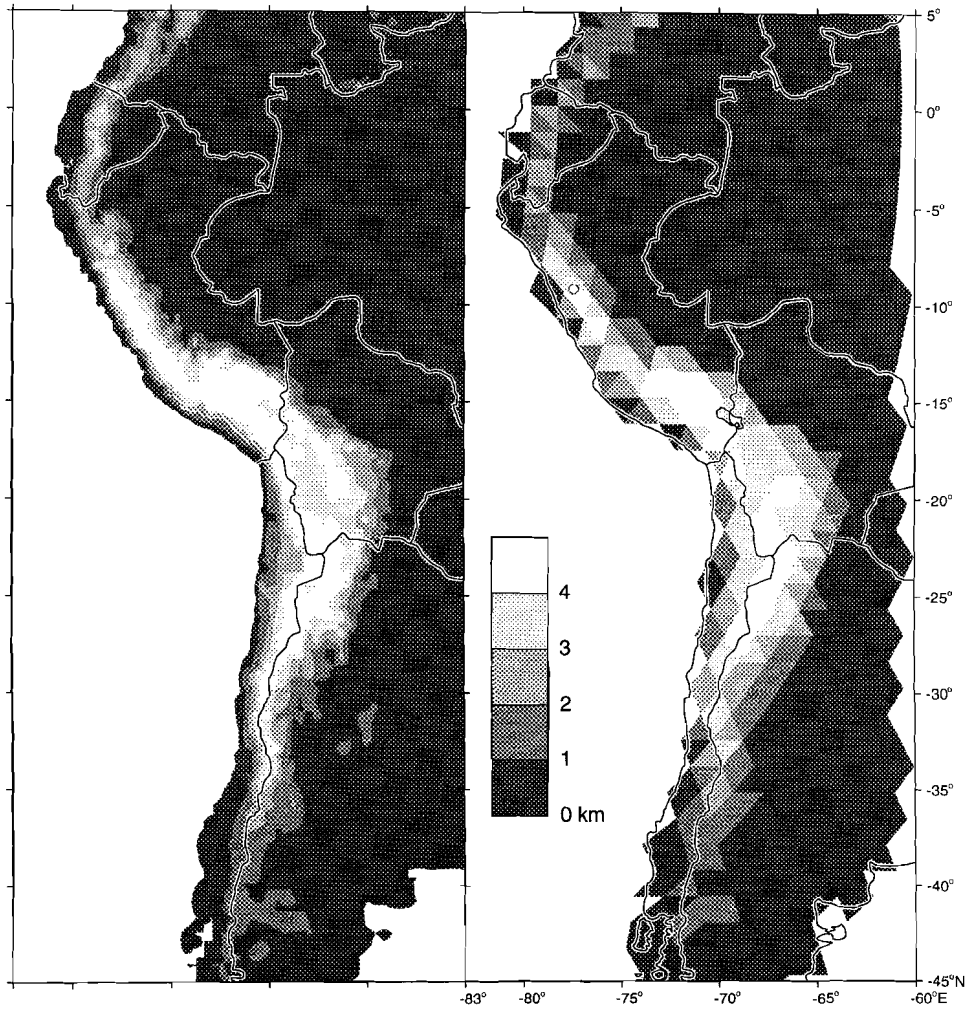


Fig. 3.7. Comparison of actual topography of the Andes (left panel) and topography averaged over the elements of the finite element mesh used in modelling (right panel). Topography is taken from the ETOPO5 data base.

Second approach. In a second approach to the problem, the effect of topography is fully integrated in the finite element calculations. This is done by taking into account horizontal body forces that are proportional to gradients in the moment of the density anomalies defined by (6). The method was outlined by *Fleitout and Froidevaux* (1983) and *Fleitout* (1991) and is in fact identical to the way ridge push is implemented (see Chapter 2).

We set out considering again the two-dimensional geometry of Figure 3.6a, a segment of which is shown enlarged in Figure 3.6b. The segment is of length dx and its width, i.e. the dimension in the direction normal to the plane of section, is considered unity. The force F_H associated with the change in topography over distance dx is equal to the difference between the vertical stress integrated along the vertical faces at x and $(x+dx)$. Thus, the force is expressed as the area between the σ_{zz} versus depth curves at x and $(x + dx)$ (cf. *Frank*, 1972).

Implicit in the above reasoning is the assumption that at both x and $(x + dx)$ there exists a lithostatic state of stress: in this case lateral changes in vertical stress correspond to lateral changes in *pressure* and are therefore associated with lateral changes in horizontal stress. It is at this point that we appear to be in conflict with our earlier inference that, as a result of topography, σ_{xx} does not vary with x (expression 3). However, this apparent contradiction stems directly from the difference between the two ways of approach. If we start by assuming horizontal and vertical equilibrium - which implies (3) - we directly obtain an expression for the average non-lithostatic stress ($\bar{\sigma}_{xx} - \bar{\sigma}_{zz}$); which is the approach outlined in (1) through (6). Alternatively, we may start by imagining a hypothetical situation of lithostatic stress at all x and derive expressions for the associated forces. In order to satisfy the equations of equilibrium (1) and (2) these forces have to be compensated by non-lithostatic stresses, which are exactly those arrived at directly with the first approach. In the finite element calculations we wish to include topography as just one of several sources of stress and require explicitly the related forces. Hence, the second approach is used.

A remark before proceeding concerns the formulation in terms of gravitational potential energy (e.g. *Le Pichon*, 1982; *Molnar and Lyon-Caen*, 1988; and *Molnar et al.*, 1993). The gravitational potential energy PE of a column of unit area at x is defined as

$$PE = \int_{-\zeta(x)}^L \sigma_{zz}(z) dz \quad (9)$$

Clearly, PE equals the area below the corresponding σ_{zz} versus depth curve and the force exerted between adjacent columns as a result of a change in topography is equal to their difference in potential energy.

Returning to Figure 3.6b we introduce F_{AD} as the integrated vertical stress over the trajectory from point A to D and likewise define F_{BC} and F_{CD} . We may then write

$$F_H = F_{AD} - (F_{BC} + F_{CD}) \quad (10)$$

Our method of calculation of F_H follows *Artyushkov* (1973) in that we develop the term F_{CD} . Adopting the notation of *Artyushkov* (1973) we assume a reference crustal thickness h_0 , indicate the depth of the crustal root by ξ , and define angle ψ as the deviation of the base of the crust from the horizontal (Figure 6). Given isostatic equilibrium and dx being small:

$$F_{CD} = \rho_c g h(x) \tan \psi dx \quad (11)$$

where ρ_c is the density of the crust and $h(x)$ its thickness at x . Substituting $\tan \psi = -d\xi/dx$ we obtain

$$F_{CD} = -\rho_c g h(x) \left(\frac{d\xi}{dx} \right) dx \quad (12)$$

Isostatic equilibrium (with the reference column) implies:

$$\rho_c \zeta + \rho_c \xi = \rho_m \xi \quad (13)$$

where ρ_m is the density of the lithospheric mantle. (13) can be used to substitute for ζ in the expression for crustal thickness:

$$h = h_0 + \zeta + \xi \quad (14)$$

yielding, after differentiation

$$\frac{d\xi}{dx} = \left(\frac{\rho_c}{\rho_m} \right) \frac{dh}{dx} \quad (15)$$

Substituting (15) into (12) we obtain

$$F_{CD} = -\left(\frac{\rho_c}{\rho_m}\right)^2 gh \left(\frac{dh}{dx}\right) dx \quad (16)$$

Next, we define $P(x)$ as the vertical stress integrated over the crustal thickness at x and write:

$$F_{AD} = P(x) = \int_{-\zeta}^{h_0+\xi} \rho_c g(z+\zeta) dz = \frac{1}{2} \rho_c g h^2(x) \quad (17)$$

Moreover, at $(x+dx)$, dx being small

$$F_{BC} = P(x) + \left(\frac{dP}{dx}\right) dx \quad (18)$$

Substituting (16), (17), and (18) into (10) we have:

$$F_H = \left(-\frac{dP}{dx} + \frac{\rho_c}{\rho_m} gh \frac{dh}{dx}\right) dx \quad (19)$$

which, with (17) can be written as

$$F_H = \left(\frac{-\rho_c(\rho_m - \rho_c)}{\rho_m} gh \frac{dh}{dx}\right) dx \quad (20)$$

Using (13) and (14) to substitute for h we finally derive

$$F_H = \left\{ \rho_c g \left(h_0 - \frac{\rho_m}{\rho_m - \rho_c} \zeta \right) \frac{d\zeta}{dx} \right\} dx \quad (21)$$

Thus, by separately evaluating the term F_{CD} we are able to express the force contributed by a segment dx in terms of topography and the gradient of topography. It is easily checked that, when extended to three dimensions, we obtain an additional expression similar to (21) describing the component in the horizontal direction perpendicular to the x - and z -axis.

In practice, calculation of F_H proceeds as follows. For each grid point of the ETOPO5 database, ζ and $\nabla\zeta$ are calculated and, subsequently, F_H is derived. Next, for each element of the finite element mesh that falls within the Andes the contributions from all grid points it encompasses are summed and the resulting force is distributed evenly over the three nodal points. Some of the elements near the western plate margin encompass areas that are actually below sea-level. F_H associated with these off-shore parts has been neglected so as not to "contaminate" the body forces corresponding to the Andes with effects related to the presence of the trench system.

Comparison of Model and Observations

When comparing model results with observations we need to consider the fact that different types of observations are not equally good indicators of stress. In particular, whereas inversion of fault slip data may provide an estimate of the principal axes of stress, the P and T axes of an earthquake focal mechanism, in fact, pertain to strain. One way of comparing modelled stress and focal mechanisms is to assume that P and T axes do indeed indicate stress, but with a larger uncertainty than for example the results of fault slip inversion. This forms part of the rationale behind the quality scheme applied in the World Stress Map. In the same manner other types of observations and differences between the significance of observations of the same type can be handled.

In order to be able to compare model and data in terms of tectonic regime we use the plunge of the observed P and T axes or principal stresses to classify an observation (see caption to Figure 3.1). Classification of a *modelled* state of stress in terms of tectonic regime is straightforward. We will denote the average horizontal non-lithostatic principal stresses provided by the FE model by $\Delta\bar{\sigma}_{Hmax}$ and $\Delta\bar{\sigma}_{Hmin}$, and assume that the vertical principal stress equals the lithostatic pressure. When, for example, $\Delta\bar{\sigma}_{Hmax}$ is compressive and $\Delta\bar{\sigma}_{Hmin}$ is tensile we are dealing with a strike-slip regime. Taking compressive stress positive and with $\sigma_1 > \sigma_2 > \sigma_3$ it follows that, in this case, σ_1 acts in the direction of $\Delta\bar{\sigma}_{Hmax}$, σ_2 is vertical, and σ_3 is parallel to $\Delta\bar{\sigma}_{Hmin}$.

Earthquake focal mechanisms can be compared to a modelled stress field in more detail if we make additional assumptions concerning the relation between stress and the direction of fault slip. Firstly, we assume that an observed seismic event represents a reactivation of a pre-existing fault plane. Since we are studying the current stage of a region with a long history of deformation this assumption appears warranted. Secondly, we assume that slip along a given plane occurs in

the direction of maximum resolved shear stress. This assumption was first formulated by *Bott* (1959) and is made implicitly whenever we compare a modelled stress field with the results of inversion of geological fault slip measurements; it is on this assumption that the inversion techniques are based. From the second assumption it follows that the direction of slip on a pre-existing fault is controlled by (1) the orientation of the fault with respect to the principal axes of stress, and (2) the relative magnitude of the principal stresses (*Bott*, 1959; *Carey and Brunier*, 1974). The latter can for example be described by the stress ratio Φ of *Angelier* (1979a), defined as

$$\Phi = \frac{\sigma_2 - \sigma_3}{\sigma_1 - \sigma_3} \quad (22)$$

The stress ratio varies from 0 to 1 and expresses the magnitude of the intermediate principal stress relative to the maximum and minimum principal stress.

Let us consider again the case of a model-derived strike-slip regime. Denoting the lithostatic pressure at depth z by $p(z)$ we may write for the (total) principal stresses at z

$$\begin{aligned} \sigma_1(z) &= p(z) + \Delta\bar{\sigma}_{Hmax} \\ \sigma_2(z) &= p(z) \\ \sigma_3(z) &= p(z) + \Delta\bar{\sigma}_{Hmin} \end{aligned} \quad (23)$$

Substitution of (23) into (22) yields:

$$\Phi = \frac{-\Delta\bar{\sigma}_{Hmin}}{\Delta\bar{\sigma}_{Hmax} + \Delta\bar{\sigma}_{Hmin}} \quad (24)$$

which demonstrates, firstly, that it is possible to calculate the value of Φ at each position in our numerical model, and secondly, that the value of Φ is independent of depth. The latter stems from the fact that a hydrostatic component of stress does not affect resolved shear stress and the fact that the model provides vertically averaged stresses. Expressions similar to (24) can be derived for the case of a normal or a reverse faulting regime.

We conclude that the FE model results contain all information required to compute the direction in which a given fault would slip according to the

modelled stress field. This leads us to propose the following method of comparison of model and focal mechanisms. Assuming it is not known which of the nodal planes of a focal mechanism represents the fault we consider both planes. Next, for each plane the direction in which slip would occur according to the modelled state of stress is computed. The angle between observed and modelled slip vector then provides a measure of the fit between model and data.

The sensitivity of the direction of slip along a given fault to small changes in the orientation of the fault plane can be shown to depend on the average orientation of the plane relative to the principal axes and the value of the stress ratio. Thus, in other words, even when all focal mechanisms of a given dataset are known with the same accuracy, the meaning of the inferred misfit angles may vary from event to event. In order to get a grip on the significance of the inferred misfits we calculate - for each mechanism of a given set - the range over which misfit varies when fault strike and dip are varied by 10° in both directions. In doing this we assume the rake of the observed slip vector to be constant.

Finally, it must be noted that in the forward calculation of fault slip we consider orientation, but not magnitude, of the resolved shear stress. Thus, we do not check whether the fault reactivation satisfies any criterium for fault strength. Indeed, this aspect is disregarded also in most of the inversion techniques that have been applied in the neotectonic studies of the Andes.

Analysis I. The First Order Model

Based on knowledge of the nature of the boundaries of the South American plate we have proposed a first order model for the dynamics (see Figure 2.3a). Incorporated are ridge push (F_{rp}) which drives the plate westwards and is counteracted by resistance associated with transform faults (F_{tf}), plate contact resistance due to subduction below the west margin (F_{pcr}), and resistance associated with Caribbean-South America convergence (F_{Car}). In this chapter we will again adopt the abbreviations of force names introduced in Chapter 2, Table 2.1. Plate contact resistance is modelled as a force parallel to the direction of convergence at the western plate margin. Finally, we included basal drag force (F_{dr}) in the form of a shear stress σ_{dr} parallel to the direction of absolute plate motion, that acts either as resistive (negative value) or driving force (positive value). Of these forces, ridge push can be quantified independently. The magnitude of F_{tf} , F_{pcr} and F_{Car} is determined as a function of σ_{dr} on the basis of the requirement that the net torque acting on the plate must vanish in order for the plate to be in equilibrium. Apart from the value of σ_{dr} , the first order model comprises as variable factors the orientation of F_{Car} and the absolute motion pole used to define the orientation of σ_{dr} . The full range of solutions of the torque balance equation can be found in Chapter 2; in this section we will examine the associated intra-plate stress field.

Defining a Reference Model

As a starting point for the analysis we assume an azimuth for F_{Car} of N135°E and zero basal shear stress. The reason for choosing this particular azimuth of F_{Car} is that we expect it to be close to the correct orientation: observed deformation is commonly interpreted as resulting from WNW-ESE to NW-SE convergence between South America and the Caribbean plate (see Chapter 2). The assumption of zero basal shear stress implies that we take a neutral standpoint regarding the nature of basal drag and has the advantage that it renders the reference model independent of assumptions regarding absolute plate motion. The corresponding nodal point forces are shown in Figure 3.8. Relatively large forces act at the Caribbean margin, forces representing the ridge push and transform fault resistance along the SAM-Sco boundary are of about equal magnitude and somewhat smaller than forces exerted at the western plate margin. Nodes within the continent and the old sea-floor off Argentina remain unloaded apart from the (very small) distributed balancing force (not shown in Figure 3.8). The relative importance of the various forces is also illustrated by a histogram of torque magnitudes. For each force type we show the magnitude of the corresponding torque in the model under scrutiny versus the magnitude of the “unscaled” torque (see Chapter 2, Table 2.2). In this case, as in all subsequent models, the magnitude of Caribbean resistance is slightly larger than the corresponding value determined in the previous chapter. To prevent unrealistically large stresses near the NW-SE striking segment of the South America - Caribbean margin this short segment - orientated strongly parallel to the acting force - has been left unloaded in all experiments presented below. This modification does not affect the net torque due to Caribbean resistance.

The stress field associated with the reference model (Figure 3.9) is characterised by E-W compression in the central part of the plate and in the Andes from Colombia southwards. F_{Car} causes compression to rotate towards NW-SE in the northwestern part of the continent. The effect of F_{Car} is still notable at considerable distance from the Caribbean-South America boundary. Compression is orientated WSW-ENE to NE-SW inwards from the central SAM-Sco boundary. Southern South America, including the Andes, is characterised by a strike-slip regime with significant N-S tension in addition to the E-W compression. Stress magnitudes are fairly uniform throughout most of the plate but relatively low near the Mid-Atlantic Ridge and the American-Antarctic ridge.

Several experiments have been aimed specifically at finding the cause of the occurrence of N-S tension in the southwestern part of the plate. This feature proved to be independent of (i) the amount of transform resistance on the western segment of the SAM-Sco boundary, (ii) the orientation of F_{per} , in particular the change in orientation of F_{per} when crossing the Nazca-South America-Antarctica triple junction, (iii) the slight change in strike of the plate margin from NNE-SSW towards NNW-SSE in southernmost Chile, (iv) the choice of fixed nodal points, (v) the correction for a net in-plane force. It follows that the

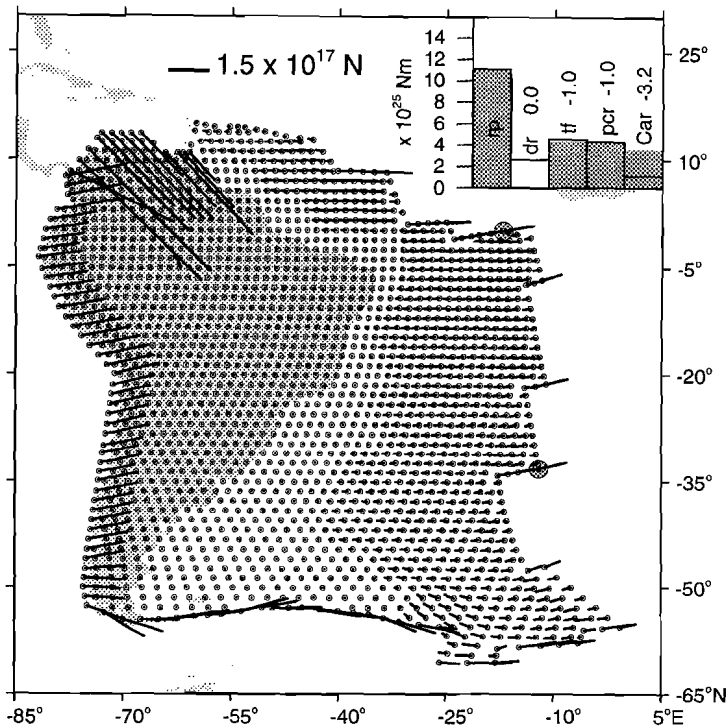


Fig. 3.8. Nodal point forces of the reference model for the stress field of the South American plate. Nodal points are indicated by dots, the associated forces are given by black lines. Force scale as indicated. The order of magnitude of the forces, 10^{17} N, is understood by realising that (e.g.) the contributing plate boundary forces, typically of the order of 10^{12} N/m, are integrated over distances of the order 10^5 m, to yield the nodal point forces. Encircled are the two nodes held fixed in the stress calculations. Histogram in upper right corner illustrates importance of each type of force featured by the model. Shown is the magnitude of the net torque vector for each force type. Grey bars pertain to the model under scrutiny; bars outlined in black give unscaled torque magnitudes. Values next to force names give force magnitude in 10^{12} N/m, or shear stress magnitude in bars in the case of basal drag, for the model under investigation. This and all subsequent model results are shown in a cartesian projection.

occurrence of N-S tension is a combined effect of F_{pcr} and ridge push. As will be shown later, the component of tension is reduced in force models including a more resistive F_{pcr} .

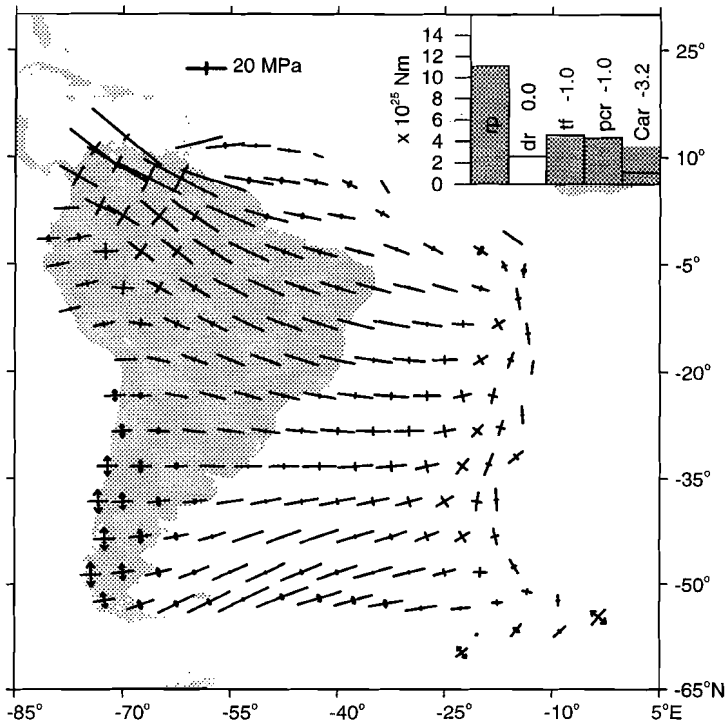


Fig. 3.9. Intra-plate stress field computed for the reference model. Stresses have been averaged over the area of each of the elements of the mesh depicted in Figure 2.2; stresses are shown for a selection of these elements. Calculations are performed using a much finer mesh (see distribution of nodal points in Figure 3.8). Short line: principal axis of compression; double arrow: principal axis of tension. Stress scale as indicated. Stress magnitudes are average values for a plate thickness of 100 km. Histogram as in previous figure.

Variation of Basal Shear

In order to define the orientation of basal shear we will consider the HS2-NUVEL1 absolute motion pole for South America (*Gripp and Gordon, 1990*) and the pole derived by *Chase (1978a)*. The former represents the most recent estimate available; of all absolute motion poles considered in Chapter 2 the latter is the one that predicts motion deviating most from that according to HS2-NUVEL1.

Since the torque balance permits only small values of *resistive* basal shear we consider a value of -1 bar (although intra-plate stress will be expressed in Pascals, we continue using bar for the basal shear stress in order to stay consistent with Chapter 2). In combination with the HS2-NUVEL1 pole this basal shear resistance leads to a reduction of resistance on the western plate margin (Figure 3.10). In general, the magnitude of the resulting intra-plate stress is somewhat smaller than in the reference model. The orientation of the principal axes, however, is very similar. Due to the reduced contribution of F_{pcr} , the effect of F_{Car} extends further to the south.

When we consider basal drag to drive plate motion, larger amounts of shear stress were found to be possible (Chapter 2). Assuming a value of +5 bar we obtain the stress field depicted in Figure 3.11. As in the previous model the orientation of the principal stresses is little different compared with the reference model. However, magnitudes of stress are much increased. F_{Car} is found to have a relatively small effect on the stress field. We may note that in spite of the correction for a net in-plane force some spurious effect of the fixed nodes is visible in this particular model.

Using the absolute motion pole of *Chase* (1978a) and a basal shear of -1 bar, the only significant difference with the equivalent model including the HS2-NUVEL1 pole lies in the less resistive F_{Car} (Figure 3.12). According to the *Chase* (1978a) pole, basal shear is directed east-southeastwards and takes over part of the resistance otherwise solely provided by F_{Car} . The associated stress field (Figure 3.12) is similar to that in Figure 3.10 apart from the northwestern region where now compression is also E-W directed. The effect of F_{Car} is restricted to the edge of the plate.

Setting basal shear stress to +5 bar results in an increase of, in particular, resistance due to F_{Car} (Figure 3.13). The latter is now found to dominate the stress field in the northern half of the plate. Parallel to the western margin, north of 15°S, a component of tension is developed.

The effect on the intra-plate stress field of a non-uniform distribution of basal shear is not illustrated here. In Chapter 2 we determined the effect on the magnitude of F_{tr} , F_{pcr} , and F_{Car} of a reduction of the amount of shear below the oceanic part of the plate relative to that below the continent. Knowing the stress field for the situation of either zero basal shear or uniform basal shear the effect of non uniform distributions of shear can be easily envisaged.

As is apparent from the associated torque balance solutions, the absolute motion models discussed in Chapter 2 but not treated explicitly in this section, result in stress fields that are intermediate between the ones shown here for the case of the HS2-NUVEL1 and *Chase* (1978a) absolute motion poles.

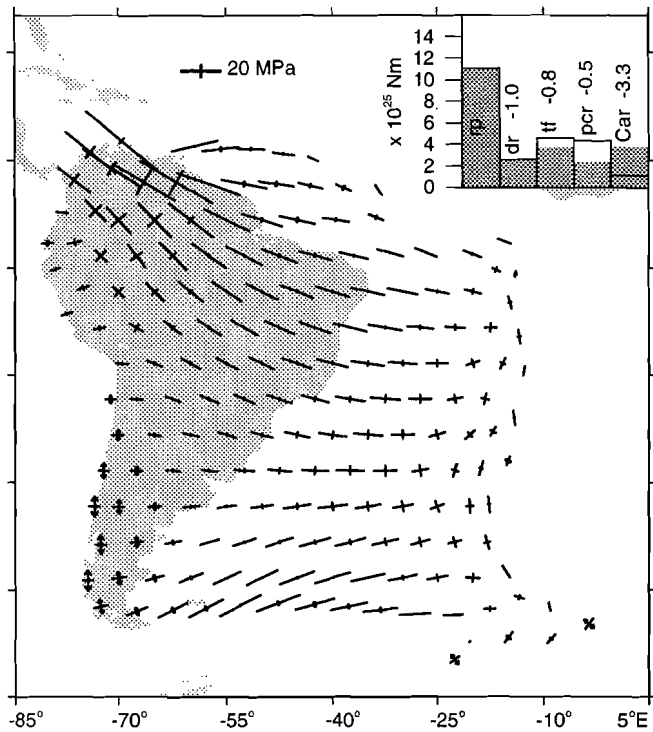


Fig. 3.10. Modelled intra-plate stress field. Basal shear -1 bar; absolute motion according to HS2-NUVEL1.

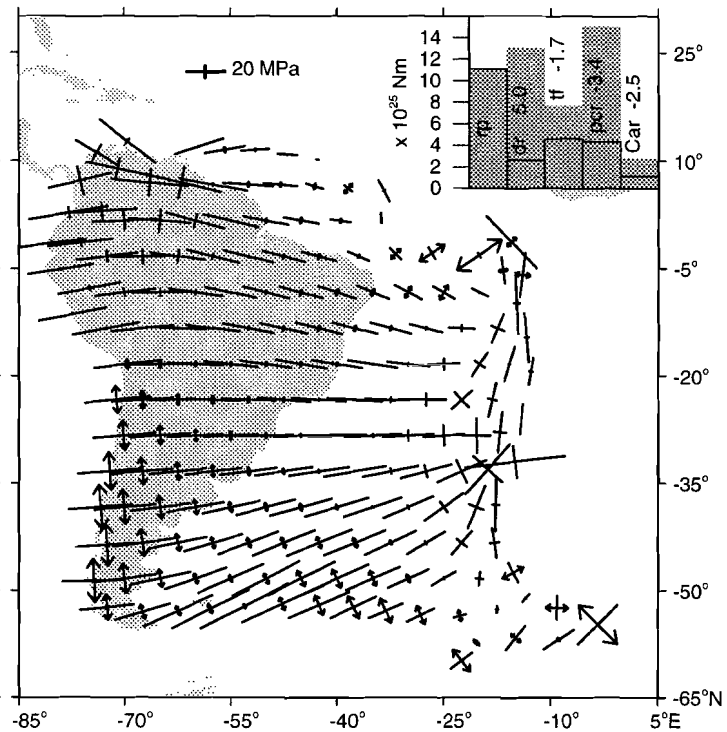


Fig. 3.11. Modelled intra-plate stress field. Basal shear +5 bar; absolute motion according to HS2-NUVEL1.

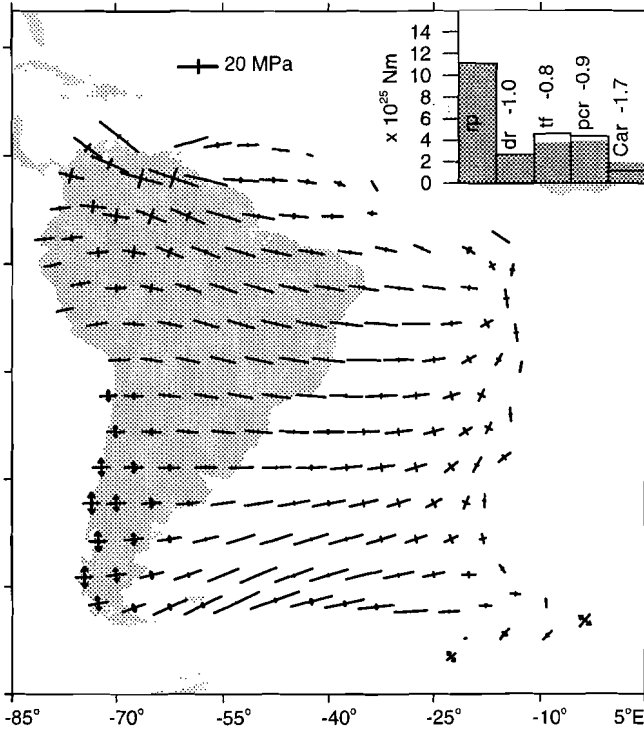


Fig. 3.12. Modelled intra-plate stress field. Basal shear -1 bar; absolute motion according to Chase (1978a).

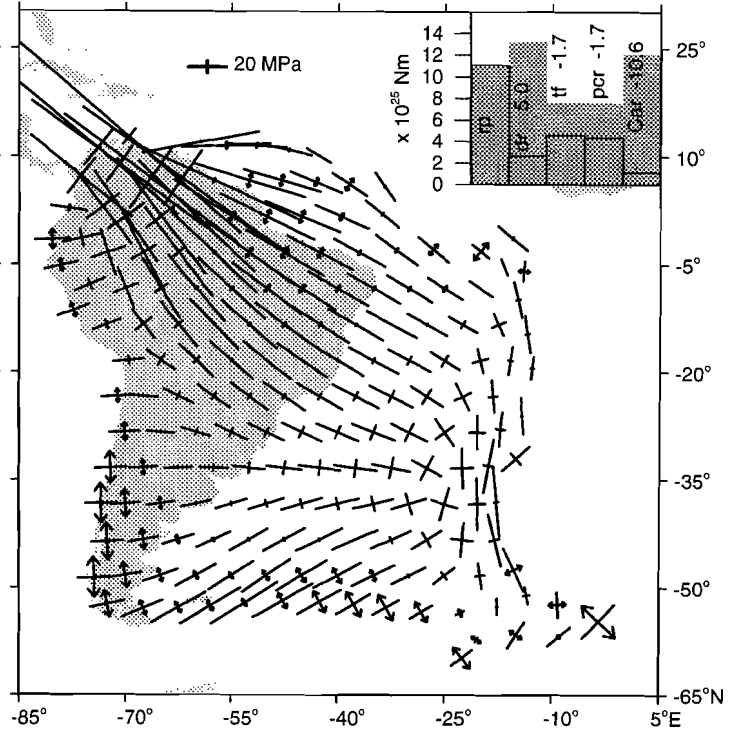


Fig. 3.13. Modelled intra-plate stress field. Basal shear +5 bar; absolute motion according to Chase (1978a).

Variation of the Azimuth of F_{Car}

Returning to the case of zero basal shear stress we change the orientation of F_{Car} to N120°E, i.e. F_{Car} is directed further towards the east than in the reference configuration. This results in an increase of resistance due to F_{if} and a reduced importance of F_{pcr} which has a notable effect on the stress field (Figure 3.14). The latter is now dominated by WNW-ESE to NW-SE compression originating at the SAM-Car boundary and by a strike-slip regime with NE-SW directed compression inwards from the SAM-Sco boundary. Along the western margin, tension approximately parallel to the coast is developed. This tension is largest in northern Chile. Westward directed ridge push, in combination with the ESE directed resistance applied to the northwestern margin and east directed resistance on the southern margin, result in a bending of the western margin.

Changing the orientation of F_{Car} to N150°E has the opposite effect: resistance due to F_{if} is reduced while resistance due to F_{pcr} is increased (Figure 3.15). As a result of the latter, compression inwards from the western plate margin is larger. N-S tension in the southwestern part of the plate is much reduced in comparison with the reference model. In the northwestern part of the continent a state of near radial compression is predicted.

Reference Model vs. Observations in the Andes

The reference model will serve also as a basis for later experiments regarding the nature of F_{pcr} and the effect of topography. At this stage, therefore, we will compare in detail the stress field of the reference model with the observations in the Andes south of 5°N. Figure 3.16 shows the model derived azimuth of the principal axis of maximum compression and the tectonic regime for each element that encompasses a least one observation within its three sides. Both in anticipation of the later experiments regarding the role of the mountain range and because it provides a convenient way of presentation, we will adopt the grouping according to topographic elevation that was used to construct Figure 3.4. Observations situated on the western flank of the Andes are denoted in lighter shade. For elevation below 3 km modelled stress is also depicted at latitudes where observations are absent. These extra points correspond to elements the average topography of which falls within the limits of the given elevation interval and which line up with the elements that do coincide with data (average topography was depicted in Figure 3.7). Thus, Figure 3.16 illustrates that, in the reference model, the azimuth of calculated σ_{Hmax} changes little along the Andes. Between 3°N and 13°S the azimuth of modelled compression equals the direction of Nazca-South America convergence. In contrast, south of 13°S compression is rotated clockwise with respect to the direction of convergence. On average the model matches the observed azimuth of σ_{Hmax} reasonably well. The largest deviations occur for the northernmost observations below 1 km and at the central segment between 1 and 2 km. The modelled azimuth of σ_{Hmax} is too small in comparison with the observations above 3 km in Peru. Regarding the correspondence between

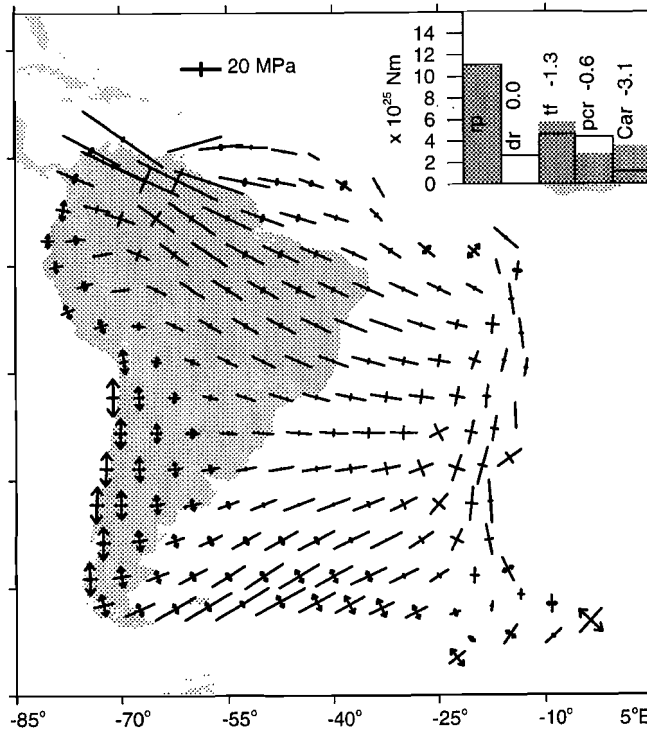


Fig. 3.14. Modelled intra-plate stress field. No basal shear; azimuth F_{Car} is N120°E.

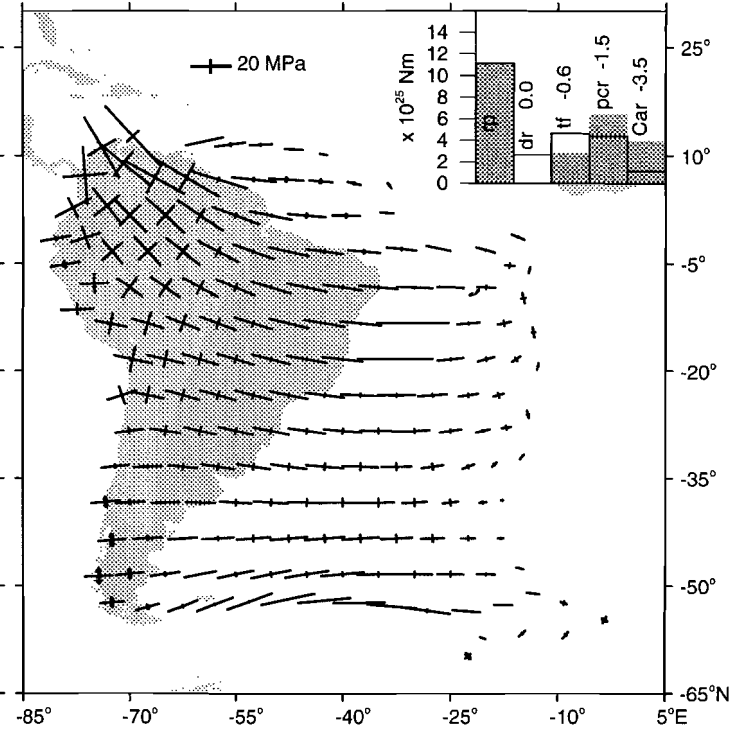
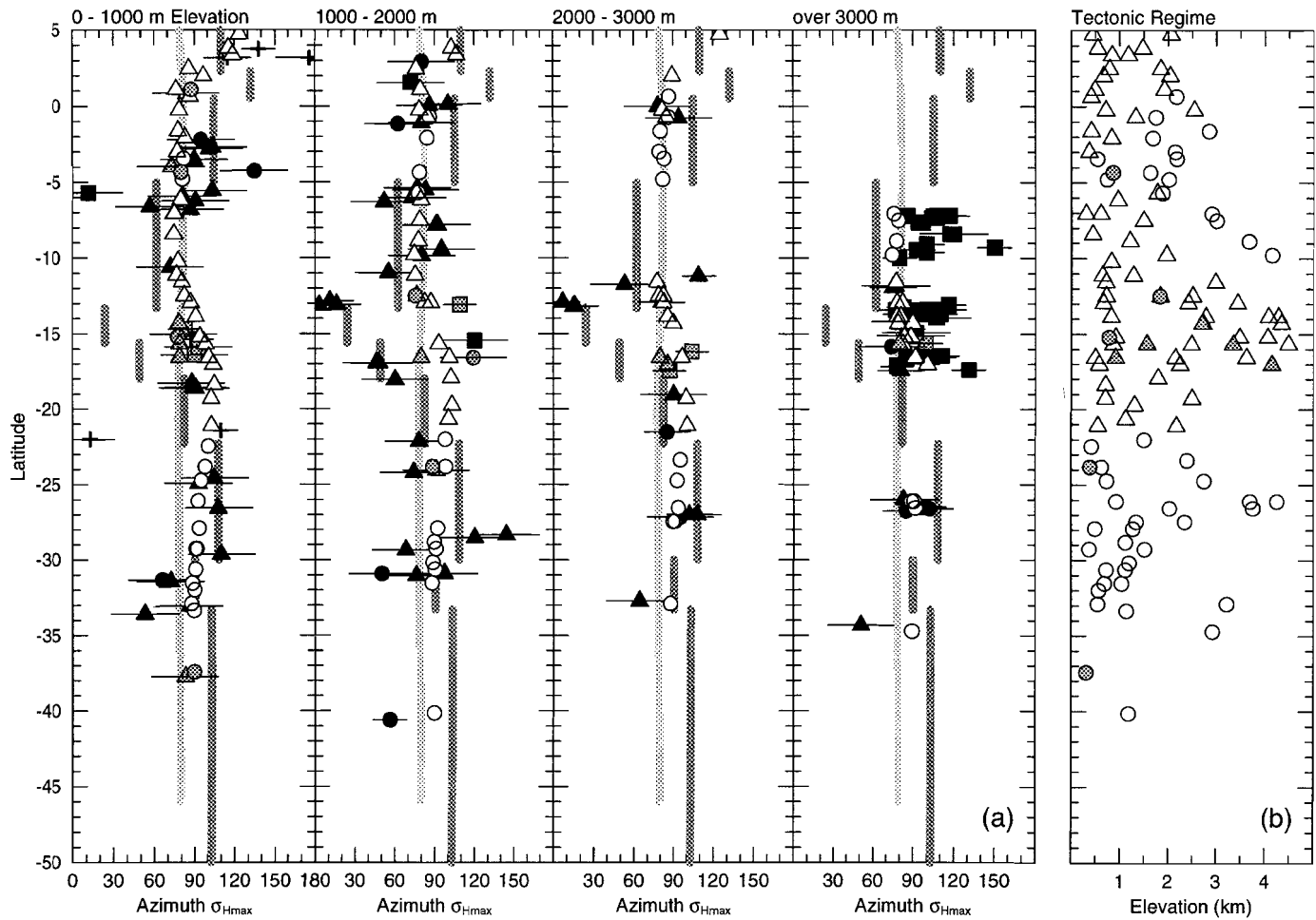


Fig. 3.15. Modelled intra-plate stress field. No basal shear; azimuth F_{Car} is N150°E.



observed and modelled tectonic regime we note two aspects. Firstly, the model predicts strike-slip in the southern Andes where reverse faulting is observed to prevail. Secondly, the model fails to match the occurrence of normal faulting above 3 km (compare Figures 3.16b and 3.4b).

For each of the focal mechanisms in the Andes south of 5°N we calculated slip vectors on both nodal planes using the state of stress obtained for the element in which the given epicentre is located. No discrimination is made between focal mechanisms of single events or average focal mechanism solutions. The result is displayed in Figure 3.17. The left panel corresponds to the nodal planes yielding the smallest angular misfit; the right panel gives the maximum misfit encountered. Angular misfit is plotted as a function of the latitude of the epicentres. We infer that, for the reference model, minimum misfit is mostly less than 20°-30°. In view of the uncertainties involved this may be considered a reasonable match. Larger misfits occur in the latitude range 20°S-35°S. The latter expresses the fact that in this region the model predicts strike-slip while reverse faulting is observed.

Evaluation of Results Part I

Basal shear stress. The model experiments suggest that observations of the actual intra-plate stress field should provide us with some constraint on the nature of the basal drag force. Most sensitive to changes in basal shear are the magnitude of roughly E-W compression inwards of the western margin and the orientation and magnitude of compression in northwestern South America. In view of the either very small (when σ_{dr} is 0 bar) or very large (when σ_{dr} is +5 bar) compression due to F_{Car} in case the Chase (1978a) pole is adopted, this absolute motion model may be considered unlikely. However, for smaller values of driving basal shear the dependence on absolute motion is found to be less pronounced, inhibiting an unambiguous conclusion. The experiments adopting the HS2-NUVEL1 pole demonstrate that in this case the orientation of compression near the western margin is largely insensitive to the value of basal shear stress. In contrast, the *magnitude* of compression is strongly dependent on σ_{dr} .

Northwestern South America. Variation of the azimuth of F_{Car} is found to have a pronounced effect on the intra-plate stress field and observations regarding the

Fig. 3.16. (previous page) (a) Modelled orientation of the principal axis of maximum horizontal compression as indicated by open symbols overlying a plot of observations identical to Figure 3.4. The type of symbol used to indicate the model result denotes the modelled tectonic regime which is determined as follows, both principal stresses compressive: reverse faulting (triangle); one axis compressive and the other tensile: strike-slip faulting (circle); both axes tensile: normal faulting (square). Model results are shown at latitude of element centres. (b) Separate depiction of *modelled* tectonic regime as a function of latitude and topographic elevation (averaged over element).

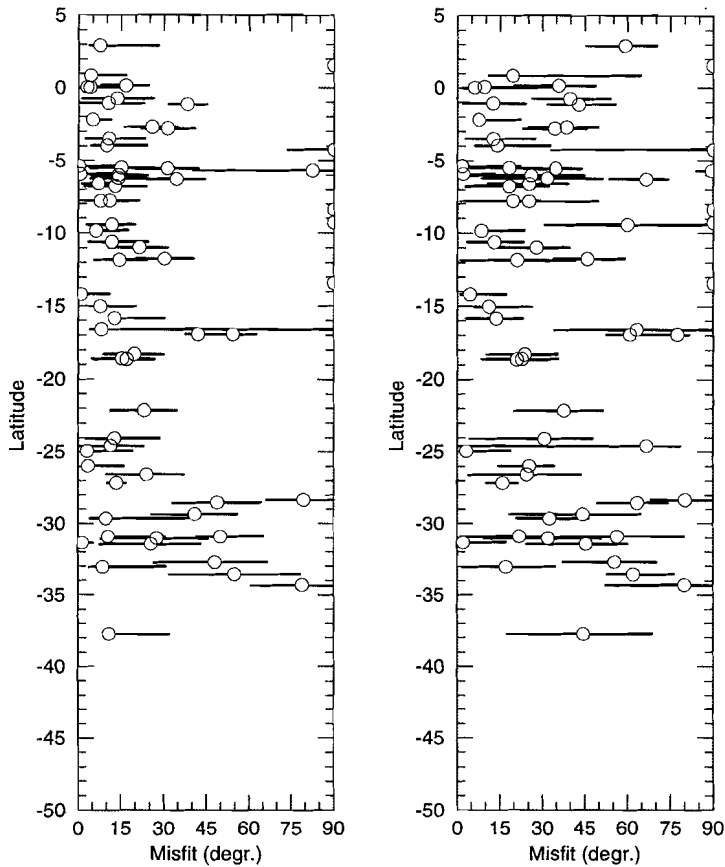


Fig. 3.17. Result of slip vector calculation for the earthquake mechanisms observed in the Andes using the stress field derived with the reference model. Shown is the absolute value of the angle between observed and modelled slip vector as a function of latitude of the earthquake epicentre. Slip vectors are computed for both nodal planes of a given mechanism; the lowest misfit value is plotted in the left panel, the highest misfit in the right panel. Horizontal bars give the range in misfit when the fault strike and fault dip are varied over $+10^\circ$ and -10° .

latter should offer an important constraint. Figure 3.18 shows in detail the modelled stress field for northwestern South America, obtained for each of the considered azimuths of F_{Car} . A first observational constraint concerns the direction of slip along the eastern boundary of the North Andes block. In reality there

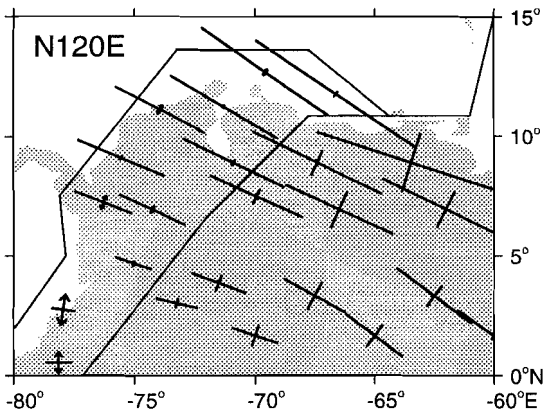
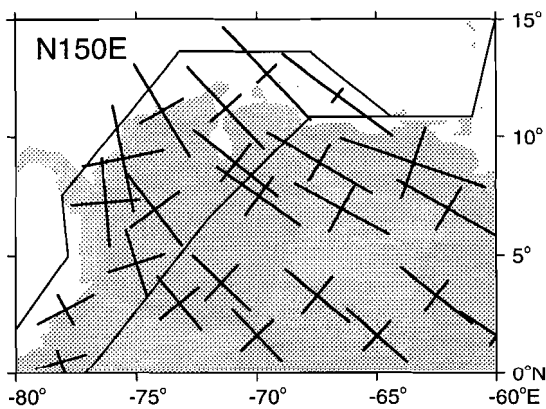
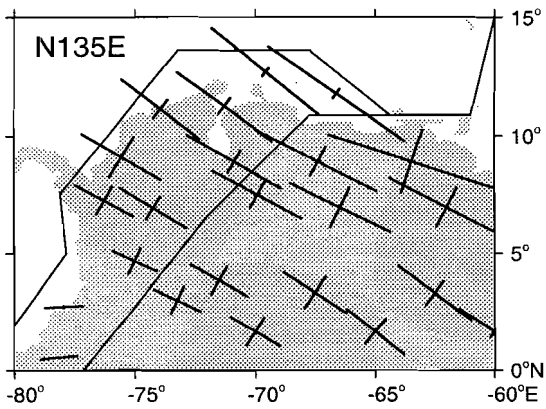


Figure 3.18. Intra-plate stress field calculated for the northwestern part of South America for three different orientations of the "Caribbean resistance" (F_{Car}).



occurs a dextral component of strike-slip along this roughly NE-SW trending fault which implies that the axis of maximum compression near the fault must be rotated anti-clockwise with respect to the normal to the fault. Obviously, this condition is satisfied by the model in which F_{Car} is orientated towards N120°E. However, Figure 3.18 shows that this condition is also satisfied when F_{Car} is taken towards N135°E because the orientation of compression changes with increasing distance from the Car-SAm boundary: a rotation of the axis of maximum compression occurs due to F_{pcr} exerted in the Colombia trench. The model with F_{Car} directed towards N150°E would predict a sinistral component of motion along the eastern boundary of the North Andes block near latitude 5°N which argues against this orientation.

The stress indicators available for the northwestern continent exhibit a large scatter and offer little constraint (Figure 3.5). Whereas relatively few orientations south of N135°E are found this does not preclude the model with F_{Car} directed towards N150°E because of the stress rotation mentioned before. Many of the available observations indicate the existence of a strike-slip regime. Although the model results demonstrate a gradual decrease of compression in the direction normal to the maximum horizontal compressive stress when F_{Car} is rotated anti-clockwise, none of the models predicts significant horizontal tension in that direction. Partly, this apparent discrepancy is due to the fact that our models predict stress while the observations - mostly earthquake focal mechanisms - express strain. This is demonstrated in Figure 3.19 which shows the result of slip vector calculation on several representative "synthetic" fault planes using the model-derived stress field in case F_{Car} is orientated due southeast. In particular on steeply dipping E-W striking faults such as observed in northern Venezuela, the modelled stress field would cause predominantly strike-slip motion in agreement with the data. It proved not possible to choose a preferred orientation of F_{Car} on the basis of slip vector calculation for the observed nodal planes.

An important constraint on the azimuth of F_{Car} is further provided by the observed state of stress along the western margin of the South American plate. Since there is no evidence for the major N-S tension predicted by the associated model, an orientation of F_{Car} towards N120°E appears unlikely. In conclusion we may state that, given the assumption that basal shear may be neglected, the orientation of F_{Car} is most likely close to N135°E.

Amazon basin. None of the models matches the NNE-SSW orientation of compression in the Amazon basin that is evidenced by two earthquake focal mechanisms and several borehole breakouts (Figure 3.1). *Zoback and Richardson* (1995) suggested that this orientation results from a rotation of the regional stress field caused by stresses that arise locally due to the density anomaly associated with the Amazon rift. These authors estimated the relative magnitude of the two superimposed stresses assuming that regional compression would trend E-W. Our model calculations suggest, instead, that regional compression is orientated

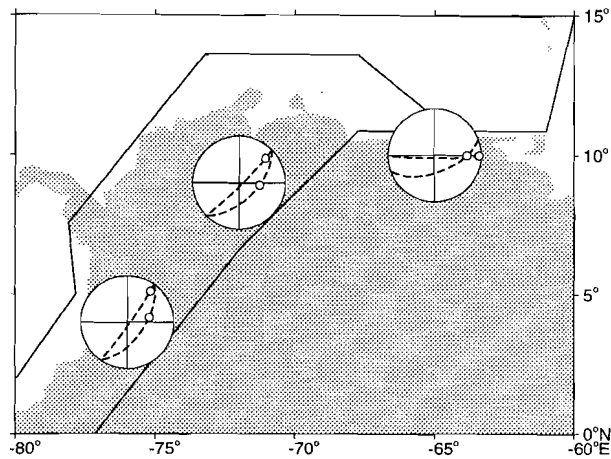


Fig. 3.19. Slip vectors (white dots) calculated for six imaginary but representative fault planes (dashed great circles) in northwestern South America on the basis of the stress field of the reference model. Dashing indicates that great circles plot in upper hemisphere of equal-area projection. Faults dip either 60° or 85°.

WNW-ESE to NW-SE due to the influence of F_{Car} . Thus, although there is still reason to believe that the density structure of the rift exerts an effect on the intra-plate stress field, the estimate of the relative importance of local and regional stresses by *Zoback and Richardson (1995)* is perhaps incorrect.

Western margin. The model result that σ_{Hmax} is rotated clockwise relative to the direction of Nazca-South America convergence south of 13°S complies with the findings of *Dewey and Lamb (1992)*. These authors inferred that the assumption that compression is parallel to convergence predicts a too large component of trench-parallel strike-slip deformation along the Chilean Andes. Our calculations suggest compression is orientated closer to the direction normal to the margin which would reduce the predicted component of strike-slip.

General. Not matched by any of the models discussed so far, are the tension observed in the high Andes and the occurrence of tension orientated perpendicular to the coast in northern Brazil.

Analysis II. Additional Plate Boundary Forces

The influence on the stress field of the six plate boundary forces of second order importance defined in Chapter 2 is examined by adding them one by one to the reference model. The magnitudes we will adopt for the additional forces were chosen so as to clearly illustrate their effect and may in fact be larger than in reality (i.e. assuming they act in the first place).

Figure 3.20 shows the effect of a trenchward pull on the South American plate in the Lesser Antilles subduction zone ($F_{LA'}$, adopted magnitude $+4 \times 10^{12}$ N/m). Eastwards of the trench tensional stresses are developed. As is true also for the other additional forces, F_{LA} not only affects the stress field in the vicinity of where it is exerted. Through its effect on the torque balance each additional force also induces changes in the magnitude of the other forces and may thus affect the overall stress field. In the present model, roughly E-W compression inwards from the west margin is larger than in the reference model. In Chile this is expressed in the form of less pronounced N-S tension. Furthermore, we observe that in response to the addition of $F_{LA'}$, compression due to F_{Car} becomes larger. The effect of incorporating a resistive F_{LA} is not shown here; it is similar to the case of a westward directed shear on the South America - North America boundary studied below.

As in the previous model, incorporation of a pull in the South Sandwich subduction zone (F_{SS} , adopted magnitude $+4 \times 10^{12}$ N/m) results in tensional stresses in the adjacent part of the plate (Figure 3.21). In contrast, whereas we are again adding a driving force, incorporation of F_{SS} does not result in a stronger compression elsewhere in the plate. Compression is amplified only near the Scotia-South America boundary. Along the western margin compression is even reduced relative to the reference model. We will not consider the situation in which the South American plate experiences a resistive force in the South Sandwich subduction zone. Such resistance would have to be caused by the mantle resisting slab penetration or originate at the contact between downgoing and overriding lithosphere. The observation that the South Sandwich subduction zone retreats eastwards, with the upper plate being characterised by back-arc spreading, renders it unlikely that such resistance is present in reality.

The inclusion of an outward pull, or "suction", normal to the central segment of the western plate margin (F_{suc} , adopted magnitude $+2 \times 10^{12}$ N/m) results in tensional stresses directed towards the loaded segment (Figure 3.22). The effect of F_{suc} on the torque balance is restricted to an increasingly resistive F_{per} . Consequently, E-W compression inwards of the west margin is larger than in the reference model north and south of the segment subject to pull.

As a second modification of the forces exerted on the overriding margin we have considered in Chapter 2 the possibility of an increased plate contact resistance on the southernmost Chile segment (F_{Chi} , adopted magnitude -3×10^{12} N/m). Incorporation of F_{Chi} results in increased compression near the southern

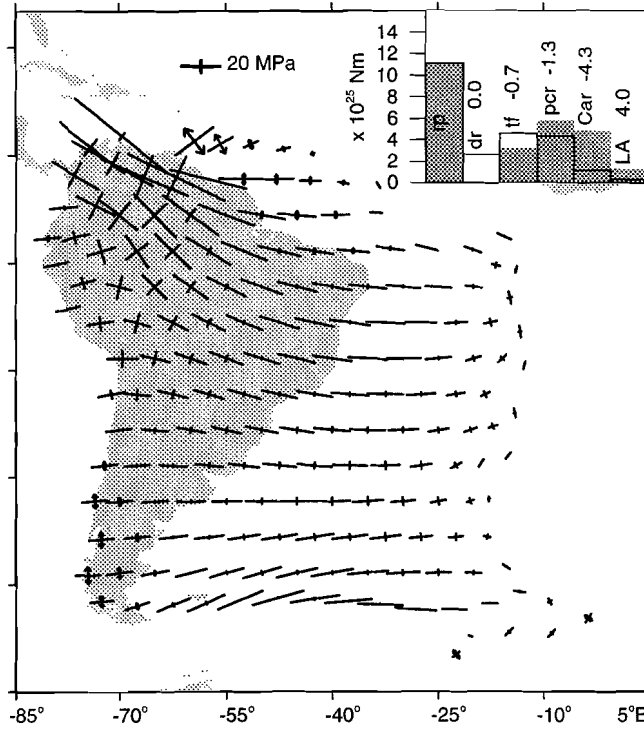


Fig. 3.20. Modelled intra-plate stress field. No basal shear; azimuth F_{Car} is N135°E. Included is additional force F_{LA} .

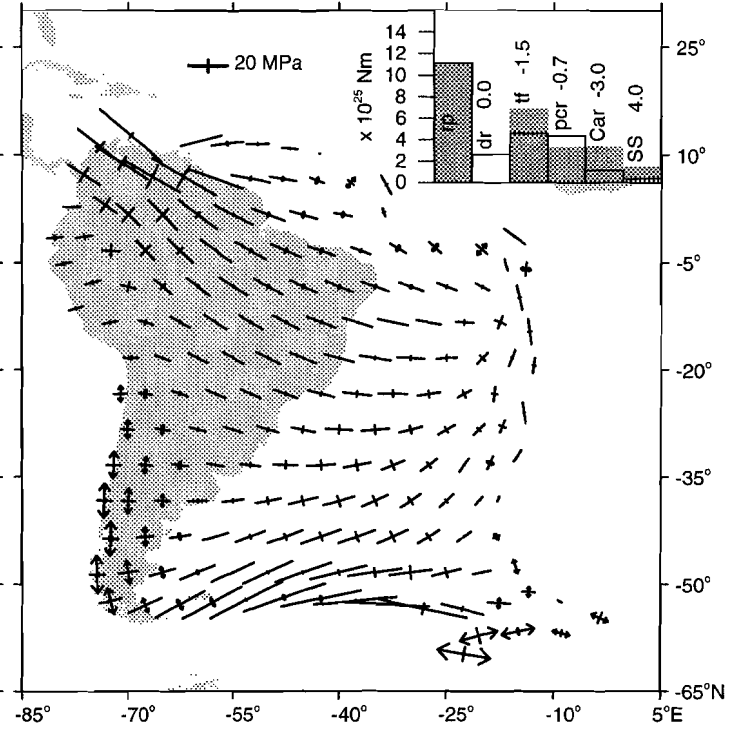


Fig. 3.21. Modelled intra-plate stress field. Included is additional force F_{SS} .

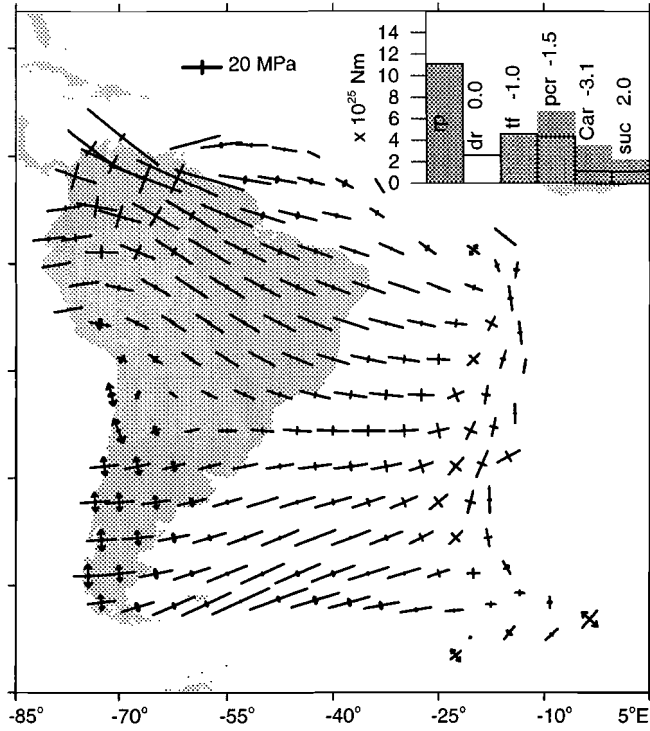


Fig. 3.22. Modelled intra-plate stress field. Included is additional force F_{suc} .

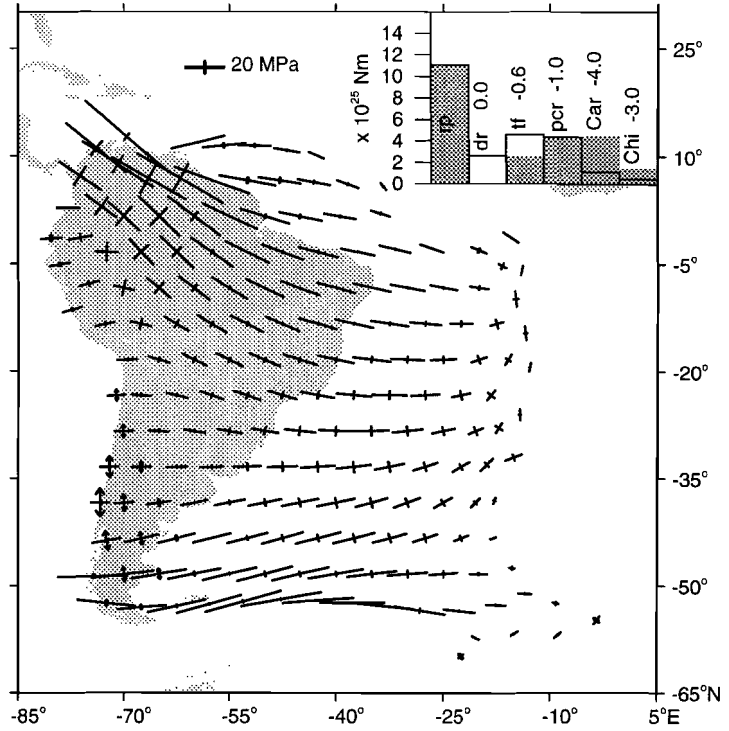


Fig. 3.23. Modelled intra-plate stress field. Included is additional force F_{Chi} .

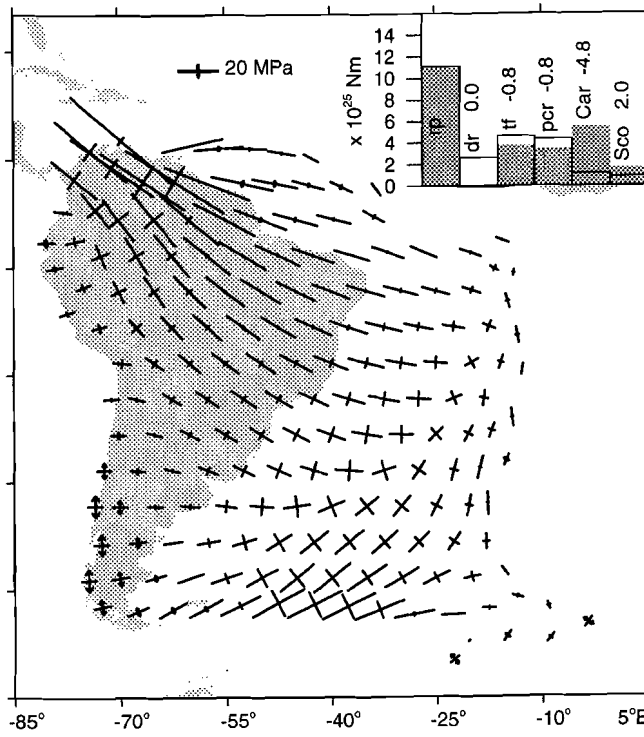


Fig. 3.24. Modelled intra-plate stress field. Included is additional force F_{Sco} .

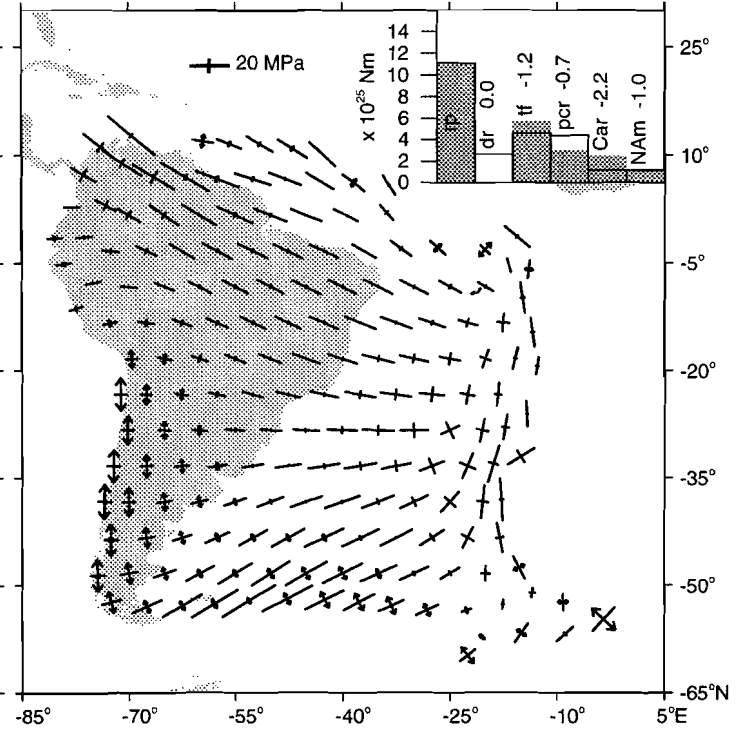


Fig. 3.25. Modelled intra-plate stress field. Included is additional force F_{NAM} .

plate margin (Figure 3.23). Regarding the torque balance, F_{Chi} is found to take over part of the contribution otherwise provided by F_{if} . This can be explained by the fact that the South America-Scotia boundary forms a major contribution to the total transform fault torque and the fact that the eastward transform shear along this margin can be replaced by an eastward directed force at the southernmost segment of the western margin. The effect of F_{Chi} on the orientation of compression near the west margin is small.

Observations suggesting that relative motion at the eastern Scotia-South America boundary comprises a component perpendicular to the contact, led us to include the additional margin-normal force F_{Sco} . Incorporation of F_{Sco} (adopted magnitude -2×10^{12} N/m) results in a rotation of the axis of maximum compression in the southeastern part of the plate (Figure 3.24). Through its effect on the torque balance, F_{Sco} leads to a stronger compression due to F_{Car} .

Finally, we assess the effect of an additional margin-parallel force on the North America-South America contact, F_{NAm} . When included as a westward directed force, i.e. driving plate motion, F_{NAm} (adopted magnitude $+1 \times 10^{12}$ N/m) proves to have a similar effect as F_{LA} (see Figure 3.20). When, instead, F_{NAm} is taken to act in eastward direction (adopted magnitude -1×10^{12} N/m) we obtain the stress field shown in Figure 3.25. F_{NAm} now results in a strike-slip regime with NW-SE orientated compression near the plate contact. Its effect on the other forces consists of a marked decrease of importance of F_{pcr} and F_{Car} which is clearly expressed in the stress field. The induced stronger transform fault resistance results in a strike-slip regime near the southern plate boundary.

Evaluation of Results Part II

Of all additional forces studied, only F_{suc} is exerted on a plate boundary segment near to which observations of the stress field are available. The observations in the central Andes do not display the stress pattern found to be characteristic for F_{suc} . Although the magnitude of F_{suc} included in our experiment may be too large, any value will result in a decreased match with the data. It follows, therefore, that F_{suc} is unlikely to be present in reality. The importance of the remaining additional forces can only be commented upon on the basis of the influence they exert on the stress field by inducing changes in the magnitude of the forces of first order significance. No firm conclusions can be drawn. The reduction of N-S tension in Chile resulting from F_{LA} and westward directed F_{NAm} leads to an improved match with the observations which could mean that these forces are indeed present in reality. In contrast, F_{SS} and eastward directed F_{NAm} further amplify the N-S tension which argues against the presence of these forces. Whether F_{Sco} occurs in reality remains unresolved. There is no observational evidence from the South American plate to confirm or deny the presence of F_{Chi} . However, the notion that transform faults are generally observed to be weak, could offer an argument in favour of F_{Chi} in view of the fact that incorporation of F_{Chi} considerably reduces the magnitude of F_{if} .

Analysis III. Lateral Variation of Plate Contact Resistance

The experiment with additional force F_{Chi} formed a first departure from the situation with a uniform magnitude of the plate contact resistance on the western margin. In this section, again on the basis of the reference model defined earlier, we will explore several other possible types of lateral variation of F_{per} . These force models were not yet defined in Chapter 2 and the associated net torques have been listed in Table 3.2.

Table 3.2. Additional Torque Data

Force	T_1 10^{25} Nm	T_2 10^{25} Nm	T_3 10^{25} Nm	Magnitude 10^{25} Nm	Longitude °E	Latitude °N
<i>Lateral Variation of F_{per}</i>						
Uniform Magnitude	0.296	1.722	-4.001	4.366	80.2	-66.4
Only Steep Segments	0.154	1.288	-2.633	2.935	83.2	-63.8
Only Flat Segments	0.142	0.434	-1.368	1.442	71.9	-71.5
Linear Age Dependence	-0.126	-0.884	2.045	2.231	-98.1	66.4
1/age Dependence	0.792	4.055	-9.583	10.436	78.9	-66.7
Latitude Dependence	0.202	0.875	-2.129	2.311	77.0	-67.1
<i>Effects of Continent-Ocean Transition</i>						
Passive Margin	0.063	-1.929	3.927	4.376	-88.1	63.8
Active Margin	-0.192	1.558	-3.762	4.076	97.0	-67.4

T_1 , T_2 , and T_3 are components of torque vectors in a Cartesian frame with x_1 : 0°E, 0°N; x_2 : 90°E, 0°N; x_3 : 90°N. The manner in which these torques are defined is explained in the text.

F_{per} Dependent on Slab Dip or Slab Age

Regarding subduction zones in general, the tectonic regime of the overriding margin has been found to correlate with the dip of the downgoing slab. Extensional "Marianas-type" overriding margins are mainly situated over steeply dipping plates whereas compressional "Andean-type" margins tend to develop over slabs that dip more shallowly (Molnar and Atwater, 1978; Uyeda and Kanamori, 1979; England and Wortel, 1980). Likewise, lateral changes in the geology of the Andes have been attributed to a segmentation of the Nazca plate in the direction parallel to the trench (e.g. Jordan et al., 1983). Generally speaking, the age of the descending lithosphere and the rate of convergence are considered to be the primary controls on slab dip (Wortel and Vlaar, 1978). In the case of subduction below the west margin of South America only slab age can contribute to the segmentation: the rate of convergence of the Nazca plate and South America changes little along their contact (Wortel, 1984; Wortel and Cloetingh, 1985). Only in the southernmost Chile trench, where the approaching oceanic lithosphere is part of the Antarctic plate, does convergence occur at a deviating, much slower, rate (see Figure 2.1).

Dependence on slab dip. Instead of making the magnitude of F_{per} proportional to the actual angle of dip of the descending slab we simplify the situation by differentiating between a value characteristic for “flat” segments and a value typical for “steep” segments (Figure 3.26). This approach is warranted by the fact that the angle of dip exhibited by the steep segments falls in a narrow range (25° - 35°) while at both flat segments the slab is orientated subhorizontally. Moreover, transition between the various segments occurs over relatively short distances. The upper plate may experience a larger resistance due to convergence at segments of flat subduction due to two reasons: (1) When subduction occurs under a shallow angle the interface between downgoing and overriding plate is larger than in the case of steep subduction. (2) To the extent that shallow dip angles result from the subduction of young lithosphere, the flat segments will be subject to a relatively high normal pressure, resulting from the small gravitational instability of the downgoing plate.

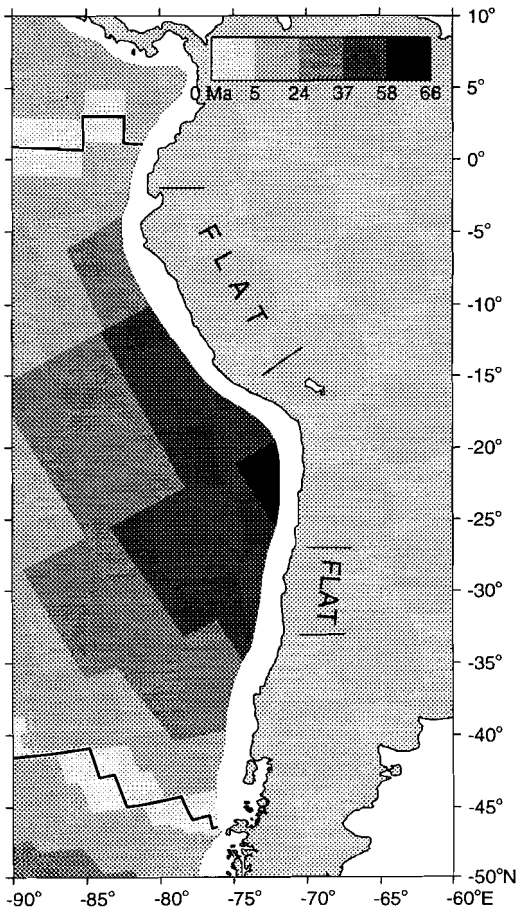


Fig. 3.26. Age distribution of the oceanic lithosphere adjacent to the western margin of the South American plate (Larson *et al.*, 1985). Also shown is the location of two segments of the Peru-Chile trench where subduction occurs at very shallow angle.

In modelling we consider the extreme situation and assume all plate contact resistance to be provided by the segments of flat subduction. Therefore, the segmentation of the subducting plate is reflected markedly in the distribution of the nodal point forces on the western margin (Figure 3.27a). The orientation of the corresponding torque vector (Table 3.2) deviates somewhat from that associated with uniform F_{pcr} which results in small changes in the magnitude of F_{tr} and F_{Car} relative to their value in the reference model. The obtained intra-plate stress field shows large compression inwards from the flat segments (Figure 3.28). Relative to the reference model the maximum increase in compression is with a factor of

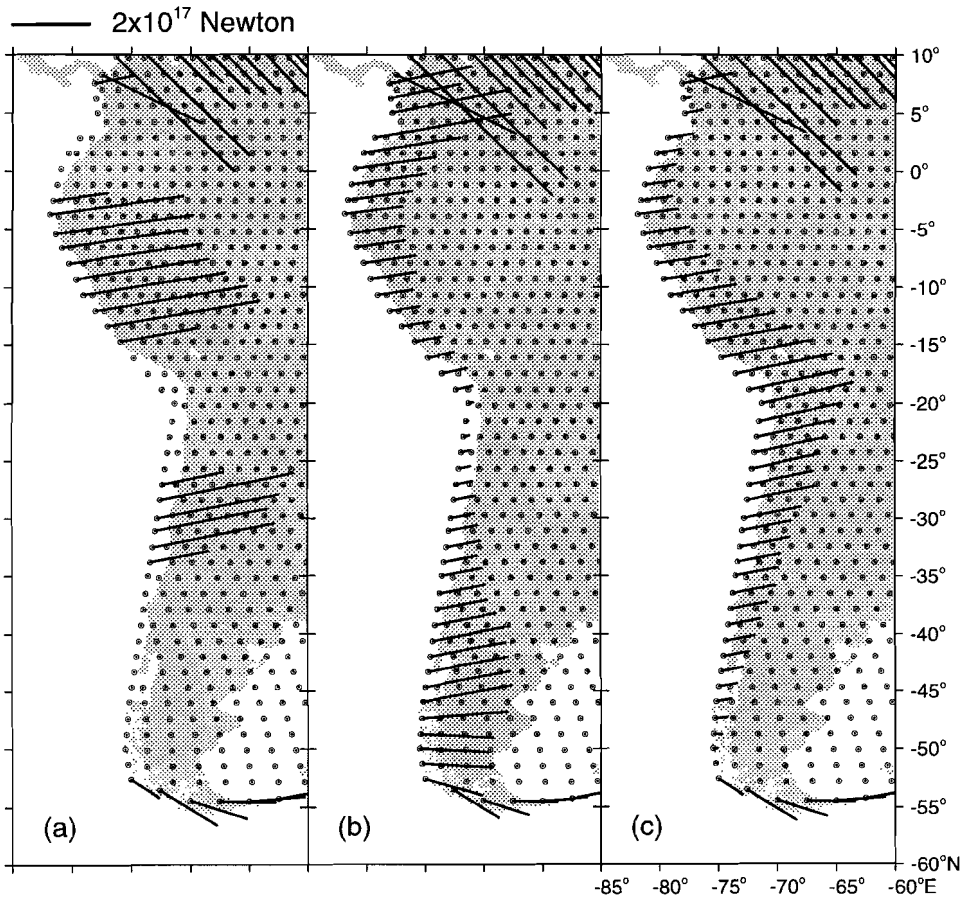


Fig. 3.27. Distribution of nodal point forces along the west margin of the South American plate for three different types of lateral variation of plate contact resistance (F_{pcr}). (a) Resistance only at segments of flat subduction. (b) F_{pcr} linearly dependent on age of the descending lithosphere. (c) F_{pcr} distributed as a function of latitude as a first approximation of the distribution suggested by *Russo and Silver (1994b)*.

about 2.7. Compression fans out from the segments of shallow subduction. N-S tension in southern Chile is much amplified.

The effect of the lateral variation of F_{pcr} on the orientation of compression is clearly illustrated by Figure 3.29. In general, the present model predicts orientations of maximum horizontal compression that deviate more from the observed orientations than does the reference model. In other words, implementation of a dependence on slab dip causes the model curves in Figure 3.29 to move away from the data. Although, in the present model the deviation is largest, the same tendency will also characterise models with less extreme differences between flat and steep segments. Most notably north of 5°S, earthquake slip vectors calculated on the basis of the model with dip dependent F_{pcr} show larger misfit angles than slip vectors associated with the reference model (not shown).

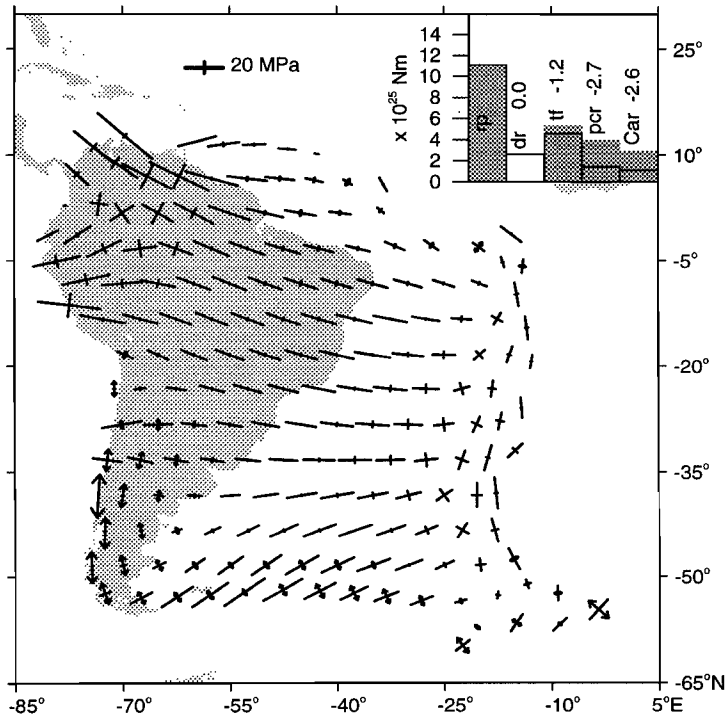
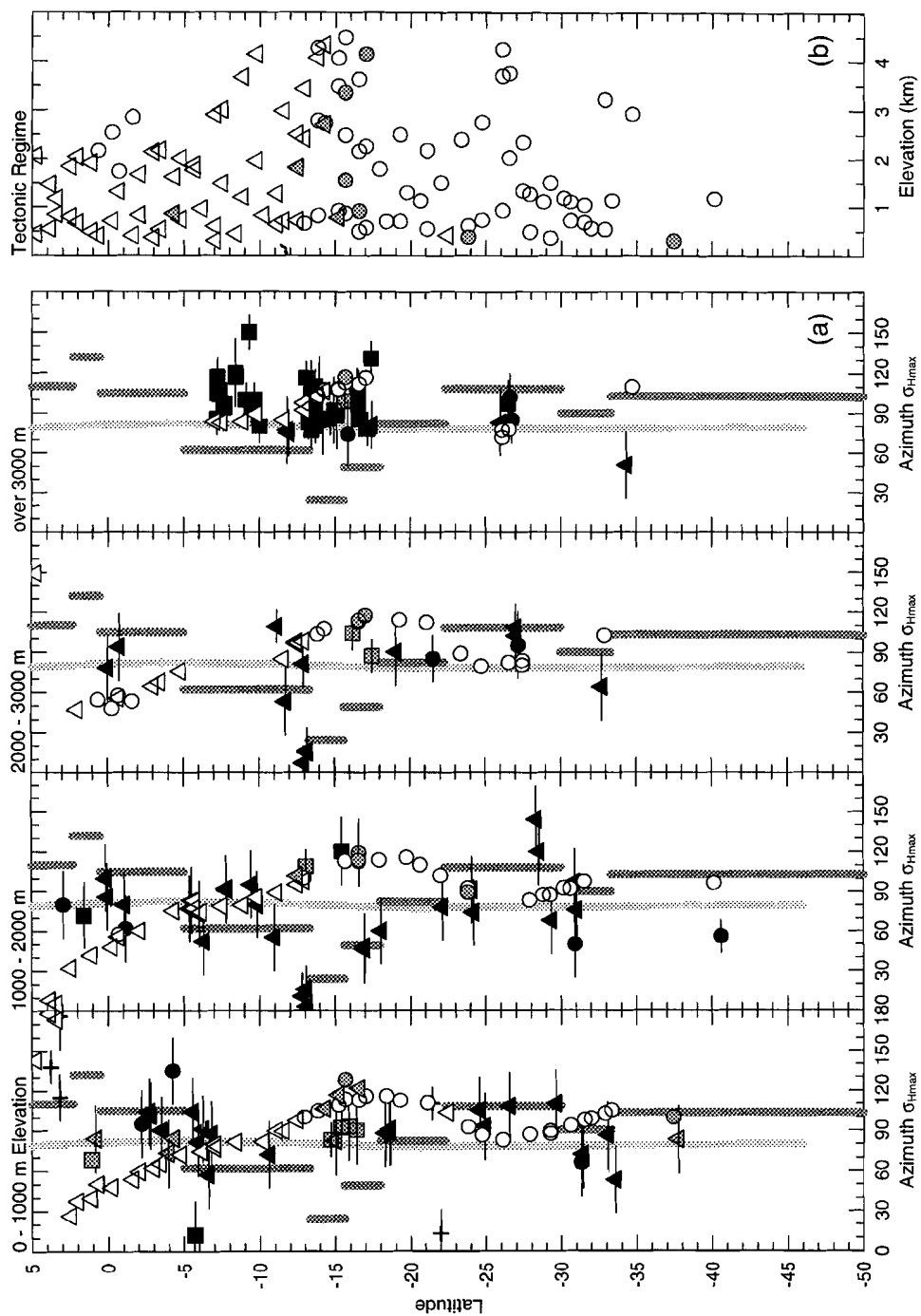


Fig. 3.28. Modelled intra-plate stress field. F_{pcr} only at flat segments.

Fig. 3.29. (next page) Modelled orientation of principal axis of maximum horizontal compression versus observed azimuth. Model incorporating F_{pcr} only at flat segments.



Dependence on slab age. For each element side situated on the western margin we determined the average age of the downgoing lithosphere using magnetic isochrons digitized from the map of *Larson et al.* (1985; Figure 3.26) in combination with a set of reconstruction poles (C.R. Scotese, personal communication, 1986). The resistance associated with convergence is expected to be inversely proportional to slab age. When downgoing lithosphere is older it is denser and has greater gravitational instability relative to the underlying mantle than young lithosphere. Consequently, older lithosphere tends to sink more rapidly which leads to steeper dip. As argued in the preceding section, steeper dip angles are associated with less resistance. We will make the assumption that there exists a linear relation between the magnitude of F_{per} and the slab age:

$$F_{\text{per}} = F^0 + \left(\frac{\text{age} - \text{age}^{\text{max}}}{\text{age}^{\text{max}} - \text{age}^{\text{min}}} \right) c F^0 \quad (1)$$

where age^{max} and age^{min} are the maximum and minimum age of downgoing lithosphere encountered (respectively 67 Ma and 2 Ma), F^0 is the value of F_{per} associated with subduction of the youngest lithosphere, and c is a value between 0 and 1 giving the fraction to which the absolute value of F_{per} is reduced at the segment where the oldest lithosphere is subducting. The value of F^0 is solved from the torque balance equation; a value for c needs to be chosen a priori. As in the previous experiment we will consider the extreme case and assume $c = 1$. This means that we assume resistance to vanish completely at the site of subduction of the oldest lithosphere. Figure 3.30 illustrates the obtained relation between F_{per} and age.

The associated nodal point forces are displayed in Figure 3.27b. Clearly expressed in the magnitude of F_{per} is the gradual increase in slab age going towards the central part of the margin. As in the case of dip dependence, the net torque of the age-dependent F_{per} deviates slightly from that associated with a

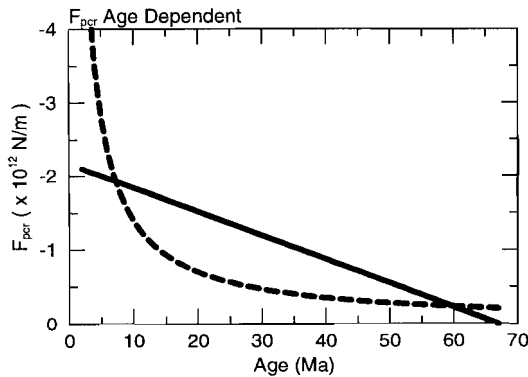


Fig. 3.30. Two alternative relations between the magnitude of plate contact resistance (F_{per}) and age of the lithosphere currently descending in the trench. Drawn line: linear dependence featured by the model of Figure 3.32. Dashed line: asymptotic relation.

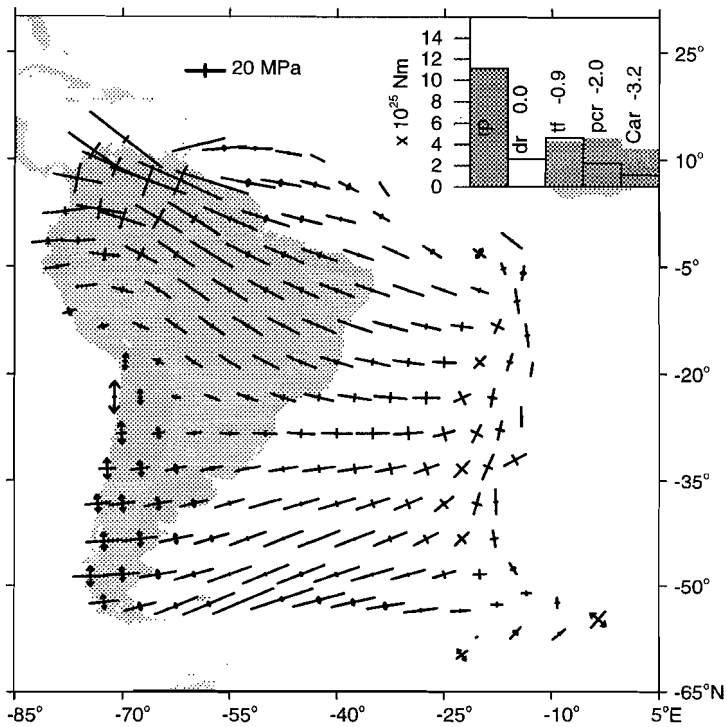
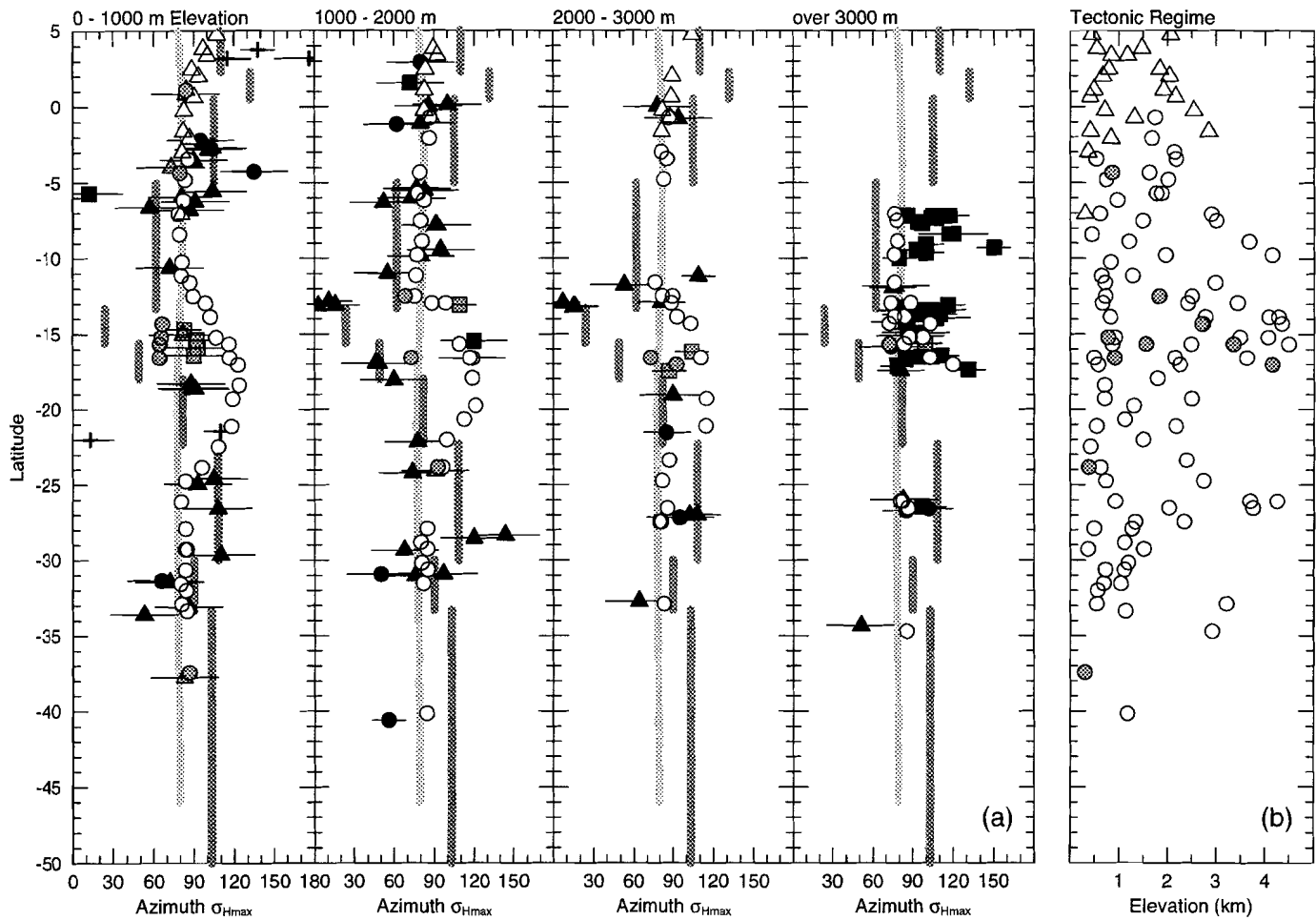


Fig. 3.31. Modelled intra-plate stress field. F_{per} dependent on age.

constant magnitude (Table 3.2). The lateral variation of F_{per} is reflected in the magnitude of roughly WSW-ENE orientated intra-plate compression near the western margin (Figure 3.31). Relative to the reference model, compression near the northern and southern end of the west margin is now about a factor 2 stronger. The lateral distribution of F_{per} causes tension orientated parallel to the strike of the margin that is largest in the central part.

A comparison of Figure 3.32 and Figure 3.16 demonstrates that the orientation of maximum horizontal compression predicted by the current model differs from that of the reference model in particular between 15°S and 25°S where there are relatively few observations. Neither the present model nor the reference model matches the available observations well. As illustrated by Figure 3.33 from about 12°S to 28°S the current model results in larger misfit to the observed earthquake slip vectors.



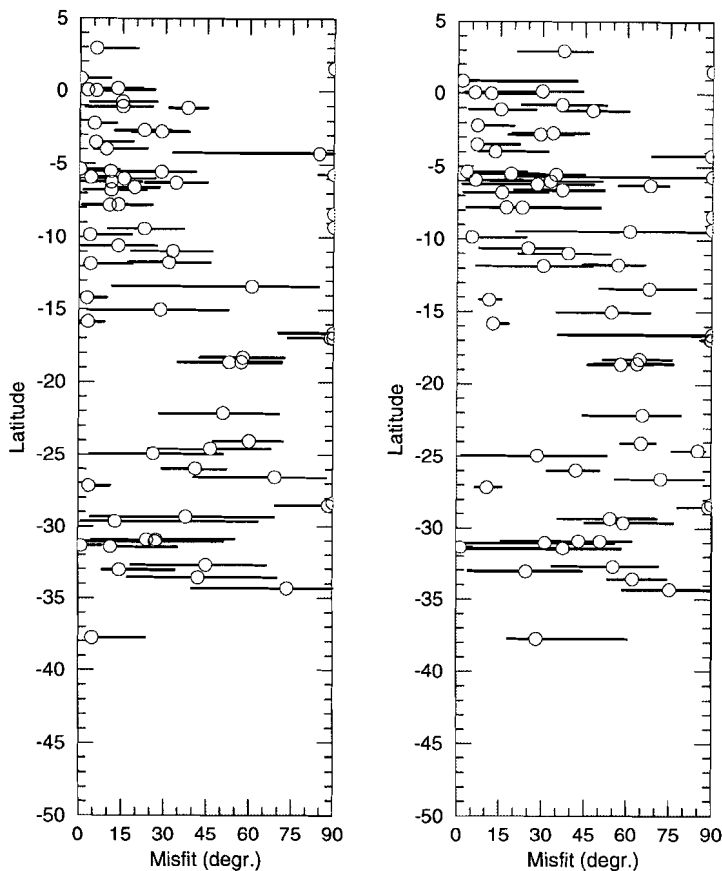


Fig. 3.33. Result of forward slip calculation using the stress field associated with age-dependent F_{pcr} .

As an alternative to the linear relation between F_{pcr} and age we have also considered a relation of the form

$$F_{pcr} = c \frac{1}{age} \tag{2}$$

In this case only one unknown is involved: the factor of proportionality c which can be solved for using the torque balance equation. The relation between F_{pcr} and

Fig. 3.32. (previous page) Modelled orientation of principal axis of maximum horizontal compression versus observed azimuth. Model incorporating age-dependent F_{pcr} .

age has also been shown in Figure 3.30. F_{pcr} is now nearly constant - at a level low compared to that found with relation (25) - for ages ranging from about 20-70 Ma. In contrast, F_{pcr} represents a large resistance for subduction of younger lithosphere. The associated torque vector nearly coincides with that corresponding to F_{pcr} of constant magnitude (Table 3.2). Adopting the 1/age dependence, differences in the value of F_{pcr} between the central segment of the overriding margin and the northern and southern end are more pronounced than in the case of the linear age dependence. Therefore, the intra-plate stress field (not shown) differs from the reference model in the same manner as the stress field derived for linear age dependence, only to a larger extent.

F_{pcr} Affected by Trench-Parallel Mantle Flow

On the basis of seismological evidence for anisotropy of the mantle underneath the subducted portion of the Nazca plate it has recently been suggested by *Russo and Silver* (1994a) that, in this region, flow in the mantle occurs parallel to the trench. The authors argue that mantle flow occurs as a consequence of the oceanward migration of the subduction zone. They envisage a flow stagnation point located somewhere halfway the horizontal extent of the trench, near latitude 20°S, from where the mantle flows sideways, i.e. north- and southwards, away from below the retreating slab. *Russo and Silver* (1994b) propose that the associated gradient in mantle pressure - high at the stagnation point, decreasing north- and southwards - is transmitted to the overriding plate via the subducting lithosphere. Thus, resistance associated with convergence is expected to be largest halfway the overriding margin of South America and should decrease going away from the central part.

As yet, it is not known how exactly the resistance on the western margin would be distributed in the case of trench-parallel mantle flow. Here we test the concept of *Russo and Silver* by constraining the magnitude of F_{pcr} to be linearly dependent on latitude λ (positive when north):

$$F_{pcr} = F^0 + \left(\frac{\lambda - \lambda^{mid}}{\lambda^{end} - \lambda^{mid}} \right) c F^0 \quad (3)$$

with

$$\begin{aligned} 0 \leq c \leq 1 \quad \text{and} \quad \lambda^{mid} = -20^\circ \\ \lambda^{end} = +9^\circ \quad \text{when} \quad \lambda \geq \lambda^{mid} \\ \lambda^{end} = -52^\circ \quad \text{when} \quad \lambda < \lambda^{mid} \end{aligned} \quad (4)$$

Thus, resistance is largest (value F^0) at latitude λ^{mid} and reduced by a factor c at the latitude of the extremities of the trench λ^{end} . We emphasize that our

experiment is not a literal representation of the configuration envisaged by *Russo and Silver* (1994b). These authors argue in terms of a resistance directed normal to the margin while we consider, as before, a resistance parallel to the direction of convergence. Moreover, Russo and Silver envisage South America to be driven westwards by asthenospheric traction whereas in the following we will assume zero basal shear stress.

As in the case of a linear dependence on slab age we will examine the extreme situation where resistance vanishes at both ends of the trench. Thus, we set c equal to 1 and solve for the value of F^0 . The resulting force distribution (Figure 3.27c) is approximately opposite to that associated with age dependence (cf. Figure 3.27b). The net torque of the latitude dependent F_{per} is orientated close to the torque vector corresponding to a uniform resistance (Table 3.2). Figure 3.34 shows the modelled intra-plate stress field. In general, the orientation of the principal stresses is not much different compared with the reference model. This is demonstrated in detail for the region of the Andes in Figure 3.35. The magnitude of compression inwards of the west margin clearly reflects the distribution of F_{per} . Near latitude 20°S compression is about a factor 1.9 larger

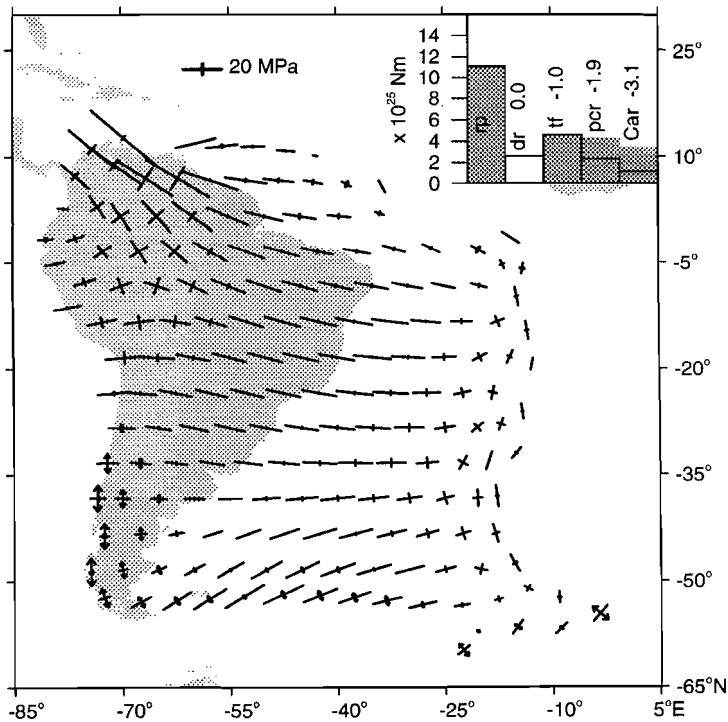
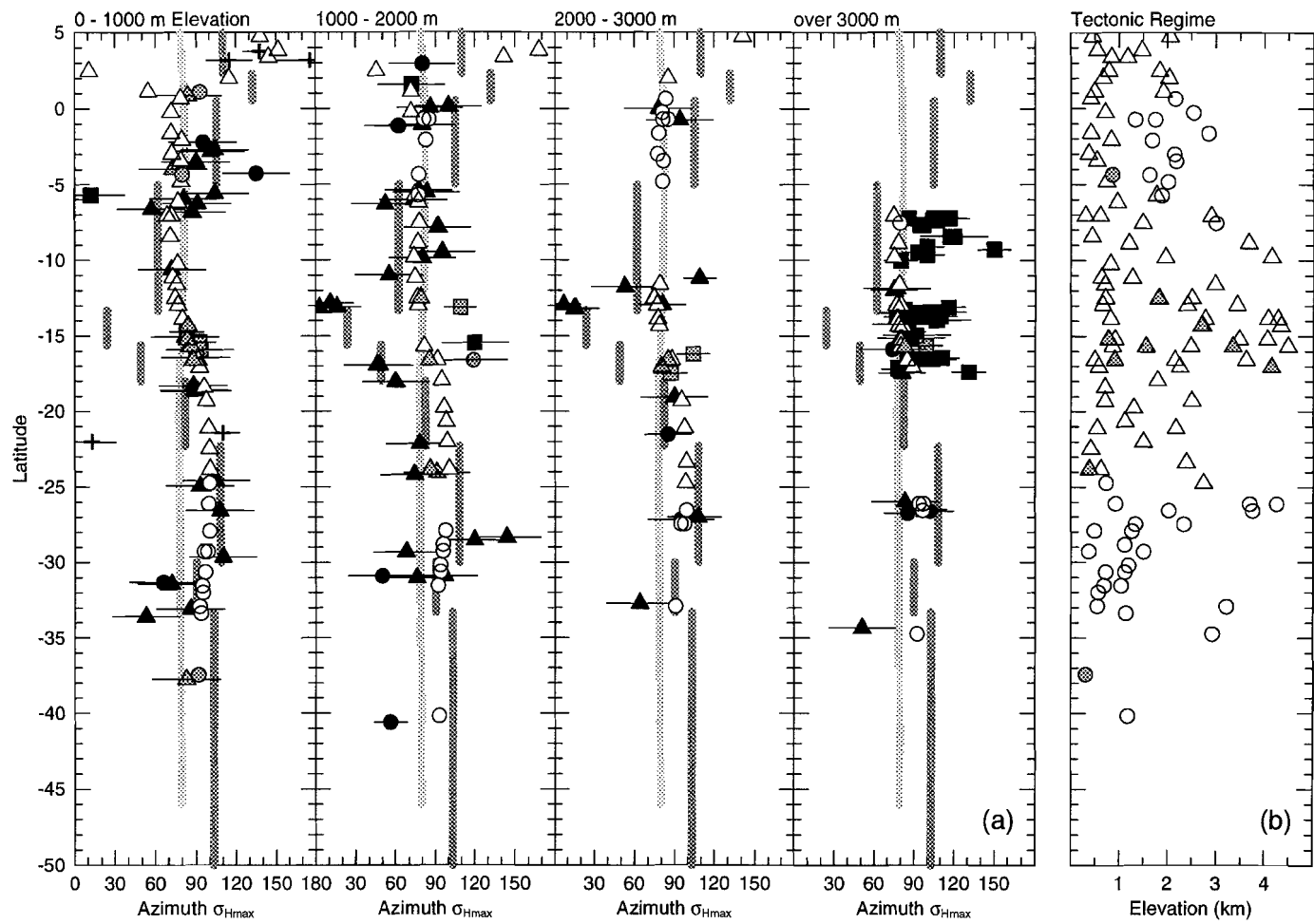


Fig. 3.34. Modelled intra-plate stress field. F_{per} dependent on latitude.



than in the reference model. The latitudinal distribution of the misfit between computed and observed earthquake slip vectors (not shown) is not significantly different from that associated with the reference model.

Evaluation of Results Part III

Under the assumption that the intra-plate stress field in western South America is mainly controlled by F_{pcr} , we can use the model results presented above to comment on the importance of lateral variation in the magnitude of this force. It would appear that the available observations rule out the possibility of a relation between F_{pcr} and slab dip. This conclusion is remarkable in view of the fact that other aspects of the overriding margin, such as topography and deformation style do seem to correlate with the dip of the downgoing plate (Jordan *et al.*, 1983; Isacks, 1988; Gephart, 1994). Furthermore, the associated increase in the misfit between modelled and observed slip vectors along part of the overriding margin argues against a dependence of F_{pcr} on slab age. In contrast, we can confirm, nor discard, the possibility of a dependence on latitude in the sense suggested by Russo and Silver (1994a, b).

Analysis IV. Effects of Continent-Ocean Transition

The Passive Margin

The passive margin of the South American continent constitutes a lateral change in lithospheric structure and may, just like the gradual increase in age of the oceanic lithosphere and the topographic high formed by the Andes, give rise to a horizontal pressure gradient. The resulting force affects both the torque balance and the intra-plate stress field. The value of the integrated vertical stress of a column of continental lithosphere is larger than the value found for a column of old oceanic lithosphere. Consequently, the gravitational forces act from the continent towards the ocean. Moreover, the forces act along gradients in integrated vertical stress and are therefore directed roughly normal to the continental margin. There is uncertainty regarding the magnitude of the force associated with a passive margin. Kuszniir (1991) gives a typical value of $1-2 \times 10^{12}$ N/m. A value of approximately 2×10^{12} N/m was inferred by Coblenz *et al.* (1994). In contrast, Fleitout and Froidevaux (1983) argue that the net force acting from continent towards ocean may well be zero. These estimates all refer to passive margins in general.

Forces associated with the continent-ocean transition can be calculated in the same manner as ridge push (Chapter 2) or the forces due to topography (this chapter). In the following, however, we will consider a simplified representation:

Fig. 3.35. (previous page) Modelled orientation of principal axis of maximum horizontal compression versus observed azimuth. Model incorporating latitude-dependent F_{pcr} .

a force of uniform magnitude exerted perpendicular to the line dividing the continental and the oceanic part of the finite element mesh (see Figure 2.2). This force, termed F_{pas} , is incorporated as a force additional to the reference model. In the experiment a magnitude of 1×10^{12} N/m is adopted. The distribution of nodal point forces is shown in Figure 3.36. Preliminary results obtained with a more realistic implementation of the continent-ocean transition indicate that the approximation as a line force is in fact rather good. Adding F_{pas} to the reference model means adding a new resistive force which takes over part of the resistance otherwise provided by F_{tf} , F_{pcr} , and F_{Car} . Since the torque of F_{pas} is orientated close to that of F_{pcr} (Table 3.2) in particular the latter resistance is much reduced. As a consequence, the intra-plate stress field displays compression near the west margin that is small in comparison with the reference model (Figure 3.37). Further east the effect of F_{pas} varies from north to south. In the northeastern part of the continent, the reference model shows predominantly WNW-ESE directed compression, the model including F_{pas} predicts an additional component of NNE-SSW directed tension. In contrast, south of about 15° S the main effect of F_{pas} consists in a marked decrease in the amount of compression on the continental side of the passive margin.

Both the reference model and the model including the effect of the passive margin match the coast-parallel orientation of the axis of maximum horizontal compression that is observed in northeastern Brazil. Whether there exists evidence for the additional component of tension found in case F_{pas} is included will be checked using fault slip vector calculation. For the events labelled 9 and 10 in Figure 3.38 the fault plane has been identified using aftershocks, for the other events both nodal planes are taken into consideration. The fault of event 10 is orientated such that the calculated slip vector displays a large scatter and this event will be disregarded. Firstly, we observe in Figure 3.38 that the reference model yields a reasonably good match between computed and observed slip vectors. Secondly, with the exception of one of the nodal planes of event 15, the fit is everywhere (slightly) improved when the effect of the passive margin is accounted for.

Regarding the observations further south along the passive margin we may note that neither the reference model nor the model including F_{pas} matches the N-S orientation of compression observed near 12° S or the NE-SW directed compression evidenced near 23° S.

The Active Margin

The overriding western margin of the South American plate constitutes an abrupt change in lithospheric structure where continental lithosphere is juxtaposed to oceanic lithosphere just as well as at the passive margin. The fact that at the overriding margin the transition between the two types of lithosphere is not continuous but occurs in the form of a fault, and the fact that this fault is not vertical but orientated such that oceanic lithosphere extends underneath a tapered

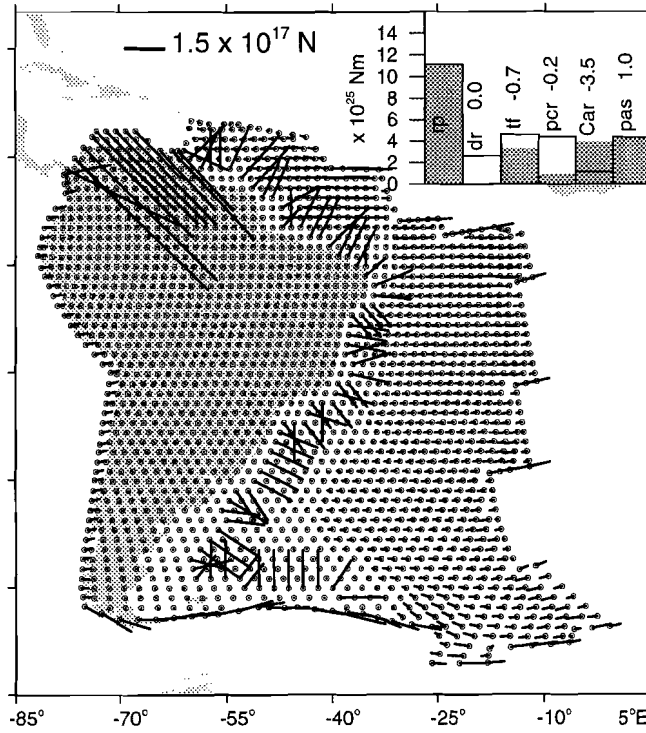


Fig. 3.36. Nodal point forces for the model incorporating the horizontal body forces associated with the passive continental margin.

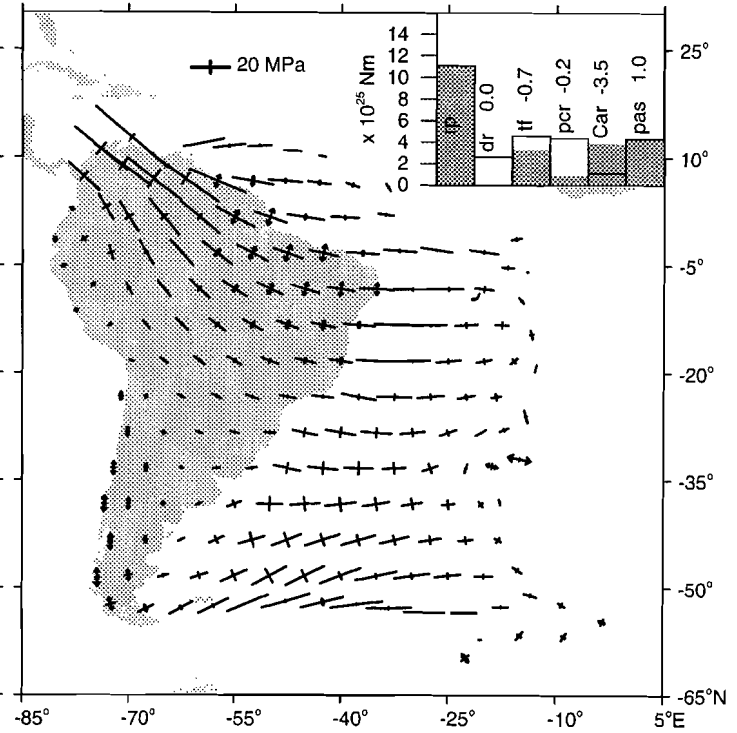


Fig. 3.37. Modelled intra-plate stress field. Model accounts for the passive margin.

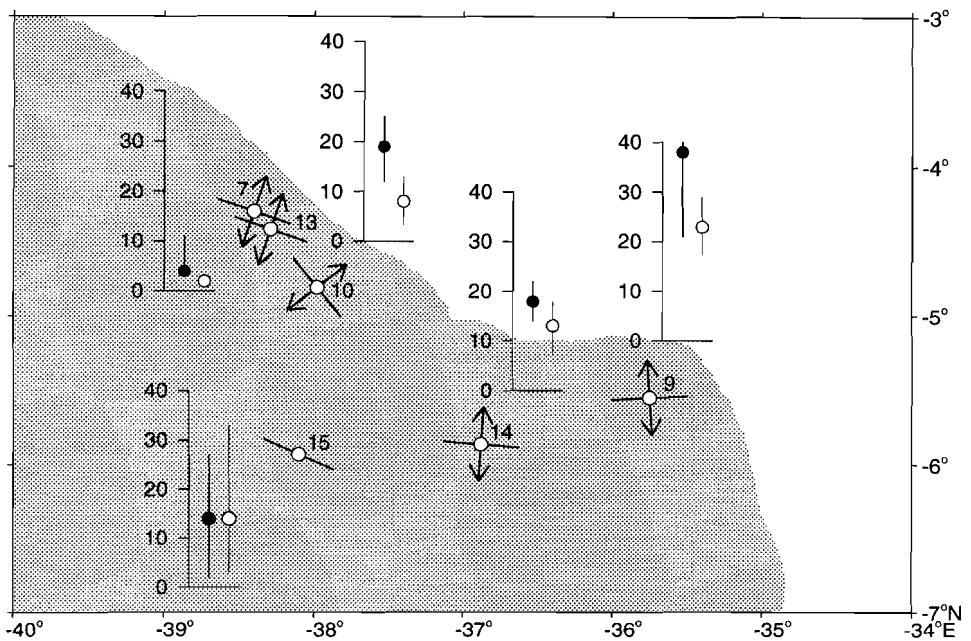


Fig. 3.38. Results of slip vector calculation for northeastern Brazil using 5 out of 6 available focal mechanisms (event labelled 10 is omitted). Diagrams shown next to the observed P- and T-axes give the misfit angle obtained for two different models of the intra-plate stress field; black dot: reference model; white dot: the model of Figure 3.37 in which the passive margin is accounted for. Vertical lines indicate the range over which misfit varies when fault strike and fault dip are varied by $+10^\circ$ and -10° .

continental edge, imply that the situation is more complex than along a passive margin. Nevertheless, it is worthwhile to investigate the hypothesis that also along the active margin the continent experiences an outward pull related to the inherent transition to oceanic lithosphere. In the following experiment we will assume the margin-normal pull is of uniform magnitude and thereby disregard the role of the lateral variation in the age of the oceanic plate at the trench. The experiment may also be regarded as a test of the finding by *Chapple and Tullis* (1977) that plate balance requires the overriding margin to be subject to a significant oceanward pull, their so-called "upper plate force". Although *Chapple and Tullis* (1977) did not consider lateral changes in lithospheric structure as the underlying cause, this upper plate force was also assumed to act normal to the margin and to be of uniform magnitude. We will not take into consideration the northwestern margin where, perhaps, the situation is comparable.

When a magnitude of 1×10^{12} N/m is adopted for the oceanward pull we obtain the nodal point forces shown in Figure 3.39. The associated torque vector is shown in Table 3.2. Via the torque balance the extra driving force mostly affects

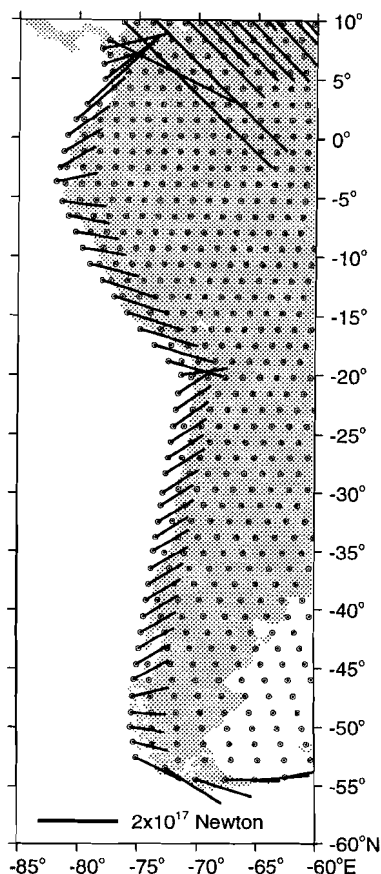


Fig. 3.39. Nodal point forces along the western plate margin for the model including an outward pull of uniform magnitude on the overriding edge.

F_{per} which becomes increasingly resistive. Therefore, the net force on the west margin is still resistive and does not - in terms of magnitude - differ much from the reference model. The fact that pull acts normal to the margin does have an effect on the orientation of the resultant force.

Associated changes in the intra-plate stress field (Figure 3.40) are most pronounced near the bend in the west margin at latitude 5°S where an additional component of NNW-SSE orientated tension is now predicted. This strike-slip regime predicted with trenchward pull is inconsistent with two focal mechanisms indicating reverse faulting near the coast. Tension inwards of the west margin in Chile is further increased relative to the reference model. Figure 3.41, showing in detail the latitudinal distribution of orientations of compression demonstrates that the effect of the pull on the west margin is small. North of 13°S misfit to the observed earthquake slip vectors is somewhat larger for the current model than for the reference model (not shown).

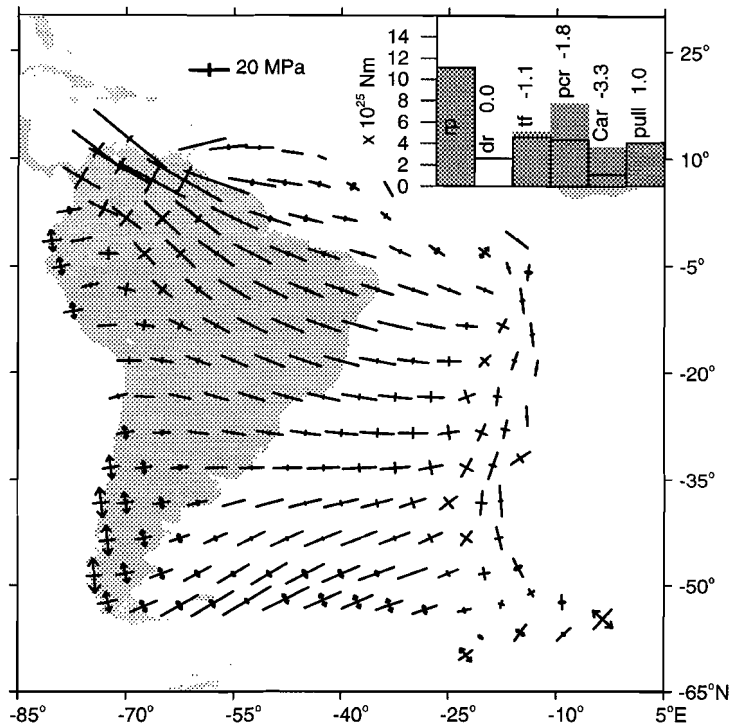


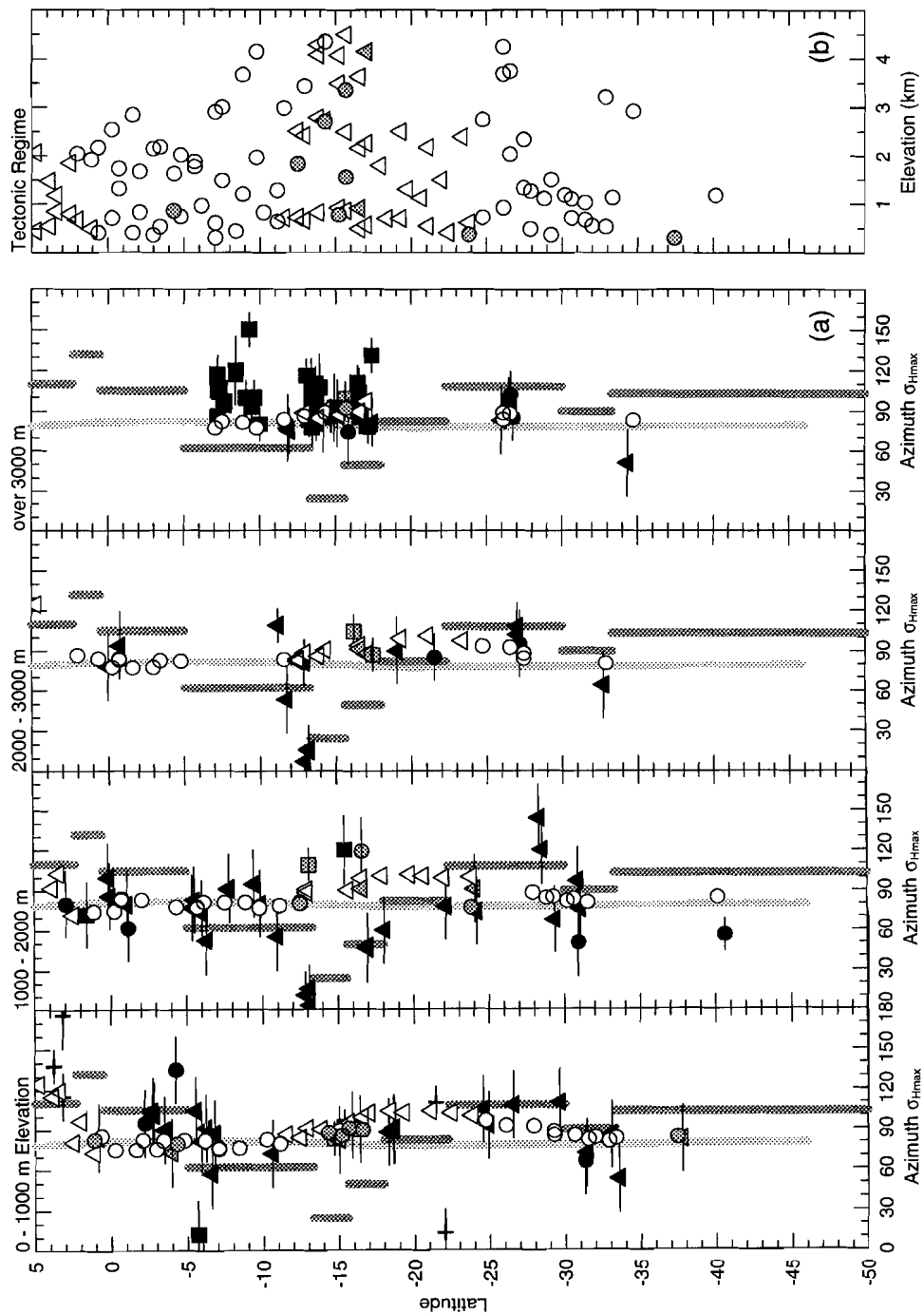
Fig. 3.40. Modelled intra-plate stress field. Including an outward pull on the western plate margin.

Evaluation of Results Part IV

Assumpção (1992) and *Coblentz and Richardson* (1992) first suggested that strike-slip faulting at the northeastern coast of Brazil expresses the combination of regional compression due to, in particular, ridge push and local tension related to the continent-ocean transition. Our model results support this notion but indicate also that the intra-plate stress field does not greatly disagree with the observations in case the continent-ocean transition is not accounted for. The latter is important with regard to estimation of the magnitude of the stresses caused by the transition. In particular, the assumption that regional compression is orientated E-W (e.g. *Assumpção*, 1992) could lead to an overestimate of the role of the passive margin.

Assumpção (1992; 1993) also envisaged that stresses caused by the passive margin would reduce compression in eastern and southeastern Brazil where the

Fig. 3.41. (next page) Modelled orientation of principal axes of maximum horizontal compression versus observed azimuth. Model with outward pull on the western margin.



coast trends roughly NE-SW and argued that this could account for the relatively low seismicity. Our calculations suggest that this effect is important only from about 15°S southwards. It was pointed by *Assumpção* (1992; 1993; see also *Stein et al.*, 1989) that flexure of the lithosphere as a result of sediment loading on the continental shelf may have a similar effect as the lateral transition in lithospheric structure.

Unfortunately, we have few observations at our disposal in the region of the bend at latitude 5°S where our calculations suggest the intra-plate stress field to be diagnostic for the occurrence of trenchward pull on the western plate margin. The available data argue against the presence of pull but a strong conclusion is not warranted.

Chapple and Tullis (1977) found that trenchward pull exceeded the resistance associated with subduction of the Nazca plate. A detailed illustration of the net force on the western margin (their Figure 6) shows trenchward directed forces except at the southernmost segment. Even without a devoted model experiment it is clear that such a force distribution is unable to account for the compression observed in the Andes.

A final remark concerns the possible role of the lateral variation in age of the oceanic lithosphere juxtaposed to the western margin. The contrast in integrated vertical stress between continental and oceanic lithosphere decreases with decreasing age of the oceanic material. Thus, assuming the structure of the continent to be the same everywhere along the active margin, trenchward pull due to the continent-ocean transition would be largest at the central segment. In this case the experiment with additional force F_{suc} may be considered an approximate representation of the situation.

Analysis V. The Effect of Topography: the Andes

Reference Model as Background

We will first explore the assumption that topography only affects the vertical component of stress (first approach). Following the procedure outlined in the section "methods" we calculate the average excess vertical stress for each element. Using these values to modify the stress field of the reference model (Figure 3.9) we obtain the stress field depicted in Figure 3.42. Comparison with the observations is illustrated by Figure 3.43. By consequence of the way topography is implemented it does not affect the orientation of the horizontal principal stresses and, in terms of σ_{Hmax} azimuth, Figure 3.42 is identical to Figure 3.16. The impact of topography on the magnitude of the principal stresses is large. Throughout much of the Andes both horizontal (non-lithostatic) principal stresses are tensional. Tension is largest in the direction where the reference model shows the least compression, i.e. in a roughly N-S direction, approximately perpendicular to the orientation of F_{pcr} and thereby to the direction of Nazca-South America convergence. Thus, the model matches well the observations of normal faulting in the high Andes apart from the already noted misfit to the azimuth of σ_{Hmax} for data from Peru. Still, in marked contradiction to the observations, the model shows normal faulting to occur also at low elevations (Figure 3.43b). As demonstrated in Figure 3.43 normal faulting prevails at all elevations above 1 km while below 1 km a strike-slip regime is predicted.

In the second approach to implementing the role of topography, the Andes contributes to the nodal point forces with which the finite element calculations are carried out (Figure 3.44). The overall shape of the cordillera is easily recognised in the associated nodal forces which, according to equation (27), are orientated in the down-slope direction. Figure 3.44 illustrates nicely the notion of a mountain range spreading sideways "under its own weight". When the net torque of the nodal forces due to topography is calculated, a vector is obtained that almost coincides with the ridge push torque. Thus, the effect on the torque balance equation of adding the topography-related forces proves to be identical to the effect of a 10% increase in ridge push. For a given value of basal shear stress the magnitude of F_{tr} , F_{pcr} , and F_{Car} is increased by 10% relative to the corresponding values in the reference model.

The stress field obtained is shown in Figure 3.45. As in the previous model, topography is found to have a pronounced effect; much of the Andes being characterised by tensional stress. The orientation of tension, however, is markedly different from that in the previous model. As a result of the outward forces, tension is largest in the direction roughly normal to the strike of the range. Also, topography is now observed to affect the state of stress in the foreland east of the Bolivian orocline. The effect of topography on the orientation of σ_{Hmax} is clearly expressed in Figure 3.46. For observations below 2 km the model matches

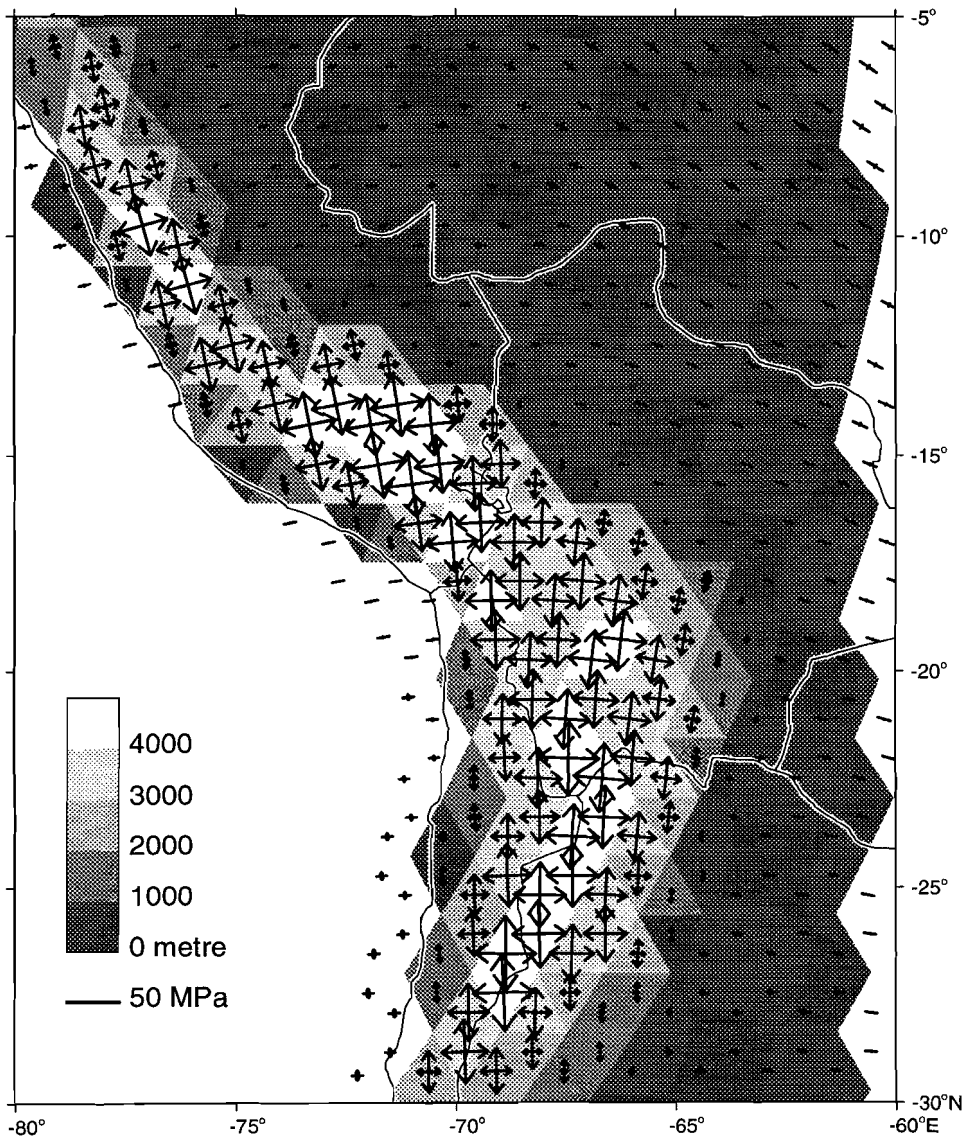
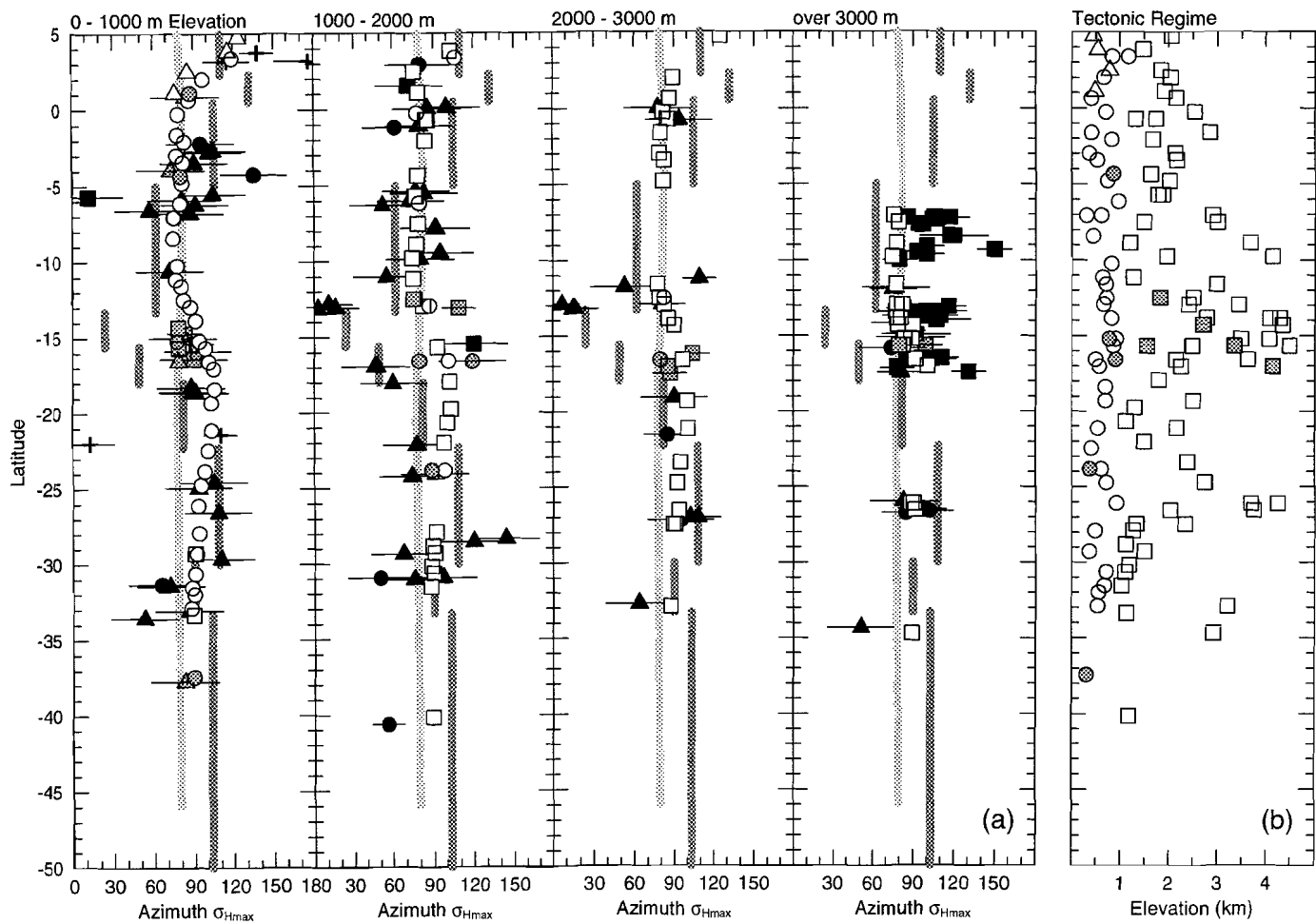


Fig. 3.42. Modelled intra-plate stress field for the central part of the Andes. No basal shear; topography affects the vertical stress only.

Fig. 3.43. (next page) (a) Modelled orientation of principal axis of maximum horizontal compression versus observed azimuth. No basal shear; topography affects the vertical stress only. (b) Modelled tectonic regime as a function of latitude and elevation.



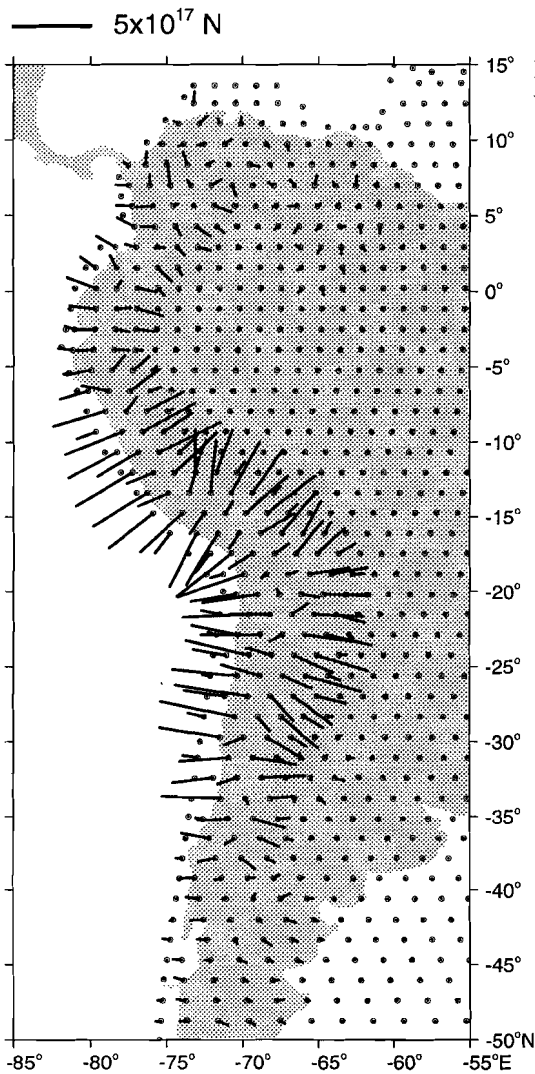


Fig. 3.44. Nodal point forces associated with the Andean Cordillera.

poorly the observed azimuth of σ_{Hmax} north of 12°S. In contrast, further south the fit is improved compared to the previous case: the model matches well the latitudinal trends in σ_{Hmax} azimuth. The same inferences pertain also to the elevation interval 2-3 km with the additional remark that the model predicts considerable latitudinal changes in σ_{Hmax} azimuth south of 22°S that can not be checked against data. Above 3 km the large cluster of observed normal faults near 15°S is matched as well by the present model as by the model where topography was assumed to affect the vertical stress only. Regarding the observations in the Cordillera Blanca region and the data from northwest Argentina, significant

differences with the present model are found. In these regions the observed orientation of tension deviates strongly from the normal-to-strike direction. With respect to the tectonic regime we find that the model is in disagreement with the observations. Already at low elevations normal faulting is predicted (Figure 3.46b) whereas in reality reverse faulting prevails (Figure 3.3 and 3.4b).

Background Model With Driving Basal Shear

This last result holds for both models examined so far and has two possible explanations. On the one hand the results may imply that we are overestimating the effect of topography, on the other that we underestimate the amount of compression due to plate tectonic forces, i.e. the amount of compression present in the reference model. Let us for the moment assume that the cause for the inferred failure of the models resides entirely on the side of the reference model. For the magnitude of intra-plate compression near the western margin to be larger it would require a more resistive F_{pcr} . Generally speaking the latter would require an extra driving force to be acting on the South American plate. In terms of our first order model such an extra driving force can only be provided by shear at the base of the lithosphere. Therefore, in this section we repeat the experiments described above now including a uniform driving basal shear stress of +5 bar.

Figure 3.47 and 3.48 show the result after incorporation of topography assuming that topography only affects the vertical stress. The average excess vertical stresses accounted for are the same as before. The orientation of σ_{Hmax} (Figure 3.48) is the same as for the corresponding model excluding topography and differs little from that obtained with zero basal shear. South of 13°S the azimuth of σ_{Hmax} is now found to deviate less from the direction of Nazca-South America convergence. Regarding the comparison with the observed σ_{Hmax} azimuth we infer the same as for the case of zero basal shear. However, with respect to tectonic regime, we find that the present model, in agreement with the observations, shows normal faulting restricted to elevations above 3 km (Figure 3.48b). At lower elevations the model still fails since it predicts strike-slip faulting.

Combining the nodal point forces due to topography calculated before (Figure 3.44) with the model where σ_{dr} equals +5 bar, we obtain the stress field shown in Figure 3.49. The presence of a larger "background" compression is expressed in the orientation of the axis of maximum tension. The latter has rotated away from the normal-to-strike direction, towards an orientation more perpendicular to the background compression. Consequently, the difference between the orientation of tension obtained via the two ways of implementing topography has become smaller. This is expressed also in Figure 3.50 which provides comparison with the data. For elevations below 2 km the trends observed in the azimuth of σ_{Hmax} south of 12°S, are matched to a lesser degree by the present model than by the corresponding model with σ_{dr} equal to zero (Figure 3.46). North of 12°S the model does better than before only for elevations between

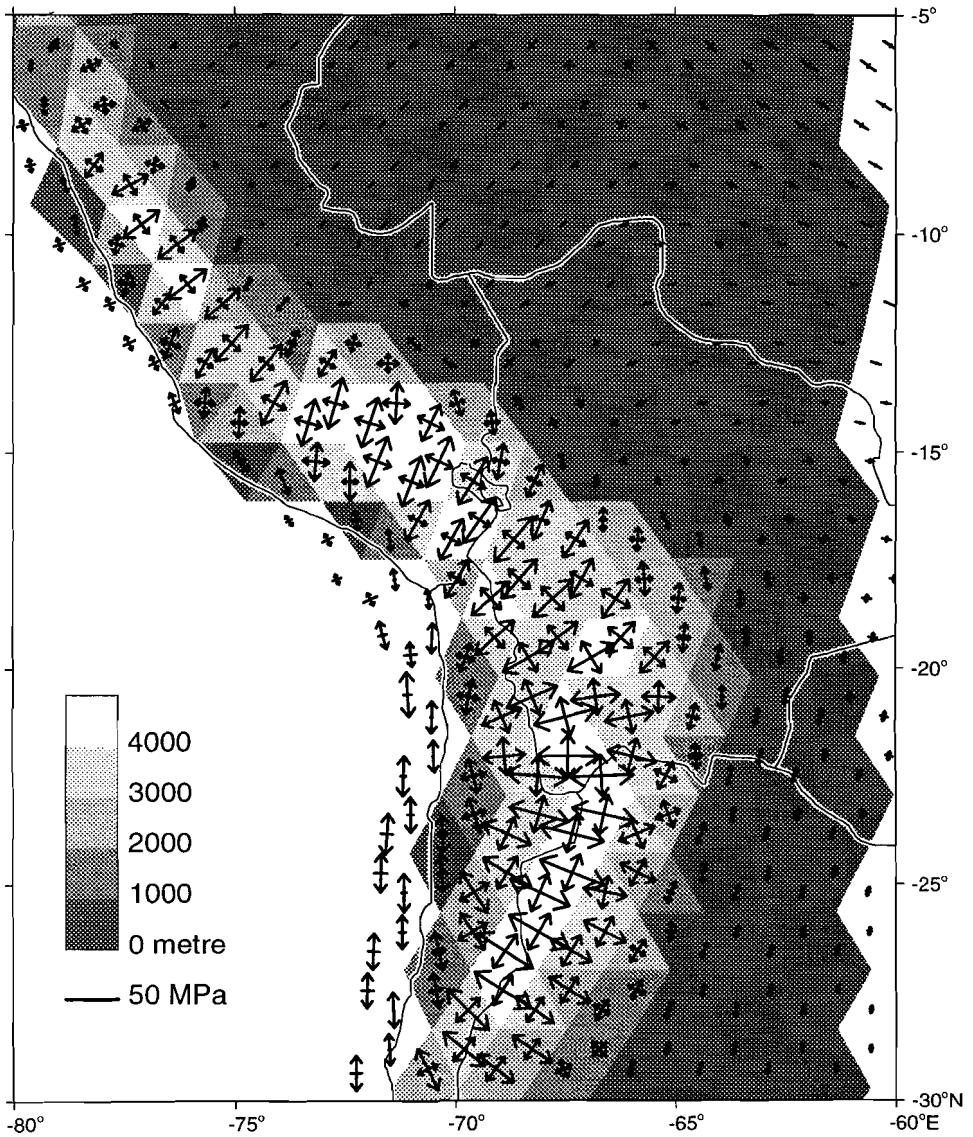
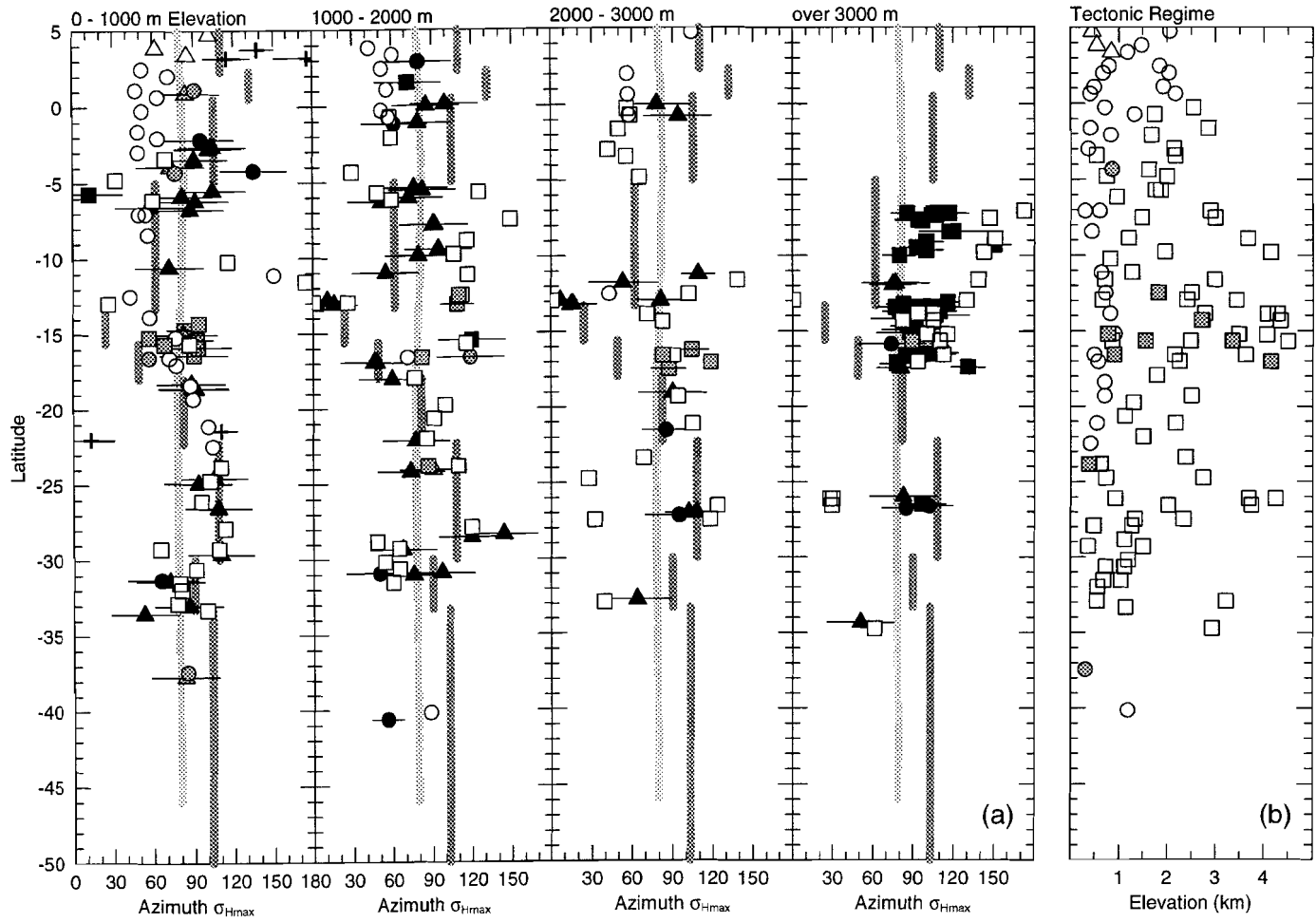


Fig. 3.45. Modelled intra-plate stress field for the central part of the Andes. No basal shear; topography is accounted for in terms of the associated horizontal body forces.

Fig. 3.46. (next page) (a) Modelled orientation of maximum horizontal compression versus observed azimuth. No basal shear; topography is accounted for in terms of the associated horizontal body forces. (b) Modelled tectonic regime as a function of latitude and elevation.



Stress Field of the South American Plate

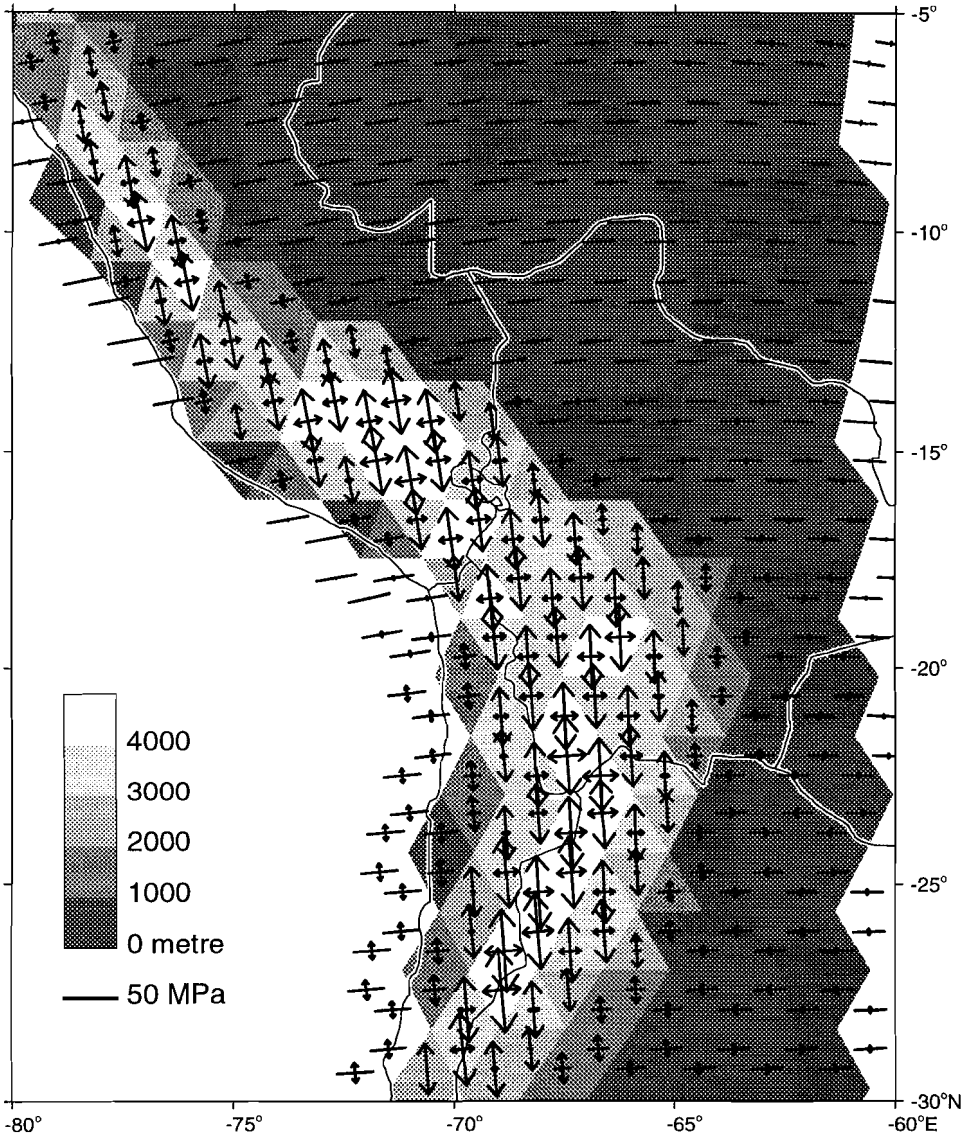
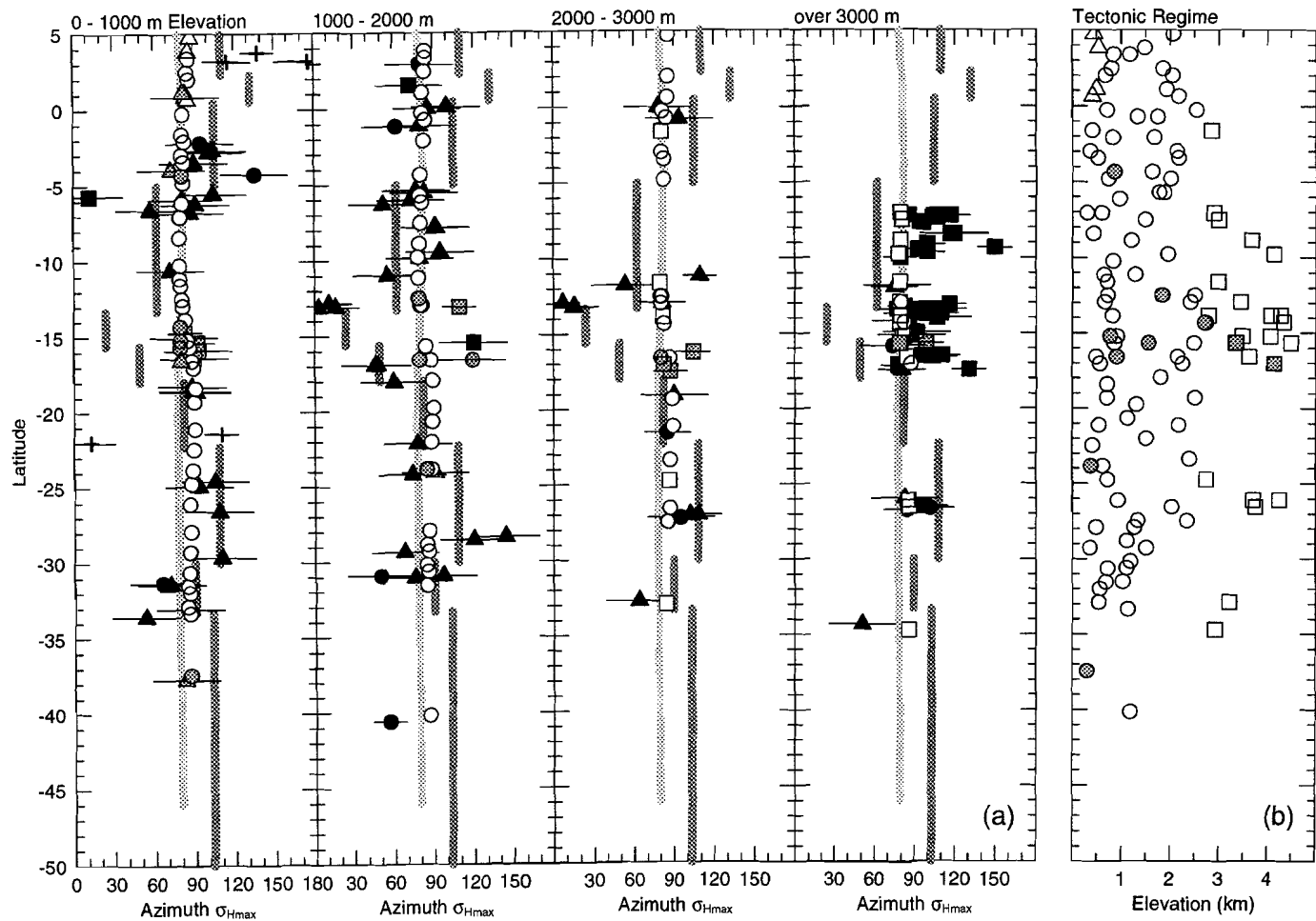


Fig. 3.47. Modelled intra-plate stress field for the central part of the Andes. Basal shear +5 bar; absolute motion according to HS2-NUVEL1. Topography affects vertical stress only.

Fig. 3.48. (next page) (a) Modelled orientation of maximum horizontal compression versus observed azimuth. Basal shear +5 bar; absolute motion according to HS2-NUVEL1. Topography affects the vertical stress only. (b) Modelled tectonic regime as a function of latitude and elevation.



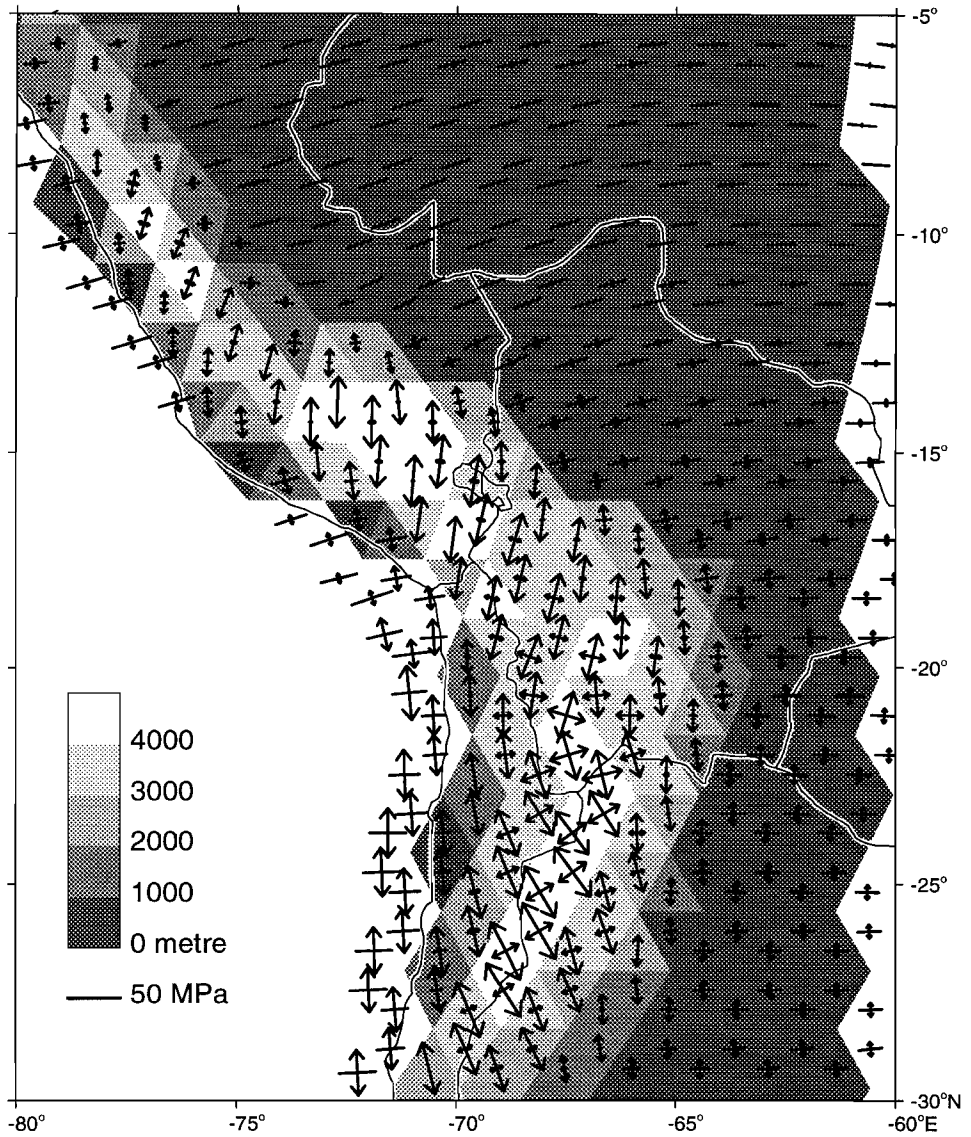
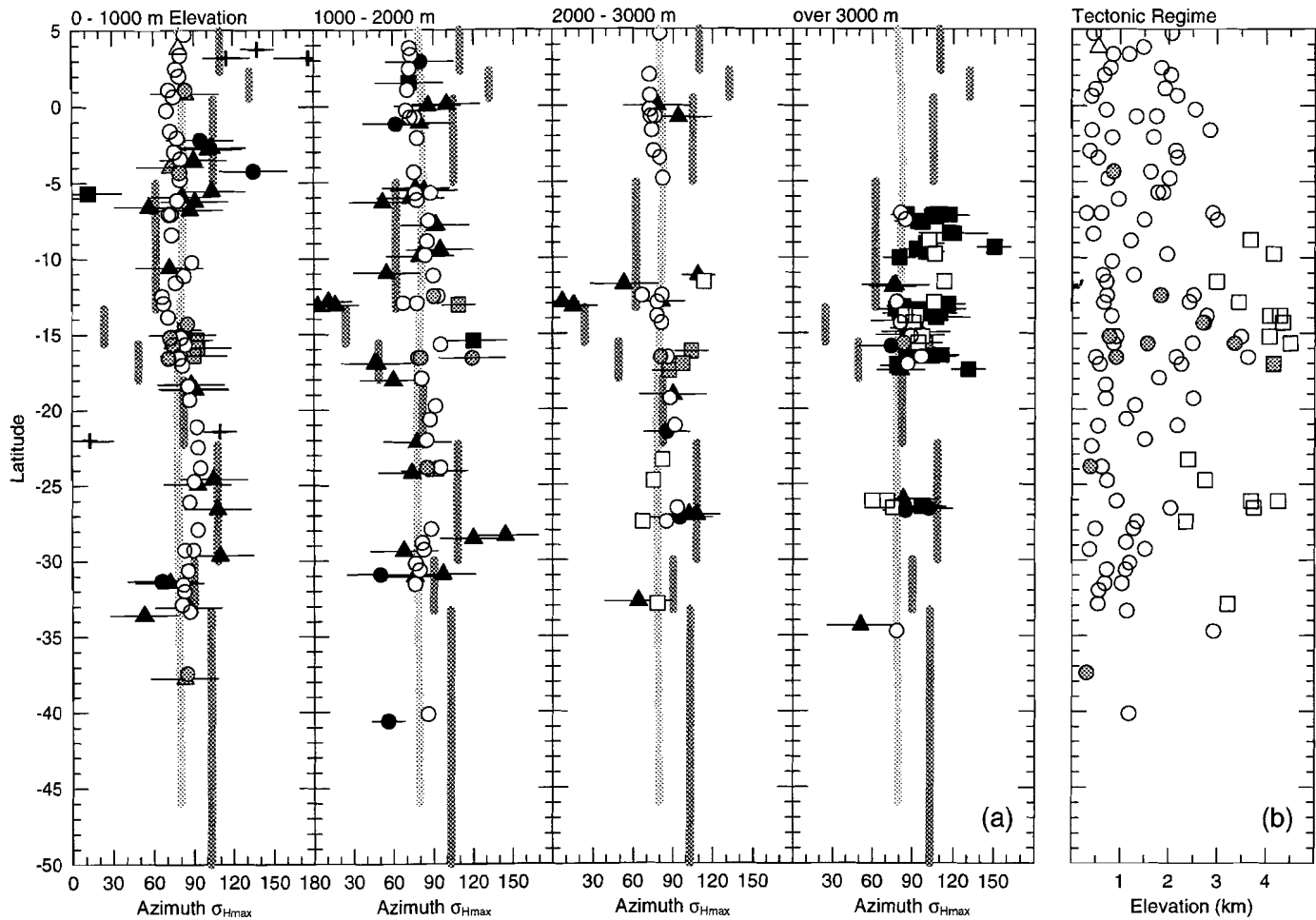


Fig. 3.49. Modelled stress field. Basal shear +5 bar; absolute motion according to HS2-NUVEL1. Topography is accounted for in terms of the associated horizontal body forces.

Fig. 3.50. (next page) (a) Modelled orientation of principal axis of maximum horizontal compression versus observed azimuth. Basal shear +5 bar; absolute motion according to HS2-NUVEL1. Topography is accounted for in terms of the associated horizontal body forces. (b) Modelled tectonic regime as a function of latitude and elevation.



1 and 2 km. At elevations between 2 and 3 km the model matches well all observations except those near 13°S. Above 3 km now also the normal faults of the Cordillera Blanca and northwest Argentina are reasonably matched. With respect to the model derived tectonic regime Figure 3.50b illustrates that elevations below 3 km are characterised mostly by strike-slip and that normal faults occur in particular above 3 km. Above 3 km, at some latitudes, the model predicts strike-slip where normal faults are observed. Still, the magnitude of any additional E-W compression is always very small. Near latitude 27°S strike-slip deformation is actually observed to occur also at higher elevations (*Allmendinger et al.*, 1989).

Evaluation of Results Part V

Dependence on density. Our choice to consider also the situation of a background model with a driving basal shear stress involved the assumption that the body forces due to topography were not overestimated. Here, we evaluate the dependence of the contribution of topography on the value of the (constant) density of crust and lithospheric mantle. To this extent Table 3.3 shows the magnitude of the average excess vertical stress (expression 5) associated with a topographic elevation of 4 km as a function of the two densities involved. Shown is $\Delta\bar{\sigma}_{zz}$ for two different values of the reference thickness of continental crust. It appears that the densities we have adopted in the model experiment provide us with a rather conservative estimate for the effect of topography. Within reasonable limits for the variables involved $\Delta\bar{\sigma}_{zz}$ could, at most, be about 28% less than the value corresponding to the densities used in our experiment. Thus, if we indeed significantly overestimated the effect of topography, this has to be due to the fact that the assumption of isostatic compensation by a crustal root only, is incorrect.

Table 3.3. Average Excess Vertical Stress (MPa)

Mantle Density [kg/m ³]	Crustal Density [kg/m ³]			
	2600	2700	2800	2900
2900	57 (51)	69 (64)	104 (99)	- (-)
3000	52 (47)	59 (54)	73 (67)	110 (104)
3100	49 (44)	55 (49)	62 (57)	77 (71)
3200	47 (42)	52 (46)	57 (52)	65 (60)
3300	46 (41)	50 (44)	54 (48)	60 (54)

Average excess vertical stress $\Delta\bar{\sigma}_{zz}$ in MPa as a function of crustal density (varies from column to column) and mantle density (varies from row to row). Densities in kg/m³; reference thickness of crust 35 km. Values in parentheses refer to a reference crustal thickness of 40 km.

Comparing the two approaches. We have applied on the scale of the entire Andes the concept that topography only affects the vertical stress, while, previously, this concept has been discussed in terms of a vertical section by *Dalmayrac and Molnar* (1981), *Froidevaux et al.* (1988), and - in most detail - by *Mercier et al.* (1992). The difference in results obtained with this approach and that involving the horizontal body forces associated with topography, are apparent: (1) In the first approach the orientation of the horizontal axes of principal stress is not affected by the mountain range. (2) In the first approach tension will always be largest in the direction perpendicular to the axis of maximum compression in the background model. In the case of the Andes this is the roughly N-S direction. In contrast, according to the second approach, tension may in fact be largest in the direction normal to the strike of the mountain range. Theoretically, the second approach is the one to follow in a thin shell model for the intra-plate stress field. The finding that the azimuth of σ_{Hmax} is matched better if we adopt the second approach offers support for the implementation in terms of body forces.

Implications of strike-slip at low elevations. Our numerical calculations indicate that implementation of the effect of topography leads to a prediction of strike-slip faulting at low elevations. This result is independent of the approach followed. Indeed, it was already pointed out by *Mercier et al.* (1992; see also *Froidevaux and Isacks*, 1984) that the transition from reverse faulting to normal faulting implies that intermediate elevations should be characterised by strike-slip faulting. The strike-slip regime is clearly brought out in our modelling because we consider the horizontal pattern of stress and not just a vertical cross section. We emphasize that the strike-slip regime is not caused by the presence of N-S tension in the background model: the latter is always further amplified. Partly, the inferred mismatch in tectonic regime - strike-slip according to the model whereas reverse faulting is observed - is due to the simplicity of the comparison. As soon as the model predicts one principal stress to be compressive and the other to be tensile, this is termed a strike-slip regime. Although, strictly speaking, the latter is correct it may distort comparison with observed faulting: a small component of horizontal tension additional to major horizontal compression could well lead to motion along a pre-existing fault that we would classify as reverse faulting. However, detailed comparison using forward slip vector calculation demonstrates that, overall, the inferred mismatch is indeed real.

Thus, we may ask what the mismatch could imply. It does probably not imply that F_{per} should be made even more resistive. The latter would further increase the E-W compression but will not prevent the second horizontal principal stress, which is almost zero in the background model, from becoming tensile due to topography. Moreover, a further increase in E-W compression would lead to an increasing misfit to the normal faulting observed at high elevations.

A possible implication of the obtained mismatch is that perhaps the background stress field is not correct. When, in reality, the regional stress field features compression in both horizontal directions, reverse faulting would extend

to higher elevations. Alternatively, the fact that the model predicts strike-slip may indicate that our representation of the effects of topography is essentially incorrect. In particular, it is possible that the assumption of local isostatic equilibrium is not warranted. Indeed, the length scale of topography, although perhaps sufficiently large relative to the thickness of the crust, is of the same order as the thickness of the lithosphere. Finally, the discrepancy between model results and observations may be due to limitations of our model. It is conceivable that thrust and reverse faulting occurring at low elevations along the Andes cannot be simulated using an elastic model of instantaneous deformation that represents the Andes as a homogeneous and isotropic body. When, for example, the present-day tectonics of the Andes are somehow partly controlled by the history of deformation, a temperature dependent model, able to account for finite deformation, would be required instead (e.g. *Govers, 1993*).

General Discussion

Ideally, we would arrive at a synthesis of the results of the five parts of the analysis by definition of a "preferred" model for the dynamics of the South American plate. In practice, however, we suffer from the fact that the importance of several of the contributing factors cannot be constrained unambiguously. Therefore, in order to conclude our study we will (1) comment on the extent to which the results of the various parts of the analysis are mutually independent, (2) summarize the results regarding the forces of first order importance, and (3) attempt to answer the question as to whether ridge push constitutes the only important driving force. A final remark concerns the state of stress in the Andes.

Combination of Model Results

Our choice to examine the various aspects that might be affecting the South American intra-plate stress field as much as possible individually has the advantage that it demonstrates clearly the characteristic effect of each relevant factor. Between them, the model experiments presented in the above provide much insight. To a large extent, the intra-plate stress field for the case of a model involving more than one deviation from the reference configuration can be thought of as resulting from the addition of the stress fields associated with each of these deviations separately. In this we need to differentiate between the direct effect of a given deviation, such as for example the increased E-W compression near the west margin resulting from F_{Chir} , and the indirect effect due to changes induced in the magnitude of the forces of the reference model. Since we are dealing with stresses in an elastic medium, the additive property will generally hold true as far as the direct effects on the stress field are concerned. Whether it also holds for the indirect effects depends on whether the deviations affect also the orientation of the torque vectors of the reference model. To illustrate this let

us consider the case of the additional force F_{suc} . Added to the reference model F_{suc} results in a more resistive F_{pcr} and causes, indirectly, an increase of the compression near the west margin outside of the central segment. The change in the magnitude of F_{pcr} associated with F_{suc} remains the same when other additional forces are involved or when, for example, the effect of topography is accounted for (hence, the introduction of the "shifts" in the previous chapter). However, when the composite model features also a lateral variation of F_{pcr} the torque vector of the latter force is orientated different in comparison with the reference model and, consequently, the shift of F_{pcr} due to F_{suc} may be different. Such differences are unlikely to be large: the orientation of the torque vector of F_{pcr} changes only slightly when lateral variation is incorporated.

The Forces of First Order Importance

The dynamical analysis in the previous chapter provided us with the picture of a plate being driven by ridge push and resisted by forces associated with subduction below the west margin, in combination with a relatively large force exerted on the northwestern margin and resistance associated with transform faults. In terms of the intra-plate stress field the situation is illustrated by the reference model: roughly E-W to WSW-ENE directed compression set up by ridge push and F_{pcr} , and a pronounced deviation from this trend due to F_{Car} .

The problem of the determination of the most likely azimuth of the Caribbean resistance is - unfortunately - an example of how uncertainty regarding other factors of relevance inhibits unambiguous conclusions to be reached. For the case that basal shear is assumed to be negligible our experiments suggest that the orientation of F_{Car} is close to N135°E. However, the effect that the resistance associated with Caribbean - South America convergence exerts on the stress field was found to be dependent also on the value of basal shear stress and the direction of absolute plate motion.

In view of this uncertainty it is worthwhile to also reverse the question. It has been argued (e.g. *Stein et al.*, 1988) that the direction of Caribbean-South America convergence is more eastwards than N135°E. However, model experiments assuming zero basal shear stress demonstrate that such an orientation is unlikely in particular in view of the associated roughly N-S tension along the entire west margin. Thus, the question may be asked: assuming an azimuth of F_{Car} of e.g. N120°E, which additional departures from the initial model with zero basal shear must be invoked to yield a realistic stress field, in particular near the western margin? In the first part of the analysis we found that the combination of a resistive basal shear and the *Chase* (1978a) absolute motion pole or a driving basal shear in conjunction with the HS2-NUVEL1 pole, both led to a reduction of the (relative) importance of F_{Car} . It can be shown that in particular in the second case the negative effect on the intra-plate stress field of a clockwise rotation of F_{Car} , i.e. N-S tension near the west margin, is much smaller. Of the additional forces studied, a pull exerted in the Lesser Antilles subduction zone

has been shown to increase the roughly N-S component of compression near the west margin. F_{LA} would also counteract the negative effects of F_{Car} rotated towards N120°E.

A uniform distribution of F_{pcr} was found to match reasonably well the average orientation of compression inwards of the west margin. Remaining differences between model-predicted maximum horizontal compression and the observed directions most likely reflect the role of topography. Other factors that might be expected to affect the pattern of compression near the west margin are the additional force F_{suc} , the occurrence of lateral variation of F_{pcr} , and the presence of an additional outward pull. These factors, however, were found to either have a negative effect on the correspondence between model and data, or yield a stress field not significantly different from that associated with uniform F_{pcr} . The conclusions regarding plate contact resistance are probably robust with respect to the uncertainty in orientation and value of basal shear stress. Basal shear will affect the magnitude of intra-plate stress but not as much the orientation.

The analysis of the torque balance in the previous chapter offered the insight that basal shear - when resistive - is only of minor importance. Our modelling does therefore not support the notion that the close correspondence between the orientation of intra-plate compression and the direction of absolute plate motion indicate basal shear is an important resistive force. The possibility of a driving basal shear stress will be considered below.

Does Ridge Push Constitute the Only Driving Force?

The constraint on the magnitude of horizontal compression offered by the observed change in tectonic regime with increasing elevation in the Andes should, in principle, allow us to answer the question whether ridge push forms the only force driving the South American plate. In fact, the use of the Andes as a "pressure gauge" (cf. e.g. *Molnar and Lyon-Caen, 1988*) may be the only way we can assess the importance of the most likely other driving force: shear at the base of the lithosphere. As mentioned in the preceding section also, results obtained for the first order model (part one of the analysis) suggest that only the magnitude, not the *orientation* of the principal axes of stress is sensitive to the value of basal shear.

When we make the assumption that topography is totally compensated by a crustal root and consider stresses averaged vertically over the thickness of the lithosphere, we infer that horizontal compression predicted by our reference model is too small. This result complies with the findings of *Froidevaux and Isacks (1984)* and *Froidevaux et al. (1988)* who considered only a vertical section through the mountain range but did include temperature dependent densities. Along the line of reasoning underlying also our "first approach" these authors estimated the horizontal compression to amount to about 50 MPa (for a 100 km thick plate). This value significantly exceeds compression present in the reference model.

Notwithstanding the consistency with previous work, our estimate of the effect of the Andes is not free of uncertainty. Three potential sources of error can be envisaged: (1) Topography may in part be compensated by a thermal root. It is not obvious how this would affect our conclusions. As stated by *Froidevaux and Isacks* (1984) a thermal root implies a greater depth of compensation. Consequently, the load of topography is "felt" throughout a larger depth range of the lithosphere which increases the average excess vertical stress. At the same time, however, the rise of the base of the lithosphere associated with a thermal root implies that stresses are carried by a thinner plate: average horizontal compression would also be increased (*Richardson and Coblenz*, 1994). Still other ways of compensation cannot be neglected. We cannot exclude the possibility that the topographic load is partly supported by flexure, nor do we know the role of the subducted Nazca plate in particular where the latter extends subhorizontally below the continent. When thickening is not restricted to the crust but occurs more nearly homogeneous throughout the entire lithosphere, the average excess vertical stress would be much smaller than the value we have adopted (*Molnar et al.*, 1993). (2) The fact that we consider vertical averages of stress. The available observations do not allow us to disregard the possibility that normal faulting occurs only at shallow depth. Again, we do not know for sure how this would affect our conclusions. *Richardson and Coblenz* (1994) used a finite element representation of a vertical section through the Cordillera Blanca which allowed them to account for variation with depth of the horizontal compression. They found that, relative to the situation with a uniform depth distribution a larger amount of total horizontal compression would still provide a match with the observations. In this case our conclusion that the reference model provides too little horizontal compression would be further strengthened. (3) The fact that the model predicts strike-slip where reverse faulting is observed. As discussed in part five of the analysis, the implications of this are uncertain. Still, it does not necessarily imply that conclusions regarding the required amount of horizontal compression are wrong. Relevant to the latter question is the relative magnitude of the vertical principal stress and the horizontal *across-strike* principal stress: it is possible that these components are correctly predicted by the model and that only the *along-strike* principal stress is incorrect.

Thus, in conclusion, we state that the model calculations certainly suggest that horizontal compression in the reference model is too small in order to explain the observed state of stress in the Andes, but that the experiments also demonstrate that there is considerable uncertainty involved.

This conclusion is contrary to that of *Richardson and Coblenz* (1994). On the basis of a finite element representation of a vertical cross section through the Cordillera Blanca these authors obtained a preferred value of 25 MPa for the magnitude of horizontal compression across the mountain range. Indeed, as argued by *Richardson and Coblenz* this value corresponds to the magnitude of ridge push ($2-3 \times 10^{12}$ N/m). However, compression along the western plate

margin depends directly on F_{pcr} and since the latter is only one of several forces opposing ridge push it will in fact be smaller than $2-3 \times 10^{12}$ N/m.

In our model analysis we have encountered several factors other than basal shear which could lead to a more resistive F_{pcr} and thereby to more compression. For example, the additional forces F_{LA} and a westward directed F_{NAm} would have the desired effect. Particularly so in view of the fact that there are also additional forces that would have the opposite effect, these forces are not expected to lead to a great increase of compression. Alternatively, it is possible that F_{pcr} is subject to lateral changes resulting in locally higher compression. Whereas significant lateral variation due to a dependence on slab dip and slab age are unlikely, a dependence on latitude sensu *Russo and Silver* (1994b) could not be excluded. The latter distribution has the advantage that it would increase compression there where the tension due to topography is largest: at the wide and high central segment of the Andes. However, even in the extreme case considered in our model experiment, latitude dependence only leads to a twofold increase of horizontal compression which is not sufficient.

We note that there are also forces left out of the reference model that would lead to a less resistive F_{pcr} and thus strengthen the conclusion that the reference model lacks a force that assists ridge push. Of the forces that would have this effect we mention in particular the force associated with the passive continental margin. Finally, we emphasize that the additional driving force need not necessarily be a *uniform* basal shear stress. It is well possible that any driving basal shear is largest below the continental part of the South American plate or distributed otherwise.

Stress Field in the Andes

We have investigated the state of stress in the Andes not by considering the range as an isolated feature but by treating it as an integral part of the whole South American plate. This approach forms an advancement over previous work in the sense that we were able to directly relate the Andean stress field to the nature of the plate tectonic forces. Moreover, the platewise approach allowed us to study the effect of the mountain range on the orientation of horizontal compression.

Being able to correctly quantify the effect of topography on the stress field is essential with regard to a matter that will not be addressed in this thesis: the temporal evolution of the intra-plate stress field and of the forces acting on the South American plate. It is in the Andes that geological studies have revealed the occurrence of changes in the state of stress through time (e.g. *Allmendinger et al.*, 1989; *Mercier et al.*, 1992). The work presented in this chapter - dealing with the present-day situation - provides a basis for study of past stages in the evolution of the South American plate.

Conclusions

In this chapter, building on the results of the dynamical analysis in Chapter 2, we have further investigated the forces acting on the South American plate by examination of the intra-plate stress field. A numerical model has been employed in order to assess the stress field characteristic for all factors considered relevant. Subsequently, comparison of model results with a recent compilation of observations of the present-day South American stress field, has allowed us determine the likeliness and (relative) importance of the proposed forces. Although it was not found possible to define a single preferred model for the dynamics of the South American plate, between them the model experiments provide much insight. Specific conclusions that could be reached are listed below, following the sequence of the five parts of the analysis (corresponding parts are indicated).

1. The choice of the absolute motion pole that is taken to define the orientation of basal shear, and the magnitude of this shear, were found to have only a minor effect on the orientation of the principal axes of intra-plate stress (an exception being northwestern South America). The magnitude of intra-plate stress, however, depends strongly on the assumed basal shear (part I).

2. For a situation in which basal shear is negligible, the azimuth of the resistive force due to Caribbean-South America convergence is close to N135°E. The extent to which this conclusion is affected in case basal shear is non-zero has been investigated (part I).

3. The existence of a significant trenchward pull on the central segment of the overriding margin (F_{suc}) can be excluded (part II).

4. A uniform magnitude of the resistance associated with subduction below the Andean margin is found to explain reasonably well the observed orientation of maximum horizontal compression along the Andes. The available data preclude the possibility that the magnitude of plate contact resistance depends on slab dip. A dependence on slab age is also argued against by the available observations, but evidence is less firm. The possibility of a lateral variation of the magnitude of F_{per} sensu *Russo and Silver* (1994a, b) can be confirmed, nor discarded (part III).

5. The orientation of the axis of maximum horizontal stress observed in northern Brasil is already matched by models excluding the effect of the passive margin. When the horizontal pressure gradient associated with the passive margin is accounted for, the observed strike-slip regime is matched (part IV).

6. The possibility of an additional trenchward pull, exerted normal to the entire overriding margin in addition to plate contact resistance, is argued against by the available data, but evidence is not conclusive (part IV).

7. By accounting for the effect of topography in terms of the associated body forces it was found possible to match the normal faulting observed in the high Andes. Moreover, when including the body forces associated with

topography, the model yields a close match to the orientation of maximum horizontal compression observed at lower elevations. However, in conflict with the available data, our models predict strike-slip faulting at these lower elevations. In reality, thrusting and reverse faulting prevails. The possible origin of this misfit between model and data has been commented upon (part V).

8. In order to match the observation that normal faulting in the Andes occurs mainly at elevations exceeding 3 km, we need to invoke an amount of horizontal compressive stress that is larger than the amount provided by plate contact resistance in case ridge push is the only driving force. Consideration of the torque balance in Chapter 2 indicated the possibility that shear stress exerted at the base of the South American plate assists plate motion. In this chapter, we have shown that a driving basal shear stress could provide the required increase in horizontal compression in the Andes. Although our calculations thus suggest that ridge push - as defined in our models - is not the only force that drives the South American plate, we have also demonstrated that this aspect involves considerable uncertainty (part V).

Late Cenozoic Dynamics of the Aegean Region

Chapter 4

Introduction

During the late Cenozoic, in what may be regarded as the final stage of convergence between the African plate and the Eurasian plate, extensional deformation affected the region of the Aegean Sea, the adjacent parts of the Greek mainland, and western Turkey (Figure 4.1 and 4.2). This region of distributed continental deformation is situated on the southern margin of the Eurasian plate and overlies a subduction zone where the lithosphere of the eastern Mediterranean Sea - part of the African plate - descends northwards. The overriding margin is formed by the Hellenic island arc.

A starting point of the investigation of the "neotectonic" evolution is perhaps the recognition by *Aubouin and Dercourt (1965)* and *Aubouin (1971)* of the importance of widespread normal faulting. Since then, the Neogene - Quaternary evolution has been given much attention from all disciplines of earth science (see *Mercier, 1979* for a review of early work). The study of tectonic structures, in particular (normal) faults, both on-land (e.g. *Angelier et al., 1982; Mercier et al., 1987*) and off-shore (e.g. *Masclé and Martin, 1990*) provides horizontal patterns of strain and stress. Information on the history of deformation is supplemented with observations of active seismic strain (e.g. *Papazachos et al., 1991; Taymaz et al., 1991; Hatzfeld et al., 1993*). Stratigraphic and sedimentological analyses of Neogene and Quaternary sedimentary deposits shed light on vertical motions, provide

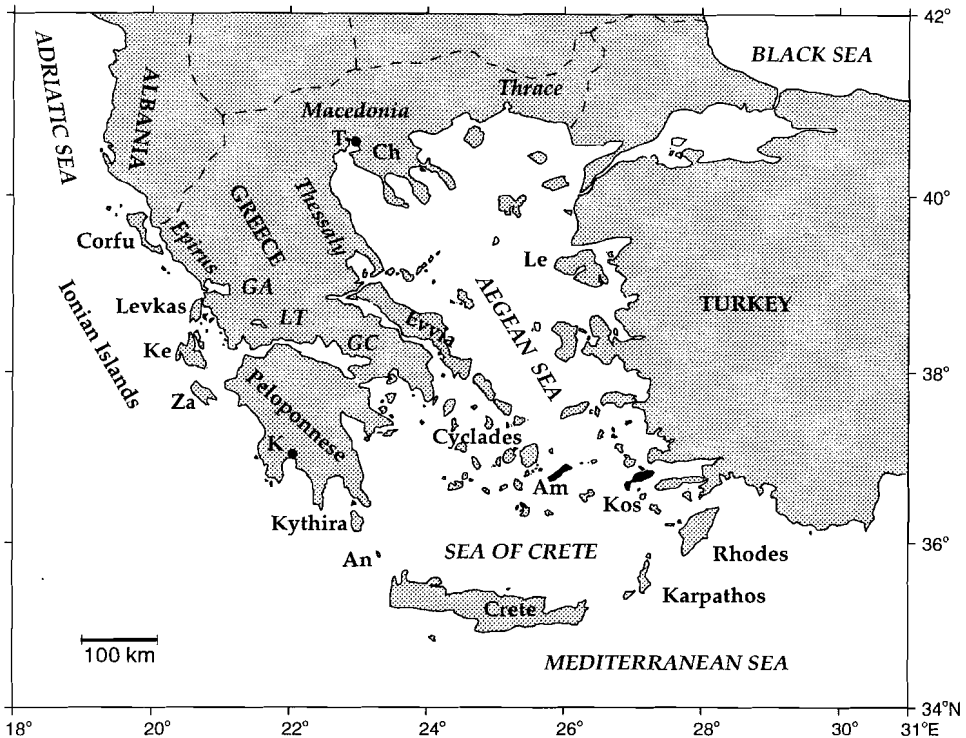


Fig. 4.1. Geographical location of places mentioned in the text. Key: GA, Gulf of Amvrakia; GC, Gulf of Corinth; LT, Lake Trikhonis; Am, Amorgos; An, Andikythira; Ch, Chalkidiki; Ke, Kefallinia; Le, Lesbos; Za, Zakythos; K, Kalamata; T, Thessaloniki.

information on tilting, and allow dating of tectonic events (Meulenkamp, 1985; Schröder, 1986). Recent vertical movements are inferred from observations of former shorelines (e.g. Pirazzoli *et al.*, 1989; Stiros *et al.*, 1992), by geodetical means (e.g. Stiros, 1986), and even, based on study of archaeological sites (e.g. Stiros, 1988; van Wamel and Gast, 1993). Paleomagnetic observations (Kissel and Laj, 1988; Márton, 1993), supplemented for the present-day with geodetical measurements (e.g. Billiris *et al.*, 1991; Kahle *et al.*, 1993; Noomen *et al.*, 1993; Oral *et al.*, 1993) constrain horizontal motions. Geochemical and petrological studies of volcanic rocks yield, for example, information on the evolution of the subducted slab (Fytikas *et al.*, 1984; Pe-Piper and Piper, 1989). The study of metamorphic rocks has proved to provide an important link between Neogene extension and the Alpine orogeny (Lister *et al.*, 1984).

As a result of these investigations, the kinematics of the Neogene - Quaternary geological evolution are well known. Moreover, several processes and mechanisms have been suggested to form the driving force of the observed

deformation. Specifically, based primarily on geological observations of faulting, dynamical concepts were proposed by two French research groups: J. Angelier, X. Le Pichon and colleagues (*Le Pichon and Angelier, 1979; Le Pichon, 1982*) and J. Mercier and co-workers (*Mercier et al., 1987*). Apart from being conflicting, suggestions concerning the dynamics are often either strictly qualitative or apply a concept which is quantitatively assessed in a general sense only, to the Aegean setting. Also, some dynamical concepts account for only part of the region.

To date, few numerical model experiments have been aimed specifically at the Aegean region. The studies which have been performed have in common that they calculate the horizontal pattern of deformation in response to a set of applied boundary conditions. *Meissner et al. (1979)* address the relation between the direction of convergence along the Hellenic arc and the internal deformation of the region. Since these authors essentially apply compression at the overriding margin their models fail to match the observed extension. Using a viscous model and applying velocity boundary conditions, *De Bremaecker et al. (1982)* demonstrate that the overall pattern of strain in the Aegean is consistent with the velocities inferred for its margins. In the context of the WEGENER/MEDLAS geodetic project, preliminary numerical modelling was carried out by *Drewes and Geiss (1986)* and *Geiss (1987)*. Evaluation of geodetic observations is also central to the recent model study of *Oral et al. (1993)*. Concentrating on the effect of evolving thermal structure on rheology, *Sonder and England (1986)* address temporal changes in the pattern of extension under a velocity applied to the overriding margin.

In order to assess, in a quantitative sense, the forces controlling the late Cenozoic extension of the Aegean region we use a forward numerical model to analyse the horizontal pattern of stress and deformation. In contrast to previous studies we apply force boundary conditions and make extensive use of observations of the intra-plate stress field. Apart from observations of active deformation, information about the evolution of deformation through time is taken into account. Of particular interest is a question which arises from the recent results of seismic tomography. The seismic velocity structure of the upper mantle below both Italy and the western Balkan suggests the presence of a discontinuity in the slab subducted below these regions (*Spakman et al., 1988; Spakman, 1990, 1991*); a result which has subsequently been tested following a forward approach (*de Jonge et al., 1994*). Interpretation of the tomographic results led to the development of the concept of lateral migration of slab detachment (*Wortel and Spakman, 1992*). In the present study we investigate whether the postulated slab detachment process, a process occurring in the upper mantle, has an expression in the late Cenozoic evolution of deformation of the overriding plate, for which information is mainly obtained from the Earth's surface.

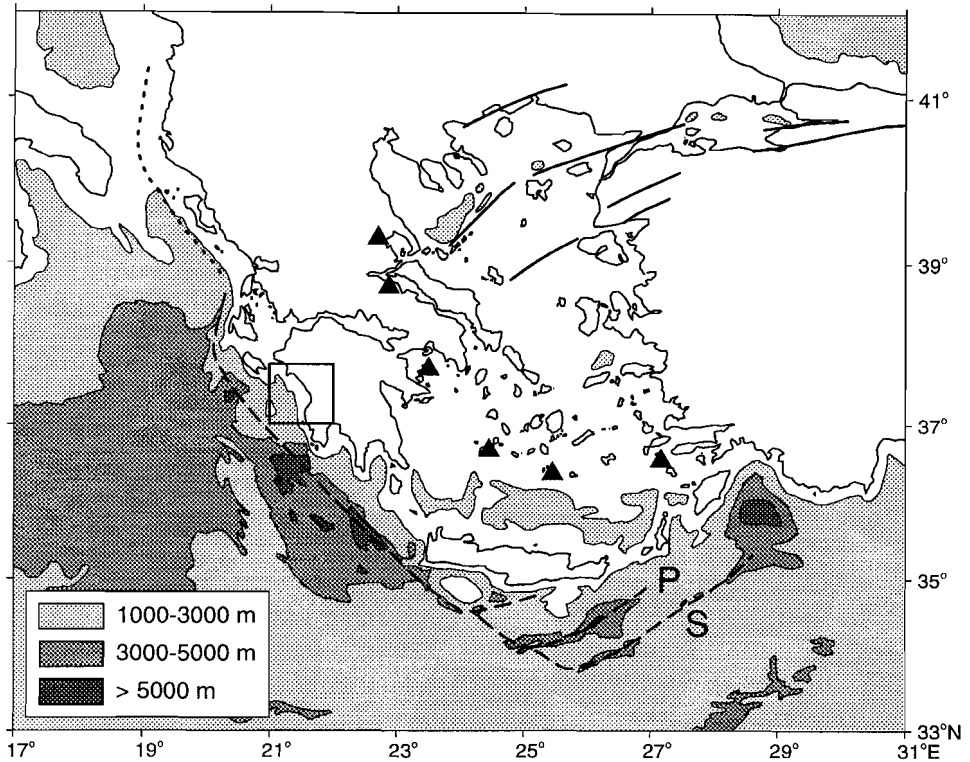


Fig. 4.2. Major structural features of the Aegean region relevant to the present study. Shading denotes bathymetry. Dashed lines indicate axes of the Hellenic trench system connecting to the northwest with the collision zone between lithosphere of the Adriatic Sea and northwest Greece-Albania (dotted line). Bold lines: faults accommodating dextral strike-slip which form the westward continuation of the North Anatolian fault zone (after *Taymaz et al.*, 1991 and *Simeakis et al.*, 1989). Black triangles: calc-alkaline volcanoes of the Late Pliocene-present. Key: P, Pliny trench; S, Strabo trench. Box indicates area of Fig. 4.3.

Outline of Geological History and Current Setting

In the Aegean region, rocks of pre-Neogene age constitute the Hellenides, i.e. the Greek segment of the Alpine chain connecting the Dinarides of the western Balkan to the Taurides of Turkey (e.g. *Jacobshagen*, 1986). Orogenic activity initiated in the Late Cretaceous when relative motion between the African plate and the Eurasian plate changed to roughly north-south convergence (e.g. *Livermore and Smith*, 1985). Sedimentary basins of the Neotethys, which formed following rifting of the northern margin of Gondwanaland during Late Permian - Middle Triassic time, were progressively closed and the rock successions were

incorporated as discrete thrust sheets into the evolving orogenic belt (e.g. *Robertson and Dixon, 1984; Dercourt et al., 1986; Robertson et al., 1991*). Shortening started with emplacement of ophiolites and, subsequently, thrusting migrated towards the more external parts forming a typical fold-and-thrust belt geometry. At the front of the advancing thrust sheets thick flysch deposits accumulated in flexurally controlled foreland basins (*Underhill, 1989; Clews, 1989*).

Tectonic burial associated with the Alpine orogeny caused, during the Middle Eocene, a high pressure - low temperature (HP/LT) metamorphism of rocks that are now exposed at the surface in the Attic-Cycladic complex (*Andriessen et al., 1979; Altherr et al., 1982; Dürr, 1986; Wijbrans et al., 1993*). HP/LT metamorphism of late Oligocene age is evidenced by the lower two thrust sheets of the south Peloponnese and Crete (*Seidel et al., 1982; Greiling, 1982*). The HP/LT rocks of the Cyclades experienced an overprint of greenschist to, locally, amphibolite facies metamorphism which preceded (*Lister et al., 1984*) or partially overlapped (*Wijbrans and McDougall, 1988*) a Middle - Late Miocene period of intrusion of granitoids. Evidence of shear deformation contemporaneous with metamorphism and granitoid emplacement led *Lister et al. (1984)* to propose that, starting during the second metamorphism, the rocks were exhumed from mid-crustal levels in the footwall of a shallow-dipping ductile shear zone, accommodating crustal extension. The ductile shear zone connected upwards with brittle low-angle normal faults - detachments - along which unmetamorphosed rocks were emplaced during a later stage. This interpretation of the Attic-Cycladic complex in terms of a metamorphic core complex has subsequently been corroborated by studies on other islands of the archipelago (*Urai et al., 1990; Buick, 1991; Faure et al., 1991; Lee and Lister, 1992; Gautier et al., 1993*).

A similar chain of metamorphic and plutonic events has recently been inferred for the Rhodope complex of Thrace, which was previously regarded as a Precambrian or Paleozoic stable massif separating two Tethyan orogenic belts (*Burg et al., 1990; Jones et al., 1992*). Moreover, data from the southwestern Rhodope suggest that the region may also be considered a core complex unroofed by extensional low-angle faulting (*Dinter and Royden, 1993; Sokoutis et al., 1993*). Evidence for extensional unroofing has been found also in the region of Mount Olympos in Thessaly (*Schermer, 1993*) and in the region between Mount Olympos and northern Evvia (*Walcott and White, 1995*).

The above-mentioned studies provide insight into the initial stages of extension. Extension of the internal zones may have started by Late Oligocene - Early Miocene time and was simultaneous with nappe emplacement in the more external parts (i.e. closer to the present-day active margin). A complete reconstruction of the kinematics, reconciling the observed directions and amounts of lengthening and shortening awaits to be proposed. Such a reconstruction would also have to account for a first phase of rotations which affected the region during the Middle Miocene as shown by paleomagnetic studies (*Kissel and Laj, 1988; Speranza et al., 1992; Márton, 1993*). During this phase and a second period

covering the last 5 Ma, the Hellenic arc acquired its pronounced curvature starting from a roughly rectilinear trend.

Progressive disruption of the Alpine edifice during the late Cenozoic is documented by Neogene sediments deposited in basins superimposed on the Alpine structures. These basins are mainly controlled by normal faults and their age varies throughout the region (e.g. *Meulenkamp, 1985; Schröder, 1986*). Although extension formed the dominant tectonic regime throughout the late Cenozoic, it was interrupted by periods of compression. In particular, folding and reverse faulting occurred on Crete prior to the Pliocene (*Meulenkamp et al., 1988; Postma et al., 1994*). The extensional deformation and associated differential vertical movements have left a pronounced expression in topography and bathymetry.

At present, the distribution of earthquakes reveals that the contact between the Aegean lithosphere and the African plate coincides with the Hellenic trench system. The latter, however, is not a typical subduction trench but rather a series of troughs developed at the contact between overriding continent and a ridge of accreted sediments carried by the downgoing plate (*Le Pichon et al., 1979; 1982; Peters and Huson, 1985*). The trench system, subangular in plan view, consists of a NW-SE striking western segment and two NE-SW trending eastern segments, the Pliny trench and the Strabo trench. To the northwest of the island of Levkas the Hellenic subduction zone connects with a zone of active collision between the Aegean lithosphere and the lithosphere of the Adriatic Sea. The subducted portion of the African plate is expressed seismically with earthquake activity deepening northwards from the trench to about 150-200 km depth (e.g. *Papazachos and Comninakis, 1971; Makropoulos and Burton, 1984*). Seismic tomography suggests the presence of an aseismic portion of the slab below this point, extending to much greater depth (*Spakman et al., 1988; Spakman et al., 1993; de Jonge et al., 1994*). The length of the subducted portion of the African plate thus evidenced implies that the Hellenic subduction zone was initiated at least 26 Ma ago, i.e. during the late Oligocene (*Meulenkamp et al., 1988; Spakman et al., 1988*). The lithosphere presently subducting below the Aegean region carries a thick sedimentary cover and may be either of oceanic or thinned continental character (*Woodside, 1977; Cloetingh et al., 1980; Makris and Stobbe, 1984*).

The Hellenic subduction zone is accompanied by active volcanism. An arc of calc-alkaline volcanoes, initiated approximately 3 Ma ago, extends parallel to the overriding margin from central Greece, through the southern Cyclades to southwest Turkey (e.g. *Fytikas et al., 1984*). Older volcanic rocks are found throughout the region to the north of the active arc. Extrusives are of Oligocene age in Thrace and become progressively younger in a southward direction (*Fytikas et al., 1984; Pe-Piper and Piper, 1989*). Being of subduction-related character, the Oligocene - Middle Miocene volcanism in the northern Aegean has been ascribed to a subduction zone preceding, and located north of, the currently active margin (*Fytikas et al., 1984*). Given the tomographic evidence for long established subduction at the present site, much of the older volcanism may in fact reflect

earlier stages of the current Hellenic subduction zone (*Spakman et al.*, 1988; *Pe-Piper and Piper*, 1989).

When continued convergence between the African plate and the Eurasian plate gave rise to collision between the Arabian promontory and Eurasia, the small Anatolian block was moved westwards, away from the zone of collision. A linear depression in the northern Aegean Sea (Figure 4.2) forms the deepest part of the continuation into the Aegean of the North Anatolian fault zone, a dextral strike-slip fault accomodating the westward motion of the Anatolian block with respect to stable Eurasia (*Ketin*, 1948; *Pavoni*, 1961; *McKenzie*, 1972; *Şengör*, 1979). East of longitude 31°E the fault zone is a narrow feature but in the northern Aegean faults accomodating dextral strike-slip are distributed over a wide area (*Dewey and Şengör*, 1979; *Barka and Kadinsky-Cade*, 1988; *Taymaz et al.*, 1991). Estimates of the time of initiation of the North Anatolian fault zone vary, but the fault zone was most likely established during Late Miocene to Early Pliocene time (e.g. *Şengör et al.*, 1985; *Dewey et al.*, 1986; *Barka and Kadinsky-Cade*, 1988; *Barka et al.*, 1994).

Observations

Aspects of the late Cenozoic geological evolution of the Aegean region that are investigated in our study are: the horizontal stress pattern derived from field observations of faulting, seismically expressed strain, and horizontal motions. The available observations are presented below.

Stress Inferred From Field Observed Faulting

Analysis of neotectonic faults on different scales, in combination with stratigraphic dating, has provided a detailed view of the late Cenozoic deformational history of the Aegean region (syntheses are given by *Angelier*, 1979b; *Angelier et al.*, 1982; *Mercier et al.*, 1987; 1989; 1993). Observations of faulting concern both minor faults developed internally within Neogene sedimentary sequences and major faults separating Neogene basin sediments from adjacent Alpine basement. In both cases, measurements of the orientation of fault planes and tectonic striae can be used in inversion schemes to obtain information about the associated state of stress. The techniques which were used in the microtectonic analyses of the Aegean region are discussed by *Carey* (1979) and *Angelier* (1979a, b). Before presenting the regional compilations we will have a close look at two areas in the southwestern Hellenic arc where fieldwork aimed at collecting additional information was carried out by the author.

Western Peloponnese. As is clearly expressed by the orientation of the three peninsulas, the major normal faults of the southern Peloponnese strike roughly NW-SE. In contrast, north of the town of Kyparissia, situated at the west coast of

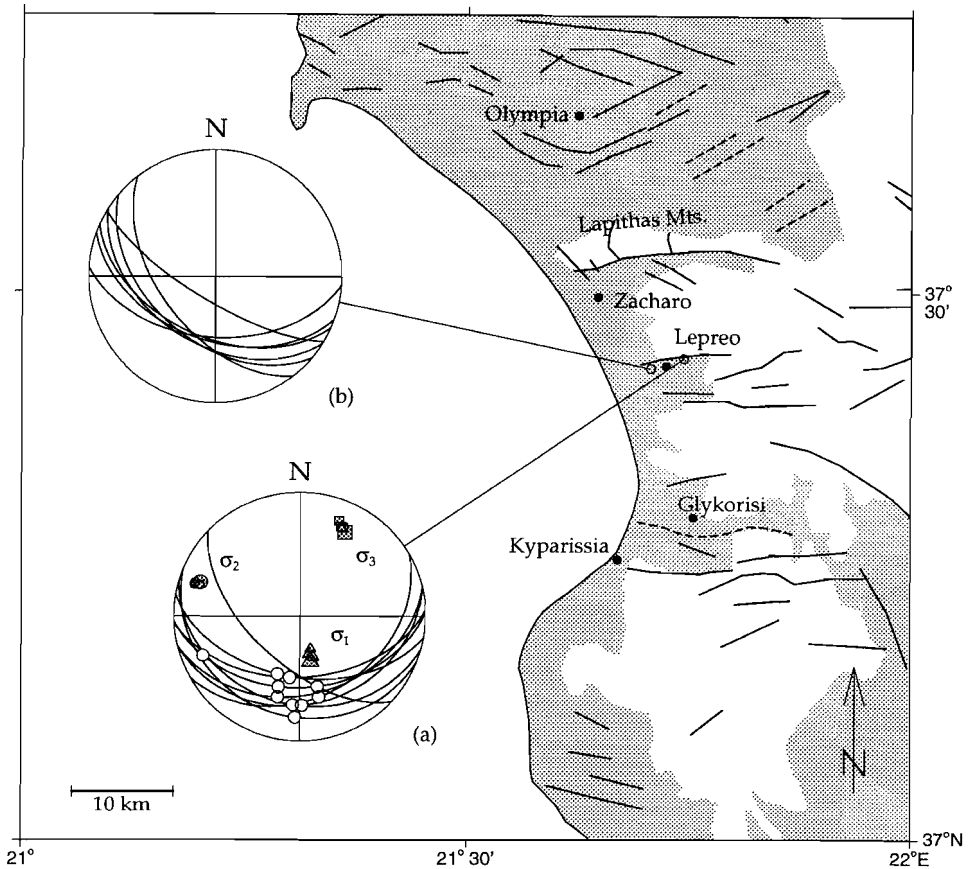


Fig. 4.3. Simplified geological map of the central western Peloponnese showing the distribution of Plio-Pleistocene sediments (grey shading) and main faults (black lines). Probable faults are shown dashed; not shown are thrusts in the pre-Neogene basement. Map digitised from IGME (1989). Insets show in lower hemisphere equal-area projection fault planes (great circles) and striae (white dots; all faults have normal component of slip) measured at two sites. (a) Measurements along km-scale Lepreo fault. Grey symbols denote the principal axes of stress obtained with the inversion method of *Reches* (1987); triangles, principal axis of maximum compression (σ_1); circles, intermediate principal stress (σ_2); squares, axis of maximum tension (σ_3). Four sets of principal axes are shown corresponding to values for friction coefficient μ of 0.2, 0.4, 0.6, and 0.8. Axes obtained for the latter value are indicated by larger symbol. The WSW plunging striation is not included in inversion. Mean misfit angle is 5° ; stress ratio varies between 0.2 and 0.4. See text for details about the inversion. (b) Metre scale faults cutting Neogene sands to the west of Lepreo.

the Peloponnese, faults striking E-W occur (Figure 4.3). Between the fault that starts at Kyparissia and the fault forming the southern boundary of the Lapithas massif, Neogene sediments are mostly restricted to a narrow strip along the coast. The sediments extend further towards the east only in a few down-faulted blocks and are generally referred to as being of Pliocene-Pleistocene age. An important question concerns the timing of activity of the E-W faults relative to that of the NW-SE faults which control vertical movements towards the east and south.

Adjacent to the Kyparissia fault the Neogene succession comprises conglomerates which are not observed further northwards in the area. The conglomerates show a large variation in component size and occur in irregular layers alternating with stratified brownish sands. Conglomerate components are mostly limestone and appear derived from the Pindos nappe which constitutes the footwall block of the Kyparissia fault and forms the basement for all Neogene deposits of the area between the latter fault and the Lapithas mountains. Neogene deposits are not reported from the footwall of the Kyparissia fault (*IGME, 1980; Lallemand, 1984*). The distribution and nature of the sediments adjacent to the Kyparissia fault suggest that their deposition is due to differential vertical motion along that fault. The E-W striking Kyparissia fault most likely bounded the basin towards the south. Marine clayey marls intercalated within the conglomerates in the vicinity of Glykorisi (Figure 4.3) were recently dated by *Frydas (1990)* as being of Late Pliocene age. Thus, it follows that the Kyparissia fault was already active by that time. No unambiguous kinematic indicators have been recovered from the fault as a consequence of which we cannot discriminate between the following two possibilities: (1) either the Kyparissia fault formed due to N-S tensional stresses during the Late Pliocene, or (2) during the Late Pliocene an existing E-W fault was reactivated.

Kinematic indicators could be observed at the east-west striking normal fault near Lepreo (Figure 4.3). East of Lepreo this fault separates Pliocene-Pleistocene deposits to the south from basement to the north. West of Lepreo both north and south block consist of Neogene rocks. Above the village, the base of the pre-Neogene massif is marked by a clear scarp. At several locations along the road east of Lepreo striated fault planes have been measured which clearly pertain to the main fault (Figure 4.3, inset a). The state of stress associated with the observed fault slip has been determined using the inversion method developed by *Reches (1987)*. Regarding the principal axes of stress we adopt the same convention as in Chapter 3 and take compressive stress as positive with $\sigma_1 > \sigma_2 > \sigma_3$. The method of *Reches (1987)* is based on two constraints: (1) the commonly used criterium that fault slip coincides with the direction of maximum resolved shear stress (cf. Chapter 3, section "methods"), and (2) the Coulomb failure criterium. Results are obtained for pre-set values of the friction coefficient μ and cohesion. As is most likely appropriate in the case of reactivation, cohesion is assumed to be zero (*Reches, 1987*), the friction coefficient has been varied between 0.2 and 0.8. The extent to which a computed stress tensor matches the

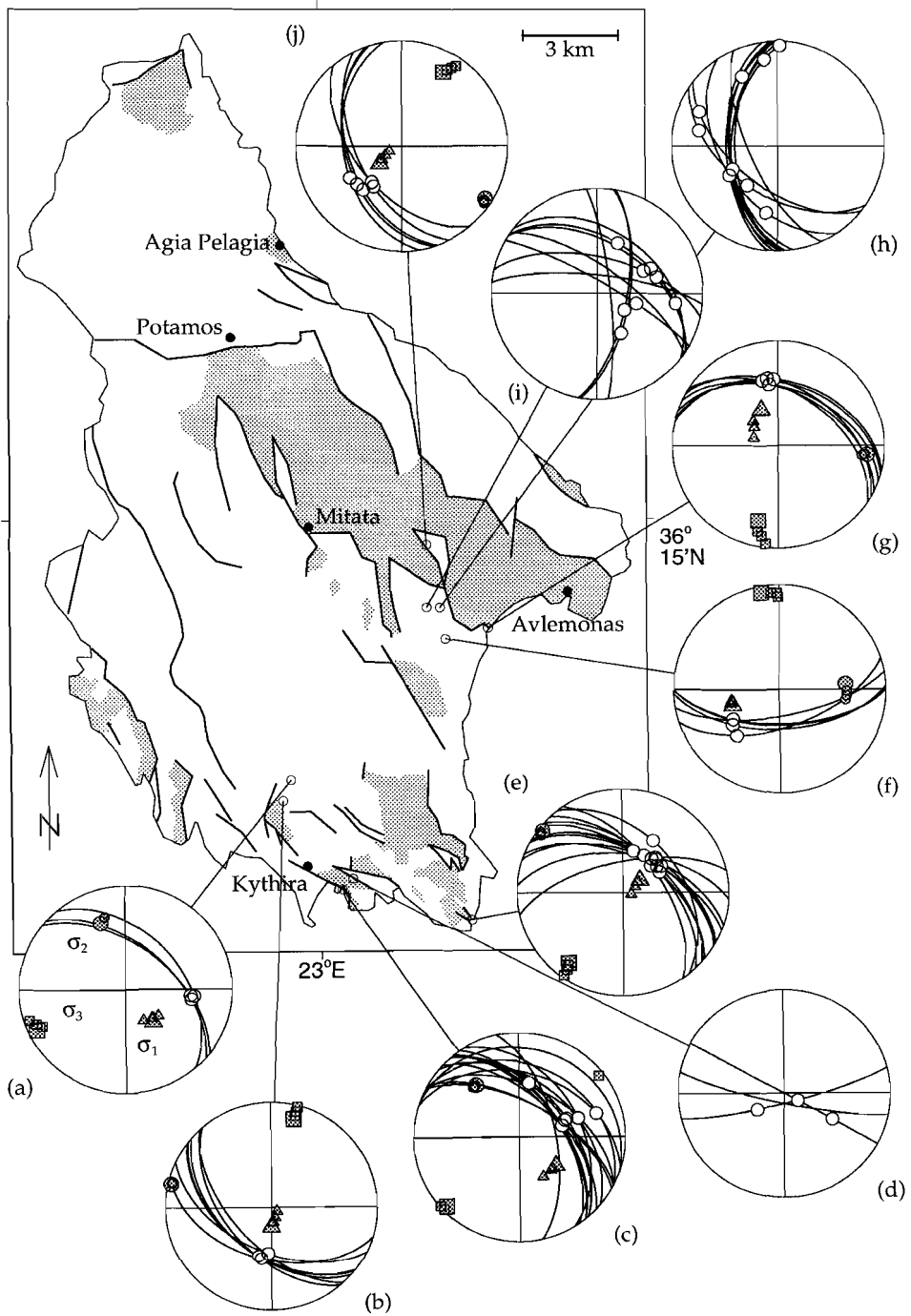
slip data is expressed in particular by the mean misfit angle: the angular deviation between observed slip vector and computed vector of resolved shear stress, averaged over all faults of the data set. For the fault at Lepreo, inversion yields a NNE-SSW orientation of the principal axis of tension (σ_3), irrespective of the assumed friction coefficient.

A small road-side quarry west of Lepreo displays metre-scale normal faults cutting the Pliocene sediments. The orientation of these faults (Figure 4.3, inset b) is also consistent with NNE-SSW directed tension. The pronounced morphological expression of the fault scarp near Lepreo suggests that the latter formed in the recent past: the stress regime with NNE-SSW orientated tension appears to be young.

The latter conclusion is in accordance with what little is known from previous studies of the western Peloponnese. *Lallemant* (1984) and *Lyberis* (1984) (see also *Lyberis and Lallemant*, 1985) report faults consistent with N-S to NNE-SSW tension that affect Upper Pliocene to Pleistocene sediments in the region of Olympia (Figure 4.3; results included in compilation of Figure 4.5a) and Upper Pliocene deposits in the southwest Peloponnese. On the basis of intra-formational faults in Upper Pliocene sediments in the Olympia region these authors conclude that a regime with N-S to NNE-SSW tension already existed by Late Pliocene time. As outlined above, the Kyparissia fault may evidence the existence of this tectonic regime also further towards the south during the Late Pliocene.

Kythira. Together with even smaller *Andikythira*, the island of *Kythira* continues the Hellenic island arc from the southeastern Peloponnese to western Crete. *Kythira* is characterised by a remarkably subdued topography with the highest point only just exceeding 500 metres. As a whole, the island rises over the seafloor towards the west and east by more than 1000 metre. The island is cut by numerous normal faults (Figure 4.4). Many of the footwalls display at their base pronounced scarps characterised by absence of vegetation, little erosion, and often

Fig. 4.4. (next page) Simplified geological map of the island of *Kythira* (from *Meulenkamp et al.*, 1977). Neogene sediments shown in grey, major faults as black lines. Insets show measurements of fault plane and striae along main faults. Lower hemisphere equal-area projection, top towards north; convention regarding fault data and calculated stress axes (grey symbols) as in Figure 4.3; all faults have normal component of slip. Details of results of inversion for stress are listed in the following. (a) Mean misfit angle 1°; stress ratio 0.2-0.4. (b) Mean misfit angle 2°; stress ratio 0.1-0.3. (c) Mean misfit angle 2°; stress ratio 0.3-0.5; NNE plunging striation not included. (d) No stress computed. Striae denoting sinistral oblique normal slip along NW-SE striking fault indicative of NW-SE to N-S directed tension. (e) Mean misfit angle 5°; stress ratio 0.3-0.5. (f) Mean misfit angle 0°; stress ratio 0.1-0.4. (g) Mean misfit angle 3°; stress ratio 0.2-0.4. (h) No stress computed. NNE to N plunging striae indicative of NW-SE tension; other striae point to E-W and SW-NE tension. (i) No stress computed. Striae indicating dextral oblique slip along N-S striking planes consistent with SW-NE directed tension; other striae point to SW-NE tension. (j) Mean misfit angle 2°; stress ratio 0.1-0.3.



well-developed slickensides. These basal strips represent the part of the footwall exposed by the latest, most likely quite recent, activity of the fault. Neogene deposits occur mainly in a long graben trending parallel to the northeast coast and in small fault-bounded depressions in the south of the island (Figure 4.4). The age of the youngest sediments present on Kythira, “middle” Pliocene (Theodoropoulos, 1973; Meulenkamp *et al.*, 1977), implies that the Pliocene to recent chronology of fault motion can not be precised on stratigraphic grounds.

As expressed by the lozenge shape of the island, the major faults of Kythira strike NW-SE and NNW-SSE to N-S. Measurements of fault planes and striae along several of the kilometre-scale faults are shown in Figure 4.4. Also shown are the results of inversion for the state of stress responsible for the observed motion. The orientation of the principal stresses proves to be little dependent on the value assumed for the friction coefficient.

As a first characteristic we note that most faults display oblique normal slip. This implies that the faults were reactivated in a stress regime with tension prevailing in one horizontal direction. In the case of radial tension the faults, irrespective of their orientation, would have slipped in the down-dip direction. The inversion method yields axes of maximum horizontal tension with orientations varying considerably from WSW-ENE to NNW-SSW. Roughly speaking, this orientation is consistent with the WSW-ENE orientation inferred for the recent regime in the southeastern tip of the Peloponnese and western Crete (see compilation Figure 4.5a). The low values of the stress ratio obtained from the inversion indicate that the second horizontal principal stress is also tensile. Assuming that our dataset is representative, it follows that there are few indications on Kythira for a stress regime characterized by maximum horizontal tension in the NW-SE direction. The latter is found to characterise the southern Peloponnese since the middle Pleistocene.

Our conclusions are mostly consistent with previous results obtained by Angelier *et al.* (1976) and Lyberis *et al.* (1982). In contrast to Angelier *et al.* (1982) we consider there to be little evidence for a subtle temporal change in the dominant direction of tension and include a tensional axes of varying orientation in the compilation for both the Pliocene and the recent period (Figure 4.5). This implies that our compilation also differs from that of Mercier *et al.* (1987) who emphasize the occurrence of NW-SE directed tension for the most recent period.

Regional compilation. It has been found that the evolution of the Aegean since the early Pliocene can be divided into two phases of extensional deformation separated by a period when compression prevailed throughout the area (see Jackson *et al.*, 1982 for an alternative view). The compression is estimated to have lasted from 1 to 0.7 Ma ago (Sorel *et al.*, 1992) and is therefore of very short duration. Our study concentrates on the extension, forming the dominant tectonic regime of the Aegean region since the early Pliocene. The available observations are compiled in Figure 4.5.

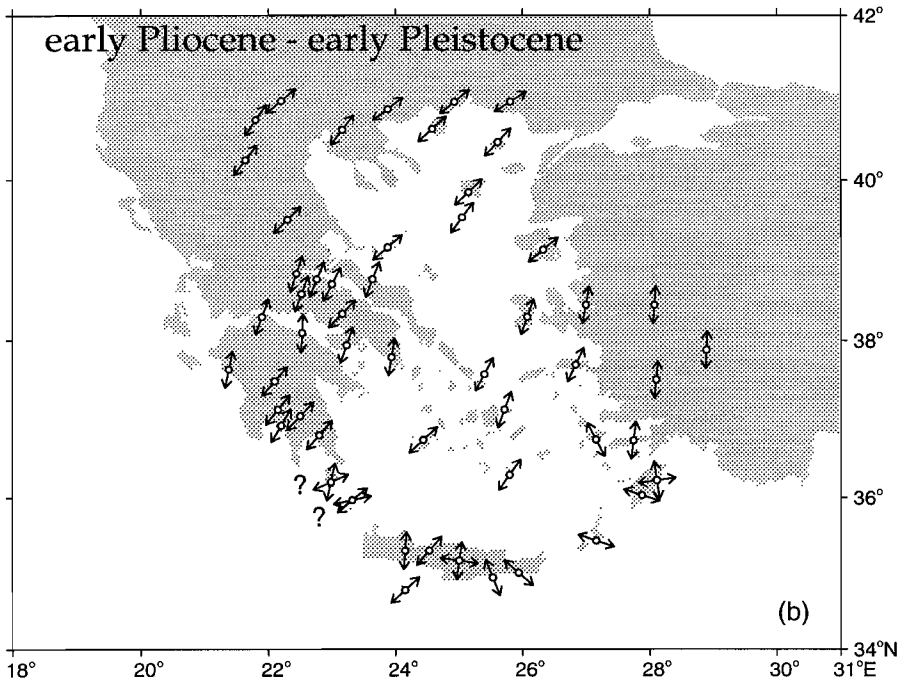
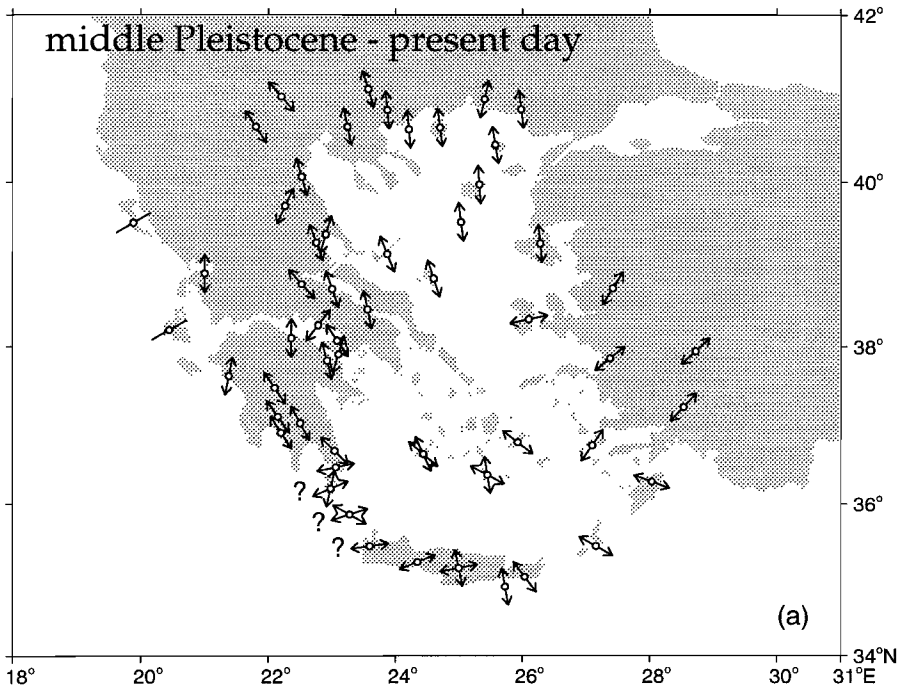
The present-day pattern of stress (Figure 4.5a) prevails since the middle

Pleistocene. Most of the Aegean region, including the island arc, is in a state of tension. The overriding margin is in compression in the Ionian islands of western Greece (Mercier *et al.*, 1972; Sorel, 1976). Although not providing information about the state of stress, geomorphological observations in the region of Epirus adjacent to the Ionian islands (King *et al.*, 1993), and seismic profiling in the straits east of Kefallinia and Zakynthos (Brooks and Ferentinis, 1984) do demonstrate active E-W to NE-SW shortening (i.e. strain).

Inwards from the active margin a regular pattern of tension can be observed (Figure 4.5a). The direction of tension is NNW-SSE to N-S in the western part: Gulf of Corinth, central Greece, Thessaly, west Macedonia and gradually changes to NNE-SSW - NE-SW in easterly direction: the northern Aegean islands, Thrace and western Turkey. Although Figure 4.5 only shows the orientation of the dominant horizontal principal axis at a given site, inversion of fault data also provides an estimate of the relative magnitude of the principal stresses. This shows that the second horizontal principal stress is often either a small tension or a compression in the northern Aegean (Mercier *et al.*, 1983; 1989) and in Thessaly (Caputo, 1990).

Fault data are more ambiguous for the southwestern Hellenic arc. Different opinions regarding the style of recent deformation have resulted in partly conflicting views on the nature of the driving forces involved (Angelier *et al.*, 1982; Lyberis and Lallemant, 1985; Mercier *et al.*, 1987; Armijo *et al.*, 1992). In the southern Peloponnese, a recent study found the present-day regime to consist of NW-SE orientated tension (σ_3 , with the second horizontal principal stress also of tensional character and of a magnitude amounting to half that of σ_3 (Mercier *et al.*, 1993; Mercier and Lalechos, in press). As on Kythira, directions of tension inferred from faults on Andikythira vary considerably and absence of recent sediments precludes establishment of a chronology (Angelier *et al.*, 1976; Angelier, 1979b; Lyberis *et al.*, 1982). Uncertain timing also holds for fault motion consistent with about E-W orientated tension on westernmost Crete (Angelier, 1979b; Lyberis *et al.*, 1982). As argued by Armijo *et al.* (1992) the fresh appearance of the fault scarps in question may imply that the inferred stress pertains to the recent regime, consistent with the interpretation of Angelier (1979b).

Notwithstanding these uncertainties we may note that, in contrast to the internal part with its gradually changing orientation of tension, the Hellenic arc from the southern Peloponnese to Turkey is characterised by approximately 90° changes in the orientation of the dominant principal axis of tension (Figure 4.5a). These occur from southern Peloponnese to west Crete (perhaps: to Kythira), from west to east Crete, and from Rhodes to southwest Turkey. The changes in orientation probably result from the two horizontal principal axes being of similar magnitude which allows a permutation of the axes of major and minor horizontal tension (Angelier *et al.*, 1982). Radial tension is suggested to prevail on central Crete where the perpendicular trending normal faults bounding the southeastern corner of the Ida mountains are inferred to have been active more or less



concurrently (Angelier, 1979b). As mentioned, significant tension in two horizontal directions characterises the southern Peloponnese (Mercier *et al.*, 1993). The islands of Karpathos and Rhodes are characterised by a dominant WNW-ESE trending tension, but on Karpathos normal faults trending perpendicular to, and simultaneously active with, the dominant normal faults orientated NE-SW are observed (Barrier and Angelier, 1981).

Separated from the present-day phase of deformation by the compressional event during the early Pleistocene was an extensional phase which commenced during the Early Pliocene (Figure 4.5b). Also during this phase, radial tension prevailed in the Hellenic arc on Crete and on Rhodes. The direction of tension in the internal part of the overriding plate during the early Pliocene - early Pleistocene was markedly different from the present-day configuration: NNE-SSW to NE-SW trending tension existed in most of the area. Following still older E-W directed tension, NE-SW trending tension also characterised the southern Peloponnese during the late Pliocene - early Pleistocene (Mercier *et al.*, 1993). Tension orientated NNE-SSW to N-S appears responsible for opening during the Late Pliocene of the Gulf of Amvrakia and Lake Trikhonis east of the Ionian islands (Doutsos *et al.*, 1987; Brooks *et al.*, 1988; Clews, 1989), but stress axes obtained by inversion of the measurements on the faults bounding these graben are not available. Tectonic structures indicative of the early Pliocene - early Pleistocene stress regime in the Ionian islands have so far not been found (Mercier *et al.*, 1993).

Seismic Strain: Earthquake Focal Mechanisms

In addition to geological studies of young faults, which provide information on the recent past, earthquakes express the deformation active at present. A compilation of published focal mechanism solutions of shallow events of moderate and large magnitude is shown in Figure 4.6. This compilation consists in the first place of focal mechanisms constrained by both body waveform analysis and first motion polarities (Taymaz *et al.*, 1990; 1991; Taymaz and Price, 1992; Taymaz, 1993; Lyon-Caen *et al.*, 1988) and is, for regions not covered by the before-mentioned studies, completed with centroid moment tensor solutions (as

Fig. 4.5. (previous page) Pattern of horizontal stress deduced from field-observed faults. Double arrow: principal axis of tension; short line: principal axis of compression. Length of symbols not proportional to stress magnitude. Two perpendicular arrows at the same site denote radial tension. Not shown is the compressive and tensional nature of the second (minor) horizontal principal stress evidenced respectively in the northern Aegean and southern Peloponnese. Question marks indicate that the age of corresponding fault activity is uncertain. (a) middle Pleistocene - present-day. (b) early Pliocene - early Pleistocene. Shown are the orientations as observed at present. Sources: compilations by Angelier (1979b), Angelier *et al.* (1982), Mercier *et al.* (1987, 1989, 1993) and original sources referenced in these papers; in addition: Lyberis and Sauvage (1985) for Thrace, Caputo (1990) for Thessaly, Papadopoulos and Pavlides (1992) for Amorgos.

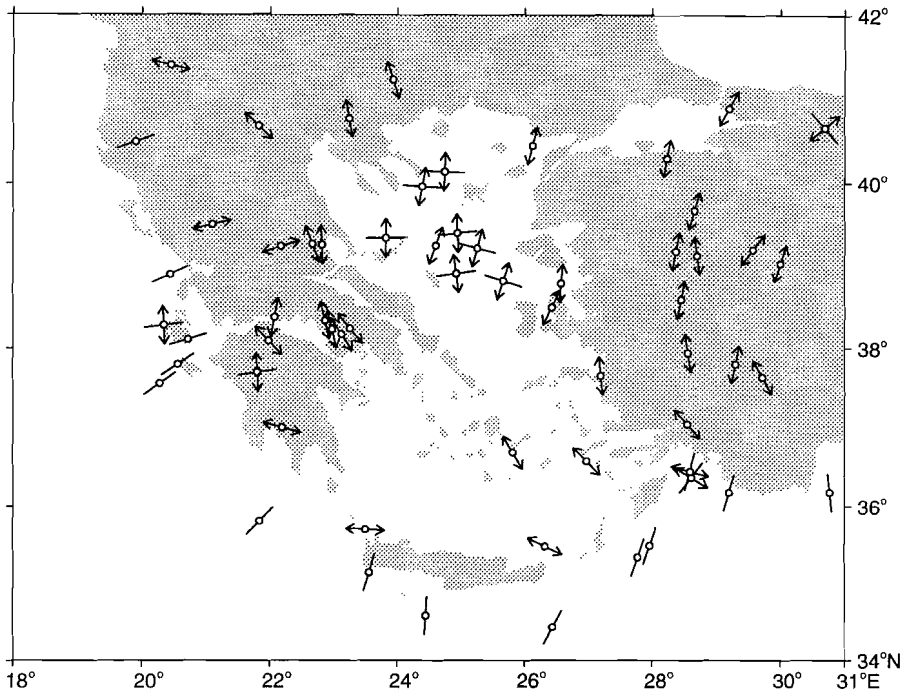


Fig. 4.6. Horizontal projection of P- and T-axes of focal mechanisms of moderate and large shallow earthquakes. Double arrow: T-axis; short line: P-axis. Extensional and thrust types of faulting are indicated by showing only T- or P-axis, respectively. Strike-slip faulting is indicated by showing both axes (because of projection not necessarily perpendicular). Although this manner of plotting does not show all information contained in a mechanism, it allows for easy comparison with observed and modelled stress and strain fields. Sources: *Taymaz et al. (1990; 1991), Taymaz and Price (1992), Taymaz (1993), Lyon-Caen et al. (1988), Ekström and England (1989), Anderson and Jackson (1987), and McKenzie (1972; 1978).*

reported in *Ekström and England, 1989*) and focal mechanisms based on first motion polarities only (*Anderson and Jackson, 1987; McKenzie, 1972; 1978*).

The horizontal pattern of T-axes (Figure 4.6), i.e. the pattern of seismically expressed extensional strain, is similar to the pattern of tensional stress derived from field observations (Figure 4.5a). Compression along the southern Hellenic arc in Figure 4.6 probably corresponds to thrusting at or near the subduction interface (*McKenzie, 1972; 1978*) and seismic slip vectors can be used to infer the direction of convergence. Earthquake data confirm the existence of a compressional margin in western Greece. Strike-slip faulting with approximately E-W directed P-axes is evidenced in the region of the northern Aegean Sea. The latter is consistent with the inference from field observations that, in the northern Aegean, horizontal stress in the direction perpendicular to σ_3 is compressive.

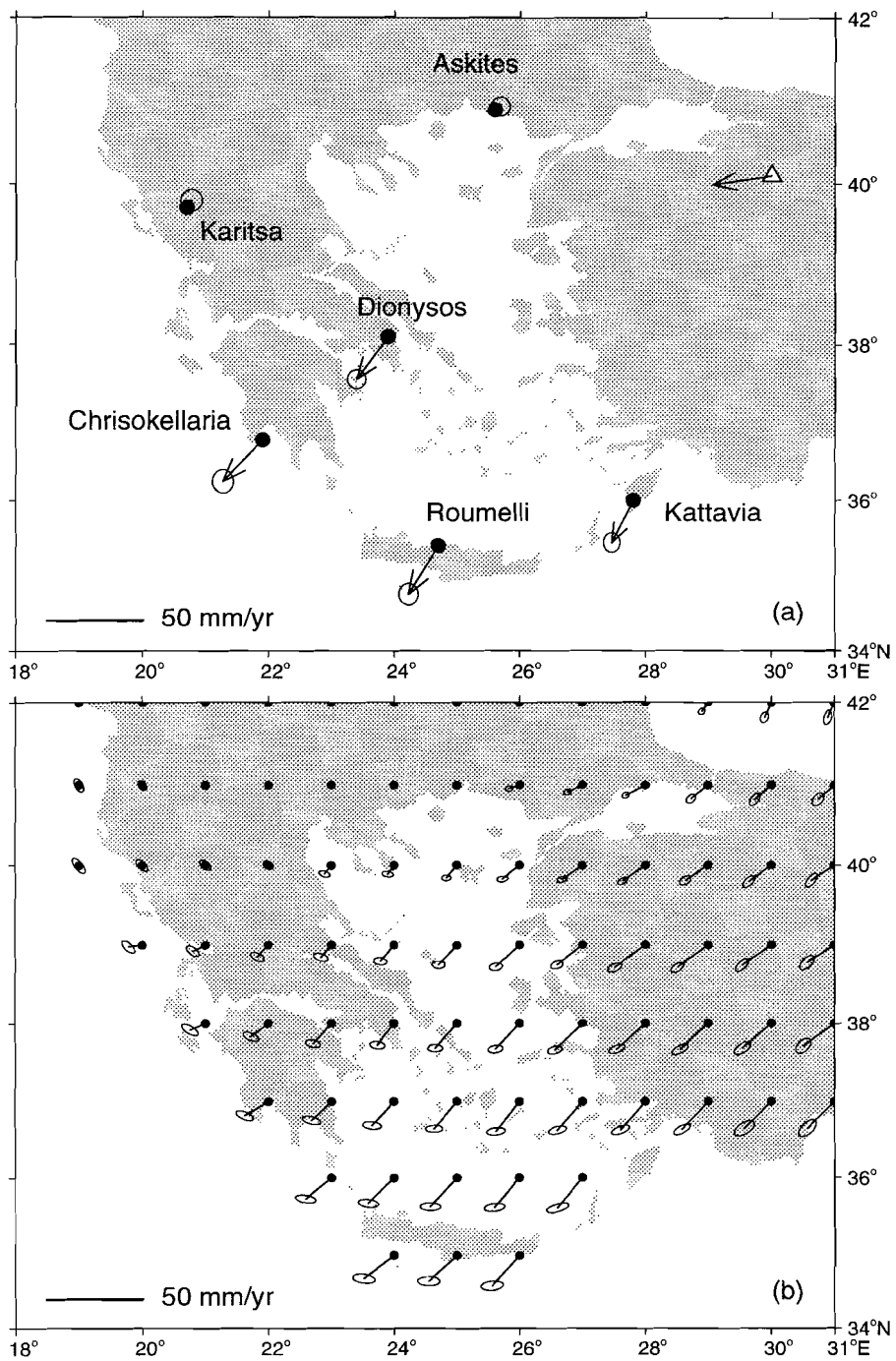
With respect to shallow events, the Sea of Crete - which was the locus of major north-south extension since the Early Pliocene - is found to be largely inactive seismically at present (*Galanopoulos, 1967; McKenzie, 1972*). The earthquake focal mechanisms which are available for the southern Aegean express E-W to NW-SE extension (*Lyon-Caen et al., 1988*). Although a state of radial tensional stress was found to characterise the Hellenic arc on the basis of field observations, the available earthquake data do not express radial extensional strain. The pattern of strain in the southern Aegean expressed by moderate and large earthquakes is consistent with that inferred from observations of microseismicity (*Hatzfeld et al., 1993*). Focal mechanisms which appear to deviate from the general trends outlined above are those indicating WSW-ENE extension below the Greek mainland and solutions showing NW-SE directed T-axes in southwestern Turkey.

Horizontal Motions

The transcurrent nature of the North Anatolian fault is evidenced by the focal mechanisms of earthquakes which have occurred along it (*McKenzie, 1972; and references therein*). Taking into account the change in slip vector azimuth observed along the North Anatolian fault, a pole of rotation of Anatolia with respect to stable Eurasia was obtained by *Jackson and McKenzie (1984)*. An upper bound for the rate of relative motion was obtained by these authors by assuming that all motion of Arabia relative to Eurasia is accommodated by strike-slip along the North and East Anatolian fault zones. The rotation pole predicts WSW directed motion of Anatolia at the longitude of the Aegean coast of Turkey. Actual crustal motion in this area will contain an additional component due to the extension deforming the Anatolian block internally (cf. *Taymaz et al., 1991*). Figure 4.7a shows the velocity calculated with the *Jackson and McKenzie (1984)* pole for a point at longitude 30°E located just south of the North Anatolian fault zone and north of the extensional domain of western Turkey. The rate of motion amounts to 31 mm/yr.

Slip vectors of earthquakes attributed to the contact between the overriding Aegean lithosphere and the subducting African plate demonstrate approximately NE-SW convergence (*McKenzie, 1972; 1978; Taymaz et al., 1990*). This implies that relative motion is close to perpendicular with respect to the western segment of the arc and is strongly parallel to the eastern segment. Further to the northwest, along the Ionian islands, relative motion is directed more towards WSW-ENE (*Mercier et al., 1972; Anderson and Jackson, 1987; Hatzfeld et al., 1993*).

Since recently, detailed information about active horizontal motions in the Aegean region is available through geodetical monitoring. Observations obtained using the Global Positioning System (GPS) have resulted in geodetical confirmation of the transcurrent nature of the North and East Anatolian fault systems (*Oral et al., 1993*). Westward motion of Anatolia relative to the area north



of the Anatolian fault zone was found to occur at an average rate of 24 mm/yr (Straub *et al.*, 1994). This value is smaller than the value inferred by Jackson and McKenzie (1984), which is consistent with the fact that the latter concerns a maximum estimate. Measurements by means of Satellite Laser Ranging in the context of the WEGENER/MEDLAS project have provided information about the motion of six stations in Greece (Noomen *et al.*, 1993; Robbins *et al.*, 1992). Figure 4.7a displays crustal motions relative to stable Eurasia according to a geodetic solution incorporating results of four SLR campaigns, organized in the period 1986-1992, and two GPS campaigns, held in 1989 and 1992 (Noomen *et al.*, 1994). Velocity vectors obtained for the three stations in the Hellenic arc and the station in central Greece are orientated towards the southwest with rates amounting to 31 mm/yr in southwest Peloponnese. No significant motion is evidenced for the stations in Epirus and in Thrace.

Further insight into tectonic motions in the Aegean region is provided by a recently established dense network of GPS stations in western Greece (Kahle *et al.*, 1993), and a GPS network employed in the southern Aegean (Gilbert *et al.*, 1994). Reoccupation with GPS of an old triangulation network has provided information regarding central Greece (Billiris *et al.*, 1991).

A continuous velocity field that describes the active overall deformation of the Aegean region at large length scale was obtained by Jackson *et al.* (1992) by fitting a velocity field to the spatial variation in seismic strain rates. Figure 4.7b shows the velocity field based on all available earthquakes with $M_s > 6.0$ from the period 1909-1983 excluding those associated with convergence along the overriding margin and with the subducted slab. Jackson *et al.* (1992) obtained a second velocity field ignoring data from a possible seismic gap in western Turkey but the difference between the two fields is small and not relevant in the present context. In general, the velocity field based on earthquakes shows slightly slower rates of motion than the geodetic solution (Figure 4.7). The directions of motion agree well; in the Hellenic arc the geodetic solution shows motion somewhat more southwards. The velocity field obtained by Jackson *et al.* (1992) again demonstrates roughly southwestward motion in the southern Aegean. In agreement with the SLR results no significant motion is inferred for points in northwestern Greece.

Fig. 4.7. (previous page) Present-day horizontal velocities in the Aegean region relative to stable Europe. (a) Motions derived by means of Satellite Laser Ranging for the six WEGENER/MEDLAS sites in Greece (black dots, station names indicated). Shown is solution SSC(DUT)94C01 (Noomen *et al.*, 1994). This solution incorporates observations of the fourth (1992) SLR campaign and combines SLR and GPS measurements. Error ellipses represent the $3\text{-}\sigma$ formal uncertainty of the vector solutions which is considered a maximum value for possible errors. Also shown in this figure is the velocity at a point in northwestern Turkey (triangle) as predicted by the Turkey-Eurasia pole derived by Jackson and McKenzie (1984). (b) Horizontal velocity field fitted to the spatial variation in seismic strain rate. Shown is the "all-data" velocity field of Jackson *et al.* (1992). Scale as in (a).

Figure 4.8 illustrates the current kinematics of the Hellenic subduction zone (cf. *Angelier et al.*, 1982; *Jackson and McKenzie*, 1988a). The geodetic solution is adopted to define motion of the central and eastern Hellenic arc relative to stable Eurasia. The NUVEL-1 Euler vector is used to describe Africa - Eurasia motion (*DeMets et al.*, 1990). Since the Euler pole is located far from the Hellenic subduction zone and the latter is of relatively small dimensions, Africa - Eurasia motion does not vary significantly along the arc. Consistent with the orientation of earthquake slip vectors at the plate contact, relative motion (vector A-C) is seen to be about normal to the western arc segment and strongly parallel to the eastern segment. Also, Figure 4.8 demonstrates that relative motion in the subduction zone is directed more towards north-south than arc-Eurasia motion. Specifically, even though motion of the eastern arc with respect to Eurasia is almost parallel to the strike of the margin (as indicated both by geodesy and the velocity field based on seismic strain), relative motion between this arc segment and Africa comprises a component of convergence due to the approach of Africa and Eurasia.

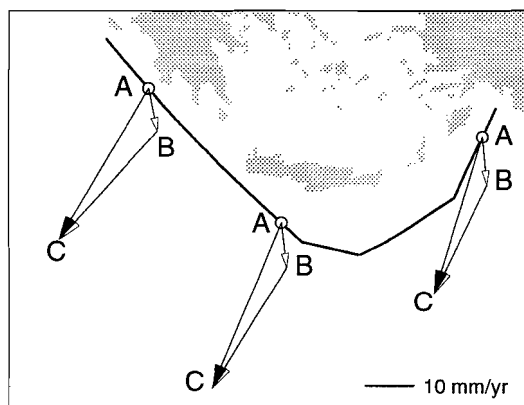


Fig. 4.8. Current kinematics of the Hellenic subduction zone. Velocity triangles illustrate relation between the relative motion vectors. Motion of the Hellenic arc relative to Africa (vector A-C) is the sum of Eurasia-Africa convergence (vector A-B) and Hellenic arc - Eurasia motion (vector B-C). The NUVEL-1 global plate motion model (*DeMets et al.*, 1990) is used to define Eurasia - Africa motion. Motion of the western, central, and eastern arc segment relative to Eurasia is assumed to be given by the geodetic velocity found for the station on Peloponnese, Crete, and Rhodes, respectively (Figure 4.7a). This figure is constructed using a geodetic solution slightly older than that displayed in Figure 4.8a; differences for the arc region are negligible, however. Present-day geography is shown for reference; thick line indicates overriding margin.

Taking into account the paleomagnetically determined rotations of the various parts of the area (*Kissel and Laj*, 1988), estimates of the amount of extension of the Aegean, and estimates of the westward motion of the Anatolian

plate, it is possible to reconstruct the paleogeography of the Aegean (*Le Pichon and Angelier, 1981; Angelier et al., 1982; Westaway, 1991, and below*). These reconstructions suggest that motion of the Hellenic arc with respect to Eurasia has been roughly southwestwards at least since the beginning of the Pliocene. Moreover, slow convergence between Eurasia and Africa has been directed approximately north-south throughout this period and, consequently, the important characteristics of the present-day pattern of subduction, mostly normal to the western segment of the arc and with a significant component parallel to the arc at the eastern segment, have prevailed at least since the beginning of the Pliocene.

Suggested Mechanisms and Present Approach

Mechanisms controlling the extensional deformation of the Aegean region which have been suggested in literature concentrate around two main factors (i) the westward motion ("escape") of the Anatolian block from the Arabia-Eurasia collision, and (ii) the Hellenic subduction zone.

Westward Motion of Anatolia

The Anatolian plate exerts a westward push on the Aegean lithosphere which is likely to be a combination of stresses transmitted from the block's trailing edge in the Arabia-Eurasia collision (*McKenzie, 1972; 1978; Tapponnier, 1977*), and buoyancy forces resulting from the thickened crust of eastern Turkey (*McKenzie, 1972; Taymaz et al., 1991*). In the concept of lateral "tectonic escape" of Anatolia from the Arabia-Eurasia collision, the combined presence of a southward bending trend of the North Anatolian fault zone (Figure 4.2), blocking continued westward motion, and an easily overridable oceanic slab in the south, is suggested to lead to southward expulsion and extension of the Aegean lithosphere (*Dewey and Şengör, 1979*). An additional factor blocking westward motion due to the displacement of Anatolia is the collision between northwestern Greece and the Adriatic lithosphere (*Taymaz et al., 1991*). The question as to the nature of the driving force of the motion of Anatolia is discussed by *Kasapoglu and Toksöz (1983), Şengör et al. (1985), and Oral et al. (1993)*. In this study we will investigate the significance of the westward push for the evolution of the Aegean region.

The Hellenic Subduction Zone

Instead of merely providing a free southern boundary to an Aegean lithosphere deforming in response to the westward push of Anatolia, the subduction zone could itself generate forces which drive the extension of the overriding plate. As suggested by *McKenzie (1978)*, the downgoing plate in the Hellenic subduction zone may generate a secondary convection current in the overlying mantle wedge which, in turn, would exert a shear stress at the base of the overriding lithosphere causing it to extend. Analysed quantitatively with a simple model by *McKenzie*

(1978), the importance of secondary convection for the evolution of the Aegean was advocated recently by *Wdowinski et al.* (1989) on the basis of a more detailed numerical model.

Alternatively, *Le Pichon and Angelier* (1979; 1981) emphasized the role of southward retreat of the subduction zone. This retreat or "roll-back" is likely to be driven by the gravitational pull acting on the subducted slab. Since, in the land-locked setting of the East Mediterranean, extension of the Aegean Sea and roll-back of the subduction zone are clearly linked in a kinematical sense, roll-back is frequently cited as the driving mechanism of the Aegean extension. However, the question to address is whether and how roll-back and upper plate extension are linked dynamically. In other words: what is the nature of the so-called "suction force" apparently experienced by the upper plate (*Elsasser*, 1971) in the particular setting of the eastern Mediterranean. Secondary convection, described above, may be regarded as one of the possible mechanisms (*Elsasser*, 1971; *Forsyth and Uyeda*, 1975).

In the concept developed by *Le Pichon and Angelier* (1979), expanding suggestions by *Makris* (1977) and *Berckhemer* (1977), roll-back is considered to provide room for gravitational spreading of the overriding plate. This hypothesis rests on the notion that, due to its different density structure as a function of depth, the Aegean lithosphere possesses a higher gravitational potential energy than the lithosphere of the east Mediterranean basin (cf. *Molnar and Lyon-Caen*, 1988). This region of relatively high potential energy will spread horizontally when roll-back causes the lateral constraint imposed at the overriding margin to be relaxed.

Slab Detachment

A schematic interpretation of the tomographic image of the oceanic slab subducted below the Aegean (*Spakman*, 1991; *Spakman et al.*, 1993) is shown in Figure 4.9. Although the subducted plate appears continuous to great depth at the longitude of the island of Crete (*Spakman et al.*, 1988) tomography indicates that further west there exists a discontinuity at a depth of 100-250 km. The gap in the subducted slab extends horizontally from below the northwestern Balkan to an ill-defined point between Crete and the Peloponnese. The presence of the discontinuity is confirmed by recent resolution tests (*de Jonge et al.*, 1994) and is interpreted to result from detachment of the deeper part of the slab. Detachment is envisaged to have initiated in the northwest and the tip of the tear is thought to have migrated southeastwards through time to yield the present-day configuration (*Wortel and Spakman*, 1992; *Yoshioka and Wortel*, in press).

When detachment occurs along a given segment of a subduction zone then the weight of the subducted slab is no longer transmitted to the shallow portion of the downgoing plate. In other words, locally, the driving force of roll-back will vanish. Depending on how roll-back of the subducting plate is related to the driving force of trenchward motion of the upper plate (which forms one

of the questions we set out to answer) slab detachment could stop such driving forces from being exerted, or could lead to an increase of the resistance against convergence, or both.

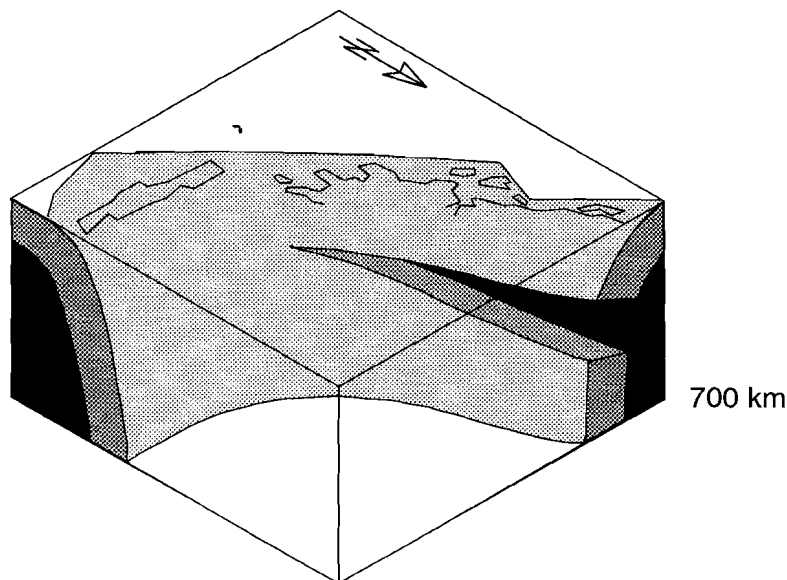


Fig. 4.9. Schematic block diagram (after Wortel and Spakman, 1992) of the eastern Mediterranean illustrating the geometry of the slab in the Hellenic subduction zone as interpreted from tomographic results (Spakman *et al.*, 1988; Spakman, 1991). View from the northeast. At a depth of 100-250 km the deeper part of the descending slab is detached, except in the region near Crete. Vertical extent of block diagram is up to a depth of 700 km.

Present Approach

The significance of the westward Anatolian push, the nature of forces possibly associated with the subduction zone, and the role of lateral migration of slab detachment will be examined by using a forward numerical model to calculate the horizontal pattern of stress and deformation associated with various force distributions. The pronounced curvature of the overriding margin and the strong lateral variation in the character of subduction along this margin, render it unlikely that the stress regime in the overriding plate can be evaluated in terms of a vertical cross section perpendicular to the trench. Moreover, only an analysis of the horizontal pattern of tectonics will elucidate the combined effects of subduction related forces and westward Anatolian push.

Model Description

We will assume that, on the scale considered in this study, the Aegean may be regarded as a continuously deforming region. The Aegean lithosphere is modelled as a thin elastic shell; calculations are done with the finite element method. Apart from a representation of the North Anatolian fault zone in some experiments, the model is homogeneous with respect to elastic properties and plate thickness. Whereas some of the force distributions which will be analysed may be taken to represent forces resulting from lateral variations in lithospheric (density) structure and topography, the latter are not explicitly accounted for.

The elastic model clearly forms a simplification of the actual lithosphere but serves as a good starting point for a numerical simulation. An elastic model provides us with the instantaneous stress and strain pattern associated with a given set of forces. This approach is clearly appropriate when applied to the present-day situation: in this case also the observations pertain to a momentary view of the on-going deformation. Given that an elastic model is incapable of simulating finite deformation, our approach to the problem of temporal evolution is to model instantaneous deformation for a specific point in time in the past. This is done on the basis of a reconstruction of the geometry of the region. The assumption of lateral homogeneity implies that localisation of deformation and strain partitioning cannot be accounted for. In particular given the fact that it may be impossible to include such effects a-priori in an unambiguous manner, the benefit of a homogeneous model is that, by comparing model results and data, it allows us to evaluate the importance of any inhomogeneities.

Even though, in finite element modelling, stress follows as a quantity derived from the displacements for which is solved, we will reverse this order in the presentation of the model results. Finite element meshes were devised representing the present-day geometry of the Aegean region and the geometry which approximately existed 2 Ma ago, during the Late Pliocene (see below). In both cases the mesh is extended sufficiently far to the north and east to ensure that the corresponding margins, considered fixed, do not affect the region of interest. Modelled displacements should be considered to represent motion relative to stable Eurasia. In the model for the present-day, the mesh boundary representing the overriding margin follows the axis of the western segment of the Hellenic trench from Kefallinia to central Crete, and from there the axis of the Strabo trench northeastwards. The latter is consistent with the observation that both sides of the Pliny trench consist of continental basement (*Peters and Huson, 1985*). Placing the mesh boundary at the Pliny trench, or smoothing the irregular margin east of Rhodes, is found not to significantly affect the computed displacements and stress. The finite element mesh is assumed to be of uniform thickness which implies in particular that the tapering of the continent near its overriding edge is not accounted for.

The curved surface of the shell is approximated using flat triangular

elements of the linear displacement type. Finite element calculations are based on Zienkiewicz (1971). All model results are displayed overlain on a conventional Mercator projection of the region of interest. Since we will not address the problem of absolute values of either forces or stress, the actual values of Young's modulus and plate thickness adopted (resp. 7×10^{10} Pa and 100 km), merely serve as scaling factor. Variation of Poisson's ratio within reasonable limits (value used: 0.25) can be shown to have no significant effect on the results. The stresses obtained by finite element calculation are horizontal non-hydrostatic principal stresses, integrated over the thickness of the plate thickness. Included in subsequent figures will be average stress values for a plate with the reference thickness of 100 km. With a plate thickness of 100 km the relation between the magnitude of the force applied at a boundary and the corresponding stress is particularly simple: an applied force of - say - $c \times 10^{12}$ Newton per metre boundary, corresponds to an average stress of $c \times 10$ MPa. For example, in the case of an applied force of 1×10^{12} N/m the associated stress amount to 10 MPa or, equivalently, 100 bar. In all model experiments presented below this relation is emphasized by using symbols of identical length for a boundary force of $c \times 10^{12}$ N/m and an intra-plate stress of $c \times 10$ MPa.

An important characteristic of the isotropic elastic shell model is the fact the orientation of the resulting principal axes of stress is identical to the orientation of the principal axes of (instantaneous) strain. In some experiments anisotropic elements will be introduced (see below); obviously, in these elements the above-mentioned characteristic does not hold. Calculated displacement fields will be evaluated using the observed horizontal velocities. Since an elastic model does not yield rates of motion we can only compare orientation and relative magnitude of computed displacements against that of the observed velocities.

Collision of the Aegean margin with the Adriatic lithosphere, northwest of the island of Levkas, is modelled by considering this part of the margin to be completely blocked. It would perhaps be more realistic to represent the collision by means of a resistive force acting on the Aegean margin. However, apart from the fact that the correct orientation of such resistance is uncertain, its magnitude relative to the other forces included in the models is not known a-priori. The effect of this particular boundary condition has been assessed by repeating the experiments also with the northwestern margin unconstrained.

Model Analysis, Present-day Situation

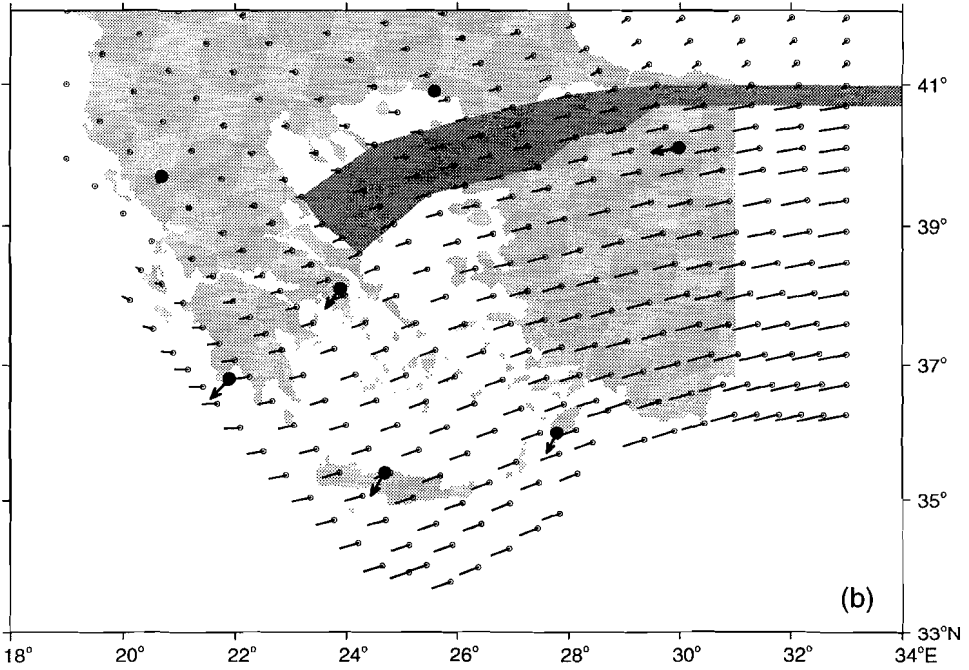
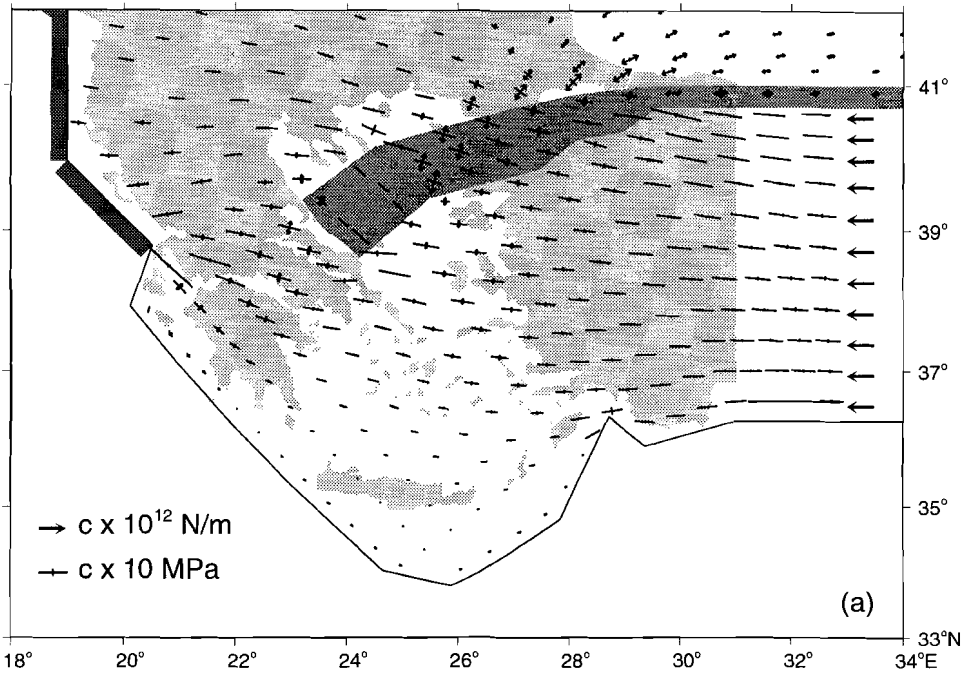
Using the mesh devised for the present-day geometry, we present in this section modelled stress, strain, and displacement patterns associated with different assumptions regarding the acting forces. Model results are evaluated using the observations of stress for the middle Pleistocene - present-day period, seismic strain, and current horizontal motions.

Consequences of Westward Anatolian Push

In order to model the deformation associated with the westward push exerted by the Anatolian plate, the North Anatolian fault zone is represented by means of anisotropic elements (Figure 4.10; Zienkiewicz (1971), see also Richardson *et al.* (1979), Drewes and Geiss (1986)). In these elements the resistance to slip in the direction parallel to the local strike of the zone is reduced by a factor of 10^3 with respect to the rest of the plate. This value was chosen so as to obtain maximum decoupling, to the east of longitude 31°E , of the motion of the Anatolian block from the part of the model to the north of the fault zone. Further reduction of the shear modulus does not significantly increase the decoupling. The highly reduced shear modulus was checked not to affect the stability of the solutions. Anisotropic elements were assumed to cover the region where faults accommodating dextral strike-slip are identified by Taymaz *et al.* (1991) and Simeakis *et al.* (1989) (Figure 4.2). Not accounted for in the model is a possible strand of the fault zone to the north of the North Aegean trough (Figure 4.2), since it is not apparent how this fault connects with the main zone to the east. The row of anisotropic elements extends eastwards from the region shown in Figure 4.10 to the distant eastern model boundary. Although the use of anisotropic elements may render stress computed for elements in the fault zone less realistic, it does provide a reasonable approximation of the effect of the fault zone as a whole on the remainder of the plate. The westward directed force is modelled as a uniform stress exerted normal to a north-south section at longitude 33°E , extending from the southern boundary of the model to just below the fault zone elements. The southern margin of the model and the part of the eastern margin south of the eastward continuation of the North Anatolian fault zone are left unconstrained. The margin northwest of Levkas is considered blocked by assigning a zero displacement boundary condition.

The calculated stress pattern (Figure 4.10a) mainly shows E-W to WNW-ESE orientated compression. A small additional component of tensional stress is observed immediately southwest of the termination of the fault zone. Compression in this model is a consequence of both the locking geometry of the North Anatolian fault zone (cf. Dewey and Şengör, 1979) and blocking of the westward

Fig. 4.10. (next page) Model of deformation associated with westward Anatolian push. Dark shading shows distribution of anisotropic elements representing the North Anatolian fault zone and its westward continuation. (a) Computed stress field. Bold arrows indicate applied stress, in this case a representation of the westward directed push; bars along model border northwest of Levkas denote zero-displacement boundary condition assigned there. The southern margin is left free. Double arrow: principal axis of tension; short line: principal axis of compression. Intraplate stress (full symbol length) is scaled relative to the applied force per metre; see text for details. (b) Computed instantaneous displacements. The exact scale is not relevant; in all the displacement fields presented in this paper the maximum displacement is shown at the same length. Bold arrows give the observed motions of Figure 4.7a for comparison (panel c on page 28).



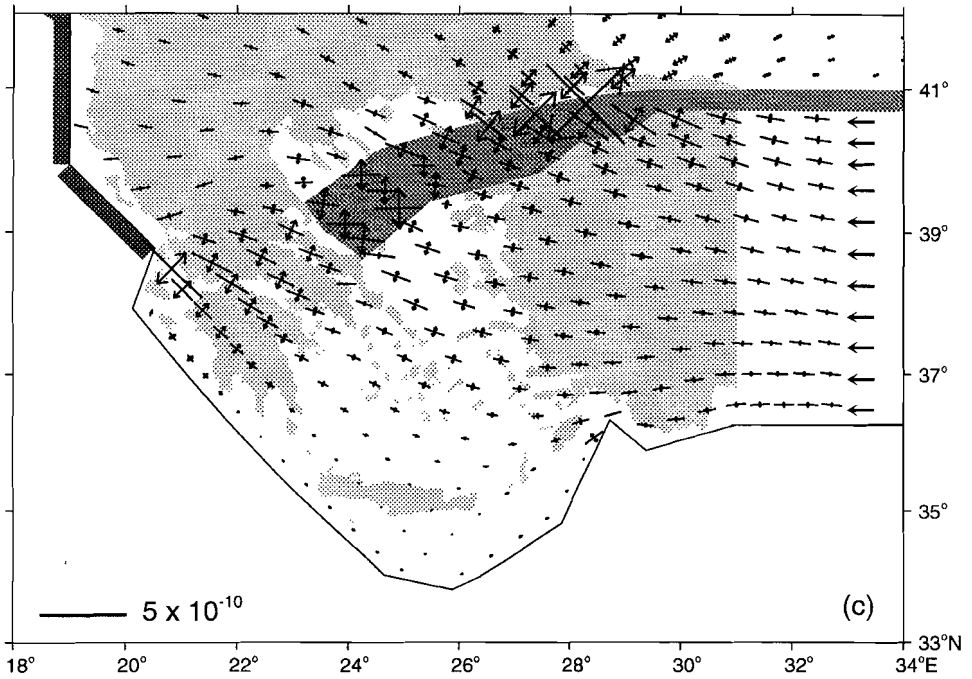


Fig. 4.10. (continued) (c) Computed strain. Double arrow: principal axis of lengthening; short line: principal axis of shortening. Scale as indicated; large strains within North Anatolian fault zone are partly omitted.

motion by the northwestern margin (cf. *Taymaz et al.*, 1991). The modelled displacement field (Figure 4.10b) clearly displays the desired right lateral displacement along the North Anatolian fault zone east of 31°E. Further west, differential displacement is distributed over an area of increasing extent. As a result of the boundary condition applied to the margin northwest of Levkas the model does not predict significant displacements in northwestern Greece in accordance with the negligible velocity found for the SLR station in Epirus and the velocity field obtained by *Jackson et al.* (1992). Calculations have also been performed assuming the northwestern margin to be blocked only northwest of latitude 42°N and leaving the Ionian segment unconstrained. In this case compressive stress in northwestern Greece is orientated more towards NW-SE and displacements towards W and WNW are found in central and northwestern Greece. Although the model shown here is in agreement with the observed motion of Anatolia relative to Eurasia, displacement predicted for the Hellenic arc is more to the west than observed (Figure 4.10b).

Figure 4.10c shows the instantaneous strain pattern associated with the model. Whereas tensional stress is largely absent, extensional strain does occur

but always in association with shortening in the perpendicular direction. Within the fault zone extensional strain is inherent to the strike-slip deformation occurring there. The orientation of the principal axes of strain computed in and close to the fault zone compares well with the orientation of P- and T-axes derived for earthquakes which occurred in the northern Aegean Sea (Figure 4.6). In northern and northwestern Greece and in western Turkey the model shows dominantly shortening. Southwest of the termination of the fault zone, in central Greece, the modelled strain pattern displays a component of NNE-SSW orientated extension in addition to the dominant WNW-ESE shortening. Both the direction of extension and the occurrence of shortening in this region are apparently in disagreement with the observed seismic strain (Figure 4.6). However, it has been argued by *Taymaz et al.* (1991) that because the blocks bounded by normal faults in central Greece are rotating about vertical axes, the region may in fact be accommodating a shortening. Rotation would also cause the direction of slip along the individual faults, and hence the orientation of derived T-axes, to deviate from the regional direction of lengthening while the latter is that predicted by a continuum model of deformation as in Figure 4.10c.

The model of the westward Anatolian push does mismatch without doubt the observations in the Hellenic arc region and western Turkey: the model does not show extensional strain while this is evidenced seismically (Figure 4.6).

On the basis of the model experiments we conclude that the westward Anatolian push is not the only force controlling the recent deformation. The mismatch between model results and observations, described in the above, is found to be independent of (1) the geometry of the fault zone, (2) the character of the restriction of the northwestern margin, and (3) the representation of the westward Anatolian push. In the following section the forces related to the subduction zone will be addressed.

Forces Associated With the Subduction Zone

In order to establish the nature of subduction related forces we will explore several models in which different forces are assumed to act along the overriding margin. Placing the forces at the extreme margin of the model may constitute a simplification of the actual situation. However, the existence of forces pulling the overriding margin is not ruled out *a priori* by the observation of compressional seismic deformation in the trench region (Figure 4.6). The latter may very well reflect shortening due to convergence of the two plates meeting at the subduction interface which is in fact caused by forces driving the overriding plate trenchwards. In contrast, northwest of about longitude $21^{\circ}30'E$ the Hellenic arc is characterised by compressional deformation extending significantly inwards from the overriding margin (Figure 4.5 and 4.6) and pulling forces on the plate boundary are only included to the east of this point. This approach is valid as a consequence of our assumption that the driving force of upper plate extension acts at the plate margin. It would perhaps be more realistic to include resistive

forces on the margin between $21^{\circ}30'E$ and the island of Levkas. However, the orientation of these resistive forces is unknown and instead of introducing more variables we will make the reasonable assumption that the effect of any resistance is small compared to that of the pull acting on the much longer remainder of the arc. In the models of the subduction related forces the margin to the northwest of Levkas is again considered to be completely blocked.

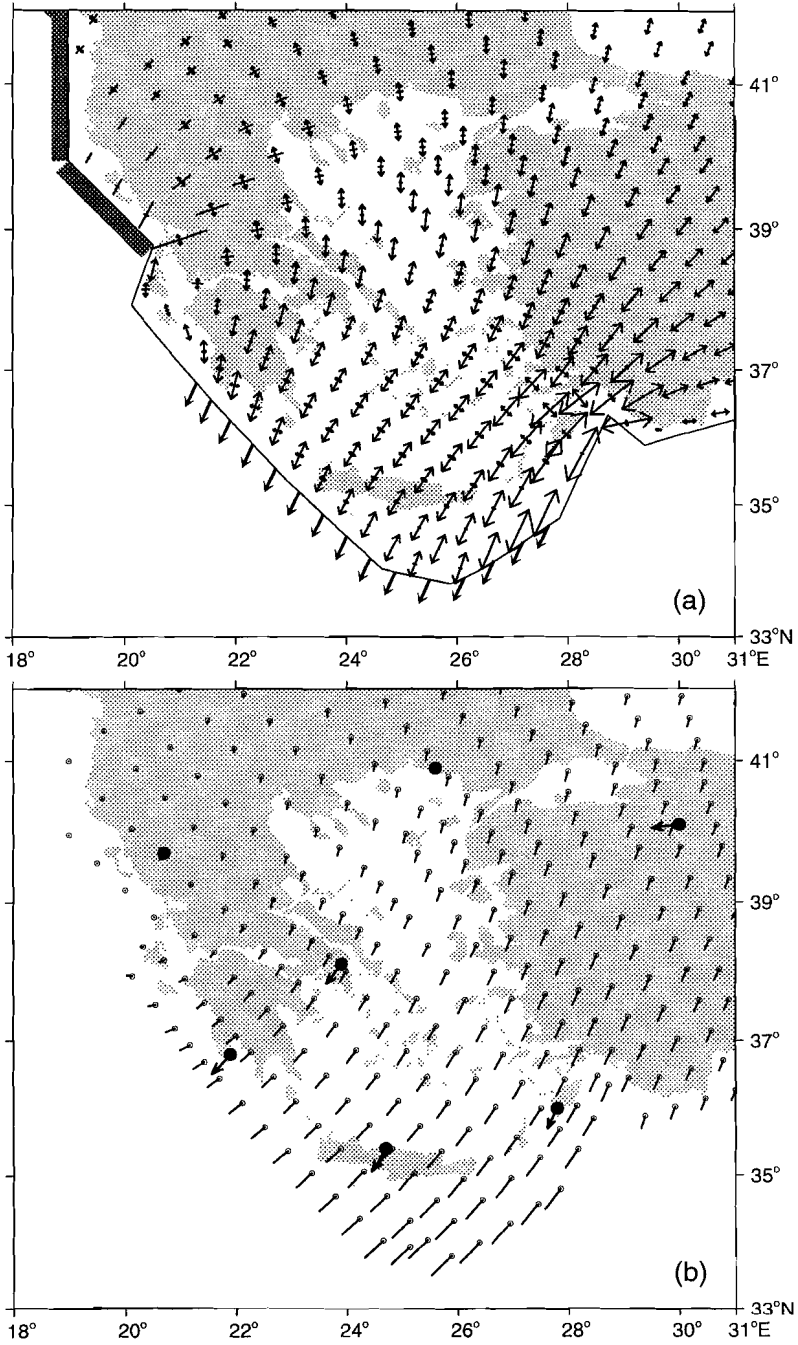
Pull parallel to relative motion. The first model which will be studied serves to examine the possibility that the subducting plate causes a pull to be exerted on the overriding margin in the direction of relative motion at the trench. Although a physical basis for this force distribution may not be obvious it is interesting to analyse this model because it is conceptually the most straightforward, following as it does from a direct translation of motions in terms of forces.

The pull acts in the direction $N155^{\circ}W$, i.e. parallel to the azimuth of Hellenic arc-Africa relative motion near West Crete determined on the basis of earthquake slip vectors by *Taymaz et al.* (1990). A constant magnitude is assumed. No force is exerted on the easternmost arc segment near Rhodes since this segment trends parallel to the applied pull. In order to isolate the deformation associated with the subduction-related forces, the North Anatolian fault zone and the westward directed push are not included in the model.

The calculated stress field is shown in Figure 4.11a, instantaneous displacements of the nodal points are depicted in Figure 4.11b. The modelled stress field shows tension in the direction of the pull in the southern Aegean and western Turkey rotating towards N-S in the central and northern parts of the region. The forces on the overriding margin pull the plate against the blocked northwestern margin. The resulting compression, NE-SW directed, affects the orientation of the small tensional stresses in this region. The magnitude of tensional stress increases towards the eastern end of the Hellenic arc. There, pull on the arc is orientated at small angle to the margin which causes intraplate stress close to the margin to be amplified. Apart from the northwestern region, the stress field can be shown not to change significantly when the northwestern margin is assumed to be blocked only to the north of latitude $42^{\circ}N$ and free slip is allowed along the Ionian segment.

The associated displacement field (Figure 4.11b) shows motion towards the SSW in the northern Aegean and western Turkey, gradually changing to SW in the southern Aegean. Along the arc from east to west displacement gradually changes from SSW directed towards WSW directed. Most nodal points within the Greek mainland show small or zero displacement. When the northwestern margin

Fig. 4.11. (next page) Model of deformation associated with forces at the overriding margin. Pull at the margin is taken parallel to the direction of relative motion in the subduction zone near western Crete. Westward Anatolian push and the North Anatolian fault zone are not accounted for. (a) Computed stress field. (b) Computed displacements. See caption to Figure 4.10 for further explanation.



is left unconstrained, the obtained displacement field differs from that shown in Figure 4.11b to the west of 22°E where now small SW displacements are predicted. In the region to the east of this longitude no significant effect is found.

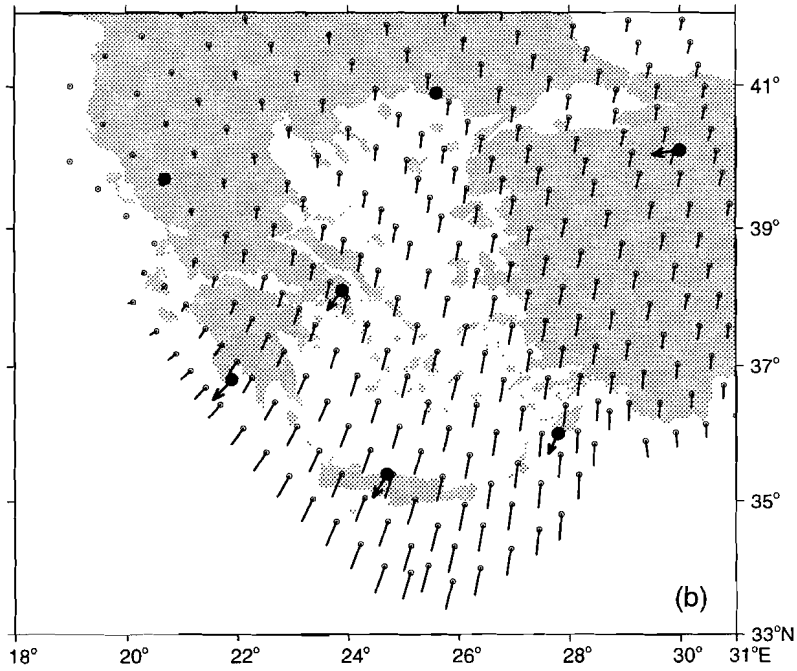
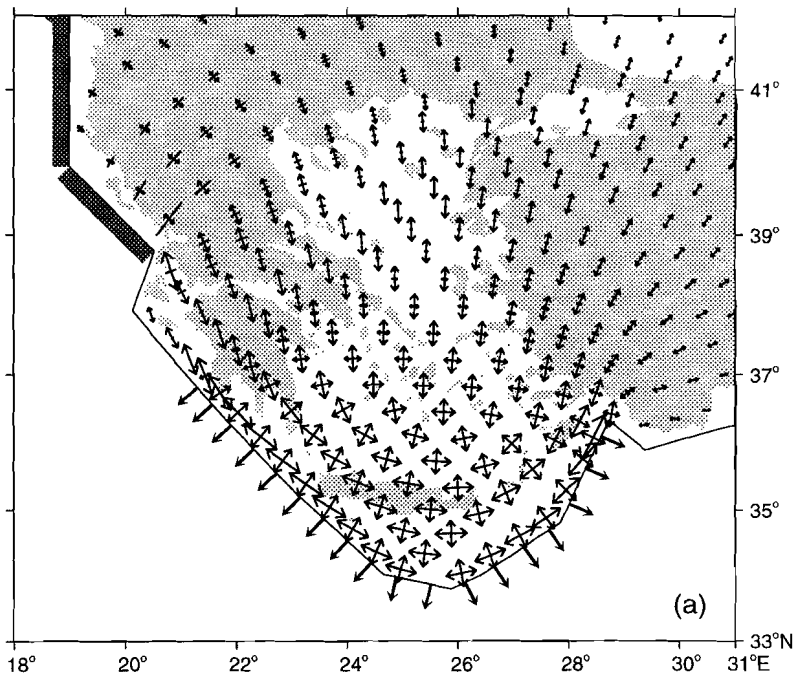
Modelled orientations of tensional stress (Figure 4.11a) correlate well with the observed directions of tension (Figure 4.5a) in western Turkey and in the region of the northern Aegean Sea including the adjacent parts of the Greek mainland. The modelled stress field does not match the observations in the southern Cyclades and the Peloponnese and fails to predict the occurrence of an additional component of approximately NW-SE tension observed along the Hellenic arc from the Peloponnese to Rhodes (Figure 4.5a).

Displacements calculated for the arc region are orientated consistently further to the west than the applied pull. The shape of the deforming region and the distribution of the pull cause the arc not to move in the direction of the exerted force. Although the restriction imposed to the margin northwest of Levkas affects displacements predicted for northwestern Greece it can be demonstrated not to control the motion of the southern arc. The displacements found for the arc are, at least in a qualitative sense, consistent with the assumption that the applied pull is in the direction of relative motion in the trench: SW motion of the arc in Figure 4.11b is with respect to Eurasia and yields, in combination with the north-south convergence between Africa and Eurasia, a SSW-NNE azimuth of relative motion along the overriding margin (cf. Figure 4.8). The orientation of the computed displacements proves to be in reasonable agreement with the geodetically determined directions of motion in the Hellenic arc and central Greece (Figure 4.11b). The model does, however, not account for the westward motion of Anatolia.

Absence in the southernmost Aegean of a state of stress with both an along-arc and an across-arc component of tension, as in the model result of Figure 4.11a, is typical when pulling forces are directed essentially in the same direction. Another example, not shown here, would be a model in which the margin from the southwestern Peloponnese to Rhodes is considered to be loaded by a uniform pull directed due southwards. In this case, the modelled stress field is found to match the observed stress field to a large extent except for the Hellenic arc region where, again, the model fails to predict along-arc tension.

Uniform arc-normal pull. As an alternative to the previous model we will investigate the possibility that pulling forces on the overriding margin associated with subduction are orientated perpendicular to the trench (cf. *Forsyth and Uyeda, 1975*; Figure 4.12). For example, such radial outward pull is expected to be associated with the mechanism of gravitational spreading since spreading forces act along the gradient in gravitational potential energy.

Fig. 4.12. (next page) Model of deformation associated with a pull of uniform magnitude acting perpendicular to the overriding margin from SW Peloponnese to Rhodes. (a) Computed stress field. (b) Computed displacements. See Fig. 4.10 for further explanation.



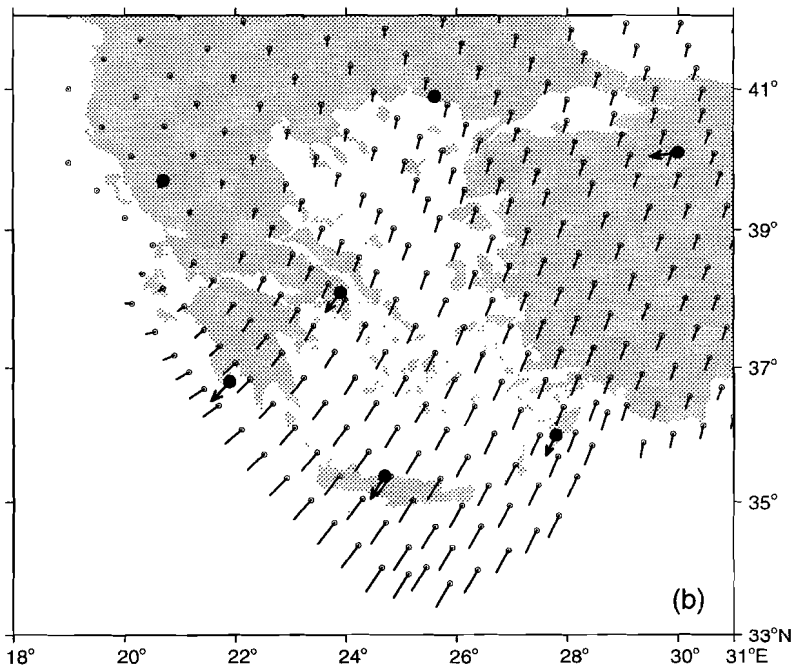
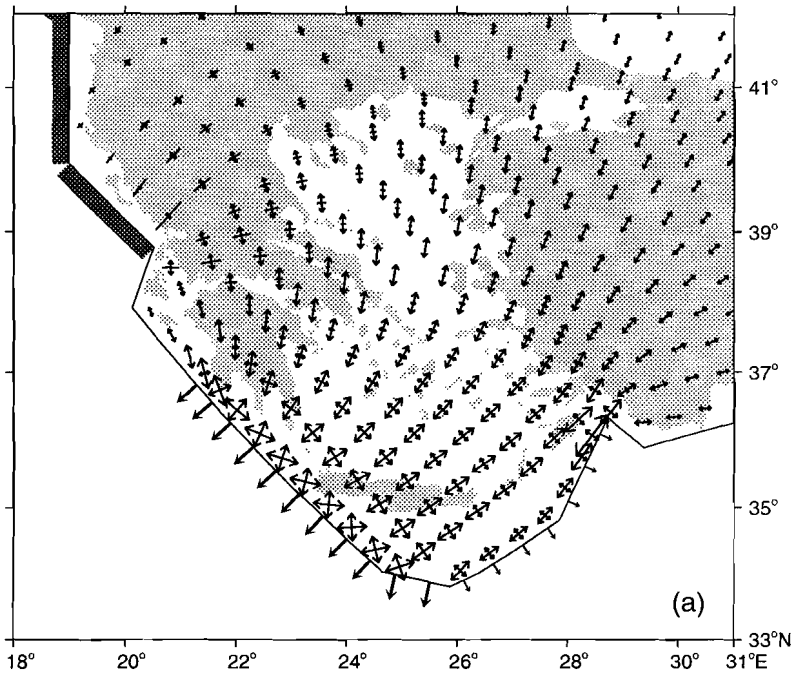
The arc-normal pull is assumed to be of uniform magnitude from the southwestern Peloponnese to Rhodes (Figure 4.12). In the stress field obtained with this configuration (Figure 4.12a) the principal axes of tension display a diverging pattern from the southern Hellenic arc northwards. The overriding margin and the region of the Sea of Crete are characterised by almost radial tension. In the overriding margin the component along the strike of the arc is slightly larger than the across-arc component. North of about latitude 38°N tension is essentially uniaxial. Inwards from the collisional northwestern margin tensional stresses are present but are subordinate to approximately NE-SW directed compression. The latter controls the orientation of the tensional principal axis in the same manner as was observed in Figure 4.11a. When the northwestern margin is left unconstrained no compression is predicted and the dominant tension in northwestern Greece rotates in a clockwise sense towards NNW-SSE. The same is true, however to a much smaller extent, for tension in the Peloponnese region. The area further to the east is unaffected.

The displacement field, shown in Figure 4.12b, displays SSW motion of the arc near western Crete changing to more westerly azimuths going along the arc to the west, and to more southerly orientations going towards the east. This southward divergence of displacements of the arc is a characteristic feature of this model and is consistent with the occurrence of along-arc tension. The divergence of motions is not the result of our specific assumption concerning the nature of the northwestern margin. When the latter is left unconstrained displacement throughout the region is directed slightly more southwards than in the case of Figure 4.12b. The described divergence, however, remains.

The modelled stress field (Figure 4.12a) matches the stress derived from field observed faults (Figure 4.5a) to a large extent. The model correctly predicts the observed northward divergence of the principal axes of tension in the internal part of the region and shows almost radial tension in the region of the arc, in accordance with the overall character of the stress field observed there. Compression predicted by the model (Figure 4.12a) is approximately at right angles to the major late Cenozoic folds and thrusts observed in the region of Epirus. However, recent and active shortening (strain) may be orientated more towards E-W (P. van Wamel, pers. comm., 1992; King *et al.*, 1993), a discrepancy with the model results perhaps due to the simplified nature of the boundary condition assigned to the northwestern margin.

Arc-normal pull, varying magnitude. In order to determine the effect of changes in the magnitude distribution of the outward pull we analyse a model in which the magnitude of arc-normal pull is reduced by a factor 0.5 from east Crete towards Rhodes relative to pull at the western arc (Figure 4.13).

Fig. 4.13. (next page) Model of deformation due to arc-normal pull where magnitude of pull at eastern arc segment is equal to half the magnitude of pull at the western segment. (a) Computed stress field. (b) Computed displacements.



Modelled stress matches the observed pattern of tension in the north and central Aegean and predicts radial tension near western Crete. Computed directions of tension deviate from those observed in the southern Peloponnese and the Cyclades. Most important is the absence in the modelled stress field of significant NW-SE orientated tension in the eastern Hellenic arc. The modelled displacement field shows motion in the southern Aegean only slightly more southwards than found for the model featuring a constant SSW directed pull (cf. Figure 4.11).

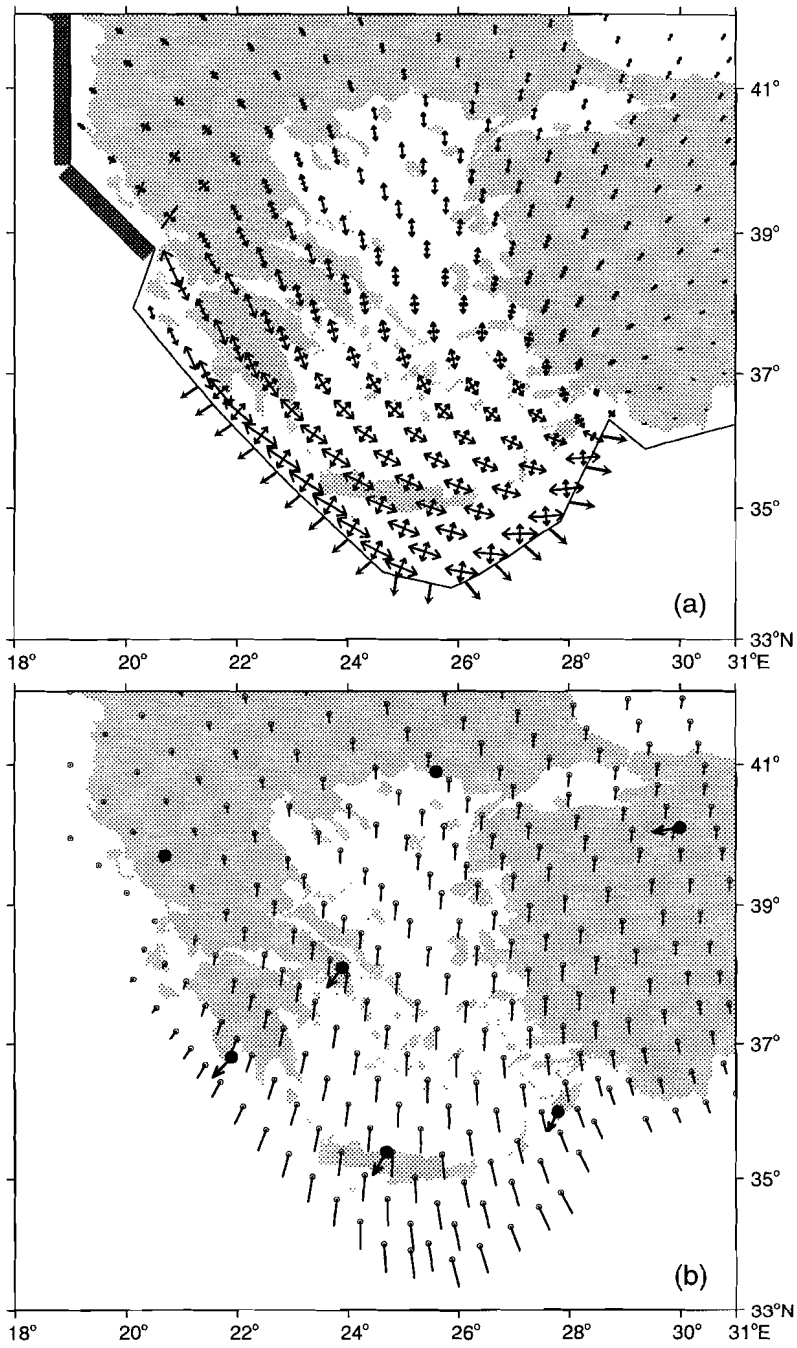
The effect of a relative reduction in the magnitude of pull acting at the western arc segment is now readily appreciated: it will be opposite to the effects seen in Figure 4.13. Less pull towards the SW will result in a prevailing NW-SE orientation of the principal tensional stresses and in displacements rotated anti-clockwise relative to those displayed in Figure 4.12b.

Arc normal pull and subduction zone resistance. Although the prevalence of normal faulting suggests that the net force experienced by the overriding Aegean margin is an outward pull, the latter may well consist of a combination of pull and a resistive force associated with convergence in the trench. As in the case of the Andean margin of the South American plate such resistance is expected, at least to first approximation, to act in the direction parallel to relative motion. Uncertain, however, is the magnitude of resistance. In this experiment we will consider the situation in which resistance is of uniform magnitude along the entire margin.

We add to the uniform distribution of arc normal pull of Figure 4.12 a resistive force with azimuth N25°E, the direction of relative motion along the Cretan segment of the arc (*Taymaz et al.*, 1990). The magnitude of resistance is taken to be relatively small; in the experiment presented here it amounts to 25% of that of the outward pull.

When we compare the stress field thus calculated (Figure 4.14a) with the stress field obtained with only arc-normal pull (Figure 4.12a), differences are observed in the southern Aegean. In case additional resistance is incorporated, tension predicted for the arc region is no longer radial but largest in a NW-SE to WNW-ESE direction. This particular pattern is caused by the additional resistance in two ways. Firstly, the NNE directed resistance preferentially reduces the magnitude of pull on the western arc segment. Secondly, additional resistance rotates pull on the western segment in a clockwise manner, and pull on the eastern segment in an anti-clockwise sense. The modelled stress field matches the fanning pattern of tension observed in the central and northern Aegean and is

Fig. 4.14. (next page) Model of deformation due to a combination of uniform arc-normal pull (as in Figure 4.12) and a resistive force in the direction of relative motion in the subduction zone. The additional resistance amounts to 25% of the pull. Shown is the resultant force distribution applied to the overriding margin. (a) Computed stress field. For clarity, dominant tensional axis is shown in bold. (b) Computed displacements.



consistent with the observations in the Peloponnese. The data available for the Cyclades, showing NNW-SSE to NW-SE oriented tension, are matched somewhat closer in case additional resistance is included. However, the model results depicted in Figure 4.14a are not consistent with observations of WSW-ENE trending tension from the southernmost Peloponnese to central Crete.

The displacement field calculated for the combination of arc-normal pull and resistance (Figure 4.14b) shows displacement orientated SSE in the southeastern Aegean where displacement was directed southward in the case of arc-normal pull alone (cf. Figure 4.12b). The deviation between modelled displacements and observed motions is thus larger in case additional resistance is incorporated.

We may note that the prevalence of WNW-ESE to NW-SE trending tension in Figure 4.14a is consistent with the pattern of T-axes in the southern Aegean (Figure 4.6). In order to examine more closely the relation between our model and the observed seismic strain, we take the inferred seismic fault planes and determine the direction in which slip would occur according to the modelled stress pattern. Slip vectors thus predicted are compared against the observed slip. The concept has been described in detail in Chapter 3. The results are shown in Figure 4.15. Both the stress field associated with uniform arc-normal pull and the stress field found with additional resistance yield a reasonable agreement for the events which occurred in the southeastern Cyclades and off western Crete. Neither of the models matches the observed slip for the Kalamata earthquake and the event near eastern Crete. The fit for the events off eastern Crete and near Kos is slightly improved if additional resistance is incorporated. The misfit found for the Kalamata event is probably somewhat misleading. The model with uniform arc-normal pull matches the general stress field in the southern Peloponnese closely and detailed investigation has shown the latter to be consistent with the focal mechanism, when the uncertainties in the data are taken into account (*Mercier and Lalechos, in press*).

Subduction Forces and Westward Push Combined

The displacement field obtained for the case of uniform arc-normal pull (Figure 4.12b, see also Figure 4.14b) shows motion of the southern Aegean which is consistently more towards the south than the geodetic observations. The result that westward Anatolian push causes a westward motion of the southern Aegean suggests that a combination of arc-normal pull and westward push could provide a match to the observed motions. The fact that a contribution of westward push must be invoked follows from the stress field also: forces associated with subduction alone do not explain the component of east-west compression evidenced in the northern and central Aegean Sea. The stress field and displacements calculated with a combined model in which the magnitude of westward push per metre north-south section is equal to half the magnitude of

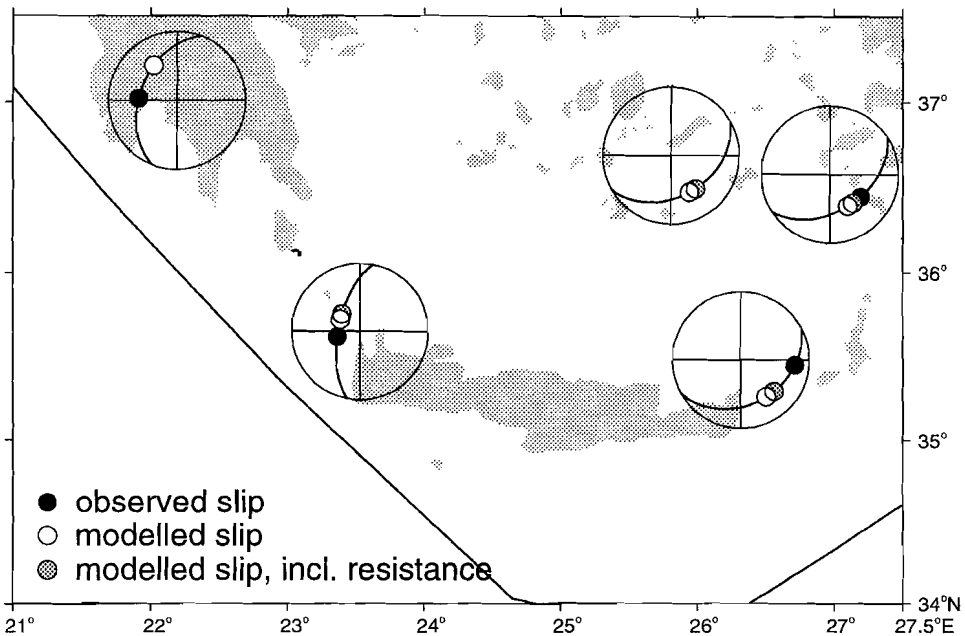
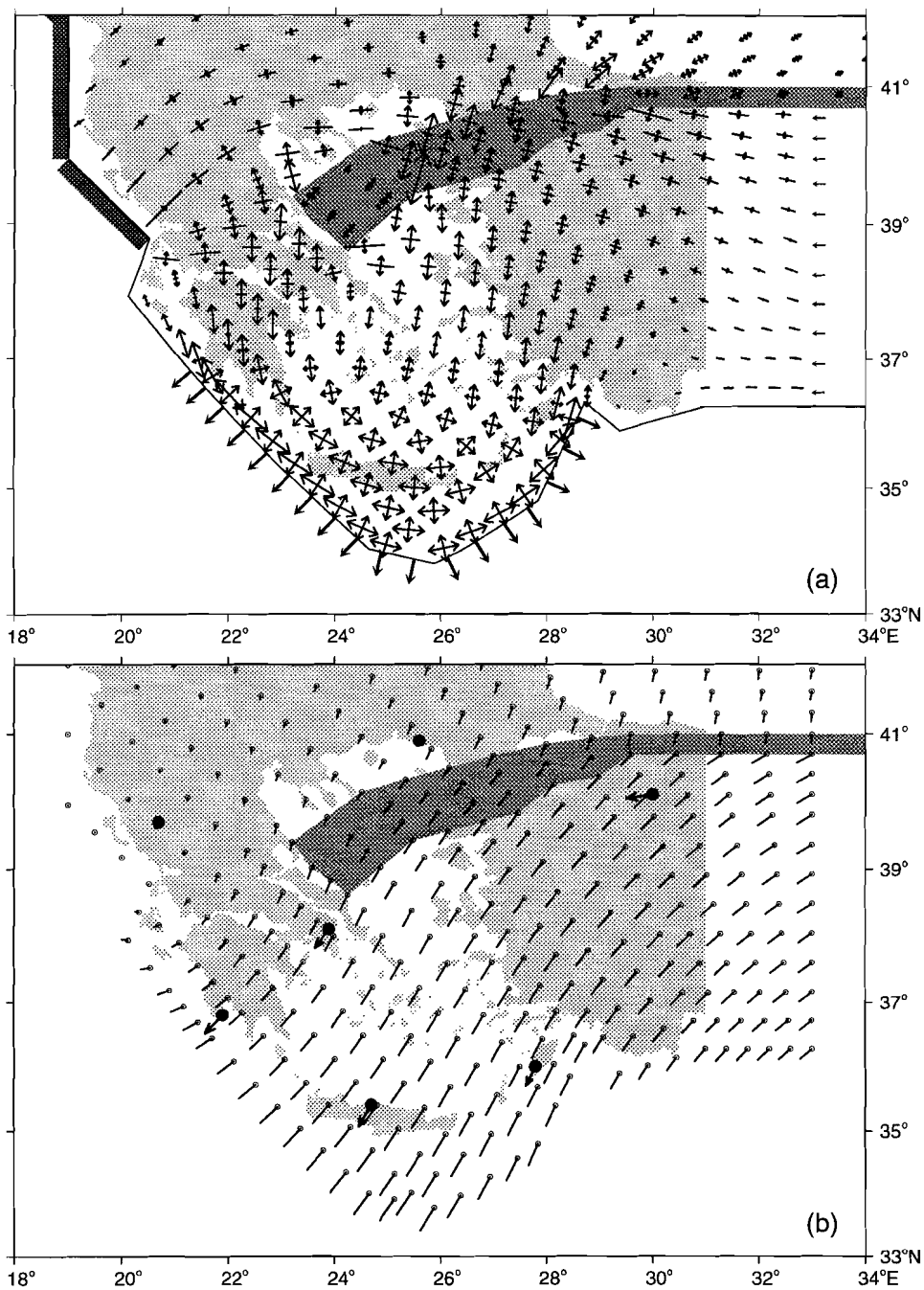


Fig. 4.15. Comparison of observed seismic slip and slip calculated on the basis of modelled stress fields in the southern part of the Aegean. Shown in lower hemisphere equal area projection are the seismic fault (great circle), observed slip vector (black dot), slip predicted according to the stress field associated with uniform arc-normal pull (white dot), and slip associated with the stress field due to arc-normal pull and additional resistance (grey dot). Note that white dot may cover grey dot; both white and grey dot may cover black dot. Both observed and modelled slip everywhere correspond to (oblique) normal faulting. Sources of focal mechanism solutions, Kalamata (date 860913) and west Crete (650427): *Lyon-Caen et al.* (1988); east Crete (790723): *Dziewonski et al.* (1987); Amorgos (560729): *Jackson and McKenzie* (1988b); Kos (681205): *McKenzie* (1972). For the latter event the fault plane was not discriminated from the two nodal planes by the author; the choice is not relevant to the present analysis, however.

the arc-normal pull per metre plate margin, are shown in Figure 4.16. The NorthAnatolian fault zone and its westward continuation are represented in the same manner as in the model isolating the effects of westward push (Figure 4.10). The northwestern margin is considered blocked.

Fig. 4.16. (next page) Model combining the westward Anatolian push (Figure 4.10) and a uniform arc-normal pull (Figure 4.12). Magnitude of westward directed force per metre north-south section equals half that of pull per metre at the overriding margin. (a) Computed stress field. (b) Computed displacements. See Fig. 4.10 for further explanation.

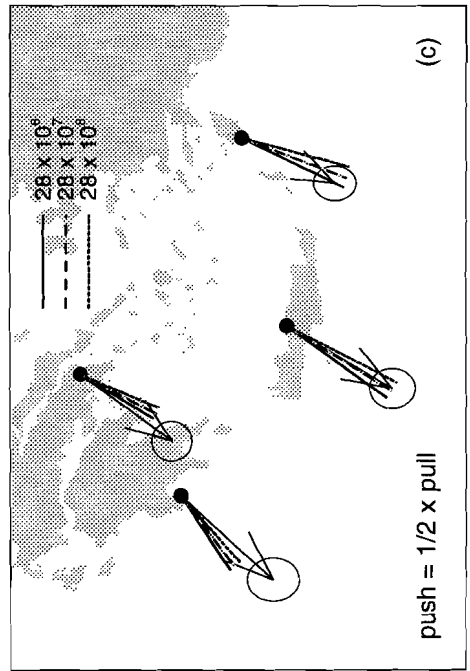
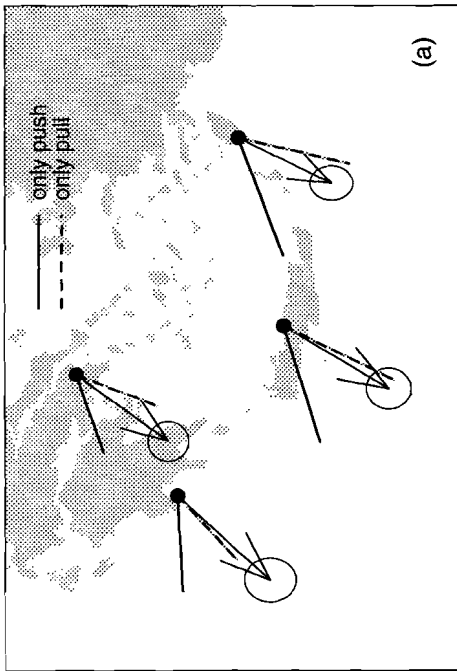
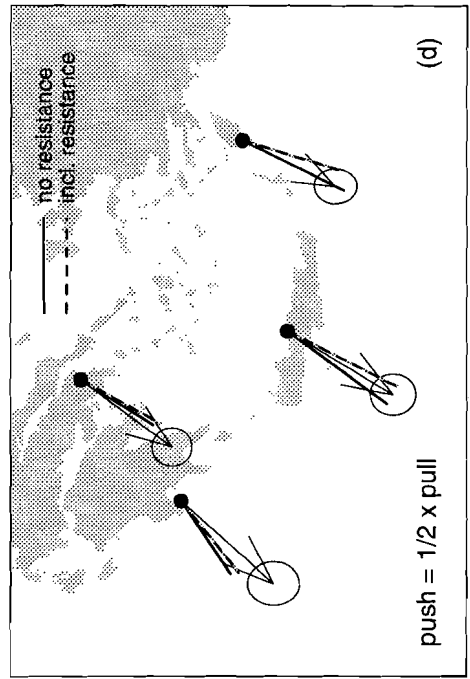
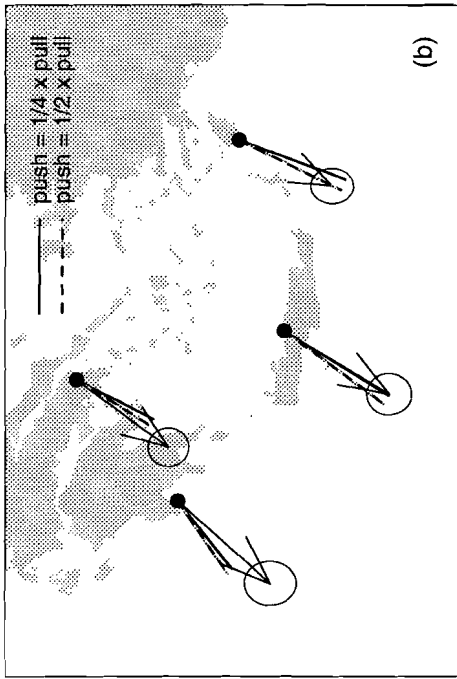


The computed stress field displays approximately east-west compression in addition to the dominant tension in the central Aegean Sea, central Greece, and western Turkey. Northwest of the fault zone, compression, as a combined effect of the blocked northwestern margin and the westward Anatolian push, now constitutes the dominant horizontal principal stress. The model is in agreement with the observed stress field (Figure 4.5a) in the sense that the model predicts radial tension in the arc, approximately north-south tension in the internal part, and additional east-west compression in the central part. In the Peloponnese the model in Figure 4.16 does not match the observed pattern of tension as closely as the model excluding the westward push since principal axes of tension are rotated by the additional east-west compression. When computing expected slip directions of seismic faults as in Figure 4.15 using the stress field of the combined model, somewhat larger angles of misfit are obtained for the events near Amorgos and Kos.

The displacement field found for the combined model is in good agreement with the observations in the southern Aegean. Including the North Anatolian fault zone in the model with uniform arc-normal pull, even without applying any westward push, already rotates the displacements closer to the observed directions. An additional relatively small westward push provides a match with the observed motion of the arc region. Of particular interest is the situation at the eastern arc segment: motion almost parallel to the strike of the margin occurs even though the margin is subject to an outward pull. Combined with Africa-Eurasia convergence the modelled pattern of motion complies with the predominantly transform nature of the eastern trench system (cf. Figure 4.8). It follows that the occurrence of strike-slip relative motion should not be interpreted as indicating that the margin is a transform fault in the sense that it is subject to horizontal compression.

In the northern part of the Aegean the modelled displacement field matches the data less well. Although relative motion across the North Anatolian fault zone is mainly right-lateral, the region as a whole is shown by the model to have a small southward motion. In other words, in northwestern Anatolia and the neighbouring region of Thrace the model predicts the motion pattern to be still influenced by the subduction related forces. This is in conflict with the negligible velocity inferred for the geodetic station in Thrace and the westward velocity inferred for a point in northwestern Turkey (Figure 4.7a). The model does agree with the velocity field derived by Jackson *et al.* (1992), shown in Figure 4.7b.

A closer look at the southern Aegean is provided by Figure 4.17 in which displacements predicted at the site of the geodetic stations are compared against the observed motion. Figure 4.17a illustrates the relation between observed motion and the model cases of only push or only pull. Results for the previously considered ratio of push over pull of 0.5 and for a value of 0.25 are shown in Figure 4.17b. We observe, firstly, that going from central Greece to the southwest Peloponnese, the model predicts a larger change in the orientation of motion than



is observed geodetically. Secondly, taking into account only the orientation of the predicted and observed motion, it follows that the ratios of 0.25 and 0.5 may be considered lower and upper limits, respectively. Push stronger than 0.5 times pull will render motion at the SW Peloponnese and Crete too far westwards. For a ratio less than 0.25 no match will be obtained for the sites in central Crete and on Rhodes. Making the assumption that the amount of modelled displacement is proportional to the rate of motion, we used the geodetic velocity inferred for the station on Crete to scale the displacement fields. It then follows from Figure 4.17a that predicted motion is slower than observed at the southwestern Peloponnese and central Greece, and slightly faster at Rhodes.

Figure 4.17c illustrates the dependence of arc displacements for a given ratio of push and pull, on the shear modulus of the fault zone elements. A stronger fault zone, i.e. with less reduced shear modulus, results in a smaller contribution to the arc displacement by the westward push: resulting displacements rotate counter-clockwise with increasing shear modulus. In view of this, the range of push over pull arrived at earlier may be considered a minimum estimate for the relative importance of westward push.

Finally, Figure 4.17d illustrates the effect of additional resistance applied to the overriding margin. The force distribution of the model in Figure 4.14 is combined with a westward push the magnitude of which amounts to 50% of that of the pull. Compared to the situation without resistance, displacements are slightly further southwards for the sites on Crete and Rhodes. The effect at the other sites is small.

Results Analysis of Present Situation

In summary, the analysis of the present-day situation has shown that (1) the observed prevalence of tensional stress can not be explained as an effect of the westward push exerted by the Anatolian block, (2) the westward push contributes to the motion of the overriding margin, (3) the observed pattern of tension is matched to a large extent by a model incorporating an arc-normal pull of uniform magnitude acting from SW Peloponnese to Rhodes, (4) a small component of additional resistance may be evidenced in particular in the pattern of seismic strain, and (5) combination of the arc-normal pull with the westward Anatolian push yields a realistic pattern of both stress and horizontal motions.

Fig. 4.17. (previous page) Comparison of geodetically derived motions in the southern Aegean (Figure 4.9a) and displacements calculated with the model combining arc-normal pull and westward push. Modelled displacement is shown at such scale that the length of the vector for the site on Crete matches that of the geodetic velocity vector. (a) Model result for the case of only push and only pull. (b) Ratio of push (force per metre north-south section) over pull (force per metre plate margin) equal to 0.25 and 0.5. (c) For a ratio of push over pull of 0.5: the effect of an increasing shear modulus of the elements of the North Anatolian fault zone. (d) For a ratio of push over pull of 0.5: the effect of including additional resistance.

Simplifications inherent to the model approach and limitations of the available observations do not allow a more precise assessment of the distribution of forces acting at the overriding margin. In particular, we cannot decide whether actual forces are decreasing more gradually at the western and eastern ends of the loaded segment, or whether the orientation of the forces shows some deviation from being purely normal to the arc. Well-established, however, is the fact that forces are diverging southwards and the fact that outward pull at the eastern arc segment is of a magnitude comparable to that at the western arc.

Model Analysis, Late Pliocene Situation

The results obtained so far confront us with two major questions regarding the Pliocene history of deformation, (1) whether the Pliocene pattern of tension can also be explained by a pull acting normal to the overriding margin from SW Peloponnese to Rhodes (given the fact that not only the observed stress field but also the geometry of the region is different), and (2) when a modification of the load is found to be required, whether it is consistent with the concept of lateral migration of slab detachment. In an attempt to answer these questions instantaneous stress and displacements are computed with a finite element mesh fitted to a paleogeographical reconstruction of the Aegean region.

This reconstruction was performed in a flat plane using a Mercator projection of the present-day coastlines; a simplification justified by the limited dimensions of the area of interest (Figure 4.18). Considering Thrace and the Black Sea area fixed, the northern part of Anatolia is placed eastwards adopting the estimate of the present-day motion relative to Eurasia of *Jackson and McKenzie* (1984). The southern part of Anatolia is shifted northwards assuming a constant rate of north-south extension amounting to $\beta=1.2$ over 5 Ma (*Angelier et al.*, 1981). Also assuming a constant rate of extension of the Aegean Sea, an estimate of a total extension of 200 km over 5 Ma (cf. *Le Pichon and Angelier*, 1981; *Jackson and McKenzie*, 1988a, b; *Westaway*, 1991) was used to determine the paleo-latitude of Crete. No rotation relative to the north-south direction was applied in accordance with paleomagnetic observations (*Valente et al.*, 1982). The island was translated towards the east in order to have it retain its position relative to southwestern Turkey (cf. *Westaway*, 1991). The reconstruction was completed assuming a clockwise rotation of 5 deg/Ma for the western margin of the Aegean (*Laj et al.*, 1982) and positioning the rotated block relative to Crete such that the continuity of the arc is retained.

Although considerable uncertainties are involved in this reconstruction, the model serves to illustrate the effects of the reduced curvature of the Hellenic arc during the Pliocene. Since, as yet, paleomagnetic data do not allow a detailed reconstruction of the rotations that affected the region, a major uncertainty encountered in examining the early Pliocene - early Pleistocene phase forms the

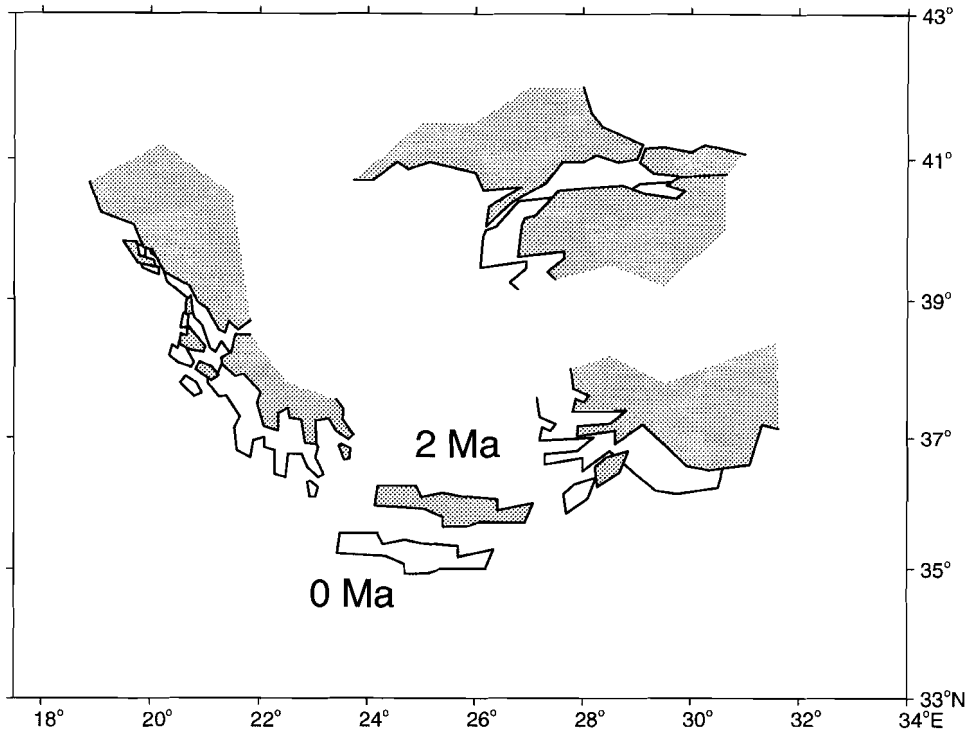


Fig. 4.18. Segments of coastline showing present-day geometry of the Aegean region (white) relative to a reconstruction of the geometry at 2 Ma b.p. (grey). See text for explanation.

original orientation of tension. Because the timing of faulting within this phase is also uncertain no hard constraints are available for the late Pliocene configuration analysed here. The model may be used to examine some general characteristics of the Aegean extension prior to the present-day. We will concentrate on the pattern of intra-plate stress and not discuss the displacement fields derived for the late Pliocene.

Arc-Normal Pull as in Present-Day Model

In the models for the Pliocene the north-south trending distant western and eastern boundaries of the mesh, and the northern boundary, are considered fixed. In view of the absence of indications for the Pliocene tectonic regime in northwestern Greece, the southern margin of the model is assigned a zero displacement boundary condition only to the margin that, at present, lies west of 18°E.

The stress field computed adopting an arc-normal pull distributed equivalent to the model which yielded a good fit for the present-day situation (Figure 4.12) is shown in Figure 4.19a. Observations of the Pliocene direction of tension in central Greece are shown in Figure 4.19a assuming that the examined sites, and with them the principal axes of tension, have rotated the same as western Greece.

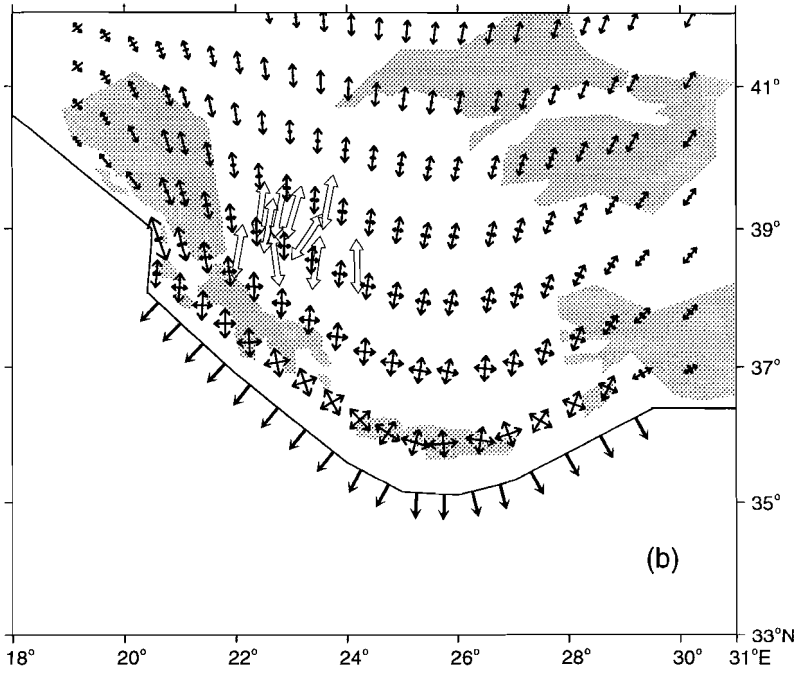
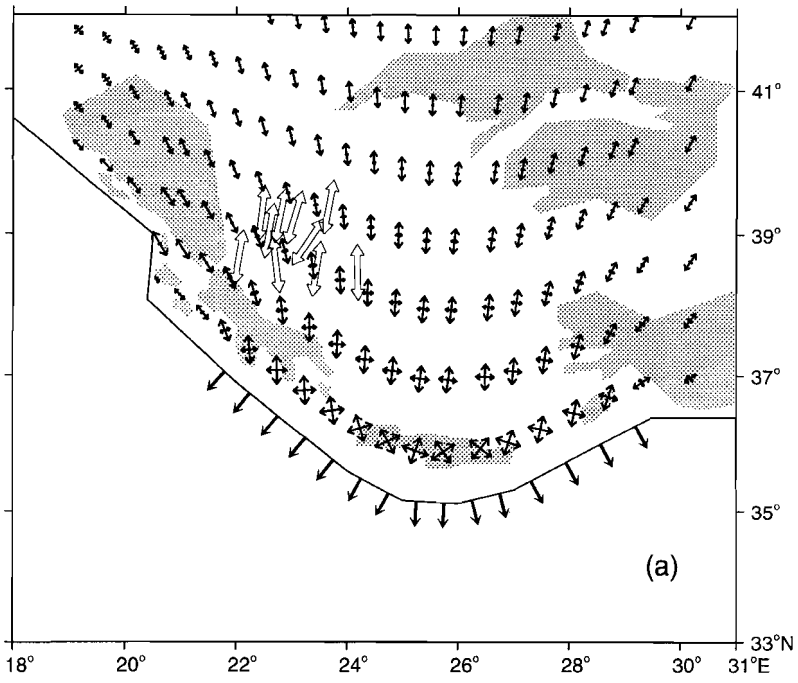
The modelled stress field shows, as was found for the equivalent present-day model (Figure 4.12a), radial tension in the region of the overriding margin and a northwards diverging pattern of tension in the internal part. Radial tension predicted for the arc is consistent with observations on Crete and Rhodes (Figure 4.5b) but the model does not show dominant tension approximately at right angles to the arc in the Peloponnese, as described by *Mercier et al.* (1993) (Figure 4.5b). Due to the reduced curvature of the overriding margin, tension computed for the region of central Greece is rotated closer to a direction normal to the western segment of the arc in comparison with the present-day case (Figure 4.12a). Still, there remains a misfit to the observed direction of tension in this area. In a broad sense the modelled pattern of tension is consistent with the observations in western and southwestern Turkey. Comparison of model calculations with the observations in the northern Aegean is complicated by the large uncertainty with respect to the original orientation of these observations. The model result in Figure 4.19a is in conflict, however, with the suggestion by *Mercier et al.* (1987) that at the time of faulting the tension in the north Aegean was directed normal to the western segment of the Hellenic arc.

The obtained results thus suggest that a modification of the load in comparison with the present-day situation is required in order to explain the Pliocene pattern of stress. We will investigate an alternative force model which stems from the concept of lateral migration of slab detachment.

Alternative Model

In view of the effect slab detachment is expected to have on the forces acting on the overriding plate, and given the present-day extent of the detachment tear as shown by tomography, we suggest that detachment might be responsible for the current compressive nature of the Ionian segment of the arc. In other words, slab detachment is thought to control the location of the westernmost extent of pulling

Fig. 4.19. (next page) Models of the deformation associated with forces at the overriding margin during the Late Pliocene, approximately 2 Ma ago. Shading illustrates paleogeography; shown is the reconstructed position of segments of present-day coastline. Large open arrows denote principal axes of tension deduced from faults observed in central Greece attributed to the early Pliocene - early Pleistocene (Figure 4.5b). The observed tensional axes are shown rotated equivalent to western Greece and the Peloponnese. (a) In this model the force distribution is taken equivalent to the model which provided a good fit to the present-day pattern of extension (Figure 4.12). (b) Model in which it is assumed that the forces acting on the overriding margin extend further to the northwest than in the previous model.



forces in our models. It follows that, if lateral migration of slab detachment has occurred, we would expect an earlier stage in the evolution of the Aegean to be characterised by outward pull extending further to the northwest along the margin.

In order to test this possibility Figure 4.19b shows the stress field obtained when also the Ionian segment of the overriding margin is assumed to be loaded by an arc-normal pull. In comparison with the model depicted in Figure 4.18a the principal axes of tension have been slightly rotated clockwise, and, consequently, the match between modelled stress field and observations in central Greece is improved. The modelled stress field is now also consistent with opening of the Gulf of Amvrakia and Lake Trikhonis, to the west-northwest of the Gulf of Corinth (Figure 4.1). In the southern Peloponnese the model shows close to radial tension. No dominant tension perpendicular to the arc is predicted (cf. Figure 4.5b). The model neither demonstrates tension approximately at right angles to the western segment of the arc in northern Greece. Instead, the computed direction of tension in northern Greece is partly controlled by the SE directed pull acting along the eastern segment of the arc. Observations of tension at right angle to the western arc in Albania (Figure 4.5b) would require the pull to extend even further northwestwards than shown in Figure 4.19b.

Discussion of Model Results

The implications of the model results for the role of Anatolian push are discussed and the inferred distribution of subduction related forces is commented upon. Interpretation of the latter in terms of the underlying mechanism and the role of slab detachment are each devoted a separate section.

Role of Anatolian Push

We would argue that, regarding the middle Pleistocene - present-day period, the westward push exerted by the Anatolian block is important in that it causes compression in the northern Aegean Sea region and partly controls the pattern of horizontal motions. The model results suggest, however, that although the *orientation* of tension may be affected by the Anatolian push, the *existence* of tensional stress is due to forces related to subduction.

Our conclusion is based on a model of instantaneous deformation in the present-day configuration and an objection would be that extension in response to shortening, such as suggested in the tectonic escape concept, will only develop after a certain amount of shortening has occurred, i.e. the extension could be an effect of finite deformation which is not accounted for in our models. In this respect it is relevant to recall that the configuration under examination came into existence less than 1 Ma ago. Moreover, prior to the middle Pleistocene, restriction to the westward motion of Anatolia may have been less pronounced

given the absence of indications for active shortening during the early Pliocene - early Pleistocene along the Ionian margin.

With respect to the present-day situation the question of the relative importance of pull at the overriding margin and westward Anatolian push has been addressed under the premise that the combined model illustrated by Figure 4.16 contains all relevant factors. Comparison of modelled and observed motion of the arc region suggests that the westward push constitutes a relatively small contribution.

Still, it is with respect to estimation of this relative importance that the limitations of our model are most apparent. Two aspects cause the obtained estimates to be uncertain. Firstly, the region where the interaction of westward push and subduction-related forces is strongest, the central and northern Aegean Sea, is represented in the models in a simplified manner. The strong variation in focal mechanism solutions for earthquakes in the central and northern Aegean Sea and northwestern Turkey and the types of faulting observed on-land can probably not be explained as a sole effect of the orientation of the fault planes with respect to a smoothly varying stress field (cf. *Chiotis and Tsoutrelis, 1992*). Instead, it appears that the compression due to the Anatolian push is concentrated along certain faults which consequently move in a strike-slip manner while in other parts extensional faulting prevails. These complex tectonics are difficult to model in a realistic manner.

Secondly, regarding the displacement field, it was found that the combined model predicts motion in northwestern Anatolia which is directed SW instead of WSW, as observed. The discrepancy in orientation may indicate that, in reality, strain dies out over a shorter length scale than in our model. The elastic rheology is a possible cause of this, but also the fact that the model considers deformation to occur homogeneously. In support of the latter is the fact that the velocity field derived by *Jackson et al. (1992)* (Figure 4.7b), which represents a continuous motion pattern averaged over a large length scale, does show SW motion in northwestern Anatolia.

The conclusions drawn from our models of the present-day situation need not be valid for the stage of initiation of extension. Nevertheless, the notion that Aegean extension and westward motion of Anatolia are not cogenetic is corroborated by recent geological evidence. An onset of extension prior to the start of the westward motion of Anatolia is indicated by the age of unroofing of the metamorphic rocks in the Cyclades and northern Greece (see above) and the timing of basin formation in western Turkey (*Seyitoğlu and Scott, 1991; Seyitoğlu et al., 1992; Barka et al., 1994; see also Şengör, 1993*).

Distribution of Forces Related to Subduction, Present-Day

The stress field calculated with a uniform elastic model, assuming a specific part of the overriding margin to be loaded by a pull of uniform magnitude, orientated normal to the margin, was found to match well the observed present-day

orientations of tension throughout the Aegean region. Collision along the margin of northwestern Greece, the westward push due to the Anatolian block, and resistive forces possibly exerted on the Zakynthos segment of the overriding margin (not modelled), induce compressional stresses which exert some control on the orientation of tension in the internal part of the region. Since the importance of this control is not well constrained, relating the orientation of tension in the central and northern Aegean to a specific distribution of forces at the overriding margin should be done with caution. However, the observation that at present the Hellenic arc is characterised by an along-arc component of tension clearly points to a radial outward orientation of the forces. This conclusion is corroborated by the result that the active motions of the Hellenic arc are consistent with a model combining the arc-normal pull with the westward Anatolian push.

We have argued that the available field data indicate that - overall - the Hellenic arc is characterised by a state of near radial tension. In this sense the observations are consistent with the present-day model incorporating arc-normal pull of uniform magnitude (Figure 4.12). However, in the arc segment between the Peloponnese and Crete, and in the segment between Crete and southwest Turkey, the model does not predict tension to prevail in one direction whereas this is suggested by the observations (Figure 4.5a; cf. *Angelier et al.*, 1982). This aspect has been demonstrated in detail for the island of Kythira (Figure 4.4). An explanation may be the fact that in reality the arc does not deform homogeneously. The arc segments to the west and east of Crete are largely submerged, indicative of higher extension than e.g. on Crete itself (*Barrier and Angelier*, 1981; *Lyberis et al.*, 1982). Moreover, it has been noted that the submerged parts of the arc may be containing transcurrent faults (*Barrier and Angelier*, 1981; *Laj et al.*, 1982; *Lyberis et al.*, 1982) in which case the along-arc component of tension predicted by the homogeneous model (Figure 4.12a) would in reality be concentrated within these depressions, causing the across-arc component to prevail in the adjacent on-shore areas.

At the location of each focal mechanism available for the arc region there is a match between the orientation of the T-axis and the direction of tension inferred from field data near the epicentre (compare Figure 4.5a and 4.6). Therefore, it is the lack of focal mechanisms consistent with roughly N-S tension, rather than the individual observations, that requires us to consider the possibility that the arc is dominated by E-W to NW-SE directed tension (as pointed out by *Lyon-Caen et al.*, 1988). We found that such a pattern of tension in the southern Aegean may result from a small deviation of the state of uniform arc-normal pull, caused by an additional resistance in the direction of convergence. The uniform magnitude of resistance assumed in the model of Figure 4.14 may be merely a rough approximation of the actual distribution. The fit between predicted and observed slip vectors was found to be only slightly improved. Nevertheless, additional resistance is likely to be small; it may have been overestimated in the

model shown in Figure 4.14 in view of the strong deviation from the observed motion in the southeastern Aegean.

In the sense that resistive forces acting on the upper plate are considered essential, our results are similar to the qualitative model of *Lyon-Caen et al.* (1988) (see also related papers *Armijo et al.*, 1992; *de Chabaliere et al.*, 1992). These authors attribute the prevalence of E-W extension in the southern Aegean to the onset of N-S collision between the Aegean and the leading edge of the African plate. Resistive forces in the direction of convergence in the subduction zone are central also to the qualitative model of *Mercier et al.* (1987).

The question then is: what causes the discrepancy between stress inferred from field-observed faulting and that expressed seismically? Although our compilation of stress data differs from that of previous studies in some respect we feel confident in our interpretation in terms of overall radial tension. Whereas *Armijo et al.* (1992) emphasize field evidence for E-W extension, consistent with the seismological data, they do not prove incorrect previous determinations of other directions of tension. Likewise, while *Mercier et al.* (1987; 1989; 1993) emphasize the importance of tension parallel to the western arc segment, their data compilation also shows NE-SW directed tension on Peloponnese and central Crete. Perhaps the most plausible explanation for the discrepancy lies in the fact that, although one principal stress dominates, the second principal stress still corresponds to a significant tension, as in Figure 4.14. Local inhomogeneities in deformation would cause faulting in directions deviating considerably from that corresponding to the regional tensor. Also, the state of stress may be varying as a function of depth: relatively high topography could enhance a state of radial tension at shallow levels in the crust.

Since the prevailing mode of deformation of the Hellenic arc is expected to be expressed in the pattern of horizontal motions (cf. Figure 4.12b and 4.14b), geodetic observations are also important. It is worth noting that preliminary results of GPS measurements indicate the Hellenic arc to be characterised by along-arc extension (*Gilbert et al.*, 1994) which would support the notion of additional resistance.

Distribution of Forces Related to Subduction, Pliocene

The early Pliocene - early Pleistocene stress field was found inconsistent with the distribution of pull which provides a fit with the observations for the present-day. Two possible causes of this discrepancy require special attention. Firstly, the misfit could be due to an underestimation of the rotation of the observations. The available paleomagnetic observations suggest, however, that clockwise rotation decreased from the western margin towards the internal region (*Kissel and Laj*, 1988) so that our assumption regarding the rotation of the observations may be considered conservative. Secondly, as comparison of the stress fields in Figure 4.12a and Figure 4.19a learned that reduction of the curvature of the arc tends to rotate tension in the region of central Greece in the required manner, the

mismatch between the computed stress field and the observations in this region, could point to an underestimation of the age of the observed faulting, or, equivalently, an overestimation of the curvature of the overriding margin. Analysis of a reconstruction obtained in the manner described above, but extrapolating back 5 Ma, has shown that reduction of the curvature alone, assuming rotation in central Greece to have been equal or less than that of the margin, does not provide a fit.

Thus, a change in the force distribution must indeed be invoked to explain the observations for the Pliocene. Extending the pull further northwestwards along the overriding margin was found to improve the fit with the direction of tension observed in central Greece. However, as mentioned, this model does not explain tension approximately at right angles to the western arc in Peloponnese and in the northern Aegean. The inability of a single force distribution to match all observations could be due to error in the reconstruction of the orientation of the paleo-stress axes or result from inappropriate basic assumptions in our model approach (e.g. homogeneity of deformation, forces concentrated at the margin). One alternative explanation worth noting is the following. Given the considerable period of time spanned by the early Pliocene - early Pleistocene phase (about 3 Ma) it is conceivable that this phase in fact comprises several stages during which the controlling forces were different. Tension normal to the western arc in Peloponnese and the northern Aegean would be consistent with pull dominantly towards the southwest. At some time during the Early Pliocene - Early Pleistocene period the situation may have been similar to that of the present-day models with pull on the eastern arc of reduced magnitude (Figure 4.13) or pull with a constant SSW azimuth (Figure 4.11).

Nature of the Subduction Related Forces

The question to address now is: what mechanism of pull on the overriding plate due to subduction do our model experiments support? Central to this question is the relation between the forces experienced by the upper plate and the kinematics of subduction, in particular, the roll-back of the subducting plate. In the following we will discuss four different mechanisms. First, however, the motion of the subducting plate will be examined.

Hinge-Retreat and Roll-Back

In dealing with the concept of roll-back a strict definition of the associated vocabulary is a prerequisite. The term "subduction hinge" is used to indicate the horizontal line along which the subducting African plate flexes downwards and disappears below the overriding plate, its location at any given stage in time coincides with that of the leading edge of the overriding continent (cf. Dewey, 1980). "Roll-back" is taken to describe a *motion* due to a specific cause: the

seaward retreat of the subduction hinge with respect to an "absolute" frame of reference (such as that formed by hotspots), caused by the gravitational pull acting on the subducted slab (Elsasser, 1971; Molnar and Atwater, 1978; Dewey, 1980). Net retreat of the subduction hinge may exceed roll-back when the continental plate is thrust over the downgoing plate, part of the retreat of the subduction hinge is then forced by the overriding plate and not due to the gravitational instability of the subducted slab (cf. Jarrard, 1986, p. 258).

Current motion of the Eurasian plate with respect to a hotspot reference frame is too slow to be significantly resolved (Minster and Jordan, 1978; Gripp and Gordon, 1990). Consequently, in the Aegean case, hinge retreat in an absolute sense is identical to hinge retreat relative to the stable interior of the overriding plate. Given that the subduction hinge coincides with the leading edge of the upper plate, absolute motion of the hinge follows directly from information on the motion of the overriding margin relative to Eurasia. At a given point along the subduction zone, hinge retreat is equal to the arc-normal component of "absolute" motion of the overriding margin (cf. Carlson and Melia, 1984). Figure 4.20 illustrates the distribution of retreat found using the geodetic velocity vectors of the three stations in the Hellenic arc. It is clear that hinge retreat is significantly slower along the margin east of central Crete and would - according to the geodetic results - be essentially zero at the segment east of Rhodes. East of Crete the arc-normal component of motion of the arc relative to Eurasia is zero. Present-day coastline shown for reference. In case that no forced hinge retreat takes place, the open arrows may be taken to illustrate the distribution of roll-back.

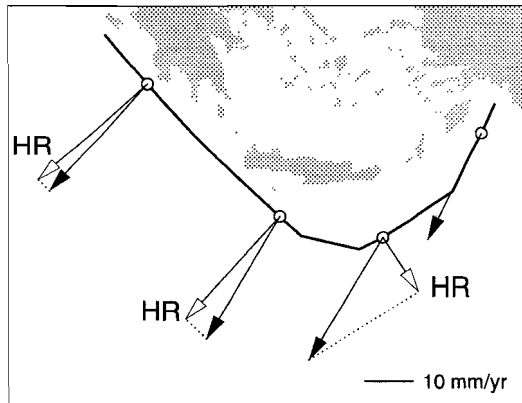


Fig. 4.20. The present-day pattern of hinge retreat. Hinge retreat (arrows marked "HR") occurs normal to the strike of the hinge and equals the arc-normal component of outward motion of the overriding margin relative to Eurasia, shown with black arrows (see text for explanation). The latter is based on the geodetic solution of Noomen *et al.* (1994); arrows correspond to vectors B-C of Figure 4.8. The geodetic vector found for the station on Crete is applied also to the margin off eastern Crete to illustrate the reduced rate of hinge retreat occurring there. East of Crete the arc-normal component of motion of the arc relative to Eurasia is zero. Present-day coastline shown for reference. In case that no forced hinge retreat takes place, the open arrows may be taken to illustrate the distribution of roll-back.

Using the geodetic data to infer hinge retreat implies the assumption that the region between the islands housing the geodetic stations and the trench system exhibits negligible deformation. Since slip vectors of earthquakes attributed to the subduction interface (e.g. *Taymaz et al.*, 1990) also point to SW to SSW directed motion of the overriding margin this assumption appears warranted. In the following both possible interpretations of the inferred pattern of hinge retreat, forced by the overriding plate or driven by slab pull, will be discussed.

Mechanism 1: Secondary Convection

In the concept of secondary convection the downgoing motion of the oceanic plate (the primary convection current) is considered to generate a corner flow in the mantle wedge separating subducting and overriding plate (the secondary convection current) capable of exerting a basal shear stress that pulls the upper plate trenchwards. Combined with slab pull causing the subduction hinge to roll-back, secondary convection would offer a mechanism for upper plate extension.

Assuming that secondary convection currents and, thereby, viscous drag at the base of the upper plate are mainly orientated parallel to the direction of convergence in the subduction zone, the model with uniform SSW directed pull (Figure 4.11) could be considered a crude representation of this mechanism. The mismatch between modelled and observed stress field would speak against the possibility of secondary convection. However, the validity of our model in this context may be questioned because it assumes driving forces are located at the overriding margin. More important, in view of the limited lateral extent of the subduction zone and its strong curvature, any pattern of secondary convection is expected to involve material transport also in other directions than in vertical planes parallel to convergence.

The strongest argument against the possibility of secondary convection is that it seems unlikely that this mechanism could explain the radial outward pull shown to be consistent with the present-day stress pattern. Moreover, the existence of roll-back renders the situation essentially different from that envisaged in the corner flow concept. Whereas corner flow requires down-dip motion of the slab to drive it, roll-back will result in more nearly vertical descend of the subducting plate. Finally, we note that, in the case of the land-locked Mediterranean, the concept of secondary convection involves a paradox. In order to generate the circulation supposed to drive extension, significant convergence at the subduction zone is required. In the case of the Hellenic subduction, convergence between Africa and Eurasia being slow, most convergence is a consequence, however, of the extension of the upper plate.

Mechanism 2: Spreading That Forces Hinge Retreat

Advocated by *Berckhemer* (1977), *Le Pichon and Angelier* (1979), and *Le Pichon* (1982) the concept that extension of the Aegean region may be a form of gravitational spreading is central also to the models of, in particular, *Mercier et al.* (1987) and

Hatzfeld *et al.* (1990). Our analysis offers quantitative support for the occurrence of gravitational spreading during the late Cenozoic by showing that the force distribution expected in the case of gravitational spreading is consistent with the observed pattern of intra-plate stress and the horizontal motions. The concept of gravitational spreading rests on the notion that the overriding plate constitutes a region of relatively high gravitational potential energy. Concerning the corresponding low in potential energy there are two possibilities: (1) The relative "low" is formed by the lithosphere of the eastern Mediterranean Sea. This corresponds to the way the concept was originally applied to the Aegean by *Le Pichon* (1982) and is the assumption that underlies this and the subsequent mechanism. (2) The region of low potential is formed as a direct result of roll-back of the subducting plate, since the latter tends to create a free boundary. This possibility will be discussed as the fourth mechanism.

Distribution of associated pull. *Le Pichon* (1982) demonstrated that the difference in surface elevation and density structure between a column of Aegean lithosphere and a column of East Mediterranean lithosphere gives rise to a horizontal spreading force sufficiently large to drive continental extension. It remains to be verified, however, that differences in gravitational potential energy are indeed largest at the overriding margin, as implied by the force distribution applied in modelling.

To this extent, Figure 4.21 shows the difference in gravitational potential energy between a column of continental lithosphere and a column of mid-ocean ridge, as a function of surface elevation and crustal thickness of the continental column. It is assumed that isostatic equilibrium with the ocean ridge is achieved at the base of the continental lithosphere. Shown are potential energy differences between columns of unit horizontal area which correspond to horizontal forces per unit length of interface between the columns (*Molnar and Lyon-Caen*, 1988; *Molnar et al.*, 1983). Figure 4.21 is constructed for an average density of the continental crust of 2854 kg/m^3 which corresponds to a surface elevation of +250 m for a column comprising 35 km of crust and 85 km of lithospheric mantle (cf. *England and Houseman*, 1989).

Squares in Figure 4.21 indicate the values of elevation and crustal thickness averaged over $1.5^\circ \times 1.5^\circ$ segments of the Aegean region. Crustal thickness is based on the Moho depth map of *Makris* (1977). The average values of elevation and crustal thickness encountered in the Aegean define a roughly linear trend with a slope that is approximately parallel to the contours of equal ΔPE : differences in potential energy within the Aegean lithosphere are small. An exception to the general trend is formed by the data of northwestern Greece. A shallower depth of the Moho, as inferred for this region by *Tselentis et al.* (1988), would render the data points closer to the general trend.

Assuming the East Mediterranean lithosphere to be oceanic and of the structure proposed by *Le Pichon* (1982), a potential energy difference per unit area of $-3 \times 10^{12} \text{ N/m}$ between an East Mediterranean column and a mid-ocean ridge

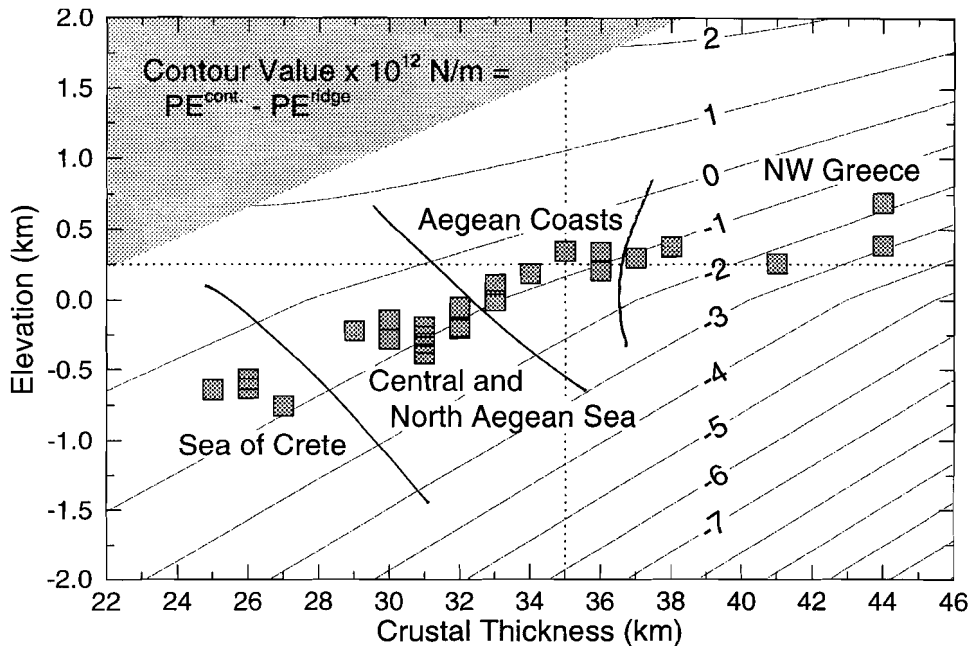


Fig. 4.21. Contour plot of gravitational potential energy of a column of continental lithosphere relative to a column of mid-ocean ridge (ΔPE), as a function of crustal thickness and surface elevation of the continental column. Contour interval 1×10^{12} N/m. Columns are of unit horizontal area so that ΔPE is identical to a horizontal force per metre interface. The mid-ocean ridge consists of 5 km of water (density 1030 kg/m^3), 5 km of oceanic crust (2900 kg/m^3), overlying asthenosphere ($\rho_a = 3200 \text{ kg/m}^3$). Assumed is an average density of the continental crust (2854 kg/m^3). A linear geotherm from temperature $T=0^\circ \text{C}$ at the top of the crust to $T=T_a$ (1300°C) at the base of the lithosphere and thermal expansion coefficient α ($3.5 \times 10^{-5} \text{ }^\circ \text{C}^{-1}$) define the density of the lithospheric mantle: $\rho_m = \rho_a(1 - \alpha(T - T_a))$. Negative elevation represents depth under water. For a given crustal thickness and elevation, lithospheric thickness follows from the requirement of isostatic balance with the ocean ridge. The shaded area represents impossible combinations of elevation and crustal thickness, its lower limit corresponds to absence of lithospheric mantle. With the chosen density of continental crust, a continental lithosphere of 120 km thick, with 35 km of crust, reaches a surface elevation of 250 m, as indicated by dotted lines. Squares denote mean values of elevation and crustal thickness averaged over $1.5^\circ \times 1.5^\circ$ segments of the Aegean region. Data points have been divided in four groups: segments covering the Sea of Crete, the central and northern Aegean Sea, the coastal areas of the Aegean Sea, and northwest Greece. Crustal thickness is based on the Moho depth map of Makris (1977).

column is found. Given this, Figure 4.21 implies that for an average density of the continental crust of 2854 kg/m^3 the potential energy difference per unit area between the Aegean region and the East Mediterranean varies from $1.5\text{-}2.5 \times 10^{12}$

between the Aegean region and the East Mediterranean varies from $1.5\text{-}2.5 \times 10^{12}$ N/m. This value is similar to that found by *Le Pichon* (1982) and significantly exceeds the potential energy differences that occur within the Aegean lithosphere. Larger potential energy differences between the Aegean lithosphere and the East Mediterranean lithosphere are found for higher values of crustal density, and vice-versa. Significantly larger differences also hold in case the East Mediterranean consists of thinned continental lithosphere, instead of being oceanic in nature.

The tentative determination of the magnitude of the force on the overriding margin provides us with a scale for the intra-plate stress fields presented in the above. An applied force of 2×10^{12} N/m corresponds to intra-plate stresses of the order of 20 MPa, averaged over the plate thickness of 100 km.

We conclude that the horizontal forces associated with lateral differences in potential energy are, indeed, expected to be largest near the overriding margin. However, the assumption that forces act at the extreme edge of the overriding plate does probably constitute a simplification. Exactly where the spreading forces act is difficult to determine. The region of the overriding margin cannot be treated in the above manner since there where the upper plate rests on the subducting plate, isostatic equilibrium with an oceanic ridge column does not hold.

Forced hinge retreat. Could the force pulling the Aegean lithosphere towards the adjacent oceanic basin be strong enough to force the subduction hinge to retreat? Although there is no conclusive evidence there exist indications that render this possibility unlikely. Since the early Pliocene extension has been the prevailing tectonic regime in the Aegean region including the island arc. Compression is expected, at least near the overriding margin, when the overriding plate forces the hinge to retreat. Moreover, convergence in the Hellenic subduction zone occurs largely aseismically (*Jackson and McKenzie, 1988b*) indicative of a low seismic coupling at the subduction interface. The maximum earthquake magnitude observed in the Hellenic trench, $M_s=7.3$ (*Jackson and McKenzie, 1988b*), implies that, in terms of seismic coupling the latter is comparable to e.g. the Marianas (*Ruff and Kanamori, 1980*). Such low seismic coupling is unlikely in the case of forced retreat but could also be due to other causes such as the presence of subducted sediments (*Jackson and McKenzie, 1988b*).

Mechanism 3: Spreading Allowed by Roll-Back

In the previous mechanism, gravitational spreading was considered to be the driving force of both upper plate extension and subduction hinge retreat. However, the gravitational instability of the subducted lithosphere is likely to at least contribute to hinge retreat. Therefore, as proposed by *Le Pichon* (1982), it is more realistic to think of the deformation of the region as being driven by the interplay of two forces, both arising from gravity (cf. *McKenzie, 1972*): the horizontal trenchward pull on the overriding plate and the vertically acting slab pull on the subducting plate.

The concept is conveniently explained in terms of a schematic vertical cross section through the subduction zone (Figure 4.22). As in the previous section the potential energy difference governing upper plate deformation is considered to be that between Aegean lithosphere and the lithosphere of the eastern Mediterranean Sea. In contrast to the previous mechanism the subduction hinge is - in the absence of slab pull causing it to retreat - considered to block seaward advance of the overriding margin and thereby prevent upper plate extension. The spreading force meets an equally large but oppositely directed resistance exerted by the hinge. However, when slab pull causes the hinge to retreat, i.e. roll-back occurs, resistance to spreading is relaxed and the overriding plate experiences a net trenchward pull.

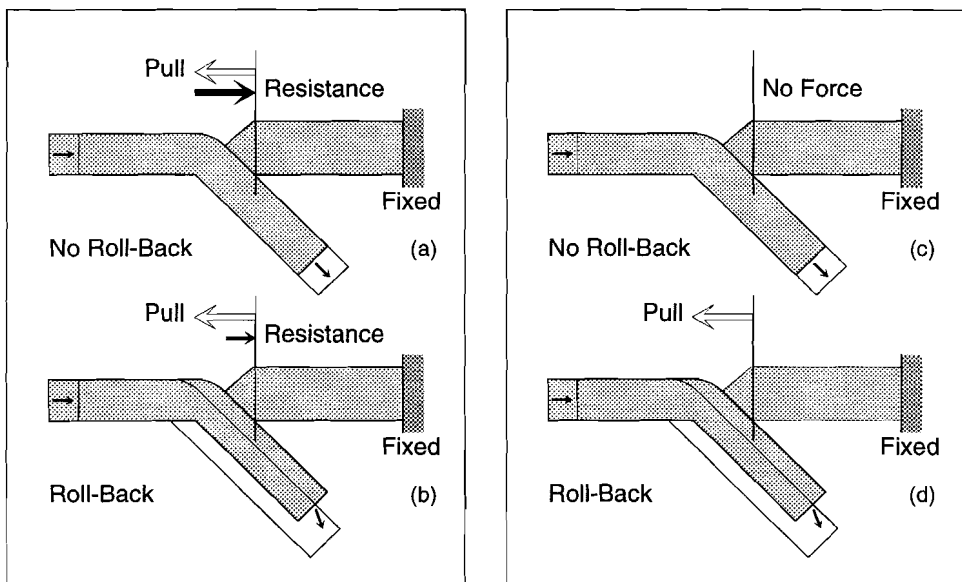


Fig. 4.22. Schematic illustration in vertical cross section of the forces acting on the boundary of the Aegean lithosphere. Panels (a) and (b) illustrate mechanism 2 discussed in text; panels (c) and (d) refer to mechanism 3. The right edge of the overriding plate is fixed, representing the non-deforming interior of the Eurasian plate. Small arrows and future outline (thin line) indicate motion of the subducting plate relative to Eurasia. Velocity components not to scale. (a) Subduction hinge is stationary. Convergence between the plates takes place by motion of the subducting plate along its shape. Pull acting on the overriding plate due to the potential energy difference between the Aegean lithosphere and the east Mediterranean lithosphere (open arrow towards left) is cancelled by a reaction force contributed by the subducting plate (black arrow towards right). (b) Subduction hinge retreats. As a result, the resistance applied to the overriding plate is reduced and the latter experiences a net trenchward pull. (c) Alternative scenario assuming that the

trenchward pull on the upper plate *results* from the release of pressure on the overriding edge due to roll-back. Hence, in the absence of roll-back no forces are present (disregarding the effect of shear at the subduction interface). (d) When roll-back occurs the upper plate experiences a trenchward pull.

Additional resistance. Whereas readily accepted in terms of a vertical section it is upon consideration of the situation in the horizontal plane that the notion of roll-back providing room for upper plate extension - as outlined in the above - is found to have an important implication. This implication stems from the fact that it is not to be expected that the overriding margin will simply follow the retreating subduction hinge. This aspect is demonstrated by our model experiment including only the uniform arc-normal pull (Figure 4.12): as a combined effect of the rigidity of the plate, the constraint imposed on the northwestern margin, and the distribution of pull, the overriding margin moves - as a whole - towards the SSW and motion does not occur radially outwards. Moreover, as is consistent with the model shown in Figure 4.10, the westward Anatolian push is expected to contribute also to the motion of the overriding margin. Based on this model experiment, westward push may be causing the eastern part of the overriding margin to move away from the trench (Figure 4.10). Since hinge retreat and thus, in the context of this mechanism, roll-back, is small or even absent along the eastern arc (Figure 4.20) it may in fact be westward push rather than slab pull that tends to separate the plates meeting in the trench and thereby relax the resistance against spreading along this arc segment. At the western segment the opposite holds: part of the trenchward migration of the overriding margin is already accounted for by the westward Anatolian push.

Knowing that there grow no gaps between overriding and downgoing plate and discarding - in view of the above - the possibility that the overriding margin exactly follows the subduction hinge, we conclude that the overriding margin must tend to overlap the hinge. The fact that an actual overlap does not occur implies that the margin not only experiences outward pull, but also a resistance constraining it to match the position of the hinge. In terms of Figure 4.22: roll-back does not necessarily completely cancel resistance but may merely reduce it.

How does the notion of additional resistance relate to our model experiments? Firstly, even though the assumption that resistance acts parallel to relative motion and is of uniform magnitude is most likely a simplification, the fact that the model experiment featuring not only pull but also a component of resistance (Figure 4.14) matches at least part of the available observations offers some support to the conclusion of the above reasoning. Secondly, the uniform distribution of pull found to already match the data to a significant extent appears a reasonable first order approximation of the effect of potential energy differences along the arc. However, in the absence of detailed knowledge

concerning the density structure on both sides of the Hellenic trench we cannot exclude the possibility that the uniform magnitude itself represents a net effect of non-uniform pull modulated by resistance.

Geometry of roll-back. The asymmetric distribution of roll-back implied by the above mechanism may be due to lateral variation of the effectivity of slab pull in driving hinge retreat, or may be related to lateral changes in slab pull associated with complex geometry of the subducted lithosphere. Seismic tomography suggests the presence of a vertical discontinuity in the subducted African lithosphere at the longitude of western Turkey (*Spakman et al.*, 1994). The nearby presence of this lateral termination may well cause the slab subducted below the eastern Hellenic arc to behave differently from the portion subducted further towards the west.

Mechanism 4: Spreading Caused by Roll-Back

In the previous two mechanisms roll-back was considered significant in the sense that it reduces the resistance against the spreading forces. Alternatively, it is conceivable that roll-back itself generates the driving force. The tendency of the two plates to separate will reduce the pressure at the overriding continental margin, a pressure gradient from the more internal part of the Aegean towards its leading edge will result, and the associated horizontal force would cause the Aegean to spread (Figure 4.22c and 4.22d). In contrast to the case of mechanism 3, spreading of the overriding lithosphere would occur even when there existed no contrast in potential energy between the adjacent plates; the relevant lateral inhomogeneity would be formed by the subduction zone itself. Trenchward pull on the upper plate as a direct consequence of freeing of the subduction fault was also argued for by *Bott et al.* (1989).

Also when spreading is thus directly induced by roll-back, the rate of roll-back controls the rate of outward motion of the overriding plate. Since the mechanism outlined here should be thought of as episodic rather than continuous (*cf. Bott et al.*, 1989) roll-back may achieve this control by governing the repeat-time of pressure release at the overriding margin.

In view of the fact that, at a given segment, the subducting plate cannot reduce pressure on the overriding margin and restrain its outward migration at the same time, pull will not act concurrently with resistance as in the previous mechanism. This, however, should not be taken to imply that the overriding margin does in general not experience resistance. The leading edge of the upper plate will experience resistance wherever it, driven by Anatolian push or by pull exerted at neighbouring segments, tends to migrate trenchwards faster than roll-back occurs. When considering the Hellenic arc as a whole the mechanism proposed here may be difficult to discriminate from that outlined in the previous mechanism.

Role of Slab Detachment

The notion that the present-day orientation of tension in the central Peloponnese is partly due to the compressive nature of the Ionian segment of the overriding margin was recognized previously by *Lyberis and Lallemand (1985)*, *Mercier et al. (1987)*, and *Hatzfeld et al. (1990)*. *Mercier et al. (1987)* argue that, throughout the Aegean, the middle Pleistocene essentially involved a change from tension orientated normal to the arc, to tension orientated perpendicular to the direction of convergence in the subduction zone. The authors suggest that the two successive stress regimes reflect an increase in the resistance applied to the overriding margin in the direction of convergence, which modifies an extensional regime related to the surface elevation and density structure of the Aegean lithosphere. The dynamical configurations envisaged by *Mercier et al. (1987)* resemble our model experiments in Figure 4.12 and 4.14. However, whereas *Mercier et al. (1987)* suggest that the evolving stress pattern of the Aegean can in essence be understood by considering a single vertical cross section, we emphasize the role of temporal variations in the lateral distribution of forces acting at the continental margin.

Given the tomographic results we suggest that the present compressive nature of the Aegean margin west of the SW Peloponnese is related to the presence of a tear in the slab subducted below this region (Figure 4.23a). It is expected to be primarily through its effect on hinge migration that slab detachment affects the dynamics of the overriding plate: the latter now meets an

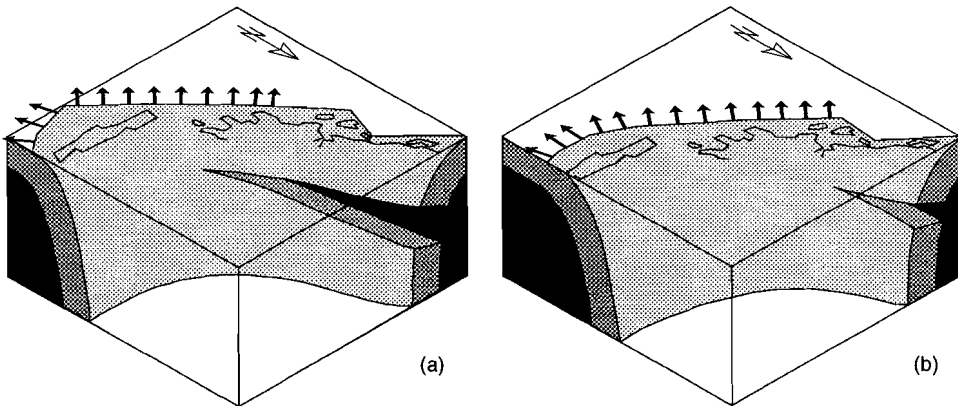


Fig. 4.23. Block diagrams schematically illustrating the relation between the horizontal extent of the detachment tear in the slab subducted below western Greece and the part of the overriding margin subject to outward pull. (a) Present-day situation (cf. Figure 4.9). (b) Hypothetical late Pliocene configuration. During the late Pliocene the tip of the detachment tear was located to the northwest of its current position; roll-back still occurred along the Ionian segment and, consequently, pull on the overriding plate extended further to the northwest than at present.

obstacle formed by the non-retreating subducted lithosphere. If gravitational spreading is the driving mechanism of the extension of the overriding plate then, along the subduction zone segment where detachment has occurred at depth, there will be no roll-back induced tendency for separation of the two meeting plates, the forces confining the continental lithosphere will not be relaxed and gravitational spreading will not occur. As demonstrated by our forward models, there may still be seaward advance of the overriding margin at a subduction segment where slab detachment has occurred. However, this will be driven by forces acting elsewhere at the plate and will cause the downgoing plate to be overthrust.

The tomographic results (*Spakman, 1991; Spakman et al., 1993*) suggest that the detachment tear extends further southeastwards than the part of the overriding margin currently in compression. Although the resolution of the tomographic images could play a role in this, some effect would in fact be expected. The gravitational pull acting on the plate subducted below the central part of the arc, where detachment has apparently not occurred, will, due to the strength of the subducting plate, also lead to some roll-back of the hinge northwestwards of the tip of the detachment tear.

As demonstrated by the model calculations for the late Pliocene, outward pull extending further to the northwest along the arc than in the preferred model for the present-day, is consistent with the observed Pliocene pattern of tension. The implied change in the forces acting on the Ionian arc segment is in line with that expected due to lateral migration of slab detachment: prior to the present the detachment tear would not yet have migrated as far to the southeast, a larger part of the hinge would still have been subject to roll-back, and pull on the overriding plate would extend further to the northwest (Figure 4.23b). The observed faulting constrains the timing of detachment below the Ionian arc segment. The latter must have occurred during the short middle Pleistocene compressive period separating the two extension phases. As mentioned in a previous section, the extent to which, during the Pliocene, outward pull extended further to the northwest along the margin compared to the present situation, and thus the length of the segment along which detachment presumably occurred during the middle Pleistocene, may have been underestimated in the model presented in Figure 4.19b.

Whether lateral migration of slab detachment is indeed the cause of the observed change in the pattern of tension during the middle Pleistocene can be investigated further by analysing the spatial and temporal variation in vertical motions. Increased roll-back and upward rebound of the downgoing plate, respectively in front and behind of the proceeding detachment tear, are suggested to affect vertical motion of the overriding continent also (*Wortel and Spakman, 1992*).

Conclusions

Using a numerical model we have calculated patterns of stress and strain for the Aegean region assuming various distributions of the tectonic forces. By considering models for the present-day situation as well as for a late Pliocene stage, we were able to address temporal variations in the dynamics. The relations thus found between the stress field and horizontal motions on the one hand, and the tectonic forces on the other, constitute the main result of our study. Both observations of the intra-plate stress field and of horizontal motions, as given by the recent results of geodetical monitoring, have been used to evaluate the model results. The following conclusions can be drawn:

1. The push exerted by the westward moving Anatolian block does not explain the observed prevalence of a normal faulting regime, as suggested in the concept of tectonic escape, but does contribute to the motion of the overriding margin.

2. The observed pattern of tension is to a large extent consistent with an outward directed pull of uniform magnitude acting normal to the overriding margin from SW Peloponnese to Rhodes. Prevalence of E-W to NW-SE orientated tension in the southern Aegean, such as suggested by the pattern of seismic strain, may be due to a relatively small amount of additional resistance.

3. When combining the distribution of uniform arc-normal pull at the overriding margin and the westward Anatolian push, the model is found to match both the observed stress field and the pattern of horizontal motions.

Apart from the fact that no constraints are available from observations of seismicity or geodetic measurement, model analysis of the Pliocene phase is hampered by uncertainties in the age of fault activity and the original orientation of the faults. Nevertheless, an additional conclusion is warranted:

4. The distribution of arc-normal pull providing a fit to the present-day pattern of tension is not consistent with the early Pliocene - early Pleistocene pattern of tensional stresses. Instead, this phase may have involved pulling forces extending further towards the northwest along the overriding margin.

In our interpretation of these results we have taken into consideration the lateral distribution of forces acting on the overriding plate, the kinematics of subduction, and the structure of the subducted slab. We conclude that a mechanism consistent with the model results is that of gravitational spreading of the Aegean lithosphere. Based on a consideration of the kinematics of the arc-trench system in plan view we argue that, in addition to the driving force associated with lateral differences in gravitational potential energy, the overriding margin is expected to experience a resistive force. Finally, we suggest that the middle Pleistocene change in the stress field in the Aegean region may reflect a change in the conditions along the western margin caused by rupture of the subducted slab present below this margin.

Conclusions

Chapter 5

Specific conclusions of the various parts of the investigation have been listed at the end of each of the three preceding chapters (see pages 46, 129, and 193). Here, the study is completed by stating several conclusions of a more general nature.

The Two Overriding Margins Compared

In the preceding chapters a numerical model has been employed in order to assess the intra-plate stress field associated with assumed sets of tectonic forces. Comparison of modelled stress fields with the available observations allowed us to decide which of the proposed force distributions is realistic. The different tectonic regimes observed to prevail in the two overriding margins of interest were assumed to reflect a different type of force distribution on the margin: resistance in the case of South America and some type of outward pull in the case of the Aegean. Subsequent model experiments have demonstrated this assumption to be correct and have provided detailed information regarding orientation and distribution of the forces experienced by the overriding margin. Resistance parallel to the direction of convergence was found to match reasonably well the pattern of compressional stress expressed by reverse faults along the Andes. Model experiments confirm the notion that normal faulting observed at higher elevation in the Andes reflects an additional contribution to the stress field of the topography and crustal root of the mountain range. Experiments were done in order to examine the possibility of a non-uniform distribution of resistance and

the likeliness of an additional component of outward pull. Notable results are that the available stress indicators preclude (1) the possibility that the magnitude of resistance is inversely correlated with the dip of the downgoing plate, and (2) the existence of a component of significant oceanward pull, in addition to resistance, on the central segment of the overriding margin. Moreover, the model results argue against the occurrence of an additional outward pull on the entire overriding margin. In the case of the Hellenic subduction zone an extensional tectonic regime is observed to characterise much of the upper plate including the overriding margin. The present-day pattern of tension was found to be explained well by a uniform distribution of outward arc-normal pull. The model experiments demonstrate that such pull also acts on the eastern segment of the overriding margin, along which relative motion is predominantly parallel to strike.

The fact that the Andean margin of South America and the Hellenic arc experience a different type of force distribution is well understood in terms of their respective plate tectonic setting. In an absolute frame of reference both plates in contact along the Andean margin advance towards the trench. The active convergence of the stable interiors of the two adjacent plates, in combination with the fact that the descending Nazca plate is relatively young, causes the upper plate to experience resistance. Oceanward retreat of the subduction hinge (again, in an absolute sense) most likely results from the push exerted by the advancing South American plate. In other words, using the terminology of Chapter 4, retreat of the hinge of the subducting Nazca plate is *forced* by the upper plate. In its turn the advance of the South American plate is driven by ridge push, possibly assisted by shear at the contact with the convecting mantle. In contrast, in the case of the Hellenic subduction zone, active convergence between the stable interiors of the African plate and the Eurasian plate has almost halted. Slab pull acting on the old oceanic lithosphere of the eastern Mediterranean causes the subduction hinge to retreat, away from the upper plate. Stating at this point that the "roll-back of the hinge causes the overriding plate to extend" would leave unanswered the question as to how these two processes are linked dynamically. The uniform arc-normal pull inferred by modelling is consistent with the suggestion that roll-back and upper plate extension are linked through the process of gravitational spreading.

Future Research

The elastic thin shell model used in this thesis has proven to be a good starting point for the study of the tectonics of the two regions of interest. This is particularly so regarding the examination of active deformation: in this case the observations clearly pertain to a momentary view. The results of neotectonic studies prompted the extension of this approach to situations back in time. When the different tectonic phases inferred from neotectonic analysis indeed represent different distributions of the acting forces, the application of a model for

instantaneous deformation at different points in time should allow us to reconstruct the temporal evolution of the controlling forces. Two main assumptions are made in this approach and it is on these aspects that future work should concentrate: (1) the assumption that the region of study deforms as a homogeneous body, and (2) the notion that the deformation of a region can be viewed upon as being built-up of separate stages. These aspects require the numerical model to incorporate a more realistic rheology. Moreover, in order to do so in the optimal way the third dimension - depth - must be incorporated explicitly in the model.

Concluding Remarks

In conclusion it can be stated that the model experiments and their interpretation presented in the preceding chapters provide us with valuable new insight regarding the dynamics of the South American plate and the Aegean region. The use of relatively simple model techniques has proved an important means of evaluating the available geological, geophysical, and geodetical observations. Forward modelling offers a visualisation of the implications of a proposed mechanism and allowed us to assess the importance of the various forces suggested to affect the observed deformation. In this manner it was possible to step beyond the existing qualitative interpretations of the data. In particular with respect to the model analysis of the state of stress in the Andes and the Aegean region, the results of this thesis may serve as a starting point for more sophisticated models including a realistic rheology or addressing the problem in 3-D. Also, the results presented here may contribute in the selection of critical areas for future data acquisition.

Although the study has concentrated on two specific regions, the results obtained are applicable in much wider context. For example, the results obtained in this thesis for the Andean margin of South America and the Hellenic arc, may serve to understand the deformation of other margins, active as well as past. This is especially so in view of the fact that, in terms of tectonic regime, the two margins studied here exemplify two "end-members". Moreover, the approach followed in this thesis may serve to inspire examination of other regions in a similar (and subsequently more advanced) manner. Methods such as the implementation of the role of topography and the technique for comparison of a modelled intra-plate stress field with earthquake focal mechanisms, are clearly of general purpose.

In both South America and the Aegean region research aimed at collecting observational evidence regarding the deformation is continuing. Although new data may require a modification of the conclusions of this study, the model experiments as such will provide important material for comparison with, and evaluation of, existing data as well as future observations.

References

- Adamek, S., C. Frohlich, and W. D. Pennington, Seismicity of the Caribbean-Nazca boundary: Constraints on microplate tectonics of the Panama region, *J. Geophys. Res.*, 93, 2053-2075, 1988.
- Allmendinger, R.W., M. Strecker, J.E. Eremchuk, and P. Francis, Neotectonic deformation of the southern Puna plateau, northwestern Argentina, *J. S. Am. Earth Sci.*, 2, 111-130, 1989.
- Altherr, R., H. Kreuzer, I. Wendt, H. Lenz, G.A. Wagner, J. Keller, W. Harre, and A. Höhndorf, A late Oligocene/early Miocene high temperature belt in the Cycladic crystalline complex (SE Pelagonian, Greece), *Geol. Jahrb.*, E23, 97-164, 1982.
- Anderson, H., and J. Jackson, Active tectonics of the Adriatic region, *Geophys. J. R. astr. Soc.*, 91, 937-983, 1987.
- Andriessen, P.A.M., N.A.I.M. Boelrijk, E.H. Hebeda, H.N.A. Priem, E.A.Th. Verdurmen, and R.H. Verschure, Dating the events of metamorphism and granitic magmatism in the Alpine orogen of Naxos (Cyclades, Greece), *Contr. Miner. Petrol.*, 69, 215-225, 1979.
- Angelier, J., Tectonic analysis of fault slip data sets, *J. Geophys. Res.*, 89, 5835-5848, 1979a.
- Angelier, J., Neotectonique de l'arc égéen, *Publ. Soc. géol. Nord*, 3, 417 pp., 1979b.
- Angelier, J., D. Théodoropoulos, and P. Tsoflias, Sur la néotectonique du seuil de Cythère, dans l'arc égéen externe (Grèce), *C. R. Acad. Sci. Paris*, 283, 1273-1275, 1976.
- Angelier, J., J.-F. Dumont, H. Karamanderesi, A. Poisson, S. Simsek, and S. Uysal, Analyses of fault mechanisms and expansion of southwestern Anatolia since the late Neogene, *Tectonophysics*, 75, 1-9, 1981.
- Angelier, J., N. Lybérís, X. Le Pichon, E. Barrier, and Ph. Huchon, The tectonic development of the Hellenic arc and the Sea of Crete: a synthesis, *Tectonophysics*, 86, 159-196, 1982.
- Armijo, R., H. Lyon-Caen, and D. Papanastassiou, East-west extension and Holocene normal-fault scarps in the Hellenic arc, *Geology*, 20, 491-494, 1992.
- Arthyushkov, E. V., Stresses in the lithosphere caused by crustal thickness inhomogeneities, *J. Geophys. Res.*, 78, 7675-7708, 1973.
- Assumpção, M., The regional intraplate stress field in South America, *J. Geophys. Res.*, 97, 11,889-11,903, 1992.
- Assumpção, M., Earthquakes and stresses in the Brazilian continental margin, *Proc. III Int. Congres Braz. Geophys. Soc.*, Rio de Janeiro, 1, 1128-1133, 1993.
- Assumpção, M., and M. Araujo, Effect of the Altiplano-Puna plateau, South America, on the regional intraplate stresses, *Tectonophysics*, 221, 475-496, 1993.

- Assumpção, M., and G. Suárez, Source mechanisms of moderate-size earthquakes and stress orientation in mid-plate South America, *Geophys. J.*, 92, 253-267, 1988.
- Aubouin, J., Réflexion sur la tectonique de faille plio-quadernaire, *Geol. Rdsch.*, 60, 833-848, 1971.
- Aubouin, J., and J. Dercourt, Sur la géologie de l'Égée: regard sur la Crète (Grèce), *Bull. Soc. géol. France*, 7, 787-821, 1965.
- Barazangi, M., and B. L. Isacks, Spatial distribution of earthquakes and subduction of the Nazca plate beneath South America, *Geology*, 4, 686-692, 1976.
- Barka, A.A., and K. Kadinsky-Cade, Strike-slip fault geometry in Turkey and its influence on earthquake activity, *Tectonics*, 7, 663-684, 1988.
- Barka, A.A., M. Sakinc, N. Gorur, Y. Yilmaz, A.M.C. Sengor, and V.S. Ediger, Is Aegean extension a consequence of the westerly escape of Turkey?, *Eos Trans. AGU*, 75, 116, 1994.
- Barker, P.F., Plate tectonics of the Scotia Sea region, *Nature*, 228, 1293-1296, 1970.
- Barker, P.F., A spreading centre in the east Scotia Sea, *Earth Planet. Sci. Lett.*, 15, 123-132, 1972.
- Barker, P.F., and I.A. Hill, Asymmetric spreading in the back arc basins, *Nature*, 285, 652-654, 1980.
- Barker, P.F., and L.A. Lawver, South American-Antarctic plate motion over the past 50 Myr, and the evolution of the South American-Antarctic ridge, *Geophys. J.*, 94, 377-386, 1988.
- Barrier, E., and J. Angelier, Structure et néotectonique de l'arc hellénique oriental: les îles de Kassos et Karpathos (Dodécanèse, Grèce), *Rev. Geol. Dyn. Geogr. Phys.*, 23, 257-276, 1981.
- Bassay Blum, M. de L., Cálculo de magnitudes, estimativa do parâmetro "b" e considerações sobre a atividade sísmica de Areado, MG, Outubro de 1991, *Proceedings III Int. Congres Braz. Geophys. Soc.*, Rio de Janeiro, 1, 694-699, 1993.
- Bell, C.M., Introduction to "Geology of the Andes", *J. Geol. Soc. London*, 141, 781-782, 1984.
- Berckhemer, H., Some aspects of the evolution of marginal seas deduced from observations in the Aegean region, in *International Symposium on the Structural History of the Mediterranean Basins*, edited by B. Biju-Duval and L. Montadert, pp. 303-314, Editions Technip, Paris, 1977.
- Billiris, H., D. Paradissis, G. Veis, P. England, W. Featherstone, B. Parsons, P. Cross, P. Rands, M. Rayson, P. Sellers, V. Ashkenazi, M. Davison, J. Jackson, and N. Ambraseys, Geodetic determination of tectonic deformation on central Greece from 1900 to 1988, *Nature*, 350, 124-129, 1991.
- Bott, M.H.P., The mechanics of oblique slip faulting, *Geol. Mag.*, 96, 109-117, 1959.

- Bott, M.H.P., G.D. Waghorn, and A. Whittaker, Plate boundary forces at subduction zones and trench-arc compression, *Tectonophysics*, 170, 1-15, 1989.
- Brooks, M., and G. Ferentinos, Tectonics and sedimentation in the Gulf of Corinth and the Zakynthos and Kefallinia channels, western Greece, *Tectonophysics*, 101, 25-54, 1984.
- Brooks, M., J.E. Clews, N.S. Melis, and J.R. Underhill, Structural development of Neogene basins in western Greece, *Basin Research*, 1, 129-138, 1988.
- Buick, I.S., The late Alpine evolution of an extensional shear zone, Naxos, Greece, *J. Geol. Soc. London*, 148, 93-103, 1991.
- Burg, J.-P., Z. Ivanov, L.-E. Ricou, D. Dimor, and L. Klain, Implications of shear-sense criteria for the tectonic evolution of the Central Rhodope massif, southern Bulgaria, *Geology*, 18, 451-454, 1990.
- Cahill, T., B.L. Isacks, D. Whitman, J.-L. Chatelain, A. Perez, and J.M. Chiu, Seismicity and tectonics in Jujuy province, Northwestern Argentina, *Tectonics*, 11, 944-959, 1992.
- Cande, S.C., R.B. Leslie, J.C. Parra, and M. Hobart, Interaction between the Chile ridge and Chile trench: Geophysical and geothermal evidence, *J. Geophys. Res.*, 92, 495-520, 1987.
- Cande, S.C., J.L. LaBrecque, and W.F. Haxby, Plate kinematics of the South Atlantic: Chron C34 to present, *J. Geophys. Res.*, 93, 13,479-13,492, 1988.
- Caputo, R., Geological and structural study of the recent and active brittle deformation of the Neogene-Quaternary basins of Thessaly (central Greece), *Sci. Ann. Geol. Dept.*, 12, Aristotle University, Thessaloniki, 1990.
- Carey, E., Recherche des directions principales de contraintes associées au jeu d'une population de failles, *Rev. Géol. Dyn. Géogr. Phys.*, 21, 57-66, 1979.
- Carey, E., and B. Brunier, Analyse théorique et numérique d'un modèle mécanique élémentaire appliqué à l'étude d'un population de failles, *C.R. Acad. Sci. Paris*, D279, 891-894, 1974.
- Carlson, R.L., and P.J. Melia, Subduction hinge migration, *Tectonophysics*, 102, 399-411, 1984.
- Chapple, W.M., and T.E. Tullis, Evaluation of the forces that drive the plates, *J. Geophys. Res.*, 82, 1967-1984, 1977.
- Chase, C.G., Plate kinematics: The Americas, East Africa, and the rest of the world, *Earth Planet. Sci. Lett.*, 37, 355-368, 1978a.
- Chase, C.G., Extension behind island arcs and motions relative to hot spots, *J. Geophys. Res.*, 83, 5385-5387, 1978b.
- Chinn, D.S., and B.L. Isacks, Accurate source depths and focal mechanisms of shallow earthquakes in western South America and in the New Hebrides Island Arc, *Tectonics*, 2, 529-563, 1983.
- Chiotis, E.D., and C.E. Tsoutrelis, Estimation of the potential type of faulting in relation to the stress field: the North Aegean case study, *J. Struct. Geol.*, 14, 215-223, 1992.

- Clews, J.E., Structural controls on basin evolution: Neogene to Quaternary of the Ionian zone, western Greece, *J. Geol. Soc. London*, 146, 447-457, 1989.
- Cloetingh, S., and R. Wortel, Regional stress field of the Indian plate, *Geophys. Res. Lett.*, 12, 77-80, 1985.
- Cloetingh, S., and R. Wortel, Stress in the Indo-Australian plate, *Tectonophysics*, 132, 49-67, 1986.
- Cloetingh, S., G. Nolet, and R. Wortel, Crustal structure of the eastern Mediterranean inferred from rayleigh wave dispersion, *Earth Planet. Sci. Lett.*, 51, 336-342, 1980.
- Coblentz, D.D., and R.M. Richardson, Constraints on continental margin dynamics from GEOSAT ERM geoid data, *Eos Trans. A.G.U.*, 73, 571, 1992.
- Coblentz, D.D., R.M. Richardson, and M. Sandiford, On the gravitational potential of the Earth's lithosphere, *Tectonics*, 13, 929-945, 1994.
- Dalmayrac, B., and P. Molnar, Parallel thrust and normal faulting in Peru and constraints on the state of stress, *Earth Planet. Sci. Lett.*, 55, 473-481, 1981.
- De Bremaecker, J.-C., Ph. Huchon, and X. Le Pichon, The deformation of Aegea: a finite element study, *Tectonophysics*, 86, 197-212, 1982.
- de Chabaliér, J.B., H. Lyon-Caen, A. Zollo, A. Deschamps, P. Bernard, and D. Hatzfeld, A detailed analysis of microearthquakes in western Crete from digital three-component seismograms, *Geophys. J. Int.*, 110, 347-360, 1992.
- de Jonge, M.R., W. Spakman, and M.J.R. Wortel, Forward and inverse modelling of mantle structure in the Alpine-Mediterranean region, *Ann. Geophys.*, 12, suppl. 1, C50, 1994.
- DeMets, C., R.G. Gordon, D.F. Argus, and S. Stein, Current plate motions, *Geophys. J.*, 101, 425-478, 1990.
- Dercourt, J., and 18 others, Geological evolution of the Tethys belt from the Atlantic to the Pamirs since the Lias, *Tectonophysics*, 123, 241-315, 1986.
- Deverchère, J., C. Dorbath, and L. Dorbath, Extension related to high topography: results from a microearthquake survey in the Andes of Peru and tectonic implications, *Geophys. J. Int.*, 98, 281-292, 1989.
- Dewey, J.F., Episodicity, sequence, and style at convergent plate boundaries, in *The Continental Crust and Its Mineral Deposits*, edited by D.W. Strangway, pp. 553-573, Geol. Ass. Can. Spec. Pap. 20, 1980.
- Dewey, J.F., Extensional collapse of orogens, *Tectonics*, 7, 1123-1139, 1988.
- Dewey, J.F., and S.H. Lamb, Active tectonics of the Andes, *Tectonophysics*, 205, 79-95, 1992.
- Dewey, J.F., and A.M.C. Şengör, Aegean and surrounding regions: complex multiplate and continuum tectonics in a convergent zone, *Geol. Soc. Am. Bull.*, 90, 84-92, 1979.

- Dewey, J.F., M.R. Hempton, W.S.F. Kidd, F. Saroglu, and A.M.C. Şengör, Shortening of continental lithosphere: the neotectonics of Eastern Anatolia- a young collision zone, in *Collision Tectonics*, edited by M.P. Coward and A.C. Ries, pp. 3-36, Geol. Soc. Spec. Publ. 19, 1986.
- Dewey, J. W., Seismicity and tectonics of western Venezuela, *Bull. Seismol. Soc. Am.*, 62, 1711-1751, 1972.
- Dinter, D.A., and L. Royden, Late Cenozoic extension in northeastern Greece: Strymon Valley detachment system and Rhodope metamorphic core complex, *Geology*, 21, 45-48, 1993.
- Doser, D.I., The Ancash, Peru, earthquake of 1946 November 10: evidence for low-angle normal faulting in the high Andes of northern Peru, *Geophys. J. R. Astron. Soc.*, 91, 51-71, 1987.
- Doutsos, T., N. Kontopoulos, and D. Frydas, Neotectonic evolution of north-western-continental Greece, *Geol. Rundsch.*, 76, 433-450, 1987.
- Drewes, H., and E. Geiss, Simulation study on the use of MEDLAS derived point motions for geokinematic models, *Adv. Space Res.*, 6, 71-74, 1986.
- Dumont, J.F., Lake patterns as related to neotectonics in subsiding basins: the example of the Ucamara depression, Peru, *Tectonophysics*, 222, 69-78, 1993.
- Dürr, St., Das Attisch-kykladische Kristallin, in *Geologie von Griechenland*, edited by V. Jacobshagen, pp. 116-148, Gebr. Borntraeger, Berlin, 1986.
- Dziewonski, A.M., and J.H. Woodhouse, An experiment in systematic study of global seismicity: Centroid-moment tensor solutions for 201 moderate to large earthquakes of 1981, *J. Geophys. Res.*, 88, 3247-3271, 1983.
- Dziewonski, A.M., G. Ekström, J.E. Franzen, and J.H. Woodhouse, Global seismicity of 1979: centroid-moment tensor solutions for 524 earthquakes, *Phys. Earth Planet. Inter.*, 48, 18-46, 1987.
- Ekström, G., and P. England, Seismic strain rates in regions of distributed continental deformation, *J. Geophys. Res.*, 94, 10,231-10,257, 1989.
- Elsasser, W.M., Sea-floor spreading as thermal convection, *J. Geophys. Res.*, 76, 1101-1112, 1971.
- England, P., and G. Houseman, Extension during continental convergence, with application to the Tibetan plateau, *J. Geophys. Res.*, 94, 17,561-17,579, 1989.
- England, P., and R. Wortel, Some consequences of the subduction of young slabs, *Earth Planet. Sci. Lett.*, 47, 403-415, 1980.
- Faure, M., M. Bonneau, and J. Pons, Ductile deformation and syntectonic granite emplacement during late Miocene extension of the Aegea (Greece), *Bull. Soc. géol. France*, 162, 3-11, 1991.
- Ferreira, J.M., R.T. de Oliveira, M.K. Takeya, and M. Assumpção, Superposition of local and regional stresses in NE Brazil: evidence from focal mechanisms around the Potiguar marginal basin, *IV Congr. Braz. Geophys. Soc.*, Rio de Janeiro, 1995.

- Fleitout, L., The sources of lithospheric tectonic stresses, in *Tectonic Stress in the Lithosphere*, edited by R.B. Whitmarsh, M.H.P. Bott, J.D. Fairhead, and N.J. Kusznir, pp. 73-81, Roy. Soc. London, London, 1991.
- Fleitout, L., and C. Froidevaux, Tectonics and topography for a lithosphere containing density heterogeneities, *Tectonics*, 1, 21-56, 1982.
- Fleitout, L., and C. Froidevaux, Tectonic stresses in the lithosphere, *Tectonics*, 2, 315-324, 1983.
- Forsyth, D.W., Fault plane solutions and tectonics of the South Atlantic and Scotia Sea, *J. Geophys. Res.*, 80, 1429-1443, 1975.
- Forsyth, D., and S. Uyeda, On the relative importance of the driving forces of plate motion, *Geophys. J. R. Astron. Soc.*, 43, 163-200, 1975.
- Forsythe, R., and E. Nelson, Geological manifestations of ridge collision: Evidence from the Golfo de Penas-Taitao basin, southern Chile, *Tectonics*, 4, 477-495, 1985.
- Frank, F.C., Plate tectonics, the analogy with glacier flow, and isostasy, in *Flow and Fracture of Rocks*, edited by H.C. Heard, I.Y. Borg, N.L. Carter, and C.B. Raleigh, pp. 285-292, Geophys. Mon., 16, 1972.
- Froidevaux, C., and B. L. Isacks, The mechanical state of the lithosphere in the Altiplano-Puna segment of the Andes, *Earth Planet. Sci. Lett.*, 71, 305-314, 1984.
- Froidevaux, C., S. Uyeda, and M. Uyeshima, Island arc tectonics, *Tectonophysics*, 148, 1-9, 1988.
- Frydas, D., Plankton-Stratigraphie des Pliozäns und unteren Pleistozäns der SW-Peloponnes, Griechenland, *Newsl. Stratigr.*, 23, 91-108, 1990.
- Fytikas, M., F. Innocenti, P. Manetti, R. Mazuolli, A. Peccerillo, and L. Villari, Tertiary to Quaternary evolution of volcanism in the Aegean region, in *The Geological Evolution of the Eastern Mediterranean*, edited by J.E. Dixon and A.H.F. Robertson, pp. 687-699, Geol. Soc. Spec. Publ. 17, 1984.
- Galanopoulos, A.G., The seismotectonic regime in Greece, *Ann. Geof.*, 20, 109-119, 1967.
- Gautier, P., J.-P. Brun, and L. Jolivet, Structure and kinematics of Upper Cenozoic extensional detachment on Naxos and Paros (Cyclades islands, Greece), *Tectonics*, 12, 1180-1194, 1993.
- Geiss, E., Die Lithosphäre im mediterranen Raum, Ein Beitrag zu Struktur, Schwerefeld und Deformation, Ph.D. thesis, 115 pp., Ludwig-Maximilians Universität, Munich, 1987.
- Gilbert, L.E., K. Kastens, K. Hurst, D. Paradissis, G. Veis, H. Billiris, W. Höppe, and W. Schlüter, Strain results and tectonics from the Aegean GPS experiment, *Eos Trans. AGU*, 75, 116, 1994.
- Gordon, R.G., and D.M. Jurdy, Cenozoic global plate motions, *J. Geophys. Res.*, 91, 12,389-12,406, 1986.
- Govers, R., Dynamics of Lithospheric Extension: a Modeling Study, Ph.D. thesis, Utrecht University, 240 pp., *Geologica Ultraiectina*, 105, 1993.

- Grange, F., D. Hatzfeld, P. Cunningham, P. Molnar, S.W. Roecker, G. Suarez, A. Rodrigues, and L. Ocola, Tectonic implications of the microearthquake seismicity and fault plane solutions in southern Peru, *J. Geophys. Res.*, *89*, 6139-6152, 1984.
- Greiling, R., The metamorphic and structural evolution of the Phyllite Quartzite Nappe of western Crete, *J. Struct. Geol.*, *4*, 291-298, 1982.
- Gripp, A. E., and R. G. Gordon, Current plate velocities relative to the hotspots incorporating the NUVEL-1 global plate motion model, *Geophys. Res. Lett.*, *17*, 1109-1112, 1990.
- Harper, J.F., Plate dynamics: Caribbean map corrections and hotspot push, *Geophys. J. Int.*, *100*, 423-431, 1990.
- Hatzfeld, D., G. Pedotti, P. Hatzidimitriou, and K. Makropoulos, The strain pattern in the western Hellenic arc deduced from a microearthquake survey, *Geophys. J. Int.*, *101*, 181-202, 1990.
- Hatzfeld, D., M. Besnard, K. Makropoulos, and P. Hatzidimitriou, Microearthquake seismicity and fault-plane solutions in the southern Aegean and its geodynamic implications, *Geophys. J. Int.*, *115*, 799-818, 1993.
- Henneberg, H.G., Geodetic control on neotectonics in Venezuela, *Tectonophysics*, *97*, 1-15, 1983.
- Henry, S.G., and H.N. Pollack, Heat flow above the Andean subduction zone in Bolivia and Peru, *J. Geophys. Res.*, *93*, 15,153-15,162, 1988.
- IGME, Geological Map of Greece, Filiatra sheet, scale 1:50.000, Institute of Geology and Mineral Exploration, Athens, 1980.
- IGME, Seismotectonic Map of Greece, scale 1:500.000, Institute of Geology and Mineral Exploration, Athens, 1989.
- International Hydrographic Organization/Intergovernmental Oceanographic Commission/Canadian Hydrographic Service, GEBCO general bathymetric map of the oceans, Ottawa, Ont., Canada, 1984.
- Isacks, B.L., Uplift of the central Andean Plateau and bending of the Bolivian Orocline, *J. Geophys. Res.*, *93*, 3211-3231, 1988.
- Isacks, B., and P. Molnar, Distribution of stresses in the descending lithosphere from a global survey of focal-mechanism solutions of mantle earthquakes, *Rev. Geophys.*, *9*, 103-174, 1971.
- Jackson, J., Active tectonics of the Aegean region, *Ann. Rev. Earth Planet. Sci.*, *22*, 239-271, 1994.
- Jackson, J., and D. McKenzie, Active tectonics of the Alpine-Himalayan belt between western Turkey and Pakistan, *Geophys. J. R. astr. Soc.*, *77*, 185-264, 1984.
- Jackson, J., and D. McKenzie, Rates of active deformation in the Aegean Sea and surrounding regions, *Basin Res.*, *1*, 121-128, 1988a.
- Jackson, J., and D. McKenzie, The relationship between plate motions and seismic moment tensors, and the rates of active deformation in the Mediterranean and Middle East, *Geophys. J.*, *93*, 45-73, 1988b.

- Jackson, J.A., G. King, and C. Vita-Finzi, The neotectonics of the Aegean: an alternative view, *Earth Planet. Sci. Lett.*, 61, 303-318, 1982.
- Jackson, J., J. Haines, and W. Holt, The horizontal velocity field in the deforming Aegean Sea region determined from the moment tensors of earthquakes, *J. Geophys. Res.*, 97, 17,657-17,684, 1992.
- Jacobshagen, V. (Ed.), *Geologie von Griechenland*, 363 pp., Gebr. Borntraeger, Berlin, 1986.
- Jarrard, R.D., Relations among subduction parameters, *Rev. Geophys.*, 24, 217-284, 1986.
- Jones, C.E., J. Tarney, J.H. Baker, and F. Gerouki, Tertiary granitoids of Rhodope, northern Greece: magmatism related to extensional collapse of the Hellenic Orogen?, *Tectonophysics*, 210, 295-314, 1992.
- Jordan, T. H., The present-day motions of the Caribbean plate, *J. Geophys. Res.*, 80, 4433-4439, 1975.
- Kahle, H.-G., M.V. Müller, S. Mueller, and G. Veis, The Kephallonia transform fault and the rotation of the Apulian platform: evidence from satellite geodesy, *Geophys. Res. Lett.*, 20, 651-654, 1993.
- Kasapoglu, K.E., and M.N. Toksöz, Tectonic consequences of the collision of the Arabian and Eurasian plates: finite element models, *Tectonophysics*, 100, 71-95, 1983.
- Kellogg, J. N., and W. E. Bonini, Subduction of the Caribbean plate and basement uplifts in the overriding South American plate, *Tectonics*, 1, 251-276, 1982.
- Kellogg, J. N., and W. E. Bonini, Reply, *Tectonics*, 4, 785-790, 1985.
- Kellogg, J., T. Dixon, and R. Neilan, CASA Central and South America GPS geodesy, *Eos Trans. AGU*, 70, 649-656, 1989.
- Keraudren, B., and D. Sorel, Relations entre sédimentation, tectonique et morphologie dans le Plio- Pléistocène de Karpathos (Grèce); mouvements verticaux et datations radiométriques, *L'Anthropologie*, 88, 49-61, 1984.
- Ketin, I., Über die tektonisch-mechanischen Folgerungen aus den grossen Erdbeben des letzten Dezenniums, *Geol. Rundsch.*, 36, 77-83, 1948.
- King, G., D. Sturdy, and J. Whitney, The landscape geometry and active tectonics of northwest Greece, *Geol. Soc. Am. Bull.*, 105, 137-161, 1993.
- Kissel, C., and C. Laj, The Tertiary geodynamical evolution of the Aegean arc: a paleomagnetic reconstruction, *Tectonophysics*, 146, 183-201, 1988.
- Kulm, L. D., W. J. Schweller, and A. Masias, A preliminary analysis of the subduction processes along the Andean continental margin, 6° to 45°, in *Island Arcs, Deep Sea Trenches and Back-Arc Basins*, edited by M. Talwani, and W. C. Pitman, pp. 285-302, Maurice Ewing Ser., 1, AGU, Washington, D.C., 1977.
- Kusznir, N.J., The distribution of stress with depth in the lithosphere: thermo-rheological and geodynamic constraints, in *Tectonic Stress in the Lithosphere*, edited by R.B. Whitmarsh, M.H.P. Bott, J.D. Fairhead, and N.J. Kusznir, pp. 95-110, Roy. Soc. London, London, 1991.

- Ladd, J.W., M. Truchan, M. Talwani, P.L. Stoffa, P. Buhl, R. Houtz, A. Mauffret, and G. Westbrook, Seismic reflection profiles across the southern margin of the Caribbean, in *Caribbean-South American Plate Boundary and Regional Tectonics*, edited by W. E. Bonini, R. B. Hargraves, and R. Shagam, pp. 153-159, Geological Society of America, Boulder, Colo., 1984.
- Laj, C., M. Jamet, D. Sorel, and J.P. Valente, First paleomagnetic results from Miocene series of the Hellenic sedimentary arc, *Tectonophysics*, 86, 45-67, 1982.
- Lallemant, S., La transversale nord-Maniote etude geologique et aeromagnetique d'une structure transverse a l'arc egeen externe, Thèse 3ème cycle, 164 pp., Université Pierre et Marie Curie, Paris, 1984.
- Larson, R. L., W. C. Pitman III, X. Golovchenko, S. C. Cande, J. F. Dewey, W. F. Haxby, and J. C. LaBrecque, The Bedrock Geology of the World, W. H. Freeman, New York, 1985.
- Lawver, L. A., and H. J. B. Dick, The American-Antarctic Ridge, *J. Geophys. Res.*, 88, 8193-8202, 1983.
- Lee, J., and G.S. Lister, Late Miocene ductile extension and detachment faulting, Mykonos, Greece, *Geology*, 20, 121-124, 1992.
- Lehner, P., H. Doust, G. Bakker, P. Allenbach, and J. Gueneau, Active margins-Caribbean margin of South America, profiles C-1422, C-1412, and C-1413, in *Seismic Expression of Structural Styles 3*, edited by A. W. Bally, pp. 3.4.2.-111-3.4.2-128, American Association of Petroleum Geologists, Tulsa, Okla., 1983.
- Le Pichon, X., Land-locked oceanic basins and continental collision: the Eastern Mediterranean as a case example, in *Mountain Building Processes*, edited by K. Hsü, pp. 201-211, Academic Press, London, 1982.
- Le Pichon, X., and J. Angelier, The Hellenic arc and trench system: a key to the neotectonic evolution of the eastern Mediterranean area, *Tectonophysics*, 60, 1-42, 1979.
- Le Pichon, X., and J. Angelier, The Aegean Sea, *Phil. Trans. R. Soc. London. A*, 300, 357-372, 1981.
- Le Pichon, X., J. Angelier, J. Aubouin, N. Lybérís, S. Monti, V. Renard, H. Got, K. Hsü, Y. Mart, J. Mascle, D. Matthews, D. Mitropoulos, P. Tsofliás, and G. Chronis, From subduction to transform motion: a Seabeam survey of the Hellenic trench system, *Earth Planet. Sci. Lett.*, 44, 441-450, 1979.
- Le Pichon, X., N. Lyberis, J. Angelier, and V. Renard, Strain distribution over the east Mediterranean ridge: a synthesis incorporating new sea-beam data, *Tectonophysics*, 86, 243-274, 1982.
- Lister, C.R.B., Gravitational drive on oceanic plates caused by thermal contraction, *Nature*, 257, 663-665, 1975.
- Lister, G.S., G. Banga, and A. Feenstra, Metamorphic core complexes of Cordilleran type in the Cyclades, Aegean Sea, Greece, *Geology*, 12, 221-225, 1984.

- Livermore, R.A., and A.G. Smith, Some boundary conditions for the evolution of the Mediterranean region, in *Geological Evolution of the Mediterranean Basin*, edited by D.J. Stanley and F.-C. Wezel, pp. 83-100, Springer, New York, 1985.
- Lu, R.S., and K.J. McMillen, Multichannel seismic survey of the Colombia basin and adjacent margins, in *Studies in Continental Margin Geology*, edited by J. S. Watkins and C. L. Drake, pp. 395-410, AAPG Mem., 34, 1982.
- Ludwig, W.J., and P.D. Rabinowitz, The collision complex of the North Scotia Ridge, *J. Geophys. Res.*, 87, 3731-3740, 1982.
- Ludwig, W.J., C.C. Windisch, R.E. Houtz, and J.I. Ewing, Structure of Falkland Plateau and offshore Tierra del Fuego, in *Geological and Geophysical Investigations of Continental Margins*, edited by J. S. Watkins et al., pp. 125-137, AAPG Mem., 9, 1978.
- Lybérís, N., Géodynamique de domaine égéen depuis le Miocène supérieur, *Mém. Sc. Terre Univ. Curie, Paris*, 84-18, 367 pp., 1984.
- Lyberis, N., and S. Lallemand, La transition subduction-collision le long de l'arc egeen externe, *C. R. Acad. Sci. Paris*, 300, 885-890, 1985.
- Lybérís, N., and J. Sauvage, Evolution tectonique de la région nord égéenne (Grèce) du Pliocène au Pléistocène, *Bull. Soc. géol. France, ser. 8, vol. 1*, 581-595, 1985.
- Lyberis, N., J. Angelier, E. Barrier, and S. Lallemand, Active deformation of a segment of arc: the strait of Kythira, Hellenic arc, Greece, *J. Struct. Geol.*, 4, 299-311, 1982.
- Lyon-Caen, H., R. Armijo, J. Drakopoulos, J. Baskoutass, N. Delibassis, R. Gaulon, V. Kouskouna, J. Latoussakis, K. Makropoulos, P. Papadimitriou, D. Papanastassiou, and G. Pedotti, The 1986 Kalamata (south Peloponnesus) earthquake: detailed study of a normal fault, evidences for east-west extension in the Hellenic arc, *J. Geophys. Res.*, 93, 14,967-15,000, 1988.
- Makris, J., Geophysical investigations of the Hellenides, *Hamb. Geophys. Einzelschr.*, 34, 124 pp., 1977.
- Makris, J., and C. Stobbe, Physical properties and state of the crust and upper mantle of the eastern Mediterranean Sea deduced from geophysical data, *Mar. Geology*, 55, 347-363, 1984.
- Makropoulos, K., and P.W. Burton, Greek tectonics and seismicity, *Tectonophysics*, 106, 275-304, 1984.
- Márton, E., Paleomagnetism in the Mediterranean from Spain to the Aegean: a review of data relevant to Cenozoic movements, in *Recent Evolution and Seismicity of the Mediterranean Region*, edited by E. Boschi, E. Mantovani, and A. Morelli, pp. 367-402, NATO ASI Series C, 402, 1993.
- Masclé, J., and L. Martin, Shallow structure and recent evolution of the Aegean Sea: a synthesis based on continuous reflection profiles, *Mar. Geology*, 94, 271-299, 1990.

- McKenzie, D., Active tectonics of the Mediterranean region, *Geophys. J. R. astr. Soc.*, 30, 109-185, 1972.
- McKenzie, D., Active tectonics of the Alpine-Himalayan belt: the Aegean Sea and surrounding regions, *Geophys. J. R. astr. Soc.*, 55, 217-254, 1978.
- Meissner, B., M. Shulman, and W. Skala, Finite-Element-Berechnungen zur Auswertung herdmmechanischer Daten und deren Beziehungen zum Störungsmunster des Ägäis-Raumes, *Geol. Rundsch.*, 68, 225-235, 1979.
- Mercier, J.L., Signification néotectonique de l'Arc Égéen. Une revue des idées, *Rev. Geol. Dyn. Geogr. Phys.*, 21, 5-15, 1979.
- Mercier, J.L., Extensional-compressional tectonics associated with the Aegean Arc: comparison with the Andean Cordillera of south Peru - north Bolivia, *Phil. Trans. R. Soc. Lond.*, A300, 337-355, 1981.
- Mercier, J.L., and S. Lalechos, The mid-recent Pleistocene NW-SE extension in southern Peloponnesus and the kinematics of the seismic fault of the 1986 Kalamata earthquake (Greece), *Proc. 2nd Congress Hellenic Geophysical Union, 5-7 May 1993, Macedonia, Greece*, in press.
- Mercier, J., B. Bousquet, N. Delibasis, I. Drakopoulos, B. Keraudren, F. Lemeille, and D. Sorel, Déformations en compression dans le Quaternaire des rivages Ioniens (Céphalonie, Grèce) Données néotectoniques et séismiques, *C. R. Acad. Sci. Paris*, 275, 2307-2310, 1972.
- Mercier, J.L., E. Carey-Gailhardis, N. Mouyaris, T. Roundoyannis, and C. Angelidhis, Structural analysis of recent and active faults and regional state of stress in the epicentral area of the 1978 Thessaloniki earthquakes (Northern Greece), *Tectonics*, 2, 577-600, 1983.
- Mercier, J.L., D. Sorel, and K. Simeakis, Changes in the state of stress in the overriding plate of a subduction zone: the Aegean arc from the Pliocene to the present, *Annales Tectonicæ*, 1, 20-39, 1987.
- Mercier, J.L., D. Sorel, P. Vergely, and K. Simeakis, Extensional tectonic regimes in the Aegean basins during the Cenozoic, *Basin Research*, 2, 49-71, 1989.
- Mercier, J.L., M. Sebrier, A. Lavenu, J. Cabrera, O. Bellier, J.-F. Dumont, and J. Machare, Changes in the tectonic regime above a subduction zone of Andean type: the Andes of Peru and Bolivia during the Pliocene-Pleistocene, *J. Geophys. Res.*, 97, 11,945-11,982, 1992.
- Mercier, J.L., D. Sorel, S. Lalechos, and B. Keraudren, The tectonic regimes along the convergent border of the Aegean arc from the late Miocene to the present; southern Peloponnesus as an example, in *Recent Evolution and Seismicity of the Mediterranean Region*, edited by E. Boschi, E. Mantovani, and A. Morelli, pp. 141-160, NATO ASI Series C, 402, 1993.
- Meulenkamp, J.E., Aspects of the late Cenozoic evolution of the Aegean region, in *Geological Evolution of the Mediterranean Basin*, edited by D.J. Stanley and F.-C. Wezel, pp. 307-321, Springer, New York, 1985.
- Meulenkamp, J.E., D. Theodoropoulos, and V. Tsapralis, Remarks on the Neogene of Kythira, Greece, *Proc. VI coll. geol. Aegean reg.*, 355-362, 1977.

- Meulenkamp, J.E., M.J.R. Wortel, W.A. van Wamel, W. Spakman, and E. Hoogerduyn Strating, On the Hellenic subduction zone and the geodynamic evolution of Crete since the late Middle Miocene, *Tectonophysics*, 146, 203-215, 1988.
- Minster, J.B., and T.H. Jordan, Present-day plate motions, *J. Geophys. Res.*, 83, 5331-5354, 1978.
- Minster, J.B., T.H. Jordan, P. Molnar, and E. Haines, Numerical modelling of instantaneous plate tectonics, *Geophys. J. R. Astron. Soc.*, 36, 541-576, 1974.
- Molnar, P., and T. Atwater, Interarc spreading and Cordilleran tectonics as alternates related to the age of subducted oceanic lithosphere, *Earth Planet. Sci. Lett.*, 41, 330-340, 1978.
- Molnar, P., and H. Lyon-Caen, Some simple physical aspects of the support, structure, and evolution of mountain belts, *Geol. Soc. Am. Spec. Pap.*, 218, 179-207, 1988.
- Molnar, P., and L. R. Sykes, Tectonics of the Caribbean and Middle America regions from focal mechanisms and seismicity, *Geol. Soc. Am. Bull.*, 80, 1639-1684, 1969.
- Molnar, P., P. England, and J. Martinod, Mantle dynamics, uplift of the Tibetan plateau, and the Indian monsoon, *Rev. Geophys.*, 31, 357-396, 1993.
- Noomen, R., B.A.C. Ambrosius, and K.F. Wakker, Crustal motions in the Mediterranean region determined from laser ranging to LAGEOS, in *Contributions of Space Geodesy to Geodynamics: Crustal Dynamics*, edited by D.E. Smith and D.L. Turcotte, pp. 331-346, *Geodyn. Ser.*, 23, 1993.
- Noomen, R., B.A.C. Ambrosius, D.C. Kuyper, G.J. Mets, B. Overgaauw, T.A. Springer, and K.F. Wakker, Crustal deformation in the Mediterranean area computed from space-geodetic observations, *Eos Trans. AGU*, 75, 115, 1994.
- Oliver, R.A., N. Vatin-Perignon, and G. Laubacher (Eds.), *Andean Geodynamics, Tectonophysics*, 205, 1-355, 1992.
- Oral, M.B., R.E. Reilinger, M.N. Toksöz, A.A. Barka, and I. Kinik, Preliminary results of 1988 and 1990 GPS measurements in western Turkey and their tectonic implications, in *Contributions of Space Geodesy to Geodynamics: Crustal Dynamics*, edited by D.E. Smith and D.L. Turcotte, pp. 407-416, *Geodyn. Ser.*, 23, 1993.
- Papadopoulos, G.A., and S.B. Pavlides, The large 1956 earthquake in the south Aegean: macroseismic field configuration, faulting, and neotectonics of Amorgos island, *Earth Planet. Sci. Lett.*, 113, 383-396, 1992.
- Papazachos, B.C., and P.E. Comninakis, Geophysical and tectonic features of the Aegean arc, *J. Geophys. Res.*, 76, 8517-8533, 1971.
- Papazachos, B.C., A.A. Kiratzi, and E. Papadimitriou, Fault plane solutions for earthquakes in the Aegean area, *PAGEOPH*, 136, 405-420, 1991.
- Pavoni, N., Die nordanatolische Horizontalverschiebung, *Geol. Rundschau*, 51, 122-139, 1961.

- Pelayo, A.M., and D.A. Wiens, Seismotectonics and relative plate motions in the Scotia Sea region, *J. Geophys. Res.*, *94*, 7293-7320, 1989.
- Pennington, W.D., Subduction of the eastern Panama basin and seismotectonics of northwestern South America, *J. Geophys. Res.*, *86*, 10,753-10,770, 1981.
- Pe-Piper, G., and D.J.W. Piper, Spatial and temporal variation in Late Cenozoic back-arc volcanic rocks, Aegean Sea region, *Tectonophysics*, *169*, 113-134, 1989.
- Pérez, O.J., and Y.P. Aggarwal, Present-day tectonics of the southeastern Caribbean and northeastern Venezuela, *J. Geophys. Res.*, *86*, 10,791-10,804, 1981.
- Peters, J.M., and W.J. Huson, The Pliny and Strabo trenches (eastern Mediterranean): integration of seismic reflection data and seabeam bathymetric maps, *Marine Geol.*, *64*, 1-17, 1985.
- Pilger, R.H., Jr, Plate reconstructions, aseismic ridges, and low-angle subduction beneath the Andes, *Geol. Soc. Am. Bull.*, *92*, 448-456, 1981.
- Pirazzoli, P.A., L.F. Montaggioni, J.F. Saliège, G. Segonzac, Y. Thommeret, and C. Vergnaud-Grazzini, Crustal block movements from Holocene shorelines: Rhodes island (Greece), *Tectonophysics*, *170*, 89-114, 1989.
- Postma, G., A.R. Fortuin, and W.A. van Wamel, Basin-fill patterns controlled by tectonics and climate: the Neogene "forearc" basins of eastern Crete as a case history, in *Tectonic Controls and Signatures in Sedimentary Successions*, edited by L.E. Frostick and R.J. Steel, pp. 335-362, Spec. Publ. Int. Ass. Sed., 1993.
- Reches, Z., Determination of the tectonic stress tensor from slip along faults that obey the Coulomb yield condition, *Tectonics*, *6*, 849-861, 1987.
- Richardson, R.M., and D.D. Coblenz, Stress modelling in the Andes: constraints on the South American intraplate stress magnitudes, *J. Geophys. Res.*, *99*, 22,015-22,025, 1994.
- Richardson, R.M., S.C. Solomon, and N.H. Sleep, Tectonic stress in the plates, *Rev. Geophys.*, *17*, 981-1019, 1979.
- Richter, F.M., and D.P. McKenzie, Simple plate models of mantle convection, *J. Geophys.*, *44*, 441-471, 1978.
- Robbins, J.W., M.H. Torrence, P.J. Dunn, R.G. Williamson, D.E. Smith, and R. Kolenkiewicz, SLR determined velocities in the Mediterranean region: implications for regional tectonic models, *Eos Trans. AGU*, *73*, 122, 1992.
- Robertson, A.H.F., and J.E. Dixon, Introduction: aspects of the geological evolution of the Eastern Mediterranean, in *The Geological Evolution of the Eastern Mediterranean*, edited by J. E. Dixon and A.H.F. Robertson, pp. 1-74, Geol. Soc. Spec. Publ. *17*, 1984.
- Robertson, A.H.F., P.D. Clift, P. Dignan, and G. Jones, Palaeogeographic and palaeotectonic evolution of the Eastern Mediterranean Neotethys, *Palaeogeogr. palaeoclimat. palaeoecol.*, *87*, 289-344, 1991.

- Ruff, L., and H. Kanamori, Seismicity and the subduction process, *Phys. Earth Planet. Int.*, 23, 240-252, 1980.
- Russo, R.M., and P.G. Silver, Trench-parallel flow beneath the Nazca plate from seismic anisotropy, *Science*, 263, 1105-1111, 1994.
- Russo, R.M., and P.G. Silver, Trench-parallel mantle flow and cordillera orogenesis, South and North America, manuscript submitted to *Geology*, 1994.
- Russo, R.M., R.C. Speed, E.A. Okal, J.B. Shepherd, and K.C. Rowley, Seismicity and tectonics of the southeastern Caribbean, *J. Geophys. Res.*, 98, 14,299-14,321, 1993.
- Sacks, I.S., Interrelationships between volcanism, seismicity, and anelasticity in western South America, *Tectonophysics*, 37, 131-139, 1977.
- Schermer, E.R., Geometry and kinematics of continental basement deformation during the Alpine orogeny, Mt. Olympos region, Greece, *J. Struct. Geol.*, 15, 571-591, 1993.
- Schröder, B., Das postorogene Känozoikum in Griechenland/Ägäis, in *Geologie von Griechenland*, edited by V. Jacobshagen, pp. 209-240, Gebr. Borntraeger, Berlin, 1986.
- Seidel, E., H. Kreuzer, and W. Harre, A late Oligocene/early Miocene high pressure belt in the external Hellenides, *Geol. Jahrb.*, E23, 165-206, 1982.
- Şengör, A.M.C., The North Anatolian transform fault: its age, offset and tectonic significance, *J. geol. Soc. London*, 136, 269-282, 1979.
- Şengör, A.M.C., Plate tectonics and orogenic research after 25 years: a Tethyan perspective, *Earth Sci. Rev.*, 27, 1-201, 1990.
- Şengör, A.M.C., Some current problems on the tectonic evolution of the Mediterranean during the Cainozoic, in *Recent Evolution and Seismicity of the Mediterranean Region*, edited by E. Boschi, E. Mantovani, and A. Morelli, pp. 1-51, NATO ASI Series C, 402, 1993.
- Şengör, A.M.C., N. Görür, and F. Şaroğlu, Strike-slip faulting and related basin formation in zones of tectonic escape: Turkey as a case study, in *Strike Slip Deformation, Basin Formation, and Sedimentation*, pp. 227-264, Society of Economic Paleontologists and Mineralogists, Tulsa, 1985.
- Seyitoğlu, G., and B. Scott, Late Cenozoic crustal extension and basin formation in west Turkey, *Geol. Mag.*, 128, 155-166, 1991.
- Seyitoğlu, G., B.C. Scott, and C.C. Rundle, Timing of Cenozoic extensional tectonics in west Turkey, *J. Geol. Soc. London*, 149, 533-538, 1992.
- Simeakis, C., J.L. Mercier, P. Vergely, and C. Kissel, Late Cenozoic rotations along the north Aegean trough fault zone (Greece); structural constraints, in *Paleomagnetic Rotations and Continental Deformation*, edited by C. Kissel and C. Laj, pp. 131-143, Kluwer Academic Publ., 1989.
- Sokoutis, D., J.P. Brun, J. van den Driessche, and S. Pavlides, A major Oligo-Miocene detachment in southern Rhodope controlling north Aegean extension, *J. Geol. Soc. London*, 150, 243-246, 1993.

- Sonder, L.J., and P.C. England, Effects of a temperature-dependent rheology on large-scale continental extension, *J. Geophys. Res.*, 94, 7603-7619, 1989.
- Sorel, D., Etude néotectonique des îles ioniennes de Céphalonie et Zante et de l'Elide occidentale (Grèce), Thèse de 3e cycle, 196 pp., Univ. Paris-Sud, Orsay, 1976.
- Sorel, D., J.-L. Mercier, B. Keraudren, and M. Cushing, Le rôle de la traction de la lithosphère subductée dans l'évolution géodynamique plio-pléistocène de l'arc égéen: mouvements verticaux alternés et variations du régime tectonique, *C. R. Acad. Sci. Paris*, 307, 1981-1986, 1988.
- Sorel, D., G. Bizon, S. Aliaj, and L. Hasani, Calage stratigraphique de l'âge et de la durée des phases compressives des Hellénides externes (Grèce nord-occidentale et Albanie), du Miocène à l'Actuel, *Bull. Soc. géol. France*, 163, 447-454, 1992.
- Spakman, W., Tomographic images of the upper mantle below central Europe and the Mediterranean, *Terra Nova*, 2, 542-553, 1990.
- Spakman, W., Delay-time tomography of the upper mantle below Europe, the Mediterranean, and Asia Minor, *Geophys. J. Int.*, 107, 309-332, 1991.
- Spakman, W., M.J.R. Wortel, and N.J. Vlaar, The Hellenic subduction zone: a tomographic image and its geodynamic implications, *Geophys. Res. Lett.*, 15, 60-63, 1988.
- Spakman, W., S. van der Lee, and R. van der Hilst, Travel-time tomography of the European-Mediterranean mantle down to 1400 km, *Phys. Earth. Planet. Int.*, 79, 3-74, 1993.
- Spakman, W., M.R. de Jonge, and M.J.R. Wortel, The complex 3D-geometry of subduction below southeastern Europe: inferences from seismic tomography, *Eos Trans. AGU*, 75, 118, 1994.
- Speed, R.C., Cenozoic collision of the Lesser Antilles arc and continental South America and the origin of El Pilar fault, *Tectonics*, 4, 41-69, 1985.
- Speranza, F., C. Kissel, I. Islami, A. Hyseni, and C. Laj, First paleomagnetic evidence for rotation of the Ionian zone of Albania, *Geophys. Res. Lett.*, 19, 697-700, 1992.
- Stanley, D.J., and F.-C. Wezel (Eds.), *Geological Evolution of the Mediterranean Basin*, pp., Springer, New York, 1985.
- Stefanick, M., and D.M. Jurdy, Stress observations and driving force models for the South American plate, *J. Geophys. Res.*, 97, 11,905-11,913, 1992.
- Stein, S., C. DeMets, R. G. Gordon, J. Brodholt, D. Argus, J. F. Engeln, P. Lundgren, C. Stein, D. A. Wiens, and D. F. Woods, A test of alternative Caribbean plate relative motion models, *J. Geophys. Res.*, 93, 3041-3050, 1988.
- Stein, S., S. Cloetingh, N.H. Sleep, and R. Wortel, Passive margin earthquakes, stresses and rheology, in *Earthquakes at North-Atlantic Passive Margins: Neotectonics and Postglacial Rebound*, edited by S. Gregersen and P.W. Basham, pp. 231-259, NATO ASI Series C, 266, 1989.

- Stiros, S.C., Geodetically controlled taphrogenesis in back-arc environments: three examples from central and northern Greece, *Tectonophysics*, 130, 281-288, 1986.
- Stiros, S.C., Archaeology - A tool to study active tectonics. The Aegean as a case study, *Eos Trans. AGU*, 69, 1633, 1639, 1988.
- Stiros, S.C., M. Arnold, P.A. Pirazzoli, J. Laborel, F. Laborel, and S. Papageorgiou, Historical coseismic uplift on Euboea island, Greece, *Earth Planet. Sci. Lett.*, 108, 109-117, 1992.
- Straub, C., H.-G. Kahle, and A. Aksoy, Active crustal deformation in the Marmara Sea region, *Eos Trans. AGU*, 75, 116, 1994.
- Tapponnier, P., Evolution tectonique du système alpin en Méditerranée: poinçonnement et écrasement rigide-plastique, *Bull. Soc. géol. France*, 19, 437-460, 1977.
- Taymaz, T., The source parameters of the Çubukdağ (W. Turkey) earthquake of 1986 October 11, *Geophys. J. Int.*, 113, 260-267, 1993.
- Taymaz, T., and S. Price, The 1971 May 12 Burdur earthquake sequence, SW Turkey: a synthesis of seismological and geological observations, *Geophys. J. Int.*, 108, 589-603, 1992.
- Taymaz, T., J. Jackson, and R. Westaway, Earthquake mechanisms in the Hellenic Trench near Crete, *Geophys. J. Int.*, 102, 695-731, 1990.
- Taymaz, T., J. Jackson, and D. McKenzie, Active tectonics of the north and central Aegean Sea, *Geophys. J. Int.*, 106, 433-490, 1991.
- Theodoropoulos, D.K., *Physical Geography of the Island of Kythira*, 94 pp., Athens, 1973.
- Tselentis, G.-A., J. Drakopoulos, and K. Dimitriadis, A spectral approach to Moho depths estimation from gravity measurements in Epirus (NW Greece), *J. Phys. Earth*, 36, 255-266, 1988.
- Underhill, J.R., Late Cenozoic deformation of the Hellenide foreland, western Greece, *Geol. Soc. Am. Bull.*, 101, 613-634, 1989.
- Urai, J.L., R.D. Schuiling, and J.B.H. Jansen, Alpine deformation on Naxos (Greece), in *Deformation mechanisms, Rheology and Tectonics*, edited by R.J. Knipe and E.H. Rutter, pp. 509-522, Geol. Soc. Spec. Publ., 54, 1990.
- Valente, J.P., C. Laj, D. Sorel, S. Roy, and J.P. Valet, Paleomagnetic results from Mio-Pliocene marine series in Crete, *Earth Planet. Sci. Lett.*, 57, 159-172, 1982.
- Van Wamel, W.A., and J.J. Gast, Analysis of tilting at Gournia (Crete) by the representative block method: a geological-archaeological technique to analyse historical tilting, *Archaeometry*, 36, 131-139, 1994.
- Vlaar, N.J., and M.J.R. Wortel, Lithospheric aging, instability and subduction, *Tectonophysics*, 32, 331-351, 1976.
- Walcott, C.R., and S. White, Structural evolution of the southern-central Pelagonian zone in Greece, *Terra Abstracts, Terra Nova*, 7, 117, 1995.

- Wdowinsky, S., R.J. O'Connell, and P. England, A continuum model of continental deformation above subduction zones: application to the Andes and the Aegean, *J. Geophys. Res.*, 94, 10,331-10,346, 1989.
- Westaway, R., Continental extension on sets of parallel faults: observational evidence and theoretical models, in *The Geometry of Normal Faults*, edited by A.M. Roberts, G. Yielding, and B. Freeman, pp. 143-169, Geol. Soc. Spec. Publ. 56, 1991.
- Wijbrans, J.R., and I. McDougall, Metamorphic evolution of the Attic Cycladic Metamorphic belt on Naxos (Cyclades, Greece) utilizing $^{40}\text{Ar}/^{39}\text{Ar}$ age spectrum measurements, *J. metam. Geol.*, 6, 571-594, 1988.
- Wijbrans, J.R., J.D. van Wees, R.A. Stephenson, and S.A.P.L. Cloetingh, Pressure-temperature-time evolution of the high-pressure metamorphic complex of Sifnos, Greece, *Geology*, 21, 443-446, 1993.
- Winslow, M.A., The structural evolution of the Magallanes basin and neotectonics in the southernmost Andes, in *Antarctic Geoscience*, edited by C. Craddock, pp. 143-154, University of Wisconsin Press, Madison, 1982.
- Woodside, J.M., Tectonic elements and crust of the eastern Mediterranean Sea, *Mar. Geophys. Res.*, 3, 317-354, 1977.
- Wortel, M.J.R., Comments on 'Lengths of intermediate and deep seismic zones and temperatures in downgoing slabs of lithosphere' by Peter Molnar, David Freedman and John S. F. Shih, *Geophys. J. R. Astron. Soc.*, 60, 307-313, 1980.
- Wortel, M.J.R., Spatial and temporal variations in the Andean subduction zone, *J. Geol. Soc. London*, 141, 783-791, 1984.
- Wortel, R., and S. Cloetingh, On the origin of the Cocos-Nazca spreading center, *Geology*, 9, 425-430, 1981.
- Wortel, R., and S. Cloetingh, A mechanism for the fragmentation of oceanic plates, in *Studies in Continental Margin Geology*, edited by J. S. Watkins, and C. L. Drake, *AAPG Mem.*, 34, 793-801, 1983.
- Wortel, M.J.R., and S.A.P.L. Cloetingh, Accretion and lateral variations in tectonic structure along the Peru-Chile Trench, *Tectonophysics*, 112, 443-462, 1985.
- Wortel, M.J.R., and W. Spakman, Structure and dynamics of subducted lithosphere in the Mediterranean region, *Proc. Kon. Ned. Akad. Wetensch.*, 95, 325-347, 1992.
- Wortel, M.J.R., and N.J. Vlaar, Age-dependent subduction of oceanic lithosphere beneath western South America, *Phys. Earth Planet. Inter.*, 17, 201-208, 1978.
- Wortel, M.J.R., M.J.N. Remkes, R. Govers, S.A.P.L. Cloetingh, and P.Th. Meijer, Dynamics of the lithosphere and the intraplate stress field, in *Tectonic Stress in the Lithosphere*, edited by R.B. Whitmarsh, M.H.P. Bott, J.D. Fairhead, and N.J. Kusznir, pp. 111-126, Roy. Soc. London, London, 1991.
- Yoshioka, S., and M.J.R. Wortel, Three-dimensional numerical modeling of detachment of subducted lithosphere, *J. Geophys. Res.*, in press.

- Zienkiewicz, O.C., *The Finite Element Method in Engineering Science*, 521 pp., McGraw-Hill, London, 1977.
- Zoback, M.L., First- and second-order patterns of stress in the lithosphere: the World Stress Map Project, *J. Geophys. Res.*, 97, 11,703-11,728, 1992.
- Zoback, M.L., and R.M. Richardson, Stress perturbation and intraplate seismicity associated with ancient continental rifts, submitted to *J. Geophys. Res.*, 1994.
- Zoback, M. L., et al., Global patterns of tectonic stress, *Nature*, 341, 291-298, 1989.

Samenvatting

Veel van de actuele deformatie van de continentale aardkorst (aardbevingen) en de deformatie opgetreden in het geologische verleden (bijv. gebergtegordels) is geassocieerd met subductiezones: zones waar een continentale lithosfeerplaat over een oceanische plaat heenbeweegt. De overschuivende rand van een continent wordt daarom ook wel aangeduid met de term "actieve" marge. Het is de doelstelling van dit proefschrift om meer inzicht te verkrijgen in de krachten verantwoordelijk voor de deformatie van deze actieve continentale marges. De studie richt zich op twee voorbeelden: de westelijke rand van de Zuid-Amerikaanse plaat, gekenmerkt door het Andes gebergte, en, ten tweede, het gebied van de Egeïsche Zee, het Griekse vasteland en west Turkije, kortweg: het Egeïsche gebied.

Het Andes gebergte en, vooral, het Egeïsche gebied zijn reeds uitvoerig bestudeerd vanuit verscheidene disciplines van de aardwetenschappen en een groot aantal observaties betreffende de deformatie is beschikbaar. Deze observaties maken het mogelijk het verloop van de deformatie (de kinematiek) in detail te reconstrueren. Uitspraken omtrent de krachten verantwoordelijk voor de geobserveerde processen (de dynamica) berusten veelal op directe (kwalitatieve) interpretatie van de beschikbare gegevens. Om de kwestie van de drijvende krachten op een meer kwantitatieve basis te kunnen beantwoorden wordt in dit proefschrift gebruik gemaakt van computermodellen.

Het door de tektonische krachten veroorzaakte intra-plaat spanningsveld dat verantwoordelijk is voor deformatie neemt in dit proefschrift een centrale rol in. De tektonische krachten werkzaam op een bepaald gebied worden onderzocht door het spanningsveld behorend bij een bepaalde krachtenverdeling te berekenen en dit modelresultaat te vergelijken met het geobserveerde spanningsveld. Inzicht in het in werkelijkheid aanwezige spanningsveld volgt uit seismologische studies van de haardmechanismen van aardbevingen en uit geologische (veld)studies van breuken. Laatstgenoemd structureel geologisch onderzoek maakt tevens reconstructie mogelijk van het spanningsveld zoals dat bestond in het geologische verleden. Ter aanvulling van de in de literatuur voor het Egeïsche gebied beschikbare gegevens is door de auteur geologisch veldwerk verricht in het zuidwesten van Griekenland. Modelleren van het spanningsveld geschiedt door de lithosfeer voor te stellen als een dunne elastische bolschil. Bij de berekeningen wordt gebruik gemaakt van de eindige-elementen methode.

Het Andes gebergte is onderzocht als onderdeel van een studie van de gehele Zuid-Amerikaanse plaat. De studie van de plaattektonische krachten aangrijpend op deze plaat valt uiteen in twee delen. In Hoofdstuk 2 wordt uitsluitend gewerkt met het criterium dat de plaat in evenwicht moet zijn. Kennis omtrent het karakter van de plaatgrenzen wordt vertaald in sets van mogelijke krachten. Het evenwichtscriterium maakt het vervolgens mogelijk de grootte van deze krachten te bepalen. Om verder onderscheid te maken tussen de sets die

voldoen aan het evenwichtscriterium worden in Hoofdstuk 3 de corresponderende spanningsvelden berekend en vergeleken met de beschikbare observaties. Vragen die hierbij aan de orde komen zijn bijvoorbeeld: Bestaat er een verband tussen, enerzijds, de grootte van de kracht die wordt uitgeoefend op de actieve westelijke rand van Zuid-Amerika en, anderzijds, de geometrie van de subducerende plaat? Is het mogelijk de spanningstoestand in het Andes gebergte te verklaren door de rol van topografie in rekening te brengen? Wat is de relatie tussen beweging van de Zuid-Amerikaanse plaat en convectie dieper in de mantel?

Het Egeïsche gebied neemt een plaats in aan de zuidrand van de Euraziatische plaat daar waar deze over de lithosfeer van de oostelijke Middellandse Zee - onderdeel van de Afrikaanse plaat - heenschuift. Terwijl het Andes gebergte is ontstaan door verkorting (compressie) van de continentale marge, wordt de Laat-Kenozoïsche ontwikkeling van het Egeïsche gebied gekenmerkt door extensie (rek). Gedetailleerde analyse van de breukdeformatie heeft uitgewezen dat het patroon van rek in de loop van de tijd is veranderd.

De modelanalyse van het Egeïsche gebied in Hoofdstuk 4 richt zich in eerste instantie op de actuele deformatie. Het onderzoek concentreert zich op de oorzaak van de waargenomen extensie. Verschillende mechanismen worden getoetst door middel van modelexperimenten. Naast informatie betreffende het spanningsveld worden ook de recentelijk via geodetisch onderzoek bepaalde horizontale korstbewegingen gebruikt als vergelijkingsmateriaal voor de numerieke modellen.

Beschouwing van een reconstructie van het gebied gedurende het Laat Pliocen, circa 2 miljoen jaar geleden, maakt het mogelijk de ontwikkeling van de plaattektonische krachten door de tijd te bestuderen. Tomografische afbeeldingen van de mantelstructuur in het Middellandse-Zeegebied duiden op de mogelijkheid dat de plaat gesubduceerd onder Griekenland wellicht deels is afgebroken. Er wordt onderzocht of dit proces een rol kan hebben gespeeld in de waargenomen verandering van het patroon van extensie.

Dankwoord

In de eerste plaats gaat mijn dank uit naar mijn begeleider Prof. Rinus Wortel. Ik heb de afgelopen jaren veel geleerd van zijn kennis van de tektonofysica en, daarnaast, van zijn wijze van benadering van de vele aspecten van het wetenschappelijk onderzoek en het onderwijs. Prof. Johan Meulenkamp introduceerde mij met de geologie van Griekenland en van hem leerde ik een aanpak van geologisch veldwerk die goed aansluit bij tektonofysische (model-)studie. Rinus Wortel en Johan Meulenkamp ben ik in het bijzonder erkentelijk voor het feit dat zij de mogelijkheid hebben geschapen tot het verrichten van gecombineerd geologisch-geofysisch onderzoek.

Discussies met Dr. Pim van Wamel en Dr. Reinoud Vissers hebben bijgedragen tot verschillende delen van dit proefschrift en worden zeer gewaardeerd. Mijn collega-promovendi, waarvan ik met name wil noemen Maarten Remkes, Rob Govers en Marc de Jonge, ben ik dankbaar voor de prettige samenwerking. Maarten Remkes leverde de basis voor de berekening van de krachtenbalans in Hoofdstuk 2. Samen met Rob Govers is gewerkt aan de kwantificering van de rol van de topografie van het Andes gebergte, opgenomen in Hoofdstuk 3. Dr. Wim Spakman was immer bereid tot het beantwoorden van vragen over zijn tomografische resultaten en de in dit proefschrift gebruikte, door hem ontwikkelde, grafische software.

Ik ben dank verschuldigd aan Ron Noomen voor het beschikbaar stellen van de resultaten van het geodetisch onderzoek in het Middellandse-Zeegebied verricht door de Technische Universiteit Delft. Fred Beekman dank ik voor zijn hulp bij het opzetten van de eindige-elementen berekeningen.

I wish to thank Prof. Jacques Mercier for the fact that he has generously provided additional information concerning fieldwork results obtained by his group in the Aegean region and for the opportunity to discuss many topics related to neotectonics. Prof. Marcelo Assumpção is thanked for sending me the latest observations regarding the South American stress field and for his additional explanation of several aspects. Dr. James Jackson kindly provided material which allowed me to reproduce his horizontal velocity field for the Aegean region.

The Institute of Geology and Mineral Exploration (IGME, Athens) is acknowledged for granting the author permission to carry out fieldwork in various parts of Greece. Royal Dutch Shell provided financial support for travel to the 1992 AGU Fall meeting.

Chapter 2 of this thesis could be improved due to critical reviews by *Journal of Geophysical Research* -referees Prof. Martin Bott and Dr. Donna Jurdy. Chapter 4 has benefitted from comments by referees Prof. John Dewey, Dr. James Jackson and an anonymous referee, concerning an earlier version of this chapter submitted to *Tectonics*. Improvements to Chapter 4 suggested by Maarten Verheul and Andrew Curtis are much appreciated.

Curriculum Vitae

De auteur van dit proefschrift is op 25 juni 1965 geboren te Amersfoort. In 1983 behaalde hij het diploma ongedeelde VWO aan het Eemland College Noord, eveneens te Amersfoort. In hetzelfde jaar werd begonnen met de studie Luchtvaarttechniek aan de Technische Hogeschool Delft. In 1984 werd echter gekozen voor de studie Geologie aan de Universiteit Utrecht. Het doctoraal-examen Geologie werd in 1989 cum laude behaald. Van 1989 tot 1995 is het in dit proefschrift beschreven onderzoek verricht. Een positie als assistent-in-opleiding werd in 1993 gevolgd door een aanstelling als toegevoegd docent. Sinds augustus 1995 is de auteur als postdoctoraal onderzoeker werkzaam op een project gefinancierd door de Nederlandse Organisatie voor Wetenschappelijk Onderzoek.